Identification and Characterisation of Mitotically Quiescent Sub-Clones in Breast Cancer

A thesis submitted for the degree of
Doctor of Philosophy

By

Lewis Quayle

Supervised by

Prof. Ingunn Holen and Dr. Penelope Ottewell

The University of Sheffield

Faculty of Medicine, Dentistry and Health

Department of Oncology and Metabolism

October 2017

Acknowledgements

I would like to begin by thanking my supervisors Prof. Ingunn Holen and Dr. Penelope Ottewell. Thank you both for believing in me and for giving me the opportunity to undertake this project in the first place. Thank you for your continued guidance and support throughout my Ph.D. and for helping me to grow as a scientist. I am very much looking forward to continuing our work together in the future.

I would like to express my utmost gratitude to Dr. Mark Jones; thanks for all the antibodies you gave me but more importantly for providing your own time to help me out with my project, I really appreciate it.

A big thank you to Alyson Evans and Diane Lefley for all the ordering and bits you have done for me personally and for all the cleaning, preparation and organising you do around the laboratory behind the scenes.

A massive thank you to Dr. Victoria Cookson and Dr. Russell Hughes; I know I have bugged you both to death with technical questions about various things over the duration of my project, so I would like to say thank you to the both of you for your friendship, your expert guidance, and for never telling me to get lost.

Cheers to all the friends I have made here for making my Ph.D. so memorable and for all the killer hangovers (after just one pint) I have suffered on the day after the night before.

I would also like to sincerely thank my long-time friend and mentor Dr. Timothy Bates for helping me to get here in the first place and for continually supporting me in my career.

Finally, a very special thank you to all of my family and to my girlfriend Maria; you have all helped me on the way to getting to where I am today and for that I am eternally grateful - I hope I have made all of you very proud.

Funding Bodies

Additional funding was provided by:

Declaration

I hereby declare that the work presented in this thesis is my own original research carried out under the guidance of my supervisors Prof. Ingunn Holen and Dr. Penelope Ottewell. All of the techniques described were carried out by myself except for fluorescent-activated cell sorting, which was performed with the assistance of Susan Clark, Kay Hopkins or Julie Swales of The University of Sheffield Flow Cytometry Core Facility, and the scoring of immunofluorescent staining, which was performed independently by Alyson Evans and William Marsden.

Permission for reproduction in this thesis has been granted by Bentham Science Publishers for the following manuscript:

Quayle, L., Ottewell, P.D., Holen, I. (2015). Bone Metastasis: Molecular Mechanisms Implicated in Tumour Cell Dormancy in Breast and Prostate Cancer. *Curr Cancer Drug Targets*, **15**, 469-80.

Publications

Publications arising from my doctoral studies include:

1. Published original manuscripts

Quayle, L., Ottewell, P.D., Holen, I. (2015). Bone Metastasis: Molecular Mechanisms Implicated in Tumour Cell Dormancy in Breast and Prostate Cancer. *Curr Cancer Drug Targets*, **15**, 469-80.

2. Published abstracts

Quayle, L., Park, S., McDonnell, D.P., Ottewell, P.D., Holen, I. *Targeting ERR-α Regulated Lactate Metabolism Eliminates Drug-Resistant Breast Cancer Cells*. The San Antonio Breast Cancer Symposium 2016, 6th – 10th December 2016, San Antonio, Texas, U.S.A.

3. Presentations at conferences

Oral Presentations:

Quayle, L.*, Ottewell, P.D., Holen, I. *Therapeutic Resistance and Unique Stemness Define Mitotically Quiescent Sub-Clones in Human Breast Cancer*. 1st Yorkshire Breast Cancer Symposium, 9th June 2017, York, England.

Quayle, L.*, Jones, M., Ottewell, P.D., Holen, I. *Mitotically quiescent human breast cancer cells are characterised by multi-drug resistance and a unique stem cell-like phenotype*. Sheffield Cancer Research Day, 8th March 2017, Sheffield, England.

Quayle, L.*, Park, S., McDonnell, D.P., Ottewell, P.D., Holen, I. *Inhibiting ERR-α Regulated Lactate Metabolism Eliminates Drug-Resistant Breast Cancer Cells*. 7th Annual Mellanby Centre Research Day, 2nd December 2016, Sheffield, England.

Quayle, L.*, Ottewell, P.D., Holen, I. *Finding New Ways of Stopping Breast Cancer from Spreading to the Skeleton*. 12th Annual Sheffield Medical School Research Meeting, 16th – 17th June 2016, Sheffield, England.

Poster Presentations:

Quayle, L.*, Ottewell, P.D., Holen, I. *Therapeutic Resistance and Unique Stemness Define Mitotically Quiescent Sub-Clones in Human Breast Cancer*. 13th Annual Sheffield Medical School Research Meeting, 15th – 16th June 2017, Sheffield, England.

Marsden, W.J.*, Holen, I., **Quayle, L.** *Autophagy as a Regulator of the Quiescent Phenotype in Breast Cancer*. 13th Annual Sheffield Medical School Research Meeting, 15th – 16th June 2017, Sheffield, England.

Quayle, L.*, Park, S., McDonnell, D.P., Ottewell, P.D., Holen, I. *Targeting ERR-α Regulated Lactate Metabolism Eliminates Drug-Resistant Breast Cancer Cells.* The San Antonio Breast Cancer Symposium 2016, 6th – 10th December 2016, San Antonio, Texas, U.S.A.

Quayle, L.*, Ottewell, P.D., Holen, I. *Therapeutic Targeting of Metastasis-Initiating Cells in Breast Cancer*. 12th Annual Sheffield Medical School Research Meeting, 16th – 17th June 2016, Sheffield, England.

Quayle, L.*, Ottewell, P.D., Holen, I. *A Novel In Vitro Model for Therapeutic Targeting of Metastasis-Initiating Cells in Breast Cancer*. Sheffield Cancer Research Day, 22nd January 2016, Sheffield, England.

Alt, I.*, **Quayle, L.**, Brown, S., Ottewell, P.D., Wilkinson, J.M., Holen, I., Cookson, V.J. *Developing a High-Throughput In Vitro Model of Breast Cancer Metastasis to Bone*. Sheffield Cancer Research Day, 22nd January 2016, Sheffield, England.

Quayle, L.*, Ottewell, P.D., Holen, I. *Novel In Vitro Models to Define Mechanisms Regulating Cellular Dormancy in Breast Cancer*. 6th Annual Mellanby Centre Research Day, 4th December 2015, Sheffield, England.

Quayle, L.*, Ottewell, P.D., Holen, I. *Unravelling the Mechanisms Regulating Cellular Dormancy in Breast Cancer Using Novel In Vitro Models*. BACR Special Conference on Breast Cancer "Breast Cancer - Bridging gaps in our knowledge to improve patient outcome", 7th – 9th October 2015, Newcastle/Gateshead, England.

Quayle, L.*, Ottewell, P.D., Holen, I. *Developing a Novel In Vitro Model for Study of Molecular Mechanisms Implicated in Breast Tumour Cell Dormancy*. Yorkshire Cancer Research Annual Research Meeting 2015, 2nd July 2015, Harrogate, England.

Quayle, L.*, Ottewell, P.D., Holen, I. *Developing a Novel In Vitro Model for Study of Molecular Mechanisms Implicated in Breast Tumour Cell Dormancy*. 11th Annual Sheffield Medical School Research Meeting, 15th – 16th June 2015, Sheffield, England.

* indicates the presenting author

Table of Contents

List of Figures

List of Tables

Summary

Metastatic disease is the major cause of death in advanced breast cancer and is supposed to be initiated by a sub-population of cancer stem cells (CSCs) that disseminate from the primary tumour at an early stage in disease pathogenesis. Detailed insight into the biology underpinning the emergence and survival of the CSC population will therefore likely be critical to the development of therapeutic strategies for prevention of breast cancer relapse. However, the isolation of CSCs based on specific marker signatures is increasingly recognised as being unreliable due to population plasticity and the ambiguous functional significance of the markers used. A number of relatively recent studies have reported pulse-chase techniques using lipophilic fluorescent dyes that enable the prospective isolation of live CSC populations based on their inherently quiescent nature.

The main aim of this thesis was to establish a lipophilic dye retention method for the isolation of mitotically quiescent human breast cancer cells from commercially available cell lines grown *in vitro*, and to establish whether quiescence was associated with characteristics of the purported metastasis-initiating breast CSC population. A latent quiescent sub-population accounting for < 2% of the total cell population was identified in the MCF-7, ZR-75-1, MDA-MB-468, MDA-MB-231 and SK-BR-3 human breast cancer cell lines based on their ability to retain the lipophilic fluorescent dye Vybrant® DiD. The relatively quiescent nature of dye-retaining cells was confirmed by their tendency to collect in the G_2/M-phase of the cell cycle and by a significant enrichment with cells that were Ki67$^-$ (G_0-phase) following immunostaining. The quiescent sub-population was shown not to be an intrinsic feature of the cell lines in which they were identified, but that they could emerge spontaneously within isolated rapidly dividing cultures. Immunoprofiling of quiescent cells illustrated only a partial overlap with the CD44$^+$CD24$^{-/low}$ signature commonly used to identify breast CSCs but showed a significant enrichment for cells that were CD44$^+$CD24$^+$ and ALDH$^+$. Quiescent cells also displayed an enhanced ability to survive chemotherapy and exclusively contained sub-clones capable of subsequent outgrowth. Further characterisation of this population could identify novel therapeutic targets for elimination of the cells responsible for *de novo* drug resistance and breast cancer recurrence.

List of Abbreviations

2D	Two-dimensional
3D	Three-dimensional
^{3}H-TdR	Tritiated thymidine
AA11	Novel anti-stem cell antigen AA11
AG10	Novel anti-stem cell antigen AG10
AHRI	Aplysia ras homology member 1
ALDH	Aldehyde dehydrogenase
ALDH1	Aldehyde dehydrogenase-1
ANOVA	Analysis of variance
ATCC	American Type Culture Collection
ATF6	Activating transcription factor-6
ATM	ATM serine/threonine kinase
AXL	Tyrosine-protein kinase receptor UFO
BAAA-DA	BODIPY-aminoacetaldehydediethylacetate
BAAA	BODIPY-aminoacetaldehyde
BCA	Bicinchoninic acid
BCL-2	B-cell lymphoma-2
BCL-XL	B-cell lymphoma-extra large
BE12	Novel anti-stem cell antigen BE12
BF4	Novel anti-stem cell antigen BF4
bFGF	Basic fibroblast growth factor
BHLHE41	Basic helix-loop-helix family member e41
BM-HMSC	Bone marrow-derived human mesenchymal stem cells
BMP	Bone morphogenetic protein
BMP7	Bone morphogenetic protein-7
BMPR2	Bone morphogenetic protein receptor type-2
BRCA1	Breast cancer 1
BrdU	5-bromo-2-deoxyuridine
BSA	Bovine serum albumin
^{o}C	Degrees Celsius
CC9	Novel anti-stem cell antigen CC9
CD24	Signal transducer CD24
CD29	Integrin β1
CD34	Hematopoietic progenitor cell antigen CD34
CD38	Cyclic ADP ribose hydrolase
CD44	Hyaluronan receptor
CD46	Complement regulatory protein
CD49f	Integrin α6
CD56	Neural cell adhesion molecule
CD57	Human natural killer-1
CD133	Prominin-1
CD147	Basigin
CD271	Low-affinity nerve growth factor receptor
CDK	Cyclin-dependent kinase
CDK4	Cyclin-dependent kinase-4

CE	Clonal evolution
c-FLIP	FLICE-like inhibitory protein
CFSE	Carboxyfluorescein diacetate succinimidyl ester
CH8	Novel anti-stem cell antigen CH8
cm	Centimetre
CO_2	Carbon dioxide
CSC	Cancer stem cell
CTC	Circulating tumour cell
CXCL12	CXC motif chemokine-12
CXCR4	CXC motif chemokine receptor-4
DA9	Novel anti-stem cell antigen DA9
DAPI	4',6-diamidino-2-phenylindole
DCIS	Ductal carcinoma *in situ*
DEAB	Diethylaminobenzaldehyde
DEC2	See BHLHE41
dH_2O	Distilled water
DMSO	Dimethylsulphoxide
DNA	Deoxyribonucleic acid
DTC	Disseminated tumour cell
EC_0	No effective concentration
EC_{25}	25% maximal effective concentration
EC_{50}	50% maximal effective concentration
EC_{100}	Maximal effective concentration
ECM	Extracellular matrix
EDTA	Ethylenediaminetetraacetic acid
EF12	Novel anti-stem cell antigen EF12
EMT	Epithelial-to-mesenchymal transition
EpCAM	Epithelial cell adhesion molecule
ER	Oestrogen receptor
ERK	Extracellular regulated kinase
ERR-α	Oestrogen-related receptor-α
FACS	Fluorescence activated cell sorting
F-actin	Filamentous actin
FAK	Focal adhesion kinase
FBS	Foetal bovine serum
fM	Femtomolar
FMO	Fluorescence minus-one
g	Gram(s)
GAS6	Growth arrest-specific 6
GD2	Ganglioside GD2
GD3	Ganglioside GD3
GFP	Green fluorescent protein
GJIC	Gap junctional intercellular communication
GLUT1	Glucose transporter-1
GRAF	GTPase regulator associated with focal adhesion kinase
GT3	Ganglioside GT3
GTPase	Guanosine triphosphate hydrolase
H&L	Heavy and light chain

HCC	Hepatocellular carcinoma cells
hEC	Human embryocarcinoma stem cells
HER2	Human epidermal growth factor receptor type-2
hES	Human embryonic stem cells
HIF-1α	Hypoxia-inducible factor-1-α
HNSCC	Head and neck squamous cell carcinoma
HRP	Horseradish peroxidase
HSC	Haematopoietic stem cell
IBC	Invasive breast cancer
IC_{50}	50% maximal inhibitory concentration
IC_{95}	95% maximal inhibitory concentration
IgG	Immunoglobulin G
IgG1	Immunoglobulin G subclass-1
IgG2b	Immunoglobulin G subclass-2b
IgG3	Immunoglobulin G subclass-3
IgM	Immunoglobulin M
ISCI	International stem cell initiative
M	Molar
MAPK	Mitogen-activated protein kinase
MARCKS	Myristoylated alanine-rich C-kinase substrate
MER	Proto-oncogene tyrosine-protein kinase MER
MET	Mesenchymal-to-epithelial transition
MFI	Median fluorescence intensity
mg	Milligram
μg	Microgram
miRNA	MicroRNA
ml	Millilitre
μl	Microlitre
mm	Millimetre
μm	Micrometre
mM	Millimolar
μM	Micromolar
MMC	Mitomycin C
MMP	Matrix metalloproteinase
MSC	Mesenchymal stem cell
mTOR	Mammalian target of rapamycin
MTT	Methylthiazolyltetrazolium bromide
NADH	Reduced nicotinamide adenine dinucleotide
$NADP^+$	Oxidised nicotinamide adenine dinucleotide phosphate
NDRG1	Protein NDRG1
NDRG2	Protein NDRG2
NF-κB	Nuclear factor κ-light-chain-enhancer of activated B-cells
NK1R	Neurokinin-1 receptor
NK2R	Neurokinin-2 receptor
NK3R	Neurokinin-3 receptor
NK1R-Tr	Truncated neurokinin-1 receptor
NK1R-FL	Full-length neurokinin-1 receptor
nm	Nanometre

nM	Nanomolar
NOTCH	NOTCH protein
NR2F1	Nuclear receptor subfamily 2 group F member 1
p21	Cyclin-dependent kinase inhibitor-1
p27	Cyclin-dependent kinase inhibitor-1B
p38	p38 mitogen-activated protein kinase
p38-α	p38 mitogen-activated protein kinase-14
p38-β	p38 mitogen-activated protein kinase-11
PBS	Phosphate-buffered saline
PBST	PBS with Tween®20
PCC	Prostate cancer cell
PDX	Patient-derived xenograft
PI3K	Phosphatidylinositide 3-kinase
PKB	Protein kinase B
pM	Picomolar
poly-HEMA	Poly-2-hydroxyethylmethacrylate
PVDF	Polyvinylidene fluoride
qPCR	Real-time quantitative polymerase chain reaction
Ras	Ras protein
RFU	Relative fluorescence units
Rheb	Ras protein homolog enriched in brain
RhoA	Ras homolog gene family member A
RIPA	Radioimmunoprecipitation assay
RNase A	Ribonuclease A
SDS	Sodium dodecyl sulphate
SEM	Standard error of the mean
SHARP1	See BHLHE41
SMAD1	SMAD family member 1
SMAD5	SMAD family member 5
shRNA	Short hairpin RNA
SSEA-1	Stage-specific embryonic antigen-1
SSEA-3	Stage-specific embryonic antigen-3
SSEA-4	Stage-specific embryonic antigen-4
TBK1	TANK-binding kinase-1
TBST	Tris-buffered saline with Tween®20
TGF-β2	Transforming growth factor-β2
TGF-βRI	Transforming growth factor-β receptor type-1
TGF-βRIII	Transforming growth factor-β receptor type-3
TNBC	Triple-negative breast cancer
TRA-1-60R	Neuraminidase-resistant podocalyxin isoform TRA-1-60
TRA-1-60S	Neuraminidase-sensitive podocalyxin isoform TRA-1-60
TRA-1-81	Podocalyxin isoform TRA-1-81
TRA-2-49	Tissue non-specific alkaline phosphatase
TRA-2-54	Tissue non-specific alkaline phosphatase
TSP-1	Thrombospondin-1
TYRO3	Tyrosine-protein kinase receptor TYRO3
uPAR	Urokinase receptor
v/v	Volume concentration

V	Volts
VEGF	Vascular endothelial growth factor
w/v	Weight concentration
x g	Times gravity
X-gal	5-bromo-4-chloro-3-indolyl-β-D-galactopyranoside
ZEB1	Zinc finger E-box-binding homeobox-1

Chapter 1

Introduction

1.1. Understanding Cellular Heterogeneity in Breast Cancer

Breast cancer is characterised by a significant degree of cellular and molecular intertumoural heterogeneity which gives rise to variability in disease progression and clinical outcome (Rich, 2016). Considerable genetic, phenotypic and functional diversity has also been documented at the cellular level within individual breast tumours. In fact, a vast body of experimental evidence reported across virtually every documented major cancer type has demonstrated intratumoural variance in terms of cell surface marker expression, genetic and epigenetic alterations, genetic stability, mitotic, invasive, metastatic, tumourigenic and angiogenic potential, and susceptibility to chemo- and radiotherapies (Burrell *et al.*, 2013; Kreso and Dick, 2014; McGranahan and Swanton, 2017). Two predominant models have historically been used to account for such intratumoural heterogeneity and explain the natural history of tumour pathogenesis, the stochastic or clonal evolution (CE) model and the hierarchy or cancer stem cell (CSC) model (**Figure 1.1.**). The former postulates that malignant cells are initially biologically homogenous but are able to accumulate genetic and epigenetic aberrations over time due to intrinsic genetic instability. The acquisition of numerous genetic and epigenetic abnormalities leads to the development of variable phenotypic and functional traits that then undergo microenvironmental selection to drive tumour progression and increased tumoural heterogeneity (Michor and Polyak, 2010; Gerdes *et al.*, 2014). In contrast, the long-standing observation of multiple similarities between normal embryonic developmental processes and abnormal neoplastic growth led to the development of the CSC model, which proposes that tumour pathogenesis is driven by a minority sub-population of transformed stem-like cancer cells that, like their non-malignant counterparts, are capable of self-renewal and differentiation to generate multiple cellular phenotypes. Accordingly, tumours are supposed to be hierarchically organised to include highly tumourigenic CSCs, transitory progenitor cells and terminally differentiated progeny (Gerdes *et al.*, 2014).

The concept that cancers are propagated by a rare, biologically distinct cellular sub-set was first suggested by the German pathologist Rudolf Virchow over 150 years ago (Nguyen *et al.*, 2012). However, it was not until the seminal study by Bonnet and Dick (1997) that direct experimental evidence to support this proposal emerged. The existence of CSCs has since become widely accepted following the demonstration of the existence of CSCs in multiple other tumour types, including those of breast, prostate, pancreas, colon, liver ovaries, head and neck, and the brain (Al-Hajj *et al.*, 2003; Singh *et al.*, 2004; Collins *et al.*, 2005; Li *et al.*, 2007; Ma *et al.*, 2007; O'Brien *et al.*, 2007; Prince *et al.*, 2007; Gao *et al.*, 2010). However, a myriad of experimental evidence that demonstrates the dynamic and reversible induced transition of non-stem cancer cells to a more stem-like phenotype, thereby supporting the CE model, has also been reported in this time (Reviewed by Plaks *et al.*, 2015). Consequently, an alternative model of reversible cellular plasticity has recently been proposed as a unifying framework that incorporates both CE and CSC models (Cabrera *et al.*, 2015). This so-called plasticity model of intratumoural heterogeneity postulates that tumour cells transiently interconvert between stem-like and differentiated states under the influence of intrinsic cellular processes and extrinsic stimuli (**Figure 1.1.**).
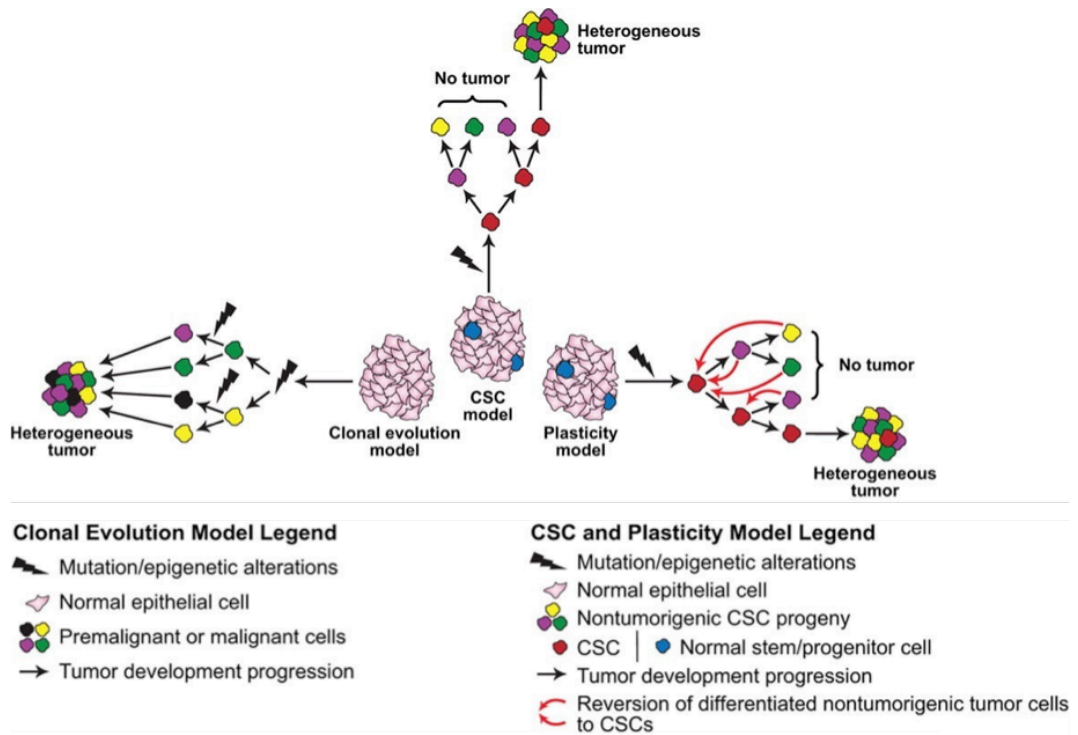
Figure 1.1. Conceptual Models of Intratumoural Heterogeneity

In the clonal evolution (CE) or stochastic model, the tumourigenic potential of cells is initially equal and is acquired over time as the cumulative result of mutational events that confer a selective advantage to particular clones in response to microenvironmental selection. In the cancer stem cell (CSC) or hierarchic model, only stem cells possess tumourigenic potential while their non-stem progeny possess little or no intrinsic tumourigenicity. According to the plasticity model, differentiation can be bidirectional so that initially non-tumourigenic cancer cells are capable of reversion to a CSC state under microenvironmental instruction. Image reprinted from Rich, J. N. (2016). Cancer stem cells: understanding tumour hierarchy and heterogeneity. *Medicine (Baltimore)*, 95, S2-7 with permission from Wolters Kluwer Health, Inc.

1.2. Metastasis: A Conceptual Overview

Metastasis, the systemic spread of a tumour to secondary sites, invariably foreshadows a poor prognosis and is ultimately responsible for greater than 90% of tumour-related patient mortality (Chaffer and Weinberg, 2011). From a clinical perspective, metastasis occurs in two distinct phases: a clinically latent stage of systemic dissemination that occurs early in disease pathogenesis (during formation of the primary tumour and prior to clinical presentation) followed by the formation of overt metastatic lesions (Klein, 2003; Husemann *et al.*, 2008; Hosseini *et al.*, 2016). Manifest metastasis is largely incurable; secondary foci frequently become refractory to chemotherapeutic agents, seed additional metastatic colonies, and eventually compromise functionality of vital organs, ultimately leading to death (Giancotti, 2013).

From a pathophysiological perspective, the conventional description of the metastatic process is that of a linear series of discrete events, the invasion-metastasis cascade (**Figure 1.2.**), that culminate in the eventual outgrowth of disseminated tumour cells (DTCs) in the distant target organ (Nguyen *et al.*, 2009). The process commences when tumour cells at the primary site undergo a partial or complete epithelial-to-mesenchymal transition (EMT). Having shed their epithelial traits, cells partially degrade and invade into the interstitial matrix, and induce the development of a supporting vasculature through neoangiogenesis. Intravasation and haematogenous dissemination subsequently occur as tumour cells exploit either local lymphatic drainage or discontinuities in the developing tumour-associated vasculature. Upon becoming arrested in the vascular beds of the distant target organ, DTCs undergo extravasation into the surrounding stroma and adopt various strategies that allow their survival and eventual successful colonisation of the non-orthotopic tissue (Valastyan and Weinberg, 2011).
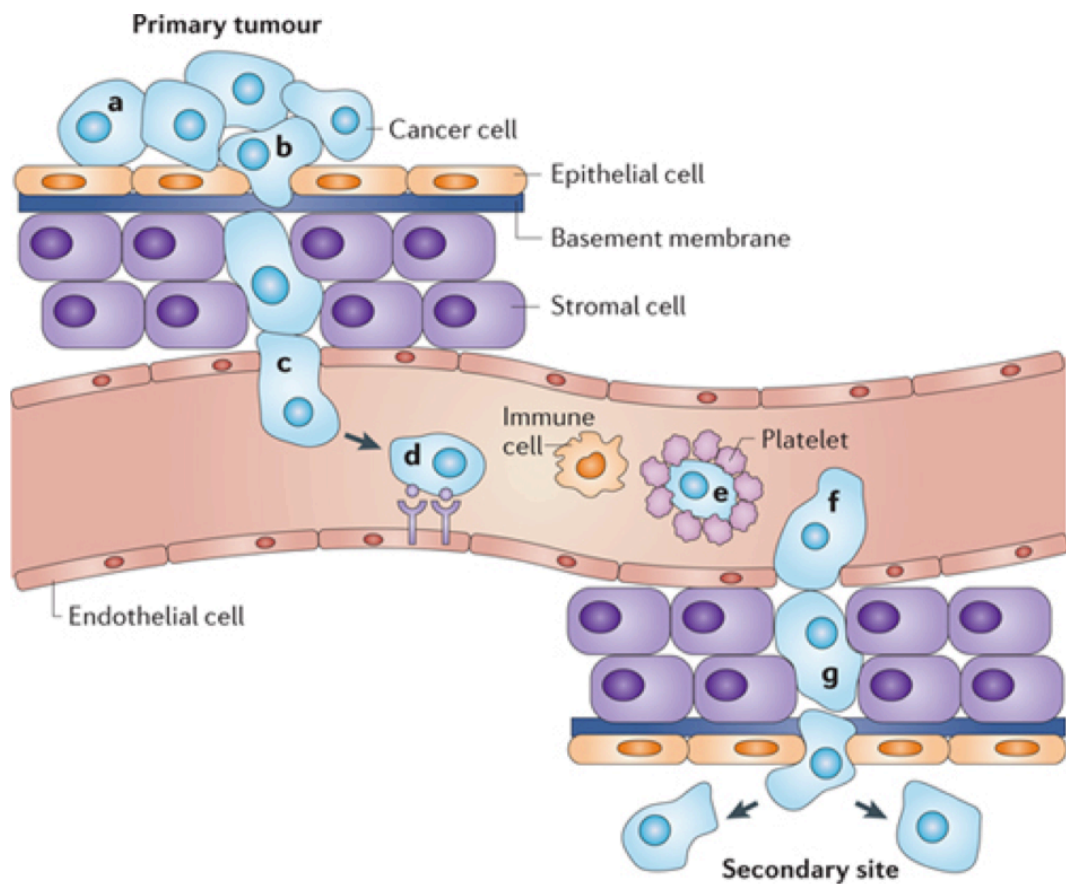
Figure 1.2. The Invasion-Metastasis Cascade

During metastasis, metastatic cancer cells reduce their adhesion to neighbouring cells (**a**) and degrade the epithelial basement membrane in order to gain access to the surrounding stroma and supporting vasculature (**b**). If the tumoural vasculature is continuous, cancer cells must undergo intravasation (**c**); endothelial cell retraction is induced by release of molecules such as vascular endothelial growth factor (VEGF) and the release of reactive oxygen species and factors including matrix metalloproteinases (MMPs) cause cell death, allowing access to the bloodstream. The distribution of circulating tumour cells (CTCs) is determined by blood flow and interactions between cancer cells and the secondary organs that they colonise; cells can get trapped in narrow capillary beds and can also express receptors that bind to vascular endothelial cells (**d**) or to platelets (**e**), which protect the cancer cells from the immune system and facilitate access to secondary tissues. Upon arrival at secondary sites, cancer cells exit the blood stream by extravasation (**f**), a process that is mechanistically comparable to intravasation. Cancer cells then proceed to invade into and take-up residence in secondary tissues (**g**). Image reprinted from Schroeder, A., Heller, D. A., Winslow, M. M., Dahlman, J. E., Pratt, G. W., Langer, R., Jacks, T. & Anderson, D. G. (2011). Treating metastatic cancer with nanotechnology. *Nat Rev Cancer*, 12, 39-50 with permission from Nature Publishing Group.

The colonisation of remote tissues by cells derived from particular primary tumours is a type-specific phenomenon (Gupta and Massague, 2006). In breast cancer, the bones, liver, lungs and brain are especially susceptible to the development of metastases, although the temporal course of disease within these target organs is often very different and varies by the molecular sub-type of breast cancer involved. In bone metastasis, and in oestrogen receptor positive (ER⁺) breast cancer in particular, relapse often occurs years and even several decades after initial diagnosis (Bragado *et al.*, 2012; Gomis and Gawrzak, 2016). These observations support the contemporary conceptualisation of the well-established "seed and soil' theory of metastasis, originally proposed by Stephen Paget over a century ago (reviewed by Langley and Fidler, 2011), which proposes that it is the compatibility or interactions between the genetic signature and cellular phenotype of the DTCs or "the seeds" and the signals encoded within specific niche microenvironments or "the soil" that is the primary determinant of whether DTCs are able to proliferate and produce overt secondary lesions, or are forced to enter a protracted state of mitotic arrest (Sosa *et al.*, 2013).

1.3. Clinical Implications of Breast Cancer Metastasis to Bone

Skeletal metastatic foci are a complication of advanced malignancy of the breast and prostate in approximately 80% of diagnoses (Smith *et al.*, 2012; Coleman *et al.*, 2014a; Coleman *et al.*, 2014b). The development of secondary tumours disrupts the tightly controlled process of bone remodelling, resulting in the well-established "vicious cycle of bone metastasis" (**Figure 1.3.**) that leads to increased bone resorption and, ultimately, tumour progression (Mundy, 1997). During the course of disease, a significant number of individuals with bone metastases will suffer frequent or recurrent skeletal related events, including; pathological fractures, spinal-compression syndromes, bone pain and hypercalcaemia (Coleman, 2006). The development of such cancer-related skeletal morbidity causes considerable personal, social and financial burden, and a markedly diminished quality of life (Kinnane, 2007). Patients are generally considered incurable once skeletal dissemination is diagnosed (Coleman *et al.*, 2014a). Although bone-targeting anti-resorptive agents have been very successful in reducing the rate of disease progression, decreasing the incidence of skeletal-related events and lengthening patient life expectancy, the median survival rate

remains around 2 years from the initial diagnosis of bone metastasis (Harries *et al.*, 2014).

Secondary skeletal foci in breast and prostate cancer are invariably derived from DTCs that are initially maintained in a protracted state of reversible mitotic arrest. This non-proliferative state confers an inherent resistance to conventional anti-neoplastic chemotherapeutics that prevents the removal of DTCs from the bone. These cells may emerge from quiescence a number of years or decades following initial treatment to form tumours that lead to skeletal destruction, complications and eventual patient mortality (Sosa *et al.*, 2014). The exact molecular mechanisms that maintain DTCs in a state of mitotic arrest and determine their reawakening to form metastatic lesions remain some of the most important unanswered questions in cancer biology. Obtaining a greater understanding of these areas will likely hold the key to vastly improving the prognosis of those patients that are diagnosed at an advanced stage of disease.
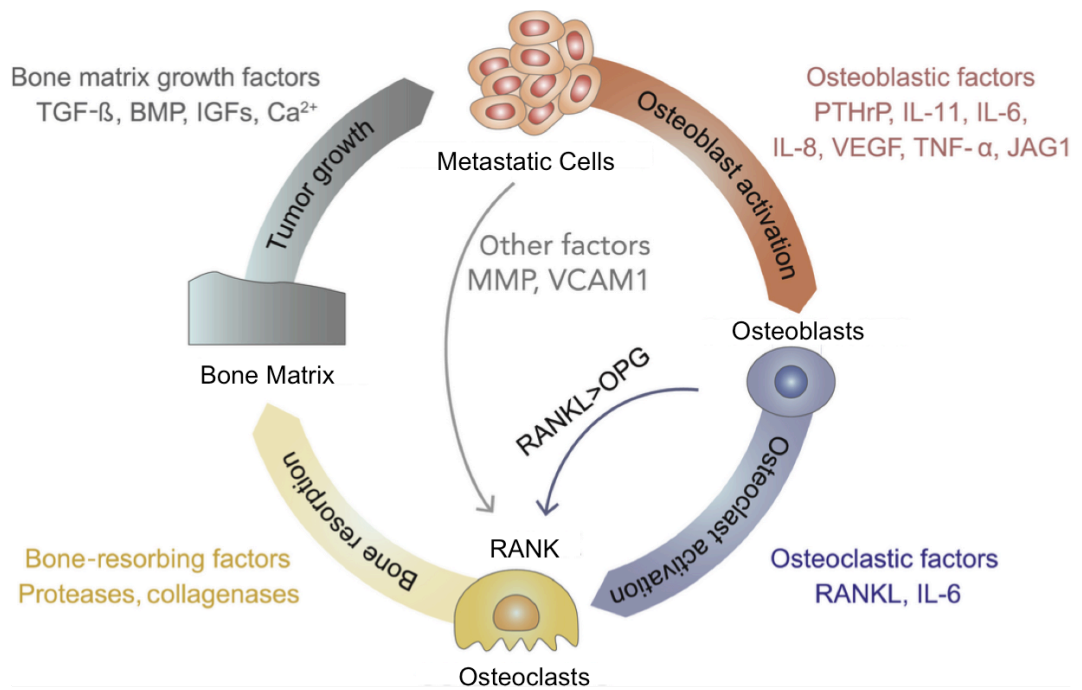
Figure 1.3. The Vicious Cycle of Bone Metastasis

Overtly growing metastatic cancer cells secrete soluble factors that act in a paracrine manner on osteoblasts and osteoclasts and ultimately stimulate bone resorption resulting in lytic bone lesions. Osteoclast activity acts to degrade the bone and releases an array of growth factors sequestered within bone tissue during osteogenesis. The action of these mitogenic factors perpetuates the cycle of tumor cell growth and osteolysis. Image reprinted from Gomis, R. R. & Gawrzak, S. (2016). Tumor cell dormancy. *Mol Oncol*. with permission from FEBS Press and John Wiley & Sons Ltd.

1.4. The Metastasis-Initiating Breast Cancer Cell Population

Metastasis itself is an inefficient process; despite the persistent shedding of vast numbers of cells into the circulation by primary tumours, very few metastatic lesions actually develop (Fidler, 1970; Weilbaecher *et al.*, 2011). Metastatic inefficiency indicates that the majority of tumour cells fail to successfully execute one of the steps of the invasion-metastasis cascade. However, a small proportion of cancer cells that arise within the primary tumour will invariably complete the metastatic process, evidenced by the fact that many cancer patients do eventually progress to develop secondary tumours (Chaffer and Weinberg, 2011). Various experimental studies indicate that these metastasis-initiating sub-clones arise within the primary tumour from progenitors that are initially devoid of significant survival or self-renewal capacity, under the influence of tumour-derived microenvironmental conditions (e.g. hypoxia and nutritional stress), and through interactions with tumour-associated stromal cells (Joyce and Pollard, 2009; Chaffer *et al.*, 2011; Scheel *et al.*, 2011; Fluegen *et al.*, 2017). The phenotypic adaptations that these cells acquire presumably do not confer a strong selective advantage at the primary site and therefore are not prevalent within the primary tumour. Instead, these changes likely act to facilitate initial entry into, and transition through, the invasion-metastasis cascade and only prove vital to cell survival and progression post-dissemination. The identification of driver mutations and the convergent adaptation of metastatic clones in a number of cancer types indicates that environmental conditions encountered during systemic spread also influences acquisition of genetic and epigenetic alterations that potentiate the metastatic capacity of tumour cells already equipped to survive the preceding stages of the dissemination process (Campbell *et al.*, 2010; Gerlinger *et al.*, 2012). The acquisition of the phenotypic attributes that enable individual tumour cells to successfully traverse the metastatic cascade can therefore be seen as a dynamic adaptation akin to the Darwinian process of natural selection; tumour cells that eventually succeed in colonising distant tissues have acquired the traits that enable emergence from each preceding stage of metastasis.

Although an exact definition of the metastasis-initiating phenotype has remained largely elusive, characteristic properties that recurrently emerge are that of multi-drug resistance, high metastatic and invasive capability, dormancy competence and features of stem cells, including; self-renewal, serial passaging ability, enhanced DNA repair, impaired apoptosis, a long doubling time, asymmetric division and cycling quiescence (Ginestier *et al.*, 2007; Singh and Settleman, 2010; Patel *et al.*, 2012; Kreso *et al.*, 2013). Cancer stem cell populations have primarily been defined by their increased functional capacity for tumour initiation and ability to subsequently recapitulate tumoural heterogeneity (Luo *et al.*, 2015). In breast cancer, a number of marker signatures have been used to identify cell populations possessing such enhanced tumourigenicity (summarised in **Table 1.1.**).

The most prolific marker signature used to identify prospective breast cancer stem cells is the $CD44^+CD24^{-/low}$ phenotype. Al-Hajj *et al.* (2003) first demonstrated that breast cancer cells possessing the $CD44^+CD24^{-/low}$ signature were significantly more tumorigenic than the corresponding $CD44^+CD24^+$ population when implanted into the mammary fat pads of the immunodeficient mice. While the prognostic significance of the $CD44^+CD24^{-/low}$ phenotype remains uncertain, the $CD44^+CD24^{-/low}$ phenotype has been shown to correlate with enhanced invasive and metastatic capability (Abraham *et al.*, 2005; Sheridan *et al.*, 2006). It has been suggested that this could be linked to the role of CD44 as the primary receptor for hyaluronan, a major component of the extracellular matrix (Orian-Rousseau, 2015). However, the diverse and complex biological functions of both CD44 and CD24 have made their exact roles in relation to the functional properties of the putative breast CSC population difficult to delineate and these still remain unclear (Jaggupilli and Elkord, 2012). Other less common markers that have been associated with enhanced tumourigenicity and have therefore been used to identify putative breast CSC populations include the cell surface glycoprotein CD133 (also called prominin-1) or the $CD29^+CD49f^+$ phenotype (expression of α6β1 integrin), although the functionality of these markers in relation to stemness, like CD44 and CD24, also remain to be elucidated.

Due to a number of progenitor functions being conserved in CSCs across multiple disease types, functional markers of stemness such as aldehyde dehydrogenase (ALDH) are also widely used to demark CSC populations. ALDH is a detoxifying enzyme responsible for the oxidation of retinol to retinoic acid, an essential process in the early differentiation of stem cells (Chute *et al.*, 2006). Enhanced ALDH activity has been observed in both normal and malignant breast stem cell, and can serve as an independent indicator for poor clinical outcome (Ginestier *et al.*, 2007). Interestingly, relatively recent studies have demonstrated that $CD44^+CD24^{-/low}$ and $ALDH^+$ phenotypes are differentially expressed depending on the sub-type of breast cancer involved; the $CD44^+CD24^{-/low}$ phenotype is more commonly associated with basal-like breast cancers, while $ALDH^+$ cells are more common in HER2-enriched and basal sub-types (Ricardo *et al.*, 2011). The specific biological mechanisms that underpin the different expression of CD44, CD24 and ALDH in breast cancer have yet to be identified.

Although the specific functionality of many of the breast CSC markers remains unclear, the correlation between their expression and the invasive properties and metastatic potential of tumours is generally well accepted. For example, DTCs expressing $CD44^+CD24^{-/low}$ and $ALDH^+$ have been detected within the axillary lymph node metastases of breast cancer patients (Wei *et al.*, 2012; Nogami *et al.*, 2014). Given that CSCs are supposed to transit through the bloodstream from the primary tumour to secondary sites, one might also expect that stem marker expression would also be highly conserved within both CTCs and DTCs. Evidence to support this hypothesis has recently been reported in a number of studies that show the expression of stem cell marker by cancer cells isolated from the peripheral blood and the bone marrow of breast cancer patients (Balic *et al.*, 2006; Theodoropoulos *et al.*, 2010; Giordano *et al.*, 2013). However, whether stem cell marker expression is stable during systemic dissemination or how their expression changes throughout the metastatic cascade is still unknown.

Table 1.1. Marker Profiles Routinely Used to Identify Breast Cancer Stem Cells

Marker Profile	Clinical-Pathological Features	Clinical Observations	References
CD44^{+} CD24[-/Low]	Enriched in claudin-low and basal sub-types Associated with BRCA1 mutational status Poor prognosis	Tumour recurrence Resistance to radiotherapy and standard chemotherapy High metastatic propensity	(Abraham *et al.*, 2005) (Li *et al.*, 2008) (Lagadec *et al.*, 2010) (Bernardi *et al.*, 2012) (Bane *et al.*, 2013)
ALDH1[+]	Associated with ER negativity, HER2 amplification and basal-like sub-type Poor prognosis	Tumour recurrence Enhanced capacity for metastatic behaviour Resistance to standard chemotherapy	(Ginestier *et al.*, 2007) (Morimoto *et al.*, 2009) (Tanei *et al.*, 2009) (Park *et al.*, 2010)
CD44^{+} ALDH1[+/High]	Enriched in high-grade DCIS Indicative of high risk patients	Predicts distant metastasis and overall survival Resistance to standard chemotherapy High metastatic propensity	(Croker and Allan, 2012) (Da Cruz *et al.*, 2014) (Da Cruz *et al.*, 2016)
CD133^{+}	Enriched in IBC Highly enriched in TNBC	Tumour recurrence Resistance to standard chemotherapy	(Meyer *et al.*, 2010) (Aomatsu *et al.*, 2012) (Liu *et al.*, 2013)
CD29^{+} CD49f^{+}	CD29 is associate with shorter disease-free survival and overall survival CD49f is a prognostic indicator and is associated with poorer clinical outcome	Tumour relapse High metastatic propensity Resistance to radiotherapy and standard chemotherapy	(Narita *et al.*, 1998) (Lim *et al.*, 2009) (Ahmed *et al.*, 2013) (Ye *et al.*, 2015)

ALDH1: aldehyde dehydrogenase 1; **BRCA1**: breast cancer 1; **CD24**: signal transducer CD24; **CD29**: integrin β1; **CD44**: hyaluronan receptor; **CD49f**: integrin α6; **DCIS**: ductal carcinoma *in situ*; **ER**: oestrogen receptor; **HER2**: human epidermal growth factor receptor type-2; **IBC**: invasive breast cancer; **TNBC**: triple-negative breast cancer.

1.5. Epithelial-to-Mesenchymal Transition and Metastasis

Pathological exploitation of the developmental EMT programme in cancer has been centrally implicated in cellular de-differentiation and acquisition of both stem cell traits and invasive capability (**Figure 1.4.**). Enhanced expression of EMT-promoting transcriptional factors Snail, Slug and Twist in breast carcinoma have been shown to induce the so-called "cadherin switch" which involves concomitant loss of tumour-suppressing junctional protein E-cadherin and up-regulation of the transendothelial migration-enabling N-cadherin, resulting in increased invasive capability (Bolos *et al.*, 2003; Yang *et al.*, 2004; Moody *et al.*, 2005; Thiery *et al.*, 2009). In addition, the E-cadherin-suppressing ZEB1 transcription factor also promotes tumour cell de-differentiation by repressing the ability of a myriad of master regulators of epithelial polarity and intercellular adhesion to inhibit the development of stemness and induce epithelial differentiation (Aigner *et al.*, 2007; Shimono *et al.*, 2009; Wellner *et al.*, 2009; Korpal *et al.*, 2011). These studies collectively demonstrate that EMT is central to the shedding of epithelial attributes and acquisition of a stem cell-like phenotype that in-turn facilitates enhanced invasive and metastatic behaviours. Interestingly, the $CD44^+CD24^{-/low}$ and $ALDH^+$ marker profiles associated with putative stem cells in breast cancer have been shown to identify spatiotemporally distinct but dynamically transitioning populations with respect to genetic signatures associated with EMT across different breast cancer sub-types (Liu *et al.*, 2014). Relatively recently, Ombrato and Malanchi (2014) proposed the "EMT-gradient model" to explain how the transient nature of the EMT process might regulate stemness and epithelial-mesenchymal phenotypes during metastasis. According to this model, the activation of the EMT program presents different threshold levels at which EMT and stemness are coupled and is instructed by microenvironmental signals; cellular phenotypes therefore exist somewhere along a spectrum, becoming more mesenchymal during invasion and more epithelial and progressively more stem-like during later stages of metastatic colonisation (**Figure 1.5.**). One notable consequence of this EMT gradient state is the differential expression of stem cell and EMT markers by the CSC population depending on their epithelial-mesenchymal phenotypic status, as exemplified by the findings of Liu *et al.* (2014).
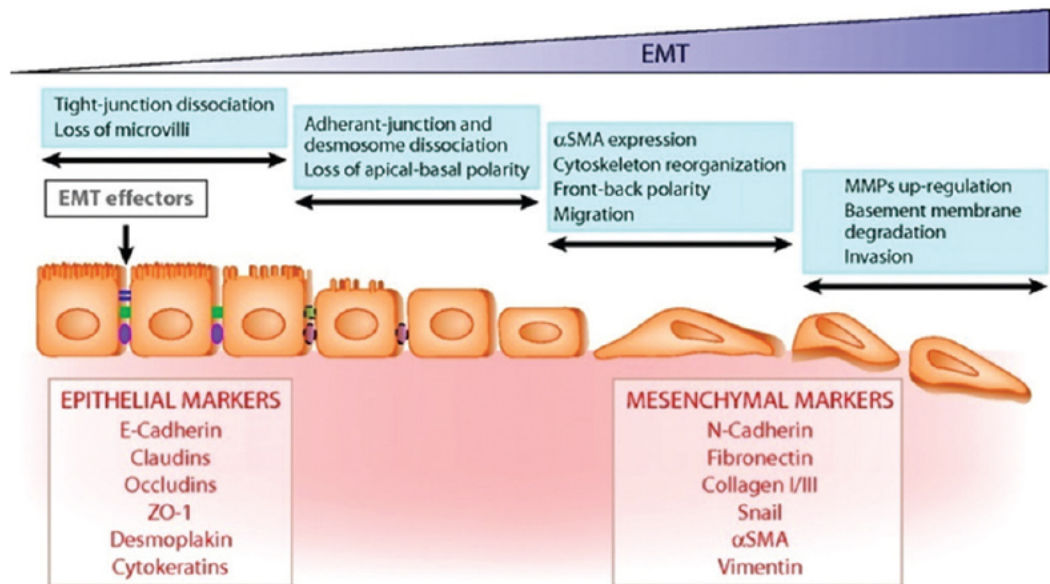
Figure 1.4. Epithelial-to-Mesenchymal Transition

During the epithelial-to-mesenchymal transition, epithelial traits and intracellular junctional complex proteins are down regulated while mesenchymal markers are increasingly expressed. These changes are accompanied by loss of apical-basal polarity and a change to lateral polarisation that aids invasive and migratory behaviour. Image reprinted from Angadi, P. & Kale, A. (2015). Epithelial-mesenchymal transition - A fundamental mechanism in cancer progression: An overview. *Indian Journal of Health Sciences and Biomedical Research (KLEU)*, 8, 77-84, with permission from Wolters Kluwer Medknow Publications.
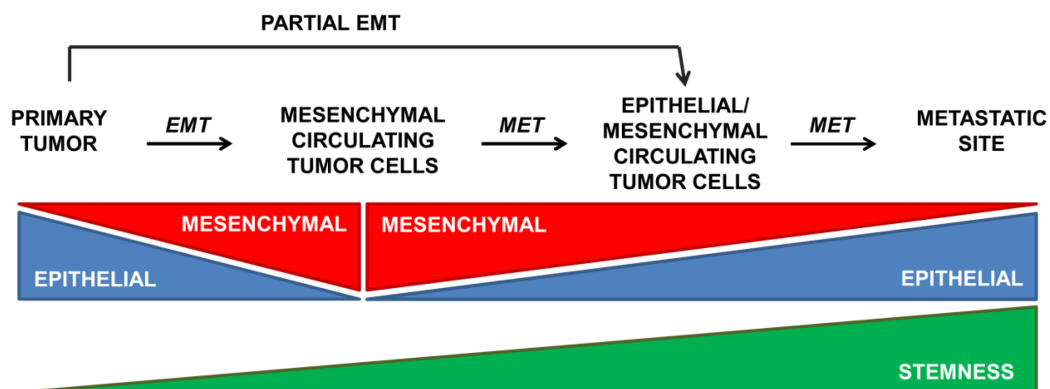
Figure 1.5. The EMT-Gradient Model of Stemness and Phenotypic Plasticity

The activation of the epithelial-to-mesenchymal transition (EMT) program during the metastatic cascade presents different threshold levels at which EMT and stemness are coupled. Cellular phenotypes therefore exist somewhere along a spectrum that is instructed by microenvironmental signals; cells gain plasticity and become more mesenchymal following initial activation of EMT during invasion, but subsequently become more epithelial and progressively more stem-like during later stages of metastatic colonisation following phenotypic reversion through mesenchymal-to-epithelial transition (MET). Image reprinted from Fabregat, I., Malfettone, A. & Soukupova, J. (2016). New Insights into the Crossroads between EMT and Stemness in the Context of Cancer. *J Clin Med*, 5, with permission from Multidisciplinary Digital Publishing Institute (MDPI).

1.6. Quiescence and the Metastasis-Initiating Cell Population

Metastatic dormancy, a period of latency between systemic dissemination and metastatic outgrowth, is a well-established concept in a number of cancer types. In breast cancer in particular, the detection of overt metastasis has been reported up to several decades post-surgery (Gomis and Gawrzak, 2016). From a cellular perspective, this asymptomatic period that precedes relapse or recurrence can be explained by either cellular mitotic quiescence, in which cells exist in a state of reversible growth-arrest, or micrometastatic dormancy, in which sub-clinical metastatic foci are unable to progress to overt disease due to insufficient vascularisation and a rate of cell death that compensates for the rate of proliferation (Aguirre-Ghiso, 2007). While these situations are likely non-mutually exclusive, the former is best supported by clinical evidence; the tumour cells isolated from bone marrow aspirates taken from patients with various bone-tropic cancers have been found to be growth arrested, and their number have been shown to directly correlate with reduced disease-free survival (Pantel *et al.*, 2008; Hartkopf *et al.*, 2014; Hartkopf *et al.*, 2015). Indeed, cellular mitotic quiescence is now recognised as a phenomenon that is integral to the pathogenesis of metastatic disease, enforced by the increasing ubiquitous association of quiescence and both *de novo* drug resistance and stemness in both normal and neoplastic cell populations (Moore and Lyle, 2011). Consequently, a number of mechanisms leading to cellular quiescence have now been described.

The balance between activated extracellular regulated kinase (ERK) and activated p38 α/β was one of the earliest quiescence inductive mechanisms elucidated. Early studies in a transgenic mouse model of breast cancer undertaken by White *et al.* (2004) reported that the loss of β1-integrin from tumour cells was linked with resistance to apoptotic cell death and entry into a growth-arrested quiescent state. Around this time, studies undertaken in human epidermoid carcinoma models *in vitro* and *in vivo* demonstrated that the induction of growth arrest followed abolition of fibronectin-dependent proliferative signalling via the FAK-Ras-ERK pathway in response to reduced urokinase receptor (uPAR)-mediated α5β1-integrin activation (Aguirre Ghiso *et al.*, 1999; Aguirre Ghiso, 2002; Liu *et al.*, 2002). In all of these studies, disruption of β1-integrin function was seen to occur in conjunction with the sustained over-activation

of the p38 mitogen-activated protein kinase (MAPK) pathway. Subsequent investigations have since demonstrated that deactivated ERK signalling in conjunction with high p38 activity can initiate the unfolded protein response pathway, promoting a protracted state of cellular quiescence through ATF6 and Rheb-mediated mTOR signalling and subsequent induction of quiescence-associated transcription factors BHLHE41 (DEC2 or Sharp1) and NR2F1, and cyclin-dependent kinase (CDK) inhibitors p21 and p27 (Schewe and Aguirre-Ghiso, 2008; Bragado *et al.*, 2013; Sosa *et al.*, 2015).

Just as the roles of uPAR- and integrin-mediated signalling identified an early link between mitotic quiescence and the cellular microenvironment, a recently published study by Fluegen *et al.* (2017) has linked the induction of quiescence-associated genes within primary tumour microenvironments to a predisposition to entry into a dormancy program at post-metastatic sites. In this study, hypoxic primary breast or head and neck squamous cell carcinoma (HNSCC) tumour microenvironments displayed up-regulation of quiescence- and hypoxia-associated genes (NR2F1/DEC2/p27 and HIF-1α/GLUT1, respectively). Tracking of individual DTCs revealed that those originating from a hypoxic microenvironment were frequently quiescent and displayed a $DEC2^{hi}p27^{hi}NR2F1^{hi}TGF-\beta2^{hi}$ signature. These post-hypoxic DTCs were shown to evade chemotherapy and were prone to enter into a state of dormancy at secondary sites. Interestingly, while p27 induction was shown to be dependent on at least HIF-1α and NR2F1 at primary sites, post-hypoxic DTCs did not appear to maintain a hypoxic gene signature, being negative for GLUT1 expression. These findings suggest that the primary tumour plays a key role in generation of quiescent, chemoresistant and metastasis-competent cells but that the post-metastatic microenvironment plays a critical role in regulating the switch between DTC dormancy and proliferation.

1.7.   The Bone Microenvironment and Post-Metastatic Regulation of Dormancy

A myriad of studies have provided evidence supporting disseminated tumour cells being maintained in a state of mitotic arrest following infiltration of a target organ (reviewed extensively by Sosa *et al.*, 2014). The collective findings of these studies indicate that the mitotically dormant state is largely the result of growth-restrictive microenvironmental conditions or deprivation of pro-proliferative signalling interactions within the post-metastatic niche. Consequently, cellular dormancy in metastasis can be seen as the result of a maladaptation that can potentially resolve following acquisition of traits that facilitate cell growth within a specific tissue microenvironment. Given that mitotic quiescence is not conducive to acquisition of genetic alterations due to a vastly decreased probability of mutational events, even in genetically unstable tumour cells, it is more likely that adaptations that favour survival and eventual outgrowth are driven by reciprocal interactions with the tissue microenvironment, reconfiguration of metastable intracellular signalling networks or modulated epigenetic states (Michor *et al.*, 2004). Gaining further insight into the quiescent cell phenotype and how signals encoded within the post-metastatic niche microenvironment modulate the signalling pathways that regulate this state to maintain long-term dormancy will be critical to identifying novel therapeutic targets for prevention of metastatic disease.

The bone marrow is characterised by high cellular heterogeneity, being composed of cells of haematopoietic origin (osteoclasts, macrophages and lymphocytes), mesenchymal origin (osteoblasts and adipocytes), neurones and endothelial cells (Shiozawa *et al.*, 2015). These cell populations compose the niche microenvironments in which haematopoietic stem cells (HSCs) and mesenchymal stem cells (MSCs) reside (reviewed by Ren *et al.*, 2015). A multitude of studies have showed that DTCs from bone-tropic cancers appropriate these microenvironments and that these either expedite or impede metastatic progression. The following sections outline established mechanisms by which the post-metastatic niche in bone can regulate DTC dormancy in bone-tropic cancers; these are summarised in **Table 1.2.** and discussed in more detail thereafter.

Table 1.2. Molecular Mechanisms Implicated in Tumour Cell Dormancy in Bone

Molecule / Pathway	Cancer Type	Implication	References
GAS6 - AXL	Prostate	High AXL:TYRO3 expression ratio on DTCs induced by osteoblastic annexin-II leads to over-stimulation by GAS6 and dormancy	(Shiozawa *et al.*, 2010) (Mishra *et al.*, 2012) (Taichman *et al.*, 2013)
TBK1	Prostate	Bone stroma induces an overexpression of TBK1 by DTCs which induces dormancy by modulating mTOR activity	(Kim *et al.*, 2013)
BMP7 - BMPR2	Prostate	Bone stroma-derived BMP7 acts on BMPR2 on DTCs to induce high p38:ERK ratio leading to dormancy	(Kobayashi *et al.*, 2011)
TGF-β2 - TGF-βRI	Breast	Bone stroma-derived TGF-β2 signalling via TGF-βRI on DTCs induces high p38:ERK ratio leading to dormancy	(Bragado *et al.*, 2013) (Marlow *et al.*, 2013)
NK1R-Tr : NK1R-FL	Breast	Bone stroma-derived CXCL12 induces reduction of NK1R-Tr expression by DTCs allowing over activation of NK1R-FL by tachykinins leading to dormancy	(Zhou *et al.*, 2014)
bFGF	Breast	Bone marrow-derived bFGF causes expression of α5β1 integrin allowing ligation by fibronectin and signalling via PI3K to induce dormancy	(Korah *et al.*, 2004) (Barrios and Wieder, 2009)
TSP-1	Breast	TSP-1 expressed on mature bone vascular endothelium induces DTC dormancy	(Ghajar *et al.*, 2013)
miRNAs via GJIC	Breast	Multiple bone-derived miRNAs act on DTCs via GJIC induced between bone stromal cells and DTCs by the paracrine action of CXCL12	(Lim *et al.*, 2011) (Ono *et al.*, 2014)

GAS6: growth arrest-specific 6; **AXL**: AXL receptor tyrosine kinase; **TYRO3**: tyrosine-protein kinase receptor TYRO3; **DTCs**: disseminated tumour cells; **TBK1**: TANK-binding kinase-1; **mTOR**: mammalian target of rapamycin; **BMP7**: bone morphogenetic protein-7; **BMPR2**: bone morphogenetic protein receptor type-2; **ERK**: extracellular signal-regulated kinase; **TGF-β2**: transforming growth factor-β2; **TGF-βRI**: transforming growth factor- β receptor type-1; **NK1R-Tr**: truncated neurokinin-1 receptor; **NK1R-FL**: full-length neurokinin-1 receptor; **CXCL12**: CXC motif chemokine-12; **bFGF**: basic fibroblast growth factor; **PI3K**: phosphoinositide 3-kinase; **TSP-1**: thrombospondin-1; **miRNA**: microRNA; **GJIC**: gap junctional intercellular communication.

GAS6 Receptor Signalling

Studies undertaken *in vivo* have demonstrated that disseminated prostate cancer cells (PCCs) preferentially migrate to osteoblast-rich regions of bone and are shown to directly compete for occupancy of the HSC niche (Shiozawa *et al.*, 2011; Wang *et al.*, 2014). Molecular pathways which are known to be critical to HSC niche selection, such as the annexin-II and chemokine receptor-4 (CXCR4)/chemokine ligand-12 (CXCL12) axes, have been centrally implicated in this process (Shiozawa *et al.*, 2008; Wang *et al.*, 2014). Exploration of the role of osteoblastic annexin-II in directing interactions between disseminated PCCs and the HSC niche showed that it significantly enhanced expression of the AXL sub-family of receptor-tyrosine kinases by PCCs (Shiozawa *et al.*, 2010). This group of receptors, which includes AXL, TYRO3 and MER, selectively bind the stromal-derived growth arrest-specific 6 (GAS6) growth factor (Hafizi and Dahlback, 2006). Enhanced expression of AXL receptors and consequent ligation by GAS6, mediated by annexin-II, was shown to increase survival, confer resistance to chemotherapy and reduce the mitotic activity of PCCs by inducing G_0 arrest (Shiozawa *et al.*, 2010).

In PC-3 and DU-145 prostate cancer subcutaneous xenograft models, DTCs isolated from bone marrow demonstrated markedly reduced proliferative activity during fluorescence-activated cell sorting (FACS) analysis of Ki67 when compared with cells of the primary tumour (Taichman *et al.*, 2013). Primary tumour cells possessed a significantly reduced AXL:TYRO3 expression ratio compared to cells grown *in vitro*, whereas DTCs isolated from tumour-free marrow showed increased expression of AXL and down-regulated TYRO3 compared with cells taken from both primary tumours and from secondary metastatic foci. Evidence from a study undertaken by Mishra *et al.* (2012) indicates that such alterations in receptor sub-type profiles might be partially dependent on stabilisation of AXL expression regulated by hypoxia-inducible factor-1-alpha (HIF-1α). Irrespective of the mechanism, the observations made by Taichman *et al.* (2013) appear to demonstrate that differential expression of AXL receptor sub-types is a key determinant of the tightly controlled switch between proliferative and dormant phenotypes in prostate cancer bone metastasis. More specifically, a low AXL:TYRO3 ratio appears to favour cellular proliferation while a high AXL:TYRO3 ratio is

suggested to be conducive to a state of dormancy. Such induction of a dormancy-permissive phenotype during niche selection closely resembles the situation that is seen during HSC occupancy of osteoblastic niche within the bone marrow (Crosier *et al.*, 1996; Darby *et al.*, 2000). Hence, it may be that other microenvironmental mechanisms known to instruct HSC function are also responsible for regulation of dormancy in DTCs resident within the bone marrow.

TBK1 Expression

Evidence reported in a study by Kim *et al.* (2013) indicates that cell-niche interactions that regulate prostate cancer cell dormancy within the bone microenvironment may be mediated by modulation of mTOR signalling. Kim *et al.* (2013) found that binding of PCCs to bone marrow stromal cells (ST2 lineage) during *in vitro* co-culture markedly increased the number of cells in proliferative arrest. This sub-population of cells, isolated based on Ki67 expression by FACS, were also noted as having significant chemoresistance to the anti-mitotic agent docetaxel. In both PC-3 and C4-2B prostate cancer cell lineages, real-time quantitative polymerase chain reaction (qPCR) analyses revealed hyper-expression of the serine/threonine-protein kinase TBK1 (TANK-binding kinase-1) in response to ST2-cell binding interactions.

TBK1 has been implicated in mediating a number of functions that facilitate both malignant transformation and cell survival in cancer (Chien *et al.*, 2006; Shen and Hahn, 2011; Baldwin, 2012). In the study undertaken by Kim *et al.* (2013), immunofluorescent staining of PCCs taken from their *in vitro* co-culture model revealed co-localisation of TBK1 with mTOR around the nuclear periphery. Rapamycin-induced inhibition of mTOR increased the proportion of dormant PCCs (Ki67$^-$) and enhanced resistance to an array of conventional chemotherapeutic agents in both PC-3 and C4-2B cell lines. Lentiviral shRNA knockdown of TBK1 resulted in a significant increase in mTOR activity and loss of chemoresistance. In addition, in stem cell-like (CD133$^+$CD44$^+$) sub-populations of PC-3 and C4-2B cells isolated from mouse bone marrow, TBK1 levels were significantly increased. *In vitro*, shRNA-induced loss of TBK1 not only caused enhanced mTOR activation but also was associated with a marked decrease in the CD133$^+$CD44$^+$ cell population. This effect was significantly reduced in

the presence of rapamycin. When taken together, these studies demonstrate that an inverse regulatory relationship exists between TBK1 and mTOR, and it appears that PCC-stromal interactions that increase TBK1-induced inhibition of mTOR are seemingly important in the formation of stem cell-like sub-populations, maintenance of dormancy, and chemoresistance in prostate cancer. However, the mechanisms by which PCC-niche interactions induce enhanced TBK1 expression, and by which TBK1-mediated inhibition of mTOR leads to the observed chemoresistance and proliferative arrest, remain to be elucidated. An earlier study in ovarian tumours undertaken by Lu *et al.* (2008) showed that dormancy was mediated by autophagic induction due to enhanced expression of aplysia ras homology member-I (AHRI) and resultant inhibition of the PI3K-PKB-mTOR pathway. The dramatic reduction in tumour regrowth in the presence of doxorubicin following chloroquine-induced inhibition of autophagy also indicated that autophagy is likely to be an important survival mechanism enabling dormant tumour cells to survive chemotherapy. In light of this, it is possible that TBK1-induced mTOR inhibition results in autophagy, and that this is responsible for the dormancy and enhanced chemoresistance in prostate cancer cells reported by Kim *et al.* (2013).

BMPR2 Signalling

While attempting to further elucidate bone stroma-derived secretory factors that may have modulatory effects on DTC dormancy in bone, Kobayashi *et al.* (2011) noted that the conditioned medium from normal bone marrow stromal cells (HS5 lineage) was able to significantly reduce prostate cancer cell proliferation but did not elicit any cytotoxic effects. On further investigation, reduced proliferative activity appeared to strongly correlate with markedly enhanced p38-MAPK signalling, loss of ERK signalling, and simultaneous induction of the N-myc downstream-regulated gene-1 (NDRG1) metastasis suppressor protein, and the CDK inhibitors p21 and p27. Addition of small molecule inhibitors that block the action of secretory factors produced by bone stromal cells showed that inhibition of bone morphogenetic protein (BMP) signalling re-establish the dormancy-associated signalling profile observed in the presence of HS5 conditioned medium. Analysis of the effects of purified BMPs *in vitro* identified only BMP7 as being able to activate p38, NDRG1, p21 and p27, and diminish ERK

signalling, eliciting a state of dormancy. This dormant state was reversed following removal of BMP7 or knockdown of its receptor, bone morphogenetic protein receptor type-II (BMPR2).

The increased expression of NDRG1, an apparent effector in BMP7-mediated dormancy, has previously been shown to inversely correlate with occurrence of bone metastasis in prostate cancer patients (Bandyopadhyay *et al.*, 2003). NDRG1 activity has also been associated with suppression of metastatic activity in cancers of the breast and colon (Guan *et al.*, 2000; Bandyopadhyay *et al.*, 2004). NDRG1 apparently achieves these effects via disruptive interactions with low-density lipoprotein receptor-related protein 6 (LRP6), the specific receptor of the Wnt ligand (Liu *et al.*, 2012). When taken together, these studies suggest that the BMP7-BMPR2-NDRG1 axis plays a pivotal role in maintaining a state of cellular dormancy that is likely to contribute to the suppression of metastasis in prostate cancer, and probably other cancer types, and that loss of BMPR2 signal transduction may precede metastatic progression.

TGF-β2 Signalling

Transforming growth factor-beta-2 (TGF-β2) is a cytokine known to be present within the bone marrow where it has been shown to regulate haematopoietic progenitor cell development (Henckaerts *et al.*, 2004). Relatively recently, Bragado *et al.* (2013) demonstrated that TGF-β2 signals present in the bone marrow are able to maintain HNSCC DTCs in a dormant state. In this study, GFP-tagged dormant HEp-3 cells isolated from the bone marrow of mice showed a prolonged 87% reduction in proliferative capacity compared to dormant cells isolated from lung. The bone marrow microenvironment thus appeared to specifically instruct activation of persistent dormancy-inductive signalling programmes within DTCs. Expression profile analyses revealed up-regulation of TGF-β2 in dormant cells from bone at greater than five-times the level present in either the parental cell line or DTCs isolated from the lungs. TGF-β2 levels were also significantly elevated in bone marrow compared to lung tissue and the basal culture medium used *in vitro*.

Within dormant DTCs, p38α/β was strongly activated while ERK signalling was diminished. The resultant high p38:ERK signalling ratio led to induction of metastatic suppressor proteins BHLHE41 and p27, and subsequent repression of CDK4, leading to a state of cellular dormancy. This dormancy-instructive phenotype was specifically restored in the presence of the β2-isoform of TGF only. However, TGF-β2-mediated dormancy was critically dependent on the co-expression of TGF-β-receptor-I (TGFβRI) and TGF-β-receptor-III (TGFβRIII) for the down-stream activation of SMAD1 or SMAD5 that is necessary for subsequent induction of p27 and mitotic arrest. Inhibition of TGFβRI or p38α/β favoured escape from dormancy and increased overall metastatic burden (Bragado *et al.*, 2013). Similar findings were reported by Marlow *et al.* (2013) following TGFβRI or p38-MAPK inhibition in growth-arrested breast cancer cell lines (MCF-7 and SUM159) generated within a 3D *in vitro* model of the dormancy-permissive bone marrow niche. This finding, therefore, strongly suggests that TGF-β2-mediated mechanisms elucidated by Bragado *et al.* (2013) may be of equal importance to dormancy in breast cancer following metastasis to bone.

NK1R-Tr Status

Tachykinin family proteins are produced by alternate exon splicing of the *Tac1* gene followed by post-translational modification, and are constitutively expressed by breast cancer and bone marrow stromal cells (Rameshwar *et al.*, 1997; Singh *et al.*, 2000). These molecules exert their biological effects through ligation of three different G protein-coupled transmembrane receptors; NK1R, NK2R and NK3R (Singh *et al.*, 2000). In both primary and metastatic breast cancer, interaction of tachykinins with the truncated variant of NK1R (NK1R-Tr) expressed by malignant cells has been shown to promote mitogenesis. In addition, reduced expression of the full-length NK1R variant (NK1R-FL) and overexpression of NK1R-Tr has been associated with a propensity for malignant transformation, as well as an enhanced capacity for invasiveness and metastatic activity (Singh *et al.*, 2000; Zhou *et al.*, 2013). In a recent study conducted by Zhou *et al.* (2014), knockdown of NK1R-Tr using shRNA in the MDA-MB-231 cell line resulted in a markedly reduced growth rate compared to cells of the parental lineage. Co-culture of MDA-MB-231 cells with bone marrow-derived human mesenchymal stem cells (BM-HMSCs) resulted in reduced NK1R-Tr expression and concomitant cell-

cycle arrest. This observation was linked to markedly increased levels of CXCL12 in the conditioned medium taken from the co-culture system which were not present in that harvested from MDA-MB-231 cells grown alone. When taken together, these results imply that reversion to a low NK1R-Tr phenotype in metastatic breast cancer is involved in regulation of DTC dormancy in bone, and that BM-HMSC-derived CXCL12 instructing reduced NK1R-Tr expression by breast tumour cells might mediate this process. However, both a detailed mechanism and evidence for the relevance of this purported dormancy mechanism to breast cancer bone metastasis *in vivo* remain to be established.

bFGF Signalling

In contrast to their suggested roles in induction of breast cancer cell dormancy, α5β1 integrin expression and re-acquisition of an activated PI3K-PKB signalling axis have been previously implicated in maintenance of breast cancer dormancy in the bone marrow. Basic fibroblast growth factor (bFGF) is a well-known mammary differentiation factor that is present in the bone marrow and is capable of modulating integrin expression. Korah *et al.* (2004) first reported that bFGF was able to induce the reversible up-regulation of α5β1 integrin lost during malignant transformation. Reconstitution of α5β1 integrin in this investigation was associated with fibronectin-ligation-dependent survival through inhibition of apoptosis that appeared to be mediated by enhanced PI3K-PKB signalling. In a subsequent investigation by Barrios and Wieder (2009), PI3K pathway activation was shown to occur in a bFGF-dependent manner, independent of α5β1 activation. In this case, the mitotic arrest necessary for maintained cellular dormancy was shown to occur through the stabilisation of cortical F-actin fibres following inactivation of RhoA. This loss of RhoA activity was preceded by PI3K-dependent activation of GTPase regulator associated with focal adhesion kinase (GRAF), a RhoA GTPase-activating protein-like complex, and the subsequent α5β1 integrin-dependent recruitment of FAK. Hence, dormancy of disseminated breast cancer cells within fibronectin-rich compartments of the bone marrow may be initiated and maintained, at least in part, through simultaneous bFGF-dependent signalling via α5β1 and PI3K.

Thrombospondin-1

The multi-functional endothelium-derived matrix glycoprotein thrombospondin-1 (TSP-1) has previously been implicated in regulating both micrometastatic and cellular dormancy, suggested to occur through negative regulation of angiogenesis (Weinstat-Saslow *et al.*, 1994; Almog *et al.*, 2009). Relatively recently, Ghajar *et al.* (2013) showed that TSP-1 surrounding the mature vascular endothelium acts as an angiocrine tumour suppressor that is able to maintain breast tumour cells (HMT-3522 T4-2, MCF-7 and MDA-MB-231 lineages) in a protracted dormant state within the murine bone marrow *in vivo*. This finding was confirmed using an organotypic model of the human bone microvascular niche *in vitro*. In a similar model of the developing vasculature, where TSP-1 expression was significantly diminished, the dormant cellular phenotype was not recapitulated. This study supports the hypothesis that endothelial cells and secretory factors deposited within their surrounding basal lamina comprise, at least in part, a dormancy-permissive perivascular niche. It also appears to demonstrate vascular regulation of tumour cell behaviour, a drastic shift from the long-established existing paradigm, and also suggests the potential existence of other, as yet uncharacterised, vascular regulators of cellular dormancy. In addition, while the anti-angiogenic activity and effects of TSP-1 on endothelial cells are well characterised (reviewed by Lawler and Lawler, 2012), the molecular mechanism by which it is apparently able to regulate cellular dormancy remains to be elucidated.

Gap Junctional Intercellular Communication and microRNAs

Park *et al.* (2013) reported that low levels of CXCL12 were able to enhance gap junctional intercellular communication (GJIC) between confluent breast cancer cells (MDA-MB-231) by increasing the translation and protein kinase-C-mediated activation of the connexin protein Cx43. In a previous study, gap junctional transmission of dormancy-inducing microRNA (miRNA) molecules miR-127, -197, -222, and -223 from primary bone marrow-derived stromal cells to cells of the MDA-MB-231 and T47D breast cancer lineages was linked to induction of dormancy during co-culture (Lim *et al.*, 2011). Transmission of these miRNAs resulted in a marked decrease in cyclins D1, D3, C and CDK4, and a concomitant increase in p21, leading to proliferative arrest in

the G_0 phase of the cell cycle. Lim *et al.* (2011) also noted that miRNA transfer via stromal-derived exosomes was linked to tumour cell dormancy, although to a lesser degree than that occurring via GJIC. However, the exosomal transfer of miRNA leading to dormancy is concurrent with a more recent investigation undertaken by Ono *et al.* (2014), in which bone marrow-metastatic MDA-MB-231 variant cells underwent growth arrest in co-culture with BM-HMSCs, in the presence of conditioned medium from BM-HMSCs, or following uptake of exosomes derived from the BM-HMSC cells. Amongst 44 miRNAs that were found to be present in BM-HSMC-derived exosomes at an elevated level, miR-23b was identified as being able to reconstitute the dormant phenotype observed in earlier experiments. Analysis of several putative target genes identified the *MARCKS* gene as the target of miR-23b action. Examination of patient bone marrow aspirates demonstrated the coexistence of BM-HMSCs amongst disseminated breast tumour cells, and that these DTCs had elevated levels of miR-23b and diminished *MARCKS* expression compared to primary breast tumour tissue. The combined findings of these studies not only identify two means by which bone marrow-derived miRNAs reach DTCs resident within the bone microenvironment, but also demonstrate that these miRNAs appear to play a role in the promotion of DTC dormancy within the metastatic niche. This finding also suggests that there are potentially several other miRNAs that might play important roles in the induction and maintenance of DTC dormancy following metastasis to bone.

1.8. The Challenge of Targeting Mitotically Inactive Cell Populations

The fact that quiescent or dormant cells are, by their very nature, mitotically inactive confers an inherent resistance to chemotherapy because the majority of chemotherapeutic agents are reliant on active cell division for their efficacy. This challenge is further confounded by a number of other drug-resistance mechanisms that have been shown to be enriched within quiescent cell populations (reviewed by Cree and Charlton, 2017). Such resistance to chemotherapy enables dormant DTCs to evade drug-induced cell death and therefore to persist at post-metastatic sites until they commence overt outgrowth. In a relatively recent position paper, Weber (2013) described two potential alternative strategies for effective treatment of metastatic disease: either prevent dissemination of cancer cells by developing drugs that would be administered in the neoadjuvant setting to remove this population, or to target pre-existing metastatic tumours. Unfortunately, both of these suggestions are likely to be of limited utility. Firstly, dissemination has been shown to be an early event in disease pathogenesis and likely occurs before the initial diagnosis (Klein, 2003; Husemann *et al.*, 2008; Hosseini *et al.*, 2016); being able to prevent dissemination therefore seems implausible. Secondly, overtly growing secondary lesions are composed of millions of tumour cells. Given that intratumoural heterogeneity has been one of the major barriers to the successful treatment of cancers, targeting a large, growing, heterogeneous post-metastatic cell mass also seems unlikely to yield any potential success. Ironically, targeting the dormant disseminated tumour cell population therefore appears the strategy most likely to offer any significant potential clinical utility. This might be achieved either by the potentially risky strategy of maintaining dormancy indefinitely, either by modulating cell-intrinsic processes or targeting the cellular microenvironment, or by specifically targeting differentially regulated metabolic pathways that enable dormant cell survival, thereby killing dormant cells *in situ* and removing any risk of their eventual overt outgrowth. Unfortunately however, the current lack of mechanistic understanding of tumour cell quiescence and post-metastatic dormancy has severely limited the development of drugs that are able to target this cell population and affect either of these strategies.

1.9. Modelling Tumour Cell Dormancy: Current Models and Future Prospects

One of the predominant challenges in studying tumour cell dormancy is that it remains virtually impossible to isolate DTCs from clinical samples in the earliest stages of metastasis. This is primarily because, by definition, minimal residual disease is not detectable by conventional whole-body imaging, and because the systemic spread of tumour cells to the bone occurs as early as the pre-invasive stages of disease when tumours are either asymptomatic or clinically undetectable (Klein, 2003; Husemann *et al.*, 2008; Hosseini *et al.*, 2016). In addition, the isolation of patient-derived DTCs is technically difficult in itself and the bone marrow biopsy procedure is associated with some risk of procedural complications, meaning that both patients and their clinicians are frequently unwilling to participate in their acquisition (Balic *et al.*, 2005). Given the restrictions surrounding the use of patient-derived DTCs, further advances in the knowledge of tumour cell dormancy in bone is likely to rely predominantly on the continued development and usage of reliable pre-clinical model systems in which the molecular mechanisms that cause cellular dormancy can be successfully unravelled. However, a number of reports by non-clinical researchers have stated that one of primary obstacles in the study of tumour cell dormancy is the lack of model systems (Yumoto *et al.*, 2014; Linde *et al.*, 2016). Although most metastasis research relies on the use of aggressively growing cancer models, in which metastases develop without latency, and often employ unsuitable endpoints, thereby completely missing the opportunity to study solitary DTCs, the notion that there are insufficient models to study dormancy is simply not correct. **Table 1.3.** outlines model systems presently available for the study of cellular dormancy.

Table 1.3. Models Available for Studying Human Tumour Cell Dormancy

Model Type	Cancer Type	Application	References
In vitro 2D culture	Multiple cancer types	Isolation of quiescent cell sub-population	(Dembinski and Krauss, 2009) (Moore *et al.*, 2012) (Yumoto *et al.*, 2014) (Wang *et al.*, 2015a)
In vitro 2D culture	Dormant breast cancer	Role of ECM in dormancy	(Guiro *et al.*, 2015)
In vitro 2D culture	Breast cancer bone metastasis	Role of ECM in dormancy	(Tivari *et al.*, 2015)
In vitro 3D culture	Dormant breast cancer	Role of ECM in dormancy	(Barkan and Green, 2011)
In vitro 3D co-culture	Breast cancer bone metastasis	Role of ECM and stroma in dormancy	(Marlow *et al.*, 2013)
In vitro 3D co-culture	Breast cancer liver metastasis	Role of ECM and stroma in dormancy	(Wheeler *et al.*, 2014)
In vitro 3D co-culture	Ovarian cancer	Role of ECM and stroma in dormancy	(Kenny *et al.*, 2015)
In vitro organotypic co-culture	Pulmonary metastasis (multiple types)	Role of lung microenvironment in dormancy	(Mendoza *et al.*, 2010)
In vitro organotypic co-culture	Breast cancer metastasis	Role of microvascular niche in dormancy	(Ghajar *et al.*, 2013)
In vitro organotypic co-culture	Prostate cancer bone metastasis	Role of microvascular niche in dormancy	(Chong *et al.*, 2014)
In vivo murine xenograft	Breast cancer bone metastasis	Complex model of tumour cell dormancy	(Lu *et al.*, 2011)
In vivo murine xenograft	Breast cancer bone metastasis	Complex model of tumour cell dormancy	(Ottewell *et al.*, 2014a)
In vivo murine xenograft	Prostate cancer bone metastasis	Complex model of tumour cell dormancy	(Ottewell *et al.*, 2014b)
In vivo murine xenograft	Lung cancer metastasis	Complex model of tumour cell dormancy	(Sakamoto *et al.*, 2015)
In vivo murine PDX	HNSCC metastasis	Isolation of DTCs	(Aguirre-Ghiso *et al.*, 2001)
In vivo murine PDX	Breast cancer metastasis	Complex model of tumour cell dormancy	(Marsden *et al.*, 2012)
In vivo murine PDX	Breast cancer metastasis	Isolation of DTCs	(Lawson *et al.*, 2015)

ECM: extracellular matrix; **2D**: two-dimensional; **3D**: three-dimensional; **PDX**: patient-derived xenograft;

HNSCC: head and neck squamous cell carcinoma; **DTCs**: disseminated tumour cells.

One notable feature of the model systems described in **Table 1.3.** is that they primarily focus on the post-metastatic microenvironmental regulation of the dormant state. Indeed, there appears to be a somewhat dogmatic opinion at present that understanding signals encoded by the post-metastatic niche is the most important element in understanding tumour cell dormancy. This is reflected in the sheer volume of research publications available regarding the microenvironment in cancer (Holen, 2016). While this is clearly an essential component of understanding metastatic biology, the conceptual framework on which much of metastasis research is based states that it is the reciprocal crosstalk between seeds (DTCs) <u>and</u> the soil (metastatic niche) that is involved in regulating the dormant state. The benefit of a more holistic approach that incorporates understanding the phenotype of the cells that are able to successfully traverse the entire metastatic cascade, as well as how the underpinning mechanisms regulating this phenotype are modulated by the post-metastatic microenvironment to maintain prolonged dormancy is perhaps most clearly exemplified by the recent work of Fluegen *et al.* (2017). The previous elucidation of a dormancy-associated gene signature by this group allowed a more comprehensive understanding of how the dormant phenotype arises within the pre-metastatic microenvironment and is then modulated in different cancers and molecular sub-types to maintain dormancy at post-metastatic sites. Understanding the intrinsic biology and phenotype of the metastasis-initiating population and developing suitable model systems in which to do so will therefore be equally critical as an understanding of the post-metastatic microenvironment in ultimately unravelling the mechanisms involved in sub-clinical disease and therefore the development of therapies for successfully treating patients diagnosed in the advanced stages of cancer.

1.10. Thesis Aims

The primary aims of the work presented in this thesis were as follows:

1. Develop a robust and reproducible *in vitro* model system enabling the isolation of mitotically quiescent human breast cancer cells.

2. Explore how modulating cellular environmental conditions affects the mitotically quiescent breast cancer cell population.

3. Establish the sensitivity of mitotically quiescent breast cancer cells to anti-cancer agents.

4. Characterise mitotically quiescent breast cancer cells and determine whether they share characteristics with the purported metastasis-initiating breast cancer stem cell population.

Chapter 2

General Materials and Methods

2.1. Cell Lines

A human breast cancer cell line panel was composed for initial investigations designed to determine the presence or absence of mitotically quiescent sub-populations using lipophilic dye retention (**Table 2.1.**). Cell lines were chosen to represent each of the main sub-types into which breast cancer can be divided based on molecular profiling. All cell lines listed in **Table 2.1.** were sourced directly from the American Type Culture Collection (ATCC) (Manassas, Virginia, U.S.A.) as fully authenticated cryogenically frozen cultures. Two further cell lines were sourced specifically for use as positive controls in particular experiments described herein; a bone homing variant of the MDA-MB-231 lineage engineered to stably express β-galactosidase (denoted as the BO2-β-gal lineage) was provided by Prof. P. Clezardin (INSERM, Lyon, France) while human cervical cancer cells of the HeLa lineage were sourced directly from the ATCC as a fully authenticated cryogenically frozen culture.

Table 2.1. Human Breast Cancer Cell Line Panel

Cell Line	Classification		Immunoprofile	References
MCF-7	Luminal A	ER Positive	$ER^+ PR^{+/-} HER2^-$	(Soule *et al.*, 1973)
ZR-75-1	Luminal B		$ER^+ PR^{+/-} HER2^+$	(Engel *et al.*, 1978)
MDA-MB-468	Basal	Triple Negative	$ER^- PR^- HER2^-$	(Cailleau *et al.*, 1978)
MDA-MB-231	Claudin-Low		$ER^- PR^- HER2^-$	(Cailleau *et al.*, 1974)
SK-BR-3	HER2	HER2	$ER^- PR^- HER2^+$	(Trempe, 1976)

Cell lines are classified according to both the clinically relevant Perou classification (left column under "classification" heading) and the traditional classification system based on receptor expression status (right column under "classification" heading). **ER**: oestrogen receptor, **PR**: progesterone receptor, **HER2**: human epidermal growth factor receptor 2.

2.2. Cell Culture Procedures

All procedures involving the handling of human breast cancer cell lines, unless otherwise stated, were carried out under laboratory containment level 2 inside of a class-2 microbiological safety cabinet using standard aseptic technique in accordance with the biosafety level requirements identified by the ATCC. All culture media and solutions to which cells were exposed were pre-sterilised and warmed to 37^oC in a water bath maintained at this temperature prior to their described usage unless otherwise stated.

2.2.1. Adherent Monolayer Cell Cultures

2.2.1.1. Maintenance of Adherent Monolayer Cell Cultures

All cell lines, with the exception of HeLa, were routinely maintained *in vitro* as adherent cultures grown in complete growth medium composed of RPMI-1640 basal medium (11mM glucose, 2mM L-glutamine) (Life Technologies Ltd., Paisley, U.K.) supplemented with 10% (v/v) dialysed foetal bovine serum (FBS) (Life Technologies Ltd.). HeLa cells were maintained as adherent cultures grown in complete growth medium composed of DMEM basal medium (25mM glucose, 3.97mM L-glutamine, 1mM sodium pyruvate) (Life Technologies Ltd.) supplemented with 10% (v/v) dialysed FBS. All cultures were routinely grown inside of sterile $75cm^2$ high-quality polystyrene tissue culture flasks (T75) (Scientific Laboratory Supplies Ltd., Hessle, U.K.). All cells were seeded at an initial optimal density as recommended by the respective supplier (**Table 2.2.**) supplemented with 0.2ml of complete culture medium per cm^2 of culture vessel surface area. Culture medium was maintained at physiological pH and temperature by equilibration with a mixture of 5% CO_2 and 95% air at 37^oC inside a humidified (100% relative humidity) water-jacketed incubator. Nutrient-depleted medium was removed from growing cultures and exchanged for an equal volume of fresh medium at intervals of approximately 48 hours. The degree of confluency (surface coverage) of growing cells was monitored daily by inverted phase-contrast microscopy. Sub-culture was undertaken at a time point corresponding with

approximately 80% of the duration of the logarithmic phase of culture growth as determined from the growth profile established for each cell line (**Section 3.4.1.**).

Table 2.2. Optimal Seeding Densities and Culture Media Used for Cell Lines

Cell Line	Seeding Density (cells per cm^2)	Complete Culture Medium
MCF-7	2.0×10^4	RPMI-1640 + 10% FBS
ZR-75-1	3.0×10^4	RPMI-1640 + 10% FBS
MDA-MB-468	2.0×10^4	RPMI-1640 + 10% FBS
MDA-MB-231	1.0×10^4	RPMI-1640 + 10% FBS
SK-BR-3	3.0×10^4	RPMI-1640 + 10% FBS
BO2-β-gal	1.0×10^4	RPMI-1640 + 10% FBS
HeLa	1.3×10^4	DMEM + 10% FBS

All initial seeding densities and the composition of complete culture media stated are as recommended by the ATCC (Manassas, Virginia, U.S.A.). Information stated for the BO2-β-gal MDA-MB-231 variant lineage is according to the information for the parental cell line.

2.2.1.2. Retrieval of Adherent Monolayer Cell Cultures

Spent growth medium was removed from the adherent cell monolayer and two repeat washes undertaken using 70μl phosphate-buffered saline (PBS) (pH 7.4 at 37°C) per cm^2. The monolayer was detached from the tissue culture flask surface by incubation in the presence of 70μl per cm^2 of trypsin-ethylenediaminetetraacetic acid (EDTA) solution (0.25% (w/v) porcine pancreatic trypsin with 0.002% (w/v) EDTA in Hank's Balanced Salt Solution) (Sigma-Aldrich Company Ltd., Dorset, U.K.) for a period of 5 minutes. An equivalent volume of complete growth medium was then added in order to neutralise the proteolytic action of trypsin, and the total volume of each trypsinised cell suspension subsequently transferred to an appropriately sized centrifuge tube. Culture vessels were rinsed once more with complete growth medium and this volume subsequently transferred to the corresponding centrifuge tube. Cells were pelleted by centrifugation of the retrieved suspension at 150 x *g* for 5 minutes at 25°C. The resultant supernatant was discarded and the cell pellet re-suspended in an appropriate volume of complete growth medium prior to haemocytometric counting.

2.2.2. Three-Dimensional Spheroid Cultures

2.2.2.1. Production of Ultra-Low Attachment 96-Well Plates

Poly-2-hydroxyethylmethacrylate (poly-HEMA) (Sigma-Aldrich Company Ltd.) was prepared as a 12% (w/v) stock solution in 95% (v/v) ethanol. Dissolution was achieved by continuous mixing with a magnetic stirrer bar at ambient temperature overnight. This stock solution was stored at ambient temperature until required. Poly-HEMA stock solution was diluted 1:24 in 95% (v/v) ethanol in order to produce a working solution with a final concentration of 0.5% (w/v). This working solution was gently vortexed before being sterile filtered through a 0.2μm polycarbonate syringe filter. A 60μl volume of the sterilised poly-HEMA solution was pipetted into each well of a Corning® Costar® 96-well round-bottomed cluster plate (Scientific Laboratory Supplies Ltd.). Plates then had their lid fitted and were removed to a non-humidified incubator maintained at 37°C for minimum period of 72 hours in order to completely evaporate the ethanol within each well. After plates were completely dried, their edges were sealed with plastic paraffin film before being stored in a refrigerator maintained at 4°C until required.

2.2.2.2. Generation and Maintenance of Three-Dimensional Spheroid Cultures

Cells were seeded into poly-HEMA-coated ultra-low attachment 96-well plates at the optimal density assuming 0.32 cm^{2} of surface area for cell growth; the equivalent surface area of flat-bottomed 96-well cluster plates. Cells were seeded in a volume of 200μl complete growth medium supplemented with 2.5% (v/v) Corning® Matrigel® basement membrane matrix (Scientific Laboratory Supplies Ltd.) that was pre-cooled to 4°C. Plates were immediately centrifuged at 1000 x g for 10 minutes at 4°C following seeding of cells, before being placed into incubation under standard growth conditions. At 48-hour intervals, 100μl of spent medium was removed from all wells and replaced with an equal volume of fresh complete growth medium.

2.2.2.3. Dispersal of Three-Dimensional Spheroid Cultures

In order to achieve a single cell suspension for subsequent analyses, three-dimensional spheroid cultures were dispersed using mechanical homogenisation and enzymatic digestion in combination. Non-adherent spheroidal cell cultures were first removed from the wells of 96-well culture plates using a sterile plastic Pasteur pipette and then decanted into an appropriately sized centrifuge tube. Centrifugation was undertaken for 5 minutes at 150 x g and 25°C in order to loosely pellet the spheroids and allow removal of the spent culture medium. Spheroids were washed twice by careful resuspension in a 5ml volume of PBS and repeating centrifugation as previously described. Dispersal of spheroids was achieved by incubation in a 1ml volume of collagenase-dispase® solution (≥ 0.1U/ml collagenase and ≥ 0.8U/ml dispase in PBS) (Sigma-Aldrich Company Ltd.) with gentle repeat aspiration being undertaken until a homogenous suspension was visibly evident. An equal volume of complete growth medium was then added before each suspension was passed through a 40μm cell strainer. The resultant suspension was immediately centrifuged at 150 x g and 25°C for 5 minutes. The supernatant was discarded and the cell pellet resuspended in a 1ml volume of serum free-culture medium prior to haemocytometric counting.

2.2.3. Haemocytometric Counting of Cells in Suspension

The cellular concentration of each retrieved cell suspension was determined by haemocytometric counting using the trypan blue dye exclusion method. Briefly, each retrieved cell suspension was mixed thoroughly by repeat aspiration followed by gentle vortexing to ensure complete homogeneity. A 50μl volume of cell suspension was then decanted into a 0.5ml microcentrifuge tube to which an equal volume of filtered 0.4% (w/v) trypan blue solution (Sigma-Aldrich Company Ltd.) was added. The suspension was gently mixed by repeat aspiration and allowed to incubate at ambient temperature for 5 minutes. During this period, a Bright-Line™ haemocytometer (Sigma-Aldrich Company Ltd.) was cleaned thoroughly with 70% (v/v) ethanol in distilled water, dried with lens tissue, and then fitted with 0.5mm thick glass coverslip. A 10μl volume of the trypan blue-cell suspension mixture was loaded into one of the haemocytometer chambers (**Figure 2.1.**). The number of viable (unstained) and non-

viable (blue-stained) cells present within each of the four corner 4 x 4 square grids were counted under inverted phase contrast microscopy at 100X magnification. The mean average viable cell count within the chamber was calculated and corrected for the dilution factor with trypan blue. Each haemocytometer counting grid has a volume of $0.1mm^3$ and 1ml has an equivalent volume of $1000mm^3$; the dilution factor-adjusted average viable cell count was therefore multiplied by 10^4 in order to express the cell count achieved as the number of cells per millilitre of suspension. The requisite volume of suspension to seed cells at the desired density was then determined from the viable cell concentration.
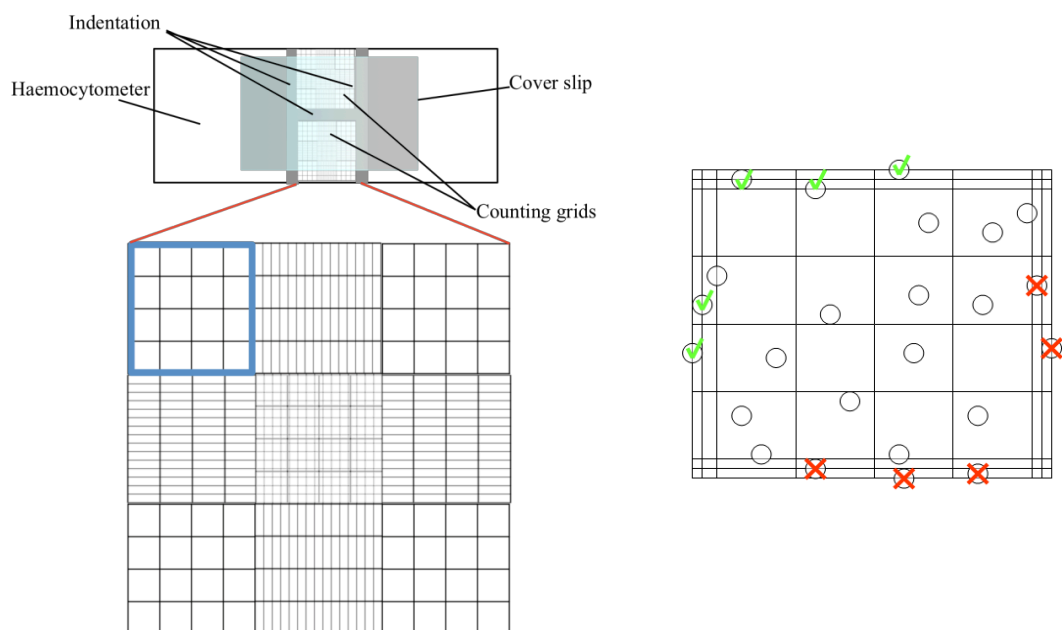
Figure 2.1. Schematic Representation of a Haemocytometer

The left diagram illustrates the main features of the haemocytometer. The right diagram represents one of the four $1mm^2$ laser-etched counting grids at each corner of a haemocytometer chamber as highlighted in blue on the left diagram. The convention for determining the number of viable (unstained) and non-viable (trypan blue-stained) cells within each of the four corner grids is also depicted by the diagram on the right; only those cells in contact with the outer two lines of the bottom and right margins were excluded from the count.

2.2.4. Cryogenic Storage and Revival of Cells

Cells were stored cryogenically frozen at a density of 1.0 x 10^6 cells per sterile cryogenic storage ampoule suspended in a 1ml volume of cryopreservation medium composed of complete growth medium supplemented with 10% (v/v) dimethylsulphoxide (DMSO). Cryogenic ampoules of cell suspension designated for long-term storage were initially preserved by controlled rate freezing (-1^oC per minute) over a 24-hour period inside of an isopropyl alcohol-jacketed freezing chamber placed into a freezer maintained at -80^oC. Frozen ampoules were stored long-term at a temperature below -135^oC in the vapour phase of nitrogen. Frozen cultures of cells required for thawing were removed from storage and immediately transferred to a water bath maintained at 37^oC. Thawing ampoules were gently agitated for approximately three minutes until the contents were completely thawed. Defrosted vials were wiped dry and decontaminated by spraying with 70% (v/v) ethanol in distilled water prior to being transferred to a class-2 microbiological safety cabinet. Vial contents were mixed gently by repeat aspiration before subsequently being transferred to a sterile 15ml centrifuge tube. A 9ml volume of pre-warmed complete growth medium was slowly added to the cell suspension and centrifugation subsequently undertaken (5 minutes at 150 x g and 25^oC). The cryoprotectant-containing supernatant was discarded from the resultant cell pellet, which was then resuspended in an appropriate volume of complete growth medium and subsequently used to seed tissue culture vessels with cells at the required density.

2.2.5. Generation of Cell Proliferation Curves

Cells were seeded in triplicate wells of 24-well cluster plates (Scientific Laboratory Supplies Ltd.) at the stipulated optimal density (**Table 2.2.**) supplemented with 0.2ml of complete growth medium per cm^2 growth area. Cluster plates were place into incubation under standard growth conditions (37^oC with 95% air, 5% CO_2 and 100% relative humidity). At each subsequent 24-hour interval, the cells within each row of three wells were retrieved by trypsinisation and the viable cell number determined by haemocytometric counting using trypan blue dye exclusion. The mean average cell count across all three replicate samples recorded at each time interval was calculated

and used to construct a growth profile by plotting viable cell count against time in culture graphically. Growth profiles were then used to identify each of the main phases of the growth cycle (**Figure 2.2.**). The doubling time of cultures during the logarithmic growth phase was calculated as the product of the incubation period and the natural logarithm of 2, divided by the natural logarithm of the ratio of the number of viable cells at the beginning and end of the incubation period.
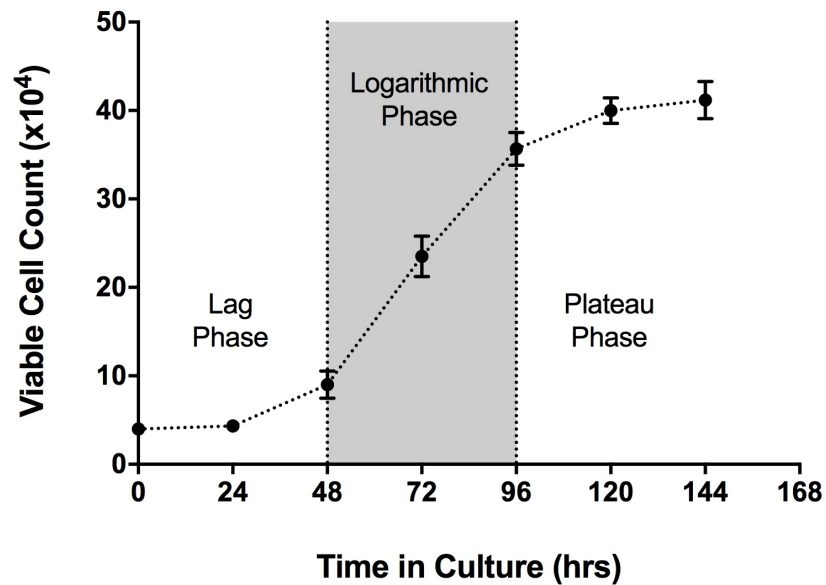
Figure 2.2. Culture Growth Profile and Phases of Population Growth

The lag-phase is defined as the period between initial seeding of cells and the point at which they enter the logarithmic growth phase. The logarithmic phase of growth (log-phase) is characterised by a constant rate of population growth per unit time. Once growth-limiting factors (e.g. depletion of essential nutrients and accumulation of inhibitory metabolic products) are encountered the rate of population growth is gradually reduced until a plateau phase occurs during which the rates of new cell formation and cell death are equal.

2.2.6. Clonogenic Assays

2.2.6.1. Adherent Colony Formation Assay

Cells were seeded at a clonogenic density of 20 cells per cm^2 of growth area in high-quality polystyrene 60mm tissue culture dishes or 6-well cluster plates (Scientific Laboratory Supplies Ltd.) and were supplemented with 0.2ml of complete growth medium per cm^2. Culture vessels were placed into incubation under standard growth conditions for a time period of at least six log-phase doubling times (determined from the respective growth curve). Following incubation for the desired period, the growth medium was carefully removed from all dishes and adherent cell colonies fixed in a 4% (v/v) solution of Pierce™ methanol-free formaldehyde (Life Technologies Ltd.) in PBS (pH 7.4 at 37°C) for 15 minutes at ambient temperature. Once fixation was complete, the fixative solution was removed and colonies immediately stained with an equal volume of 0.05% (w/v) aqueous crystal violet solution (Merck Chemicals Ltd., Nottingham, U.K.) for 30 minutes at ambient temperature. Subsequently, culture vessels were washed by two repeat immersions in a tub of tap water before being inverted onto tissue paper and allowed to dry completely. Once dried, plates were imaged using the Pixera Professional 1.2 megapixel digital camera system (Pixera U.K. Ltd., Bourne End, U.K.) and colonies counted by way of semi-automated image analysis (**Figure 2.3.**) undertaken using GeneTools software (Syngene U.K. Ltd., Cambridge, U.K.).
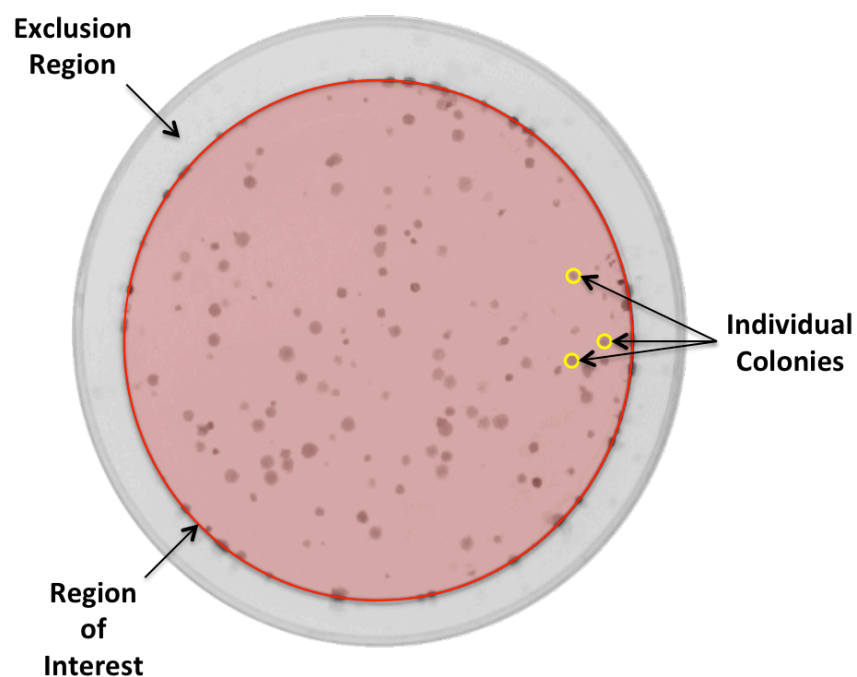
Figure 2.3. Semi-Automated Colony Number Analysis in GeneTools Software

The region of interest (red) was set manually to define the outer boundary of the area for analysis. The sensitivity and thresholds of detection were pre-set and calibrated using manual counts, allowing the software to automatically detect individual colonies (yellow circles). The lower limit of detection for a colony was set to the number of pixels approximately equivalent to 10 cells. Merged colonies, false-positives and false-negatives were manually resolved before the final colony count was recorded.

2.2.6.2. Mammosphere Formation Assay

Mammosphere assays were undertaken according to a method described by Weiswald *et al.* (2015). Mammosphere formation assay plates were made by coating each well of a 6-well cluster plate with 2ml of 1.5% (w/v) agarose in RPMI-1640 + 10% FBS. Briefly, electrophoresis grade agarose powder (Thermo Fisher Scientific, Paisley, U.K.) was pre-weighed into 50ml centrifuge tubes, to which RPMI-1640 + 10% FBS was added inside a sterile microbiological safety hood. Tubes were tightly sealed and then gently inverted several times to form a suspension before the lids were loosened and tubes were placed into a glass beaker placed inside of a microwave. Heating was undertaken in cycles of 10 seconds followed by closure of the tube lid and gentle inversion. These cycles were repeated until the agarose had completely dissolved to form a solution. Tubes of molten agarose were each placed inside a glass beaker containing water pre-heated to 90°C in order to prevent solidification. The molten agarose solution was carefully dispensed into 6-well cluster plates inside of a sterile microbiological safety hood and allowed to set completely for approximately 30 minutes with the cluster plate lid removed. Once the agarose had set, cells were seeded into these plates at a clonogenic density of 20 cells per cm^2 of growth area and were supplemented with 0.2ml of complete growth medium per cm^2. Cluster plates were placed into incubation under standard growth conditions for a time period of at least six log-phase doubling times (determined from the respective growth curve). Following incubation for the desired period, the number of non-adherent mammospheres was quantified under inverted phase-contrast microscopy.

2.2.7. Scratch Closure Cell Migration Assay

Scratch closure cell migration assays were undertaken according to the methods described by Rodriguez *et al.* (2005) and Cory (2011). Mitomycin C from *Streptomyces caespitosus* (Sigma-Aldrich Company Ltd.) was supplied as 2mg vials. Prior to use, the contents of each vial were dissolved in 200ml of serum-free RPMI-1640 basal medium to produce a solution with a final concentration of 10µg/ml. This solution was protected from light until required for use and was stored in a refrigerator maintained at $4^{o}C$ for up to two weeks. Cells were seeded in triplicate into 6-well cluster plates and supplemented with 0.2ml of medium per cm^{2} surface area. Once coverage had reached 100% confluency, spent medium was removed from the cell monolayer and two washes undertaken using PBS. Mitomycin C solution, freshly prepared using serum-free RPMI-1640 basal medium at a concentration of 10µg/ml, was added to completely cover the cell monolayer and then tissue culture vessels replaced in incubation under standard growth conditions for a three hour period. Subsequently, the Mitomycin C solution was removed and three washes of the cell monolayer undertaken using serum-free basal culture medium. A 200µl pipette tip was then used to make a linear scratch of approximately 750µm in width in the cell monolayer. Each well was then washed three times with pre-warmed complete culture medium in order to completely remove cell debris formed during the introduction of the scratch. Two reference points were marked at either end of the scratch on the underside of the plate under low-magnification (50X magnification) inverted phase-contrast microscopy using a permanent marker pen. Images were immediately captured at each reference point under inverted phase-contrast microscopy at 100X magnification and further images captured at subsequent time-intervals in an identical manner. The area of the scratch within each image field was measured using the open-source image analysis platform ImageJ (**Figure 2.4.**) and the percentage closure over the assay time period calculated.
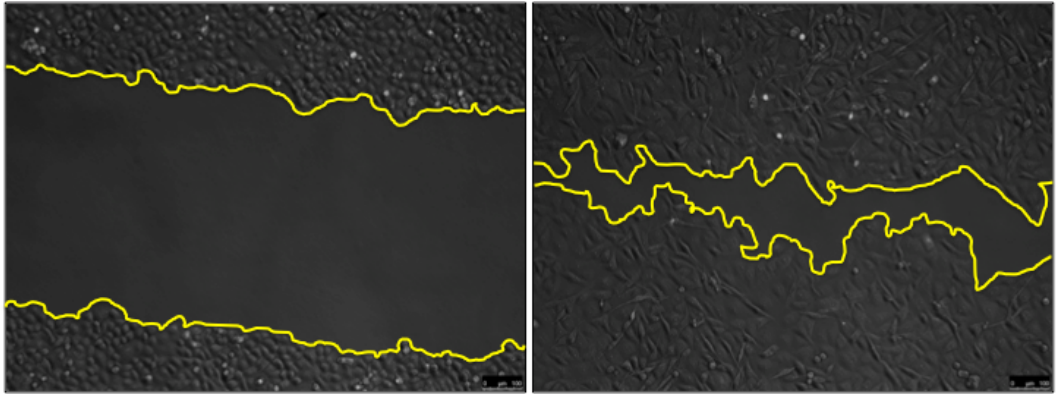
Figure 2.4. Scratch Assay Analysis Using ImageJ Software

Images were imported into ImageJ, converted to grayscale and the contrast enhanced in order to allow the scratch border to be readily defined. The border of the scratch at 0 hours (left) and 24 hours (right) was demarked using the freehand draw tool (yellow line). The physical pixel length according to the image metadata was programmed into the imageJ scale conversion plugin allowing the area within the scratch to be automatically calculated for each image and the percentage closure of the scratch over the time period determined.

2.3. Cell Labelling and Immunostaining

2.3.1. Vybrant® Lipophilic Tracer Dye Staining

Vybrant® DiO, CM-DiI and DiD were purchased from Life Technologies Ltd. All lipophilic dye staining was undertaken in suspension at a density of 1.0×10^6 cells in 1ml of serum-free basal culture medium in accordance with the supplier's instructions. Vybrant® DiO and DiD dye solutions were used at a final concentration of 5µM while Vybrant® CM-DiI dye solution was used at a final concentration of 2µM; the appropriate volume of each staining solution was added directly to cell suspension before samples were vortexed thoroughly and placed into incubation within a water bath maintained at 37^oC for a period of exactly 5 minutes while protected from light. Vybrant® DiO or DiD staining required samples to be incubated for a further 15 minutes at 37^oC while Vybrant® CM-DiI staining required cells to be immediately transferred to ice for the subsequent 15 minute period. Following the appropriate incubation period, samples were centrifuged for 5 minutes at 150 x *g*, the resultant supernatant discarded and the cell pellet resuspended in an equal amount of fresh serum-free culture medium. Centrifugation and resuspension in this way were then repeated two further times before the stained cells were ready for use in subsequent applications.

2.3.2. Immunostaining for Fluorescence Microscopy

2.3.2.1. Sample Preparation by Cytocentrifugation

Samples of cells for immunostaining were deposited onto Superfrost Plus™ glass microscopy slides by cytocentrifugation using the Shandon™ Cytospin™ 3 cytocentrifuge (both from Thermo Fisher Scientific). Cytocentrifuge funnels were first fitted with a single glass microscopy slide and white filter card and held together with a metal clip (**Figure 2.5.**). Funnels were loaded with 200µl of complete culture medium and then placed into the cytocentrifuge. Centrifugation was undertaken at 150 x *g* for 3 minutes in order to pre-wet the filter card. Each cytocentrifuge funnel was then loaded with a 200µl volume of cell suspension containing the desired number of cells for deposition. Centrifugation was then repeated for 3 minutes at 150 x *g* using medium acceleration in order to deposit cells directly onto the slides. Each glass microscopy slide was then separated from the cytocentrifuge funnel and blotting card, and transferred into a slide rack. Slides were immediately plunged into ice-cold fixative solution (either 4% (v/v) methanol-free formaldehyde in PBS or 4% (w/v) paraformaldehyde in PBS) and allowed to incubate on ice for a 10-minute period. Washing was subsequently undertaken in two changes of PBS before cells were progressed to immunostaining. Where staining was not carried out immediately post-fixation, slides were stored at 4°C immersed in PBS until required for staining.

2.3.2.2. Indirect Immunostaining of Intracellular Markers for Immunofluorescence

Fixed cytocentrifuge samples were drained of PBS and a hydrophobic barrier pen (Vector Laboratories Ltd., Peterborough, U.K.) used to draw a circular hydrophobic barrier around each cell spot. All slides were placed onto a slide tray and a 200µl volume of permeabilisation buffer (0.1% (v/v) Triton™ X-100 in PBS) deposited onto each cell spot. Incubation in the presence of permeabilisation buffer was carried out for 5 minutes at ambient temperature. Permeabilisation buffer was removed by tapping the slides onto tissue before three washes were undertaken using PBS-Tween® 20 (PBST) wash buffer (0.01% (v/v) Tween® 20 in PBS), each for 5 minutes. A 200µl volume of blocking buffer (10% (v/v) normal serum + 1% (w/v) bovine serum albumin

(BSA) in PBST) was pipetted onto slides and incubation undertaken for 1 hour. Normal serum used for blocking during any particular experiment was matched to the host species in which the secondary antibody being used was raised. All normal sera were sourced either from Vector Laboratories Ltd. or Sigma-Aldrich Company Ltd. During the blocking incubation period, primary antibodies and corresponding isotype control antibodies were diluted to the desired concentration in antibody diluent (1% (w/v) BSA in PBST). Following the blocking incubation, the solution on all samples was removed by gently tapping the slides onto tissue and a 200µl volume of the appropriate primary antibody solution or antibody diluent only (primary omitted control samples) pipetted onto each cell spot. The tissue in the base of each slide tray was then dampened with distilled water, the slide tray lid replaced and the tray placed into incubation at 4°C overnight. On the subsequent day, the primary antibody solution or diluent was removed from all samples and three washes undertaken as described previously. During the final washing step, secondary antibodies were diluted to the desired concentration in antibody diluent solution. A 200µl volume of dilute secondary antibody solution or antibody diluent only (secondary omitted control samples) was then carefully pipetted onto each cell spot and incubation undertaken for 1 hour at ambient temperature. Following this incubation, the solution on all samples was removed by gently tapping the slides onto tissue and three washes undertaken as previously described. The residual wash buffer was then carefully removed from each slide and mounting of samples undertaken using a 0.12mm thickness round glass coverslip and a minimal volume (approximately 10µl) of ProLong® Gold anti-fade mounting medium containing 4',6-diamidino-2-phenylindole (DAPI) (Life Technologies Ltd.). Mounted samples were cured on a flat surface, completely protected from light, for a period of 24 hours before imaging.

All information regarding specific primary, isotype control and secondary antibodies used in immunostaining for fluorescence microscopy is detailed later in the respective methods sections of the experiments in which they were used.
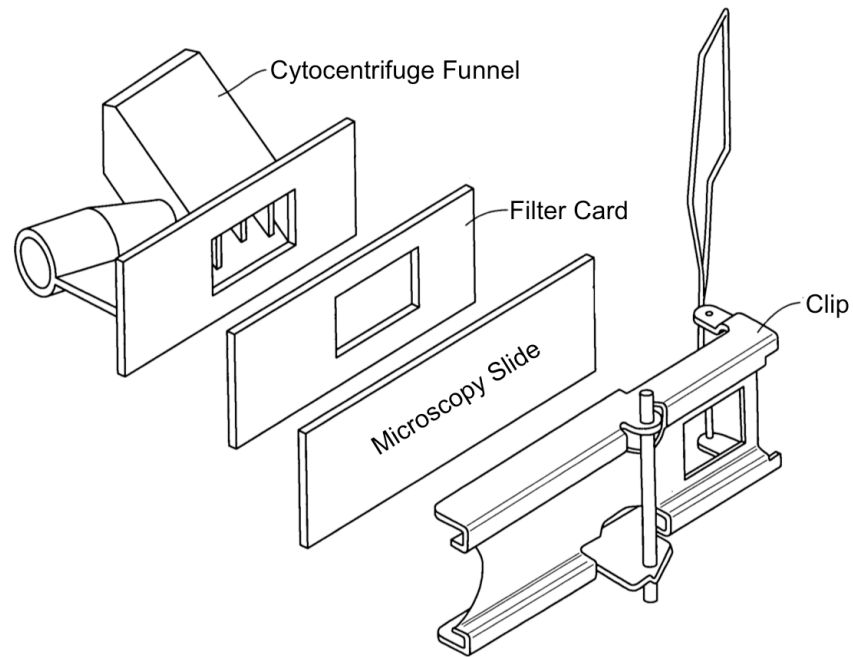
Figure 2.5. Cytocentrifuge Slide Preparation Apparatus

The apparatus and relative configuration required for preparation of samples by cytocentrifugation are shown. A glass microscopy slide was first placed carefully into a metal cytocentrifuge clip with the electrostatically positive charged side onto which cells would be deposited facing outward. A filter card was then loosely placed in apposition to this surface and the cytocentrifuge funnel placed on top. The arm of the metal clip was then drawn down and clipped into place in order to securely hold all components together. The entire configuration was then ready for loading into the cytocentrifuge.

2.3.3. Immunostaining for Flow Cytometry

2.3.3.1. Direct Immunostaining of Cell Surface Markers for Flow Cytometry

Samples of 1.0 x 10^6 live cells were prepared from harvested cell suspensions in microcentrifuge tubes and centrifuged for 5 minutes at 150 x g in a centrifuge pre-cooled to 4°C. Following centrifugation, the supernatant was discarded and the resultant cell pellet washed twice by resuspension in a 1ml volume of ice-cold flow cytometry buffer (5% (v/v) FBS in PBS) followed by immediate centrifugation as previously described. Directly conjugated primary antibodies and corresponding isotype controls were pre-diluted to the desired concentration in ice-cold flow cytometry buffer. Washed cell pellets were resuspended in 100µl of primary antibody solution and incubated for 1 hour at 4°C in total darkness under constant agitation. Following incubation, a 900µl volume of ice-cold flow cytometry buffer was added to all tubes and centrifugation undertaken at 150 x g for 5 minutes. The stained cell pellet was carefully washed two further times by resuspension in a 1ml volume of ice-cold flow cytometry buffer followed by immediate centrifugation as previously described. The washed cell pellet was resuspended in 1ml of ice-cold flow cytometry buffer and strained through 40µm cell strainer into round-bottomed polystyrene flow cytometry tubes (Beckton, Dickenson and Co. Plc., Oxford, U.K.) prior to immediate analysis.

2.3.3.2. Indirect Immunostaining of Cell Surface Markers for Flow Cytometry

Samples of 1.0 x 10^6 live cells were prepared from harvested cell suspensions in microcentrifuge tubes and stained with unconjugated primary antibodies in exactly the same manner as described in **Section 2.3.3.1.** Once washed three times following incubation in the presence of primary antibody solution, each cell pellet was resuspended in a 100µl volume of fluorophore-conjugated secondary antibody pre-diluted to the desired concentration in ice-cold flow cytometry buffer and incubated for 1 hour at 4°C in total darkness under constant agitation. Following incubation, a 900µl volume of ice-cold flow cytometry buffer was added to all tubes and centrifugation undertaken at 150 x g for 5 minutes. Each stained cell pellet was carefully washed two further times by resuspension in a 1ml volume of ice-cold flow

cytometry buffer followed by immediate centrifugation as previously described. Washed cell pellets were each resuspended in 1ml of ice-cold flow cytometry buffer and strained through a 40µm cell strainer into a round-bottomed polystyrene flow cytometry tube prior to immediate analysis.

2.3.3.3. Indirect Immunostaining of Intracellular Markers for Flow Cytometry

Samples of 1.0 x 10^6 cells were prepared in pre-cooled microcentrifuge tubes from retrieved cell suspensions following retrieval and haemocytometric counting. Cells were collected by centrifugation for 5 minutes at 150 x g in a centrifuge pre-cooled to 4^oC. Following centrifugation, the supernatant was discarded and the resultant cell pellet resuspended in a 1ml volume of ice-cold fixation solution (4% (v/v) methanol-free formaldehyde in PBS). Fixation was undertaken by incubation of samples on ice for 10 minutes. Following fixation, samples were centrifuged at 300 x g for 5 minutes and the resultant supernatant discarded. Each cell pellet was resuspended in a 1ml volume of permeabilisation and blocking solution (0.1% (v/v) Triton™ X-100 + 10% (v/v) normal serum in PBS) and incubated for 1 hour at ambient temperature. During this period, unconjugated primary antibodies and corresponding isotype controls were pre-diluted to the desired concentration in intracellular flow cytometry buffer (1% (w/v) BSA + 0.1% (v/v) Triton™ X-100 in PBS). Following blocking, samples were centrifuged at 300 x g for 5 minutes and the resultant supernatant discarded. Each cell pellet was resuspended in a 100µl volume of pre-prepared primary antibody solution and incubated for 1 hour at ambient temperature with constant agitation. During this period, fluorophore conjugated secondary antibodies were pre-diluted to the desired concentration in intracellular flow cytometry buffer. Following incubation, a 900µl volume of ice-cold intracellular flow cytometry buffer was added to all tubes and centrifugation undertaken at 300 x g for 5 minutes. The cell pellet was carefully washed two further times by resuspension in a 1ml volume of ice-cold intracellular flow cytometry buffer followed by immediate centrifugation as previous. Washed samples were resuspended in 100µl of pre-prepared secondary antibody solution and incubated for 1 hour at ambient temperature in total darkness. Following incubation, a 900µl volume of ice-cold intracellular flow cytometry buffer was added to all tubes and centrifugation undertaken at 300 x g for 5 minutes. Each stained cell pellet was

carefully washed two further times by resuspension in a 1ml volume of ice-cold intracellular flow cytometry buffer followed by immediate centrifugation as previously described. Each sample was finally resuspend in 1ml of intracellular flow cytometry buffer and strained through a 40μm cell strainer into a round-bottomed polystyrene flow cytometry tube prior to immediate analysis.

All information regarding specific primary, isotype control and secondary antibodies used in immunostaining for flow cytometry is detailed later in the respective methods sections of the experiments in which they were used.

2.4. Microscopic Imaging

All fluorescent and phase-contrast imaging was carried out using the AF6000LX Integrated Live Cell Workstation from Leica Microsystems U.K. Ltd. (Milton Keynes, U.K.). This microscope is fitted with filter cubes for imaging a range of fluorophores (**Table 2.3.**), as well as an environmental chamber maintained at 37°C and fed with a gas mixer supplying 95% air and 5% CO_2, thereby enabling live cell imaging. The Leica DMI4000B inverted microscope was used for bright-field transmitted light imaging in full colour, as was required during β-galactosidase assays (**Section 2.8.1.**).

Table 2.3. Specification of Filter Cubes Available on the Leica AF6000LX

Filter Cube	Excitation Range	Excitation Filter Type	Dichromatic Mirror	Suppression Filter Type	Example Fluorophore
A4	Ultraviolet	BP 360/40	400	LP 425	DAPI
L5	Blue	BP 480/40	505	BP 527/30	AlexaFluor® 488, Vybrant® DiO
N3	Green	BP 546/12	565	BP 600/40	Vybrant® CM-DiI
Y5	Red	BP 620/60	750	BP 810/90	Vybrant® DiD

LP: longpass filter , **BP**: bandpass filter

During analysis of immunofluorescent staining by manual scoring of positively stained cell events, three representative non-overlapping fields were required for each sample type within three technical replicate sample sets across each of three biologically independent repeats of each experiment. In order to acquire these images in a reproducible and non-biased manner, the tile-scan function of the AF6000LX was used in order to produce a 3 x 3 field image of the total area of each immunostained cell spot (**Figure 2.6.**). The three central cross sectional fields were used in each case for manual scoring of total events (indicated by staining of cell nuclei) and events positively stained for the marker of interest (indicated by immunostaining).
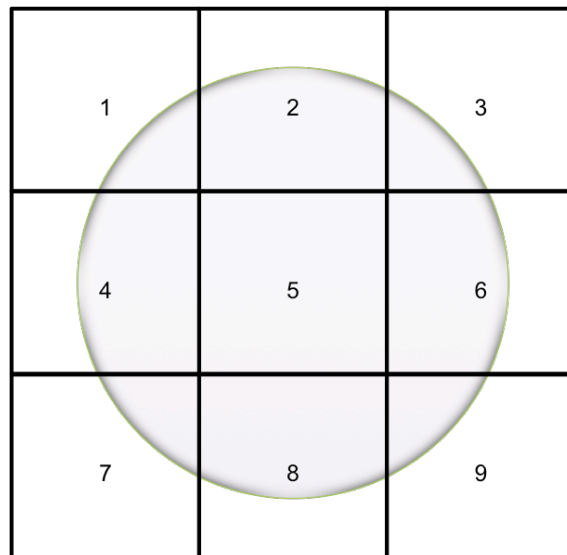
Figure 2.6. Acquisition of Non-Overlapping Fields for Scoring of Immunostaining

Once the microscope had been set up for Köhler illumination and focussed on the cell spot (represented here by a grey circle), the upper-left margin (quadrant 1) was located. Having recorded an X, Y coordinate, the microscope stage was then sequentially panned to the upper right, lower right, and lower left margins (quadrants 3, 9 and 7, respectively) and X, Y coordinates recorded for each. The coordinates recorded were used to define the boundaries of the sample, which was divided into nine equal fields for imaging. These fields were then imaged in order from 1 - 9 in an automated manner using the tile scan function of the Leica AF6000LX. Images of fields 4, 5 and 6 were used to provide a representative cross section of the each sample and were then scored manually for total number of cells and positively stained events present.

2.5. Flow Cytometry and Fluorescence Activated Cell Sorting

All flow cytofluorimetric analyses were undertaken using either the BD™ FACSCalibur™ or BD™ LSR-II™ platform, while fluorescence activated cell sorting (FACS) was undertaken using the BD™ FACSAria™ platform (Beckton, Dickenson and Co. Plc.). All flow cytometry data were analysed using the FlowJo® flow cytometry analysis platform (FlowJo LLC, Ashland, Oregon, U.S.A.).

2.5.1. General Experimental Design

An unstained sample of cells was prepared within each experimental sample set. Unstained samples were grown and processed in an identical manner to all corresponding stained samples except that they were not exposed to any fluorescent molecules (e.g. lipophilic dyes or antibodies). Unlabelled samples were used in order to measure the autofluorescence of the population of interest and to calibrate the cytometer by setting the voltage applied to each fluorescence detector channel in order that unlabelled cells were detected as negative events within the first logarithmic decade of the corresponding graphical output.

For assessment of live cell viability, 1µM TO-PRO®-3 iodide (Life Technologies Ltd.) was used when experimental samples were labelled with green or red fluorescent fluorophores, while 75µM propidium iodide (Sigma-Aldrich Company Ltd.) was used in all experiments involving the labelling of cells with fluorophores emitting far red fluorescence. A 5µl volume of the appropriate viability dye was added per millilitre of cell suspension followed by through mixing and a 1-minute incubation period in complete darkness immediately prior to analysis of samples. During cytometric analysis or FACS, the removal of cellular debris, identification of single cell events and removal of non-viable cells was routinely undertaken according to a gating tree depicted in **Figure 2.7.** The gating trees showing subsequent stages of gating for specific applications are depicted in the respective section describing the methodology for these assays.
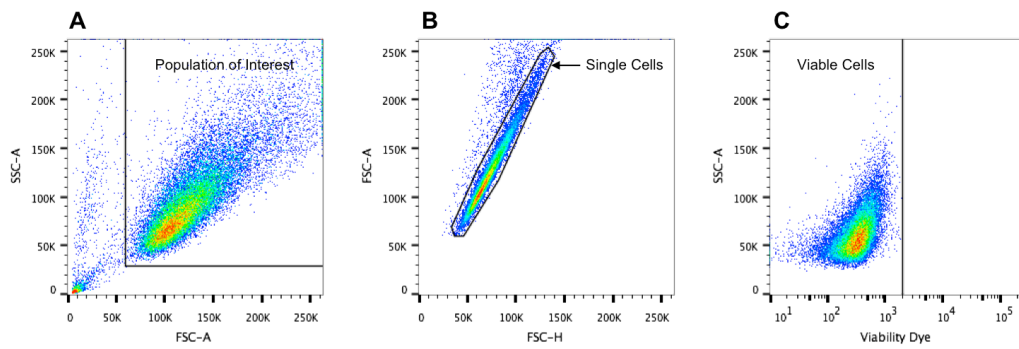
Figure 2.7. Initial Gating Strategy for Flow Cytofluorimetric Analyses

A: Cellular debris, identified by low particle size or forward-scatter (FSC) and granularity or side-scatter (SSC), was first gated-out of the event population. **B**: The resultant population was then divided into single cell and non-single cell events. **C**: Single cell events were further divided into live and dead cell populations based on fluorescence intensity of viability dye (propidium iodide or TO-PRO®-3 iodide) staining relative to autofluorescence of an unlabelled cell sample analysed at the same detector channel voltage.

Isotype control samples were prepared in all immunostaining experiments in order to determine non-epitope-specific binding of the primary antibody being used. Isotype control antibodies lacking antigenic specificity were matched to the host species, clonality, isotype and conjugation format of the corresponding primary antibody. Isotype control antibodies were always used at the same protein concentration as the primary antibody to which it was matched. Secondary antibody controls were prepared when a secondary antibody was used in an indirect immunostaining protocol (**Section 2.3.3.2.** and **Section 2.3.3.3.**). These controls were prepared by omission of the primary antibody during sample preparation and functioned to determine non-specific binding of the secondary antibody to low affinity sites in the absence of any primary antibody.

In order to determine any spectral overlap of fluorophores used in multi-colour flow cytometry experiments, a series of fluorescence minus-one (FMO) control samples was prepared. Each FMO control in a series was prepared by staining a sample with all the fluorescent conjugates to be used in the final procedure except for one, allowing the contribution of the fluorophores present to the signal in the unlabelled channel to be determined and correctly compensated as required. Single colour compensation controls were prepared in multi-colour experiments to this end, in order to calibrate the cytometer for removal of spectral overlap. Spectral overlap was also prevented, where possible, by selecting fluorophores that could be excited and detected by separate laser-detector combinations.

Positive control samples were also included, where available, by preparation of a sample of cells known to express the target protein of interest or by including a sample stained for a marker that is known to be expressed in the test cell population. These were processed in the same manner as stained experimental samples and were used to eliminate the possibility of false negative results caused by sub-optimal immunostaining due to a procedural error or ineffective antibodies.

2.5.2. Cytofluorimetric Assessment of Cell Cycle Status

2.5.2.1. Univariant Cell Cycle Analysis Using Propidium Iodide

Samples of 1.0×10^6 cells were removed from harvested cell suspensions and were transferred to separate 15ml centrifuge tubes. Centrifugation was then undertaken for 5 minutes at 150 x g and 25°C. The resultant supernatant was removed from each cell pellet and was discarded. Cells were washed twice by resuspension in PBS and repeating centrifugation as previous. The washed cell pellets were then simultaneously fixed and permeabilised by resuspension in a 1ml volume of an ice-cold solution of 70% (v/v) ethanol in ultra-pure (18MΩ) distilled water that was added drop-wise during low speed vortexing. All ethanolic cell suspensions were placed inside a refrigerator maintained at 4°C overnight. On the following day, a 5ml volume of ice-cold PBS was added to each ethanolic cell suspension followed by gentle vortexing, and then centrifugation undertaken at 1000 x g for a 5-minute period. The resultant supernatant was carefully discarded from the cell pellet before addition of a further 5ml of ice-cold PBS. Centrifugation was then undertaken exactly as previous. During this time, Ribonuclease A (RNase A) from bovine pancreas (Sigma-Aldrich Company Ltd.) was added to a 75μM solution of propidium iodide to a final concentration of 0.002% (w/v). Once centrifugation was complete, the resultant supernatant was discarded and each cell pellet resuspended in a 500μl volume of the freshly prepared propidium iodide-RNase A solution. Samples were then protected from light and incubated for at least 60 minutes before being analysed by flow cytometry.

2.5.2.2. Univariant Cell Cycle Analysis in Live Cells Using Hoechst 33342

Hoechst 33342 stock solution was purchased from Life Technologies Ltd. and was supplied at a concentration of 10mg/ml in distilled water. Immediately prior to use, an appropriate volume of a 1mg/ml working solution was prepared by undertaking a 1:10 dilution of the Hoechst 33342 stock solution using distilled water as diluent. Freshly prepared Hoechst 33342 working solution was stored at ambient temperature protected from light until required. Samples of 1.0×10^6 cells were prepared from harvested cell suspensions inside separate 15ml centrifuge tubes and centrifuged for 5

minutes at 150 x g and 25°C. The resultant supernatant was removed from each cell pellet and was discarded. Cells were then gently resuspended in 1ml of pre-warmed serum-free basal cell culture medium. A 5µl volume of the 1mg/ml Hoechst 33342 working stock solution was added to all samples (f.c. 5µg/ml), which were then mixed well by rapid vortexing, protected from light and incubated in a water bath maintained at 37°C for a 45 minute period. Following incubation, samples were strained through 40µm cell strainers into round-bottomed polystyrene flow cytometry tubes and immediately analysed by flow cytometry.

2.5.3. Aldehyde Dehydrogenase Activity Assay

Aldehyde dehydrogenase (ALDH) activity was determined using the non-immunological ALDEFLUOR™ assay kit available from STEMCELL™ Technologies U.K. Ltd. (Cambridge, U.K.). The inactive ALDEFLUOR™ reagent BODIPY-aminoacetaldehyde-diethylacetate (BAAA-DA) was supplied as a dry solid. The dry BAAA-DA was dissolved in DMSO and converted to the activated fluorescent form BODIPY-aminoacetaldehyde (BAAA) by treatment with 2N hydrochloric acid prior to use, according to the manufacturers instructions. Briefly, 25µl of DMSO was added to the vial of dry BAAA-DA, followed by immediate thorough mixing and incubation for 1 minute at ambient temperature while protected from light. A 25µl volume of 2N hydrochloric acid was then added to the vial, which was again mixed thoroughly and incubated for 15 minutes at ambient temperature while protected from light. A 360µl volume of ALDEFLUOR™ assay buffer was then added to the vial and mixed thoroughly. The dilute activated ALDEFLUOR™ reagent was aliquoted and store at -20°C until required for use.

Samples of 1.0 x 10^6 cells were removed from retrieved cell suspensions and transferred to separate microcentrifuge tubes. Centrifugation was undertaken at 150 x g for 5 minutes and the resultant supernatant discarded. Cell pellets were washed by resuspension in 1ml of PBS followed by immediate centrifugation as previous. Washed samples were resuspended in 1ml of ALDEFLUOR™ assay buffer. A 5µl volume of the activated ALDEFLUOR™ reagent was added to each millilitre of sample followed by gentle vortexing. A 0.5ml volume of suspension was then removed and transferred to

a separate control tube containing 5µl of the specific aldehyde dehydrogenase inhibitor diethylaminobenzaldehyde (DEAB) followed by immediate mixing. Both test and corresponding control tubes were incubated for 45 minutes at 37°C protected from light. Following incubation, all tubes were centrifuged for 5 minutes at 150 x *g* and the supernatant discarded. Each resultant pellet was resuspended in 0.5ml of ALDEFLUOR™ assay buffer and each tube placed on ice prior to flow cytofluorimetric analysis (**Figure 2.8.**).
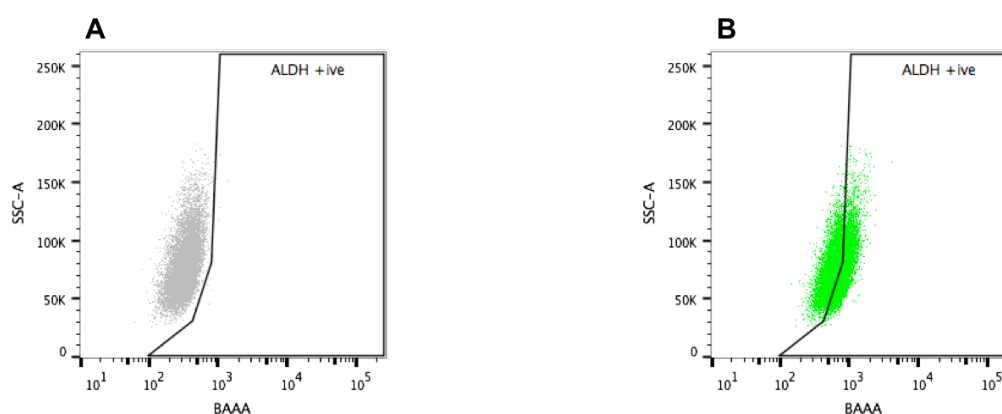
Figure 2.8. Flow Cytometric Detection of Cellular ALDH Activity

A: A sample of cells treated with the specific aldehyde dehydrogenase (ALDH) inhibitor diethylaminobenzaldehyde (DEAB) was used to set the gate in the appropriate detector channel for the detection of oxidised BODIPY-aminoacetaldehyde (BAAA) that indicates cellular ALDH activity **B**: Experimental samples were analysed using the gating strategy pre-set using DEAB treated controls, thereby allowing detection of ALDH positive cells as events exceeding the relative fluorescence profile of the corresponding DEAB treated control.

2.6. Establishing Drug Dose-Response Curves

2.6.1. Preparation of MTT Reagent

Methylthiazolyltetrazolium bromide (MTT) was prepared as a 0.5% (w/v) stock solution in PBS; 1g of MTT powder (Sigma-Aldrich Company Ltd.) was added to a final volume of 200ml of PBS. Complete dissolution was achieved by continuous stirring for a one-hour period on a heated magnetic stirrer plate maintained at 37°C. The solution was protected from light throughout. Once dissolved, the MTT stock was sterilised by filtration through a 0.2μm polycarbonate filter and was then aliquoted as 5ml volumes and stored at -20°C until required. Immediately prior to use, frozen aliquots were thawed rapidly by placing into a water bath maintained at 37°C for approximately 5 minutes, after which they were mixed thoroughly by vortexing before being diluted 1:5 in complete growth medium to produce a working solution with a final concentration of 0.1% (w/v).

2.6.2. Optimisation of MTT Assay Conditions

The optimal MTT concentration and incubation time for use during MTT assays were originally established by (Mosmann, 1983) and (Denizot and Lang, 1986); the recommended MTT concentration of 1mg/ml and an incubation period of 3 hours was used in accordance with these pre-validated recommendations. A standard curve for both MCF-7 and MDA-MB-231 cell lines was generated in order to establish the linearity of the relationship between cell number and the absorbance reading at 540nm obtained following the MTT assay procedure in order to ensure that the cell line specific optimal seeding densities to be used in subsequent cytotoxicity assays did not lead to delineation of this relationship after the intended assay period. Briefly, both MCF-7 and MDA-MB-231 cells were seeded into the wells of a high-quality polystyrene 96-well flat-bottomed cluster plate (Scientific Laboratory Supplies Ltd.) in triplicate at a range of densities (1000 - 20, 000 cells per well) and supplemented with 100μl of complete growth medium. A row of blank wells containing medium alone (no cells) was prepared at either end of the plate. Plates were incubated overnight under standard growth conditions in order to allow cells to recover and adhere to the base of

the wells. All wells (including blank wells) were then completely drained and re-filled with a 100μl volume of freshly prepared MTT reagent prepared as described previously (**Section 2.6.1.**). Plates were then replaced in incubation for a period of 3 hours. Subsequently, all wells were once again drained of their contents and 100μl of DMSO added. Plates were then protected from light by wrapping in aluminium foil and placed on a plate-shaker set to 180 revolutions per minute for a 15-minute duration prior to being read spectrophotometrically at a wavelength of 570nm using a SpectraMax® M5 multi-mode plate reader (Molecular Devices U.K. Ltd., Wokingham, U.K.).

2.6.3. Drug Dose-Response Assay Procedure

Cells were seeded at the cell line specific optimal density into the wells of a high-quality polystyrene 96-well flat-bottomed cluster plate and supplemented with 100μl of complete growth medium. A row of blank wells containing medium alone (no cells) was prepared at either end of the plate according to the plate set-up schematic depicted in **Figure 2.9.** Plates were incubated overnight under standard growth conditions in order to allow cells to recover and adhere to the base of the wells. On the subsequent day, drug solutions were freshly prepared along with solvent control solutions composed of complete growth medium and the percentage of solvent equivalent to that present in the highest drug concentration being tested. Following overnight incubation, the spent medium was removed from all wells. Each well was filled with a 200μl volume of complete growth medium (growth controls), the appropriate solvent control solution (vehicle controls), or one of the pre-prepared drug-containing solutions according to the plate set-up schematic depicted in **Figure 2.9.** Plates were then replaced in incubation for a period of time equivalent to the duration of the logarithmic phase of culture growth specific to the cell line being used. Following incubation in the presence of drug for the appropriate period, all wells (including blank wells) were completely drained and re-filled with a 100μl volume of freshly prepared MTT reagent prepared as described previously (**Section 2.6.1.**). Plates were then replaced in incubation for a further period of 3 hours. Subsequently, all wells were once again drained of their contents and 100μl of DMSO added. Plates were then protected from light by wrapping in aluminium foil and placed on a plate-shaker set to 180 revolutions per minute for a 15-minute duration prior to being read

spectrophotometrically at a wavelength of 570nm using a SpectraMax® M5 multi-mode plate reader.
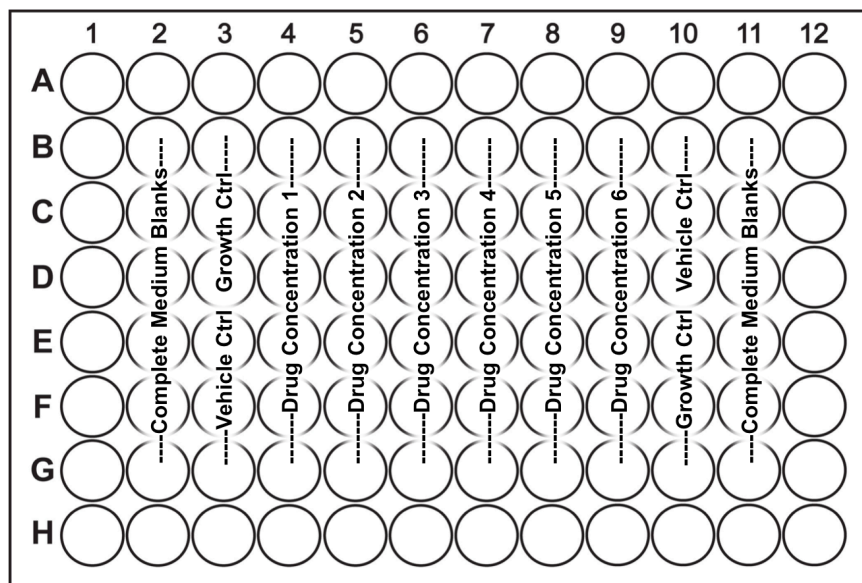
Figure 2.9. Plate Configuration for Drug-Dose Response Assessment by MTT Assay

Peripheral wells were filled with 200µl of 0.2µm filter-sterilised ultrapure (18MΩ) water. Blank wells containing only complete culture medium were prepared at either end of the plate. Growth controls (denoted as "Growth Ctrl" here) contained adherent cells and a 200µl volume of complete growth medium only while vehicle controls (denoted as "Vehicle Ctrl" here) contained adherent cells and a 200µl volume of complete growth medium along with the equivalent percentage of solvent present in the highest drug concentration being tested. Drug solutions were added to each plate in order of decreasing concentration from left to right.

2.7. Western Blotting

2.7.1. Preparation of Whole Cell Lysate

Culture vessels were placed on ice and the cells washed twice with ice-cold PBS. Cultures were harvested into 0.2ml PBS per cm^2 growth area using a plastic cell scraper. The retrieved cell suspensions were transferred to separate pre-cooled centrifuge tubes and the vessels washed with an equivalent volume of ice-cold PBS that was also transferred to the corresponding centrifuge tube. Samples were subjected to centrifugation for 5 minutes at 150 x g and 4^oC. The supernatant was drained and the cell pellet resuspended in 100µl of RIPA lysis buffer (150mM sodium chloride, 1.0% (v/v) IGEPAL® CA-630, 0.5% (w/v) sodium deoxycholate, 0.1% (w/v) sodium dodecyl sulphate (SDS) and 50mM Tris in 18MΩ distilled water, pH 8.0 at 4^oC) with 0.1% (v/v) protease inhibitor cocktail (all from Sigma-Aldrich Company Ltd.). Samples were incubated on ice with constant agitation maintained for 30 minutes before being subjected to centrifugation at 10,000 x g for 10 minutes. Tubes were placed directly on ice subsequently and the supernatant (lysate) transferred to a separate pre-cooled microcentrifuge tube while the pellet (cell debris) was discarded. Lysates were routinely used immediately but can be stored at -20^oC short-term or at -80^oC for a longer duration.

2.7.2. Determination of Lysate Protein Concentration

A series of five BSA protein standard solutions were prepared by dilution of 1mg/ml BSA protein standard (Sigma-Aldrich Company Ltd.) in lysis buffer to concentrations of 0 - 800µg/ml. Cell lysates were diluted 1:10 in lysis buffer. BCA (bicinchoninic acid) protein assay reagent was composed by addition of 1 part 0.1M copper (II) sulphate solution to 50 parts bicinchoninic acid solution (both from Sigma-Aldrich Company Ltd.). A 200µl volume of this solution was added to 10µl volumes of samples and standard solutions pipetted into triplicate wells of a 96-well assay plate. The plate was covered with paraffin film and incubation undertaken at ambient temperature for 30 minutes. The final absorbance was read at a wavelength of 500nm using a SpectraMax® M5 multi-mode plate reader.

2.7.3. Electrophoresis

Protein samples were prepared in 4x protein sample buffer (40% (v/v) glycerol, 8% (w/v) SDS, 0.04% (w/v) bromophenol blue and 240mM Tris hydrochloride in 18MΩ distilled water, pH 6.8 at 37°C) with 50mM dithiothreitol added at the time of formulation. Final total protein per sample was typically 20 - 40μg (depending on the protein concentration of cell lysates). Volumes were made up to a final volume of 15μl using 18MΩ distilled water. Denaturation of protein was achieved by heating at 95°C for 10 minutes followed by a brief centrifugation to ensure any evaporated liquid in the cap of the microcentrifuge tube was returned to the bottom. The total 15μl volume of each sample was loaded into the wells of a 4-20% Mini-PROTEAN® TGX™ precast polyacrylamide gel (Bio-Rad Laboratories Ltd., Hemel Hempstead, U.K.). A gradient gel such as this was routinely used for electrophoresis of whole cell lysates as the acrylamide concentration gradient from the beginning (top) to end (bottom) of the sample path allows the separation of a broad range of protein sizes. One well was loaded with a 7μl volume of Precision Plus Protein™ Dual Xtra Pre-stained Protein Standards (Bio-Rad Laboratories Ltd.) used as molecular weight markers. Electrophoresis was undertaken at 130V for 1 – 2 hours.

2.7.4. Transfer

A single piece of Polyvinylidene fluoride (PVDF) membrane (Thermo Fisher Scientific) cut to the exact size of the gel was soaked in absolute methanol for 30 seconds followed by washing in 18MΩ distilled water for 5 minutes with constant agitation. Following washing, the membrane was placed in transfer buffer (0.025M Tris, 0.192M glycine and 10% (v/v) methanol in 18MΩ distilled water, pH 8.5 at 37°C) and allowed to equilibrate for 5 minutes. Four pieces of blotting paper and transfer sponges were also soaked in transfer buffer during this time. The gel was sandwiched within the blotting module between sponges and blotting paper as depicted in **Figure 2.10.** ensuring that no air bubbles were trapped between layers. The blotting module was placed into the gel tank along with an ice pack before the tank was completely filled with transfer buffer. The transfer was then undertaken at 70V for 1.5 – 2 hours.
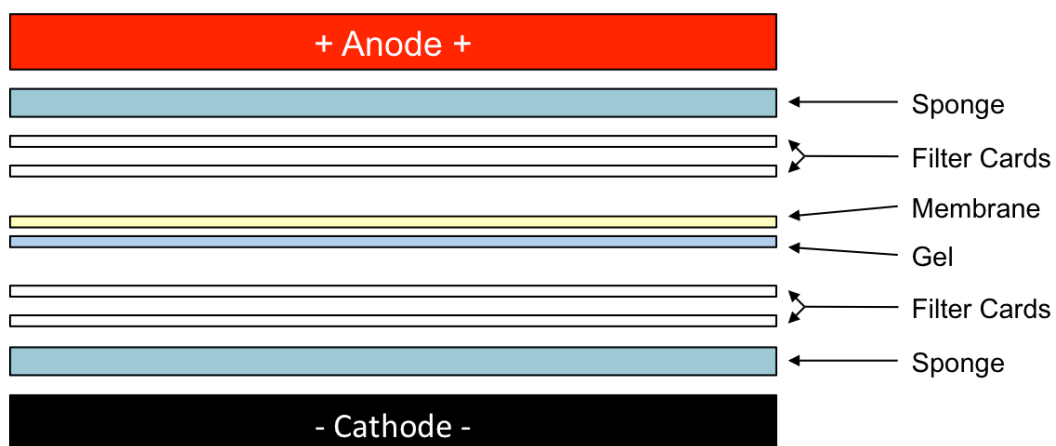
Figure 2.10. Western Blot Transfer Module Configuration

Prior to performing a wet transfer, the polyacrylamide gel was first equilibrated in transfer buffer before being placed in the "transfer sandwich" (filter cards-membrane-gel-filter cards) cushioned by sponge pads and held together by a support grid. All components of the transfer sandwich were pre-equilibrated in transfer buffer.

2.7.5. Protein Detection

Following transfer, the PVDF membrane was placed in a blocking solution of 10% (w/v) non-fat milk powder in Tris-buffered saline (25mM Tris, 0.15M sodium chloride, pH 7.5 at 37°C) with 0.05% (v/v) Tween®20 (TBST) for 30 minutes. During this time, primary antibodies against the protein of interest and a pre-selected housekeeping protein were diluted to the desired concentration in a solution of 5% (w/v) non-fat milk powder in TBST to produce a 5ml final volume of dilute antibody solution. The PVDF membrane was loaded into a 50ml centrifuge tube and the total 5ml volume of dilute primary antibody solution added. Tubes were placed onto a roller and incubated at 4°C overnight. On the subsequent day, the PVDF membrane was removed from the primary antibody solution and washed three times in TBST for 10 minutes per wash. Horseradish peroxidase (HRP) conjugated polyclonal secondary antibodies were diluted to the desired concentration in 5% (w/v) non-fat milk powder in TBST to produce a 5ml final volume of dilute antibody solution. The PVDF membrane was incubated in the presence of secondary antibody solution for 1 hour at ambient temperature. The membrane was then washed with TBST three times for 10 minutes per wash. SuperSignal™ West Pico Chemiluminescent HRP substrate (Thermo Fisher Scientific) was used for detection and localisation of antibody bound to the PVDF

membrane; equal volumes of peroxide and luminol enhancer solutions were mixed and subsequently used to cover the PVDF membrane. The membrane was then imaged immediately using the Bio-Rad ChemiDoc™ MP Imaging System with Image Lab™ software (Bio-Rad Laboratories Ltd.).

All information regarding specific primary and secondary antibodies used in western blot procedures are detailed later in the respective methods sections of the experiments in which they were used.

2.8. Biochemical Assays

2.8.1. β-Galactosidase Assay

The activity of β-galactosidase at pH 6.0 is a widely used marker of cellular senescence and is not found in pre-senescent, quiescent or immortal cells. Cellular β-galactosidase activity at pH 6.0 was assayed using the β-galactosidase staining kit available from New England Biolabs U.K. Ltd. (Hitchin, U.K.). A bone-homing MDA-MB-231 variant cell line that was engineered to stably express β-galactosidase (denoted MDA-MB-231-BO2-β-gal) was used as a positive control for β-galactosidase activity. Briefly, experimental and positive control samples of cells were seeded in triplicate into the wells of 6-well cluster plates at the cell-line specific optimal density supplemented with a 3ml volume of complete culture medium and placed into incubation under standard growth conditions for 24 hours. For each 35mm well to be stained, a staining solution comprised of 930μl of 1X staining solution (40mM citric acid/sodium phosphate, 0.15M sodium chloride and 2mM magnesium chloride), 10μl of 500mM potassium ferrocyanide, 10μl of 500mM potassium ferricyanide and 50μl of 20mg/ml 5-bromo-4-chloro-3-indolyl-β-D-galactopyranoside (X-gal) in dimethylformamide was composed inside of a polypropylene tube and the pH adjusted to pH 6.0 using 2N hydrochloric acid immediately prior to requirement. Growth medium was removed from all wells to be stained and the adherent cells rinsed once with a 2ml volume of PBS. Cells were fixed in 2% (v/v) formaldehyde and 0.2% (v/v) glutaraldehyde in PBS for 15 minutes at ambient temperature. All wells were then rinsed two times with PBS as previous. A 1ml volume of freshly prepared staining solution was added to each 35mm well, the plate edges sealed with paraffin film in order to prevent evaporation and all plates placed into a non-humidified CO_2-free incubator maintained at 37°C overnight. Following overnight incubation, positive control wells were checked for the development of the green/blue staining indicative of β-galactosidase activity prior to photomicroscopic image acquisition.

2.8.2. Determination of D-Glucose Concentration in Culture Medium

The concentration of D-glucose present in solution was determined using the D-glucose assay kit available from Eton Bioscience Inc. (San Diego, CA, U.S.A.). Briefly, the 800µM D-glucose standard and glucose assay solution contained within the assay kit were removed from storage at -80°C and thawed on ice overnight at in a refrigerator maintained at 4°C. Once thawed, the D-glucose standard and experimental samples were allowed to equilibrate to ambient temperature prior to undertaking the assay procedure, while the assay reagent was kept on ice protected from light. The D-glucose standard was first diluted 1:2 with dH$_2$O; 500µl of standard (as supplied) was diluted with 500µl of dH$_2$O. This dilute D-glucose standard (f.c. 400µM) was then used to compose a series of eight D-glucose standard solutions with concentrations between 400µM and 8µM along with a 0µM dH$_2$O blank control solution. Experimental samples were then diluted according to the maximal D-glucose content present in the basal medium as stated by the respective supplier in order to ensure that optical density readings post-assay would fall into the range of the standard curve. A 50µl volume of each standard solution and experimental sample was then added in duplicate directly to the wells of a standard 96-well assay plate. A 50µl volume of D-glucose assay reagent was then added to all wells, the plate sealed with paraffin film and placed into incubation for 15 minutes at 37°C in a non-humidified CO$_2$-free incubator. Following incubation, the reaction within all wells was stopped by addition of a 50µl volume of 0.5M acetic acid followed by gentle agitation. The absorbance was measured spectrophotometrically at a wavelength of 490nm using a SpectraMax® M5 multi-mode plate reader. The D-glucose concentration of experimental samples was determined by interpolation of the recorded absorbance measurement from the standard curve.

2.8.3. Determination of L-Lactate Concentration in Culture Medium

The concentration of L-lactate present in solution was determined using the L-lactate assay kit available from Eton Bioscience Inc. Briefly, the 3mM L-lactate standard and lactate assay solution contained within the assay kit were removed from storage at -80°C and thawed on ice overnight at in a refrigerator maintained at 4°C. Once thawed, the L-lactate standard and experimental samples were allowed to equilibrate to ambient temperature prior to undertaking the assay procedure, while the assay reagent was kept on ice protected from light. The L-lactate standard was then used to compose a series of eight L-lactate standard solutions with concentrations between 3mM and 60µM along with a 0µM dH$_2$O blank control solution. Experimental samples were then diluted according to the maximal possible L-lactate content that could be present based on complete homolactic fermentation of the entire D-glucose content of the basal medium according to the respective supplier. This process was necessary to ensure that the optical density readings post-assay would fall into the range of the standard curve. A 50µl volume of each standard solution and experimental sample was then added in duplicate directly to the wells of a standard 96-well assay plate. A 50µl volume of L-lactate assay reagent was then added to all wells, the plate sealed with paraffin film and placed into incubation for 30 minutes at 37°C in a non-humidified CO$_2$-free incubator. Following incubation, the reaction within all wells was stopped by addition of a 50µl volume of 0.5M acetic acid followed by gentle agitation. The absorbance was measured spectrophotometrically at a wavelength of 490nm using a SpectraMax® M5 multi-mode plate reader. The L-lactate concentration of experimental samples was determined by interpolation of the recorded absorbance measurement from the standard curve.

2.9. Statistical Analyses

All statistical analyses were undertaken using GraphPad Prism 7 (GraphPad Software Inc., La Jolla, U.S.A.). All data were expressed as the mean average ± the standard error of the mean (SEM). The statistical analysis applied to data, where undertaken, is indicated within the respective figure legend. Statistical significance was attributed when $P < 0.05$.

Chapter 3

Establishing an *In Vitro* Model for the Study

of Mitotically Quiescent Breast

Cancer Cells

3.1. Summary

Emerging evidence strongly suggests that putative cancer stem cells are the metastasis-initiating population in breast cancer. Breast cancer stem cells are presumed to be mitotically quiescent, like their non-malignant counterparts, and therefore capable of evading conventional anti-neoplastic therapy and driving both tumour relapse and recurrence at secondary sites. Detailed insight into cancer stem cell biology is therefore likely to be critical to the development of novel therapeutic strategies for prevention and effective treatment of metastatic breast cancer. Contemporary means of identifying cancer stem cells based on specific cell surface marker signatures have proved controversial due to the transience of this population and the lack functional significance associated with this approach. The requirement exists, therefore, for reliable and functionally informed model systems enabling the characterisation of cancer stem cell populations. Relatively recently, pulse-chase techniques for assessment of stem cells based on their inherent quiescent nature has undergone something of a renaissance due to the advent of lipophilic tracer dyes that have enabled the isolation and analysis of live cells. While a number of studies in other cancer types have demonstrated the prospective identification of cancer stem cells or stem-like populations using this approach, it's potential utility in breast cancer remains virtually unexplored. This chapter describes the development of a highly reproducible *in vitro* model system enabling prospective functional isolation of a putative stem-like mitotically quiescent sub-population from human breast cancer cell lines using a lipophilic dye retention method.

3.2. Introduction

A substantial body of evidence indicates that the pathogenesis of many cancers, including breast cancer, is driven by a sub-population that displays stem cell properties. These so-called cancer stem cells (CSCs) are thought to be responsible not only for initiation and growth of the primary tumour but also for therapeutic resistance and the initiation of metastatic lesions (recently reviewed by Luo *et al.*, 2015). Cancer stem cell populations, like their non-malignant counterparts, are hierarchically organised and maintained by a process of self-renewal in which slow-cycling stem cells divide asymmetrically to generate new stem cells and rapidly dividing transit-amplifying cells (Oakes *et al.*, 2014). Cells that exist in a slow-cycling or an absolute quiescent state are inherently less susceptible to traditional chemotherapeutic agents that rely on mitotic activity to initiate cytotoxicity (Moore and Lyle, 2011). This observation suggests an inherent recurrence mechanism in which CSCs evade therapeutic targeting. A detailed insight into the biology of quiescent CSCs is therefore likely to be critical to the development of effective novel therapeutic strategies for prevention of cancer relapse and recurrence. However, in order to study CSCs it is first necessary to isolate them using techniques that enable their differential identification amongst the bulk tumour cell population.

Contemporary approaches for selective identification of CSCs primarily rely on expression of specific cell surface marker profiles. Bonnet and Dick (1997) originated this technique when they first demonstrated initiation of acute myeloid leukaemia by a self-renewing, primitive hematopoietic cell sub-set with a unique $CD34^+CD38^-$ phenotype. Since this pioneering study, CSC populations have been identified in this manner in multiple cancers including those of breast, prostate, pancreas, colon, liver ovaries, head and neck, and the brain (Al-Hajj *et al.*, 2003; Singh *et al.*, 2004; Collins *et al.*, 2005; Li *et al.*, 2007; Ma *et al.*, 2007; O'Brien *et al.*, 2007; Prince *et al.*, 2007; Gao *et al.*, 2010). In breast cancer, a tumour initiating stem cell-like population was first identified by way of their $EpCAM^+CD44^+CD24^{-/low}$ surface marker expression profile (Al-Hajj *et al.*, 2003). When injected into immunocompromised mice, the gold standard for assessing breast CSC activity, $EpCAM^+CD44^+CD24^{-/low}$ cells exhibited over 100-fold greater tumourigenicity than cells lacking this phenotype and were also able to

recapitulate the cell-type heterogeneity of the original tumour. More recently it has been reported that both normal breast stem cells and their malignant counterparts are demarked by increased expression of ALDH, a known predictor of poor clinical outcome (Khoury *et al.*, 2012; Papadaki *et al.*, 2014; Yang *et al.*, 2016). Both the CD44$^+$CD24$^{-/low}$ and ALDH$^+$ phenotypes have been extensively used for prospective isolation of CSCs from different molecular sub-types of breast cancer over recent years. However, a study by Ginestier *et al.* (2007) conclusively demonstrated that CD44$^+$CD24$^{-/low}$ and ALDH$^+$ phenotypes identify minimally overlapping stem-like populations that are genetically, phenotypically and spatially distinct but dynamically transitioning. Meyer *et al.* (2010) more recently reported that both CD44$^+$CD24$^{-/low}$ and CD44$^+$CD24$^+$ phenotypic sub-sets identified in oestrogen receptor-negative breast cancer are tumourigenic in mouse xenograft models. These contrasting and sometimes confounding results illustrate the issues that can arise due to the plasticity of the CSC population and the uncertainty that surrounds the functional implications of putative CSC surface markers. These issues highlight the requirement for incorporating functionally significant means of identifying CSCs.

Functional approaches to isolation of CSCs can primarily be sub-divided into vital dye exclusion and label-retention assays. The dye exclusion method is predicated on the observation that both normal and malignant stem cell populations demonstrate up-regulated expression of adenosine 5'-triphosphate-binding cassette transporter proteins and therefore possess an increased capability to efflux fluorescent vital dyes (Bunting, 2002). This dye-exclusion activity results in a side-population that can be isolated for further study by FACS (Hadnagy *et al.*, 2006). A number of studies employing this technique have demonstrated the existence of side-populations enriched for stem-like properties and enhanced tumourigenicity in various molecular sub-types of human breast cancer (Patrawala *et al.*, 2005; Nakanishi *et al.*, 2010; Britton *et al.*, 2012).

The elucidation of the hierarchical self-renewal process employed by stem cell populations resulted in the development of pulse-chase label-retention approach to identification and isolation of quiescent CSCs. In early studies that employed this technique, cells were initially labelled with either tritiated thymidine (^{3}H-TdR) or 5-

bromo-2-deoxyuridine (BrdU) which then partition equally between dividing transit amplifying cells and their progeny on subsequent cell divisions resulting in an exponential decrease in signal intensity; as a result of their mitotically quiescent nature, stem cells retain their initial label and therefore remain identifiable amongst the non-label retaining population (Cotsarelis *et al.*, 1990; Potten *et al.*, 1992). More recently, nucleotide analogues such as ^{3}H-TdR and BrdU, which require cell membrane permeabilisation and antibody labelling for their detection, have been superseded by lipophilic fluorescent membrane dyes for this purpose, thereby enabling live sorting of cells for subsequent study (**Figure 3.1.**).
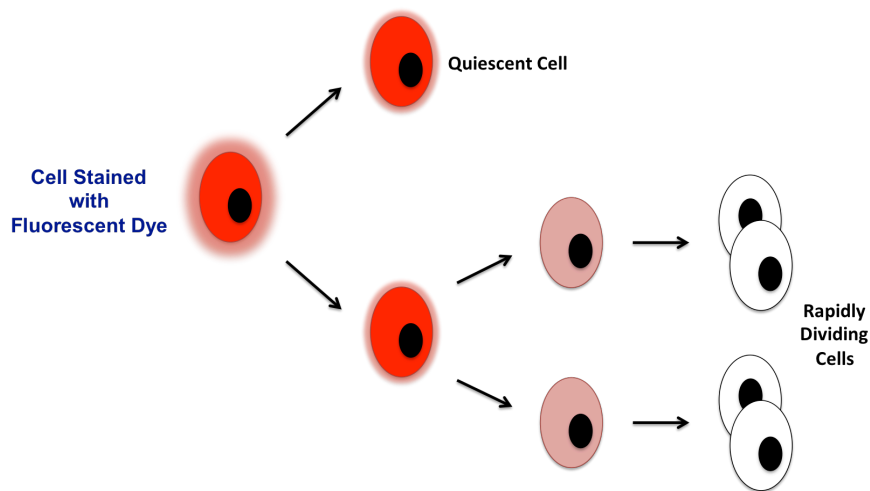
Figure 3.1. Detection of Quiescent Cells by Lipophilic Dye Label-Retention Assay

Cell cultures are initially labelled homogenously with a highly lipophilic fluorescent dye. The dye label is then subsequently lost from the rapidly dividing bulk cell population by progressive dilution during subsequent mitotic divisions while slowly dividing or mitotically quiescent cells remain identifiable as a persistent bright fluorescent signal over time.

Using this approach, Yumoto *et al.* (2014) described the identification of a slowly cycling sub-population in a number of human prostate cancer cell lines based on the persistent retention of the lipophilic tracer dye Vybrant® DiD. Expanding on these findings, Wang *et al.* (2015a) demonstrated that the label-retaining quiescent prostate cancer cell population possessed a unique gene expression profile, mimicking the deployment of a number of haematopoietic stem cell niche-associated markers. In addition, these cells were found to be significantly more bone tropic and tumourigenic *in vivo* compared to the rapidly dividing cell population isolated from the same parental culture. Label-retaining cells did however lack differential expression of commonly used prostate cancer stem cell markers (CD133, CD44 and α2/β1 integrins), suggesting that mitotic quiescence is associated with a unique phenotype that partially overlaps with stemness defined by cell surface marker expression. Similar findings were reported in a study of pancreatic adenocarcinoma undertaken by Dembinski and Krauss (2009). In this study, a slow-cycling label-retaining population comprising approximately 3% of total cell mass was shown to possess a fibroblastic morphology and marker profile indicative of epithelial-mesenchymal transition, were significantly more invasive *in vitro*, and were ten-times more tumourigenic *in vivo* than the non-label retaining population. Interestingly, when assessed for common CSC surface markers, label-retaining cells were enriched for, but only partially overlapped with, the common $CD24^+CD44^+CD133^+$ marker profile thought to demark pancreatic cancer stem cells.

In breast cancer, use of the lipophilic membrane dye retention technique has almost entirely been restricted to retrospective validation of putative cancer stem cell populations isolated using cell surface markers. Quiescent breast tumour cell populations have therefore remained relatively poorly characterised and the degree of non-mutual exclusivity between this population and stem-like cells isolated using common surface marker profiles unexplored. As a consequence, it is entirely feasible that our current understanding of breast cancer stem cell biology is not truly reflective of the entire CSC population and the true potential for their therapeutic targeting remains only partially realised.

3.3. Aims, Hypothesis and Objectives

The aim of the work described in this chapter was to establish a robust and highly reproducible *in vitro* model system enabling the isolation and subsequent characterisation of mitotically quiescent breast cancer cells.

The key hypothesis pertaining to the work described in this chapter was that ***human breast cancer cell lines contain a latent mitotically quiescent sub-population that persists amongst the rapidly dividing bulk cell population.***

The following objectives were defined in order to test this hypothesis:

1. Characterise the growth kinetics of a panel of human breast cancer cell lines in order to facilitate definition of the interval at which lipophilic dye retention would be measured in each case.

2. Determine the suitability of select fluorescent lipophilic tracer dyes for the application of detecting mitotically quiescent cells.

3. Establish whether or not a quiescent sub-population was existent within each model cell line by pulse-chase analysis of fluorescent lipophilic tracer dye labelling.

4. Determine whether dye-retaining cells were senescent, absolutely quiescent (non-senescent and non-dividing) or relatively quiescent (slowly cycling).

3.4. Method Development and Results

3.4.1. Characterising the Growth of Breast Cancer Cell Lines in Monolayer Culture

Establishing the growth characteristics of a model cell culture under optimal conditions facilitates comparison of the effects of exogenous factors to an established baseline. In addition, the descriptive statistics that describe the growth profile of any given culture can be used to inform subsequent experimental procedures. The growth profiles of MCF-7, ZR-75-1, MDA-MB-231, MDA-MB-468 and SK-BR-3 human breast cancer cell lines were therefore established initially. Growth profiles were constructed by monitoring the number of viable cells present within each culture at 24-hour intervals post-seeding according to the methods described in **Section 2.2.5.** The resultant growth curves are depicted in **Figure 3.2.**

All growth profiles largely followed the classic sigmoidal pattern. In each case, an initial period of delayed growth (lag phase) was followed by a rapid increase in the culture growth rate that preceded a period of linear expansion of viable cell number in each culture over time (logarithmic phase). Gradually, a reduction in the rate of culture expansion was recorded in all instances, likely due to the exhaustion of available nutrients and a build-up of waste metabolites in the culture medium (stationary phase). In the case of MDA-MB-231, MDA-MB-468 and SK-BR-3 cell lines, a decline phase was also evident at later time-points, during which there was a progressive reduction in the number of viable cells present within cultures. Growth profiles were used to define the time of onset, end-point and duration of the logarithmic phase of growth and the log-phase doubling time of the respective culture. These descriptive parameters are summarised for each model cell line in **Table 3.1.** Growth profiles were also used to define the time-point at which cultures were approximately 80% confluent and at which sub-culture would therefore be undertaken during routine maintenance and pulse-chase experiments. The respective sub-culture interval for each cell line is displayed in **Table 3.1.**
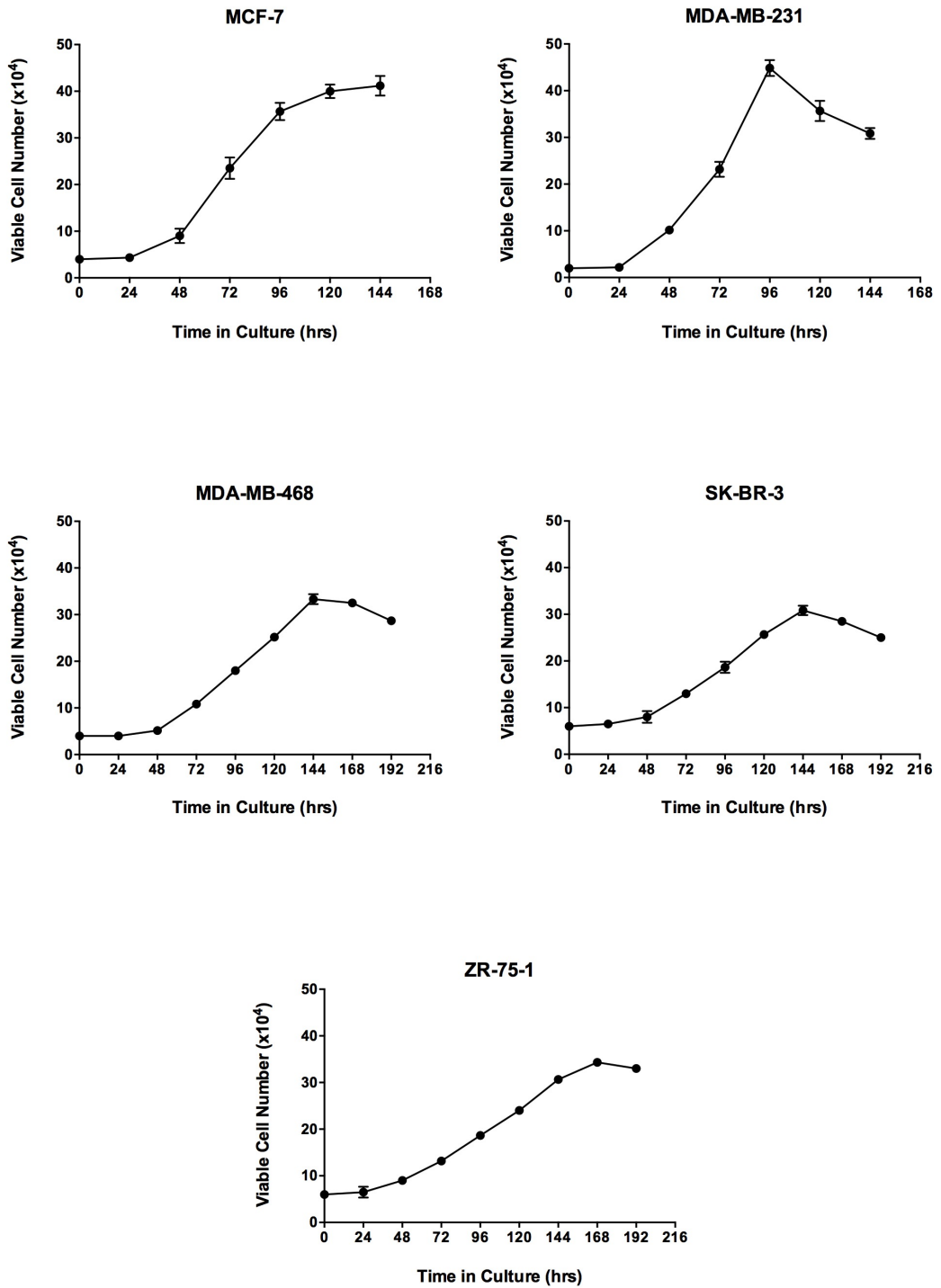
Figure 3.2. Model Cell Line Growth Curves

The proliferation curves for the MCF-7, MDA-MB-231, MDA-MB-468, SK-BR-3 and ZR-75-1 human breast cancer cell lines are shown; the number of viable cells (Y-axis) is plotted against the duration of culture post-seeding (X-axis) in each case. Data are expressed as the mean average ± SEM for n = 3 biologically independent repeat experiments.

Table 3.1. Summary of Descriptive Statistics for Model Culture Growth Curves

Cell Line	MCF-7	ZR-75-1	MDA-MB-468	MDA-MB-231	SK-BR-3
Molecular Sub-Type	Luminal A	Luminal B	Basal	Claudin Low	HER-2
Log-Phase Start (Hours)	24	24	48	24	48
Log-Phase End (Hours)	96	168	144	96	144
Log-Phase Duration (Hours)	72	144	96	72	96
Log-Phase Doubling Time (Hours)	25	60	36	17	44
Sub-Culture Interval (Hours)	96	144	120	72 - 96	120

The descriptive statistics describing the key features of the respective growth curve for each model cell line are shown. All times displayed are stated to the nearest 24-hour period, as determined graphically, with the exception of the log-phase doubling time which was calculated as described in Section 2.2.5. using graphically determined input variables.

3.4.2. Selection of Tracer Dyes for Identification of Quiescent Sub-Clones

The lipid intercalating long alkyl side-chain carbocyanine derivatives, such as the Vybrant® dye series, and the structurally related PKH dye series are by far the most frequently used supravital lipophilic fluorochromes for cell tracing and tracking applications in cancer studies (Progatzky *et al.*, 2013; Luo *et al.*, 2015). Dyes of both series are stably incorporated into the lipid bilayer of cell membranes and subsequently diffuse laterally to result in uniform staining of individual cells and homogenous staining of cultures. When present within biological membranes, dyes of both series characteristically exhibit strong fluorescence and photostability as a result of their extremely high extinction coefficients, modest quantum yields, and short excited-state lifetimes within lipid environments, making their lipid intercalating and photochemical properties ideally suited to long-term lineage tracing applications (Horan and Slezak, 1989; Samlowski *et al.*, 1991). However, the potential for confounding results due to inadvertent lateral dye transfer, cytotoxicity and loss of cellular function following initial staining is greater when using PKH rather than Vybrant® dyes based on literary reports (Li *et al.*, 2013; Progatzky *et al.*, 2013). In addition, the initial labelling of cells with PKH dyes requires resuspension of cells in an

isosmotic mannitol-based loading medium while the Vybrant® dyes can be added directly to culture medium, making handling less complicated and permitting uniform labelling of cells either in suspension or when growing as adherent monolayers (Honig and Hume, 1986). The Vybrant® dyes DiO, CM-DiI and DiD were therefore chosen for further assessment of their suitability for tracing mitotically quiescent cells (**Figure 3.3.**). Vybrant® CM-DiI is a modified analogue of Vybrant® DiI that exhibits the same photochemical properties but incorporates a thiol-reactive chloromethylbenzamido group. Unlike Vybrant® DiI and the equivalent PKH26, Vybrant® CM-DiI is retained in cells following aldehyde fixation and permeabilisation procedures as a result of dye conjugation to membrane-bound sulfhydryl-containing peptides and proteins (Andrade *et al.*, 1996). Owing to the potential utility of these additional properties in later experiments, Vybrant® CM-DiI was chosen for initial assessment of suitability for mitotically quiescent cell tracing over Vybrant® DiI.
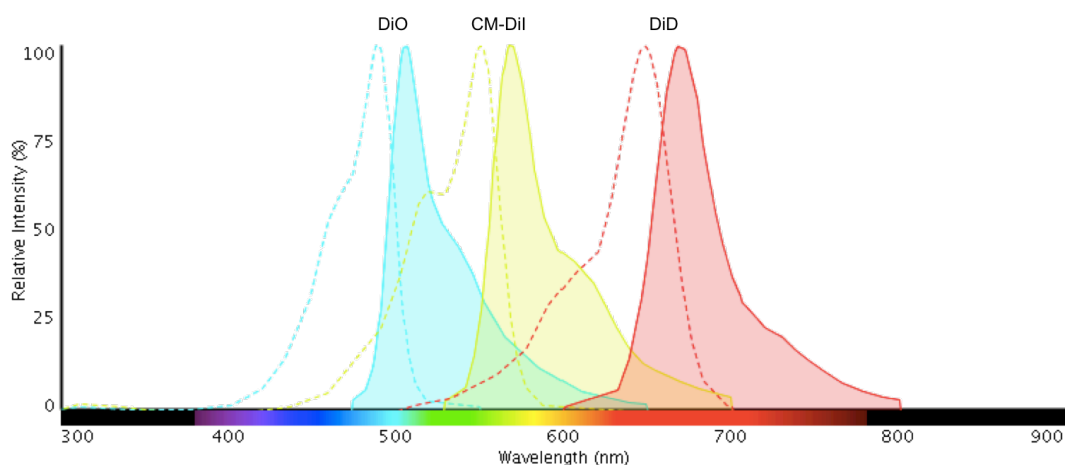
Figure 3.3. Fluorescence Spectra of Vybrant® Lipophilic Tracer Dyes

Vybrant® dyes DiO (Ex. 484, Em. 501), CM-DiI (Ex. 549, Em. 565) and DiD (Ex. 644, Em. 665) exhibit green, orange-red and far-red fluorescence respectively. DiO and CM-DiI are detectable using standard fluorescein and rhodamine optical filters while DiD has much longer-wavelength excitation and emission spectra and requires a 670nm long-pass optical filter or a close equivalent for detection. Original image generated using Thermo Fisher Scientific Fluorescence SpectraViewer available at https://www.thermofisher.com/uk/en/home/lifescience/cellanalysis/labelingchemistry/fluorescence-spectraviewer.html - Last Accessed: 01/08/2017.

3.4.2.1. Cytofluorimetric Assessment of Vybrant® Dye Staining

The identification of mitotically quiescent cells by label retention methods is reliant on the persistent retention of a bright fluorescent label following loss of this label from the mitotically active bulk cell population after numerous passages of continuous culture. Homogenous initial staining of cultures and the brightness of staining are the two critical considerations when assessing the staining produced by a fluorescent dye. The suitability of the Vybrant® dyes DiO, CM-DiI and DiD for tracing quiescent cells was therefore initially assessed for the ability to homogenously stain cells and the relative brightness of the staining produced.

MDA-MB-231 cells were stained in suspension according to the supplier instructions as detailed in **Section 2.3.1.** and were analysed cytofluorimetrically immediately after staining. During flow cytometric analyses, single live cell events were determined as described in **Section 2.5.1.** Negativity was defined as having the same fluorescence profile in the respective detector channel as an unlabelled sample of cells while positivity was initially defined by events possessing relative fluorescence exceeding that of events within the negative gate (**Figure 3.4.**).
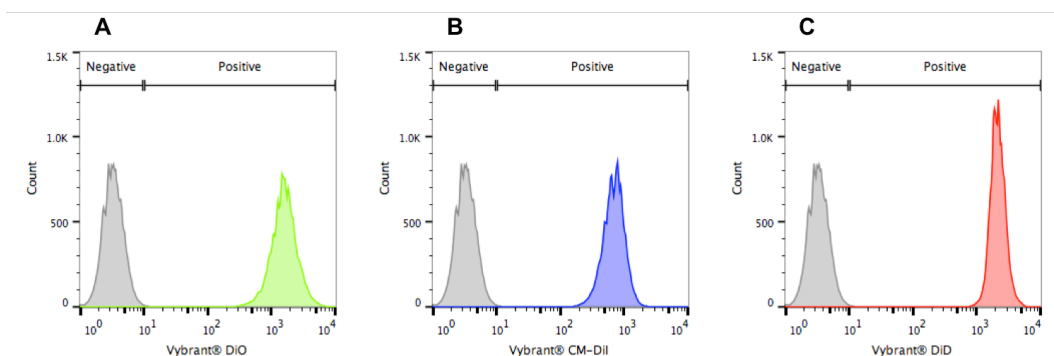
Figure 3.4. Cytofluorimetric Analysis of Newly Vybrant® Dye-Stained Samples

Gates for the analysis of Vybrant® dye labelling were initially defined by the fluorescence profile of an unlabelled sample when the detector channel voltage was adjusted to centre this population in the first decade of the respective graphical output. The fluorescence profiles of samples stained with Vybrant® DiO (**A**) Vybrant® CM-DiI (**B**) and Vybrant® DiD (**C**) immediately after labelling are shown.

The percentage of positive events within freshly labelled samples can be used to provide an indication of homogeneity of staining while the fold-change in median fluorescence intensity (MFI) of stained samples relative to unlabelled control samples can provide an indication of relative brightness of staining. The staining index (**Figure 3.5.**) is a more comprehensive assessment of relative brightness that accounts for peak separation, which is dictated by the width of the negative peak produced by the unlabelled control sample. Comparison of staining indices calculated for Vybrant® DiO, CM-DiI and DiD based on initial staining are displayed in **Figure 3.6.** Representative images of initial staining of MDA-MB-231 cells are also depicted in **Figure 3.6.**
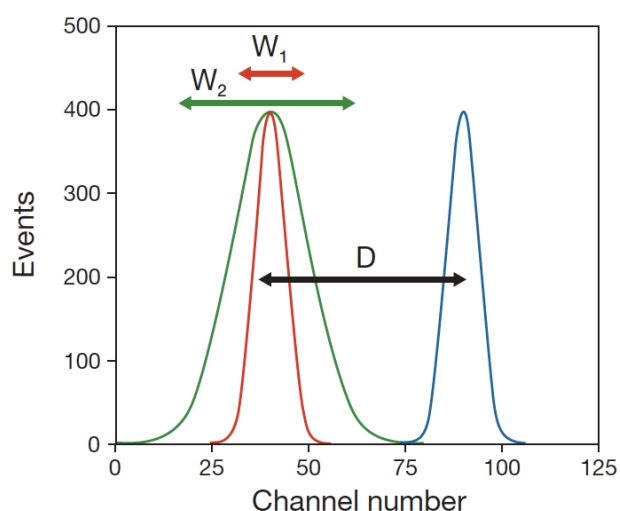
Figure 3.5. Calculation of Staining Index

Staining index is calculated as the ratio of the difference in negative and positive peak median fluorescence intensity (MFI) (**D**) and the width of the negative peak (**W**), which is twice the robust standard deviation. The width of the negative peak affects the separation of the positive and negative signals; as exemplified by the figure, a sample with a narrow spread (**W$_1$**) and a wide spread (**W$_2$**) possess the same MFI but different staining indices, making staining index the preferred means of comparing fluorophore staining brightness.
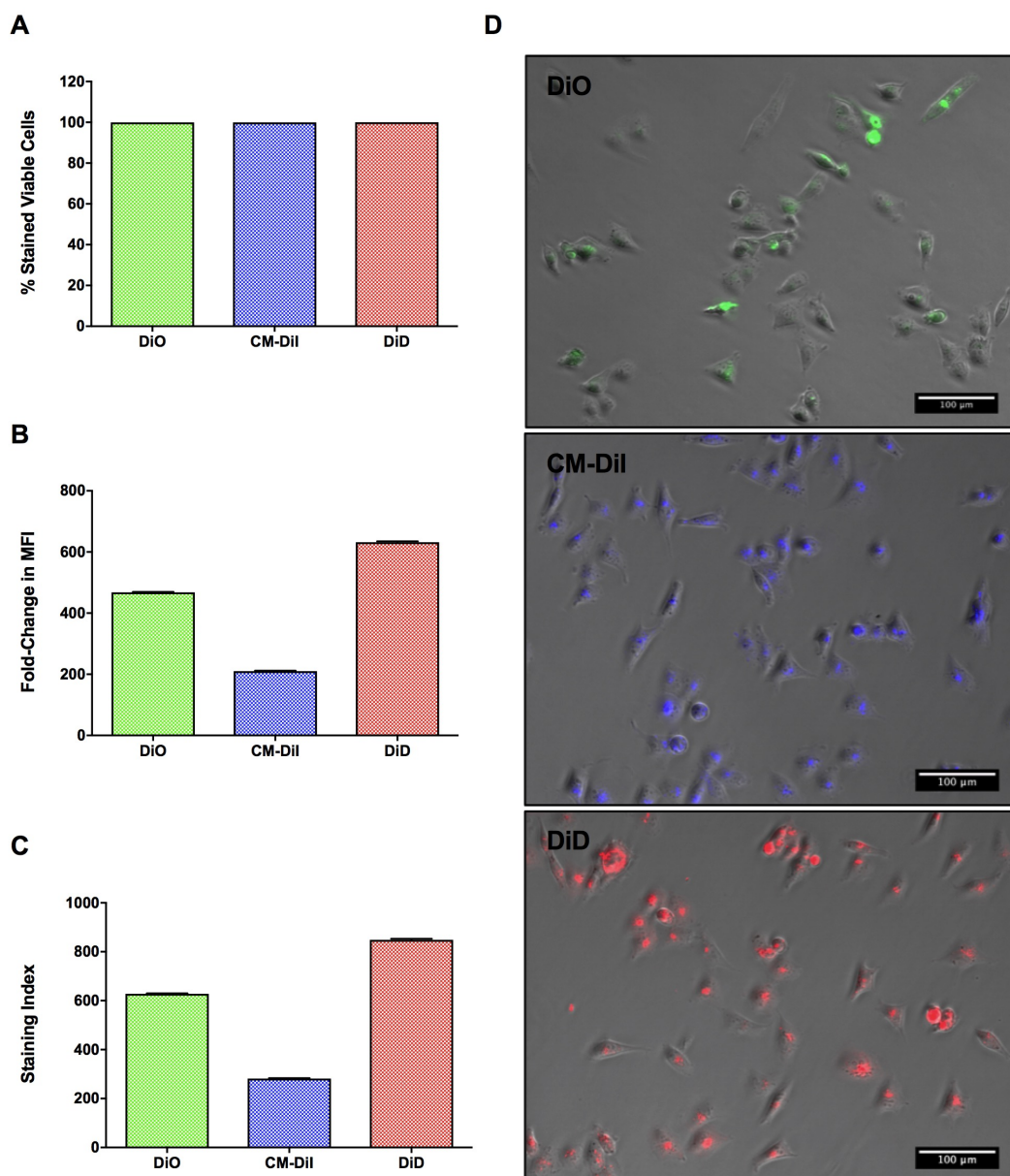
Figure 3.6. Initial Staining of MDA-MB-231 Cultures by Vybrant® Dyes

A: The percentage of stained viable cells is shown for each of the Vybrant® dyes DiO, CM-DiI and DiD immediately after staining was undertaken. **B**: The fold-change in median fluorescence intensity (MFI) relative to cellular autofluorescence in the appropriate flow cytometer detector channel is shown for each dye. **C**: Staining indices calculated for initial staining of Vybrant® dyes compared to unlabelled controls. Data are expressed as the mean average ± SEM for n = 3 biologically independent repeat experiments. **D**: Representative images of initial staining produced by Vybrant® DiO (top) CM-DiI (middle) and DiD (bottom). All images were captured using a 10x objective lens (scale bar = 100µm).

All dyes initially stained 100% of cells when gating during flow cytofluorimetric analysis was set as described in **Figure 3.4.** The average fold-change in MFI for samples labelled with Vybrant® DiO- and Vybrant® CM-DiI was 469 and 211 times that of an unstained sample, respectively, while samples labelled with Vybrant® DiD showed an average 632-fold increase in MFI. All stained samples were measured relative to an unlabelled MDA-MB-231 sample, meaning that the negative peak in all cases was very similar and that staining index was therefore primarily reliant on MFI. As a result, both MFI and staining index measurements follow the same pattern and indicated that Vybrant® DiD resulted in the brightest labelling of cultures.

Based solely on the assessment of their initial staining characteristics, any of the Vybrant® dyes used might have been suitable for long-term tracer applications; each of the three dyes tested demonstrated homogenous and relatively bright initial staining. However, while no significant effects on breast cancer cell growth or function has previously been reported, some carbocyanine dyes have been shown to cause concentration-dependent inhibition of the mitochondrial electron transport chain, thereby having the potential to impact cell growth and functions such as motility (Anderson and Trgovcich-Zacok, 1995). It was deemed prudent to first ascertain that Vybrant® dye staining did not impact the growth or basic functional characteristics of stained cells before selecting a dye for use in identifying mitotically quiescent cells, due to the requirement to identify an intrinsic sub-population without altering the inherent properties of the parent culture.

3.4.2.2. Establishing the Effects of Vybrant® Dye Staining on Cell Function

The growth profile of MDA-MB-231 human breast cancer cells was established following staining with Vybrant® DiO, CM-DiI and DiD. The growth profile of each stained culture was compared to the growth profile obtained for an unstained control sample grown under identical conditions in order to determine whether staining with Vybrant® dyes significantly altered culture growth. Samples of 1.0×10^6 cells were prepared in serum-free basal culture medium and stained in suspension according to the supplier instructions (**Section 2.3.1.**). Stained cells were seeded at the optimal density and growth profiles established by monitoring the number of viable cells present within each culture at 24-hour intervals post-seeding, as detailed in **Section 2.2.5.** The results are displayed in **Figure 3.7.** The intrinsic growth characteristics of MDA-MB-231 cells remained unaltered following staining with Vybrant® DiO, CM-DiI and DiD; there was no significant difference in the number of viable cells present at any time point following staining across all three of the dyes tested. This lack of alteration to the inherent growth properties indicated no evidence of cytotoxicity following Vybrant® dye staining. While these results suggested it was also unlikely that Vybrant® dye staining would have any profound effect on other basic functional properties of cell behaviour, colony forming ability and migratory capability were subsequently assayed to ensure that this was the case.
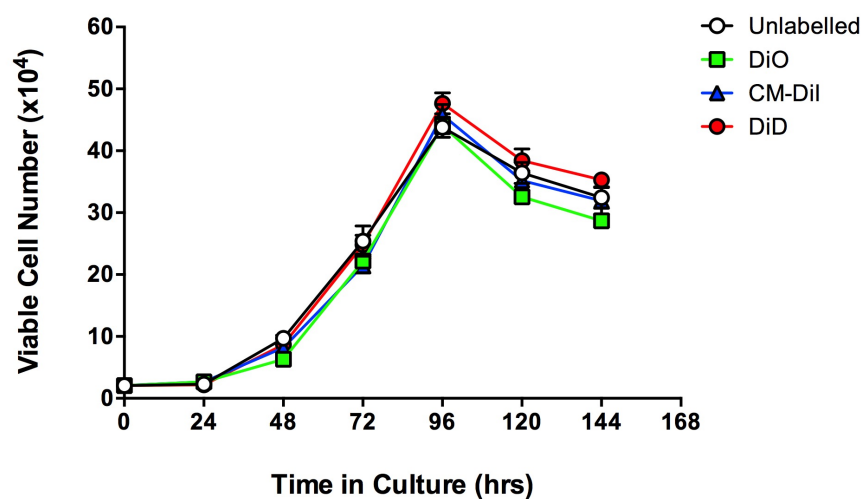
Figure 3.7. Growth Profiles of Vybrant® Dye-Stained MDA-MB-231 Cultures

The growth profiles of unstained and Vybrant® DiO-, CM-DiI- and DiD-stained MDA-MB-231 human breast cancer cells grown *in vitro* as adherent monolayer cultures are shown; viable cell count (Y-axis) is plotted against the duration of culture (X-axis) in each case. Data obtained for stained cultures was compare to those recorded for unstained cultures using two-way ANOVA followed by Dunnett's Multiple Comparison Test. No statistically significant difference was found between unstained and stained samples at any time point. Data are expressed as the mean average ± SEM for n = 3 biologically independent repeat experiments.

Colony forming ability of Vybrant® DiO-, CM-DiI- and DiD-stained MDA-MB-231 cells was assessed in order confirm the findings of proliferation assays and thereby demonstrate that staining does not significantly affect cell growth capability. Samples of 1.0×10^6 MDA-MB-231 cells were prepared in serum-free basal culture medium and stained in suspension according to the supplier instructions (**Section 2.3.1.**). Stained cells were seeded at a clonogenic density of 20 cells per cm^2 of growth area in high-quality polystyrene 60mm tissue culture dishes, supplemented with 0.2ml of complete growth medium per cm^2 and placed into incubation under standard growth conditions for 6 days; a time period covering at least six log-phase doubling times, which for MDA-MB-231 cells was previously determined as approximately 17 hours. The number of colonies formed by unstained and stained cells was established following fixation and crystal violet staining as described in **Section 2.2.6.1.** The results, depicted in **Figure 3.8.**, demonstrated no significant difference in the colony forming ability of Vybrant® DiO- CM-DiI- or DiD-stained cells compared to unstained control cells, supporting the findings of proliferation assays which indicated that Vybrant® dye staining did not alter cell growth.
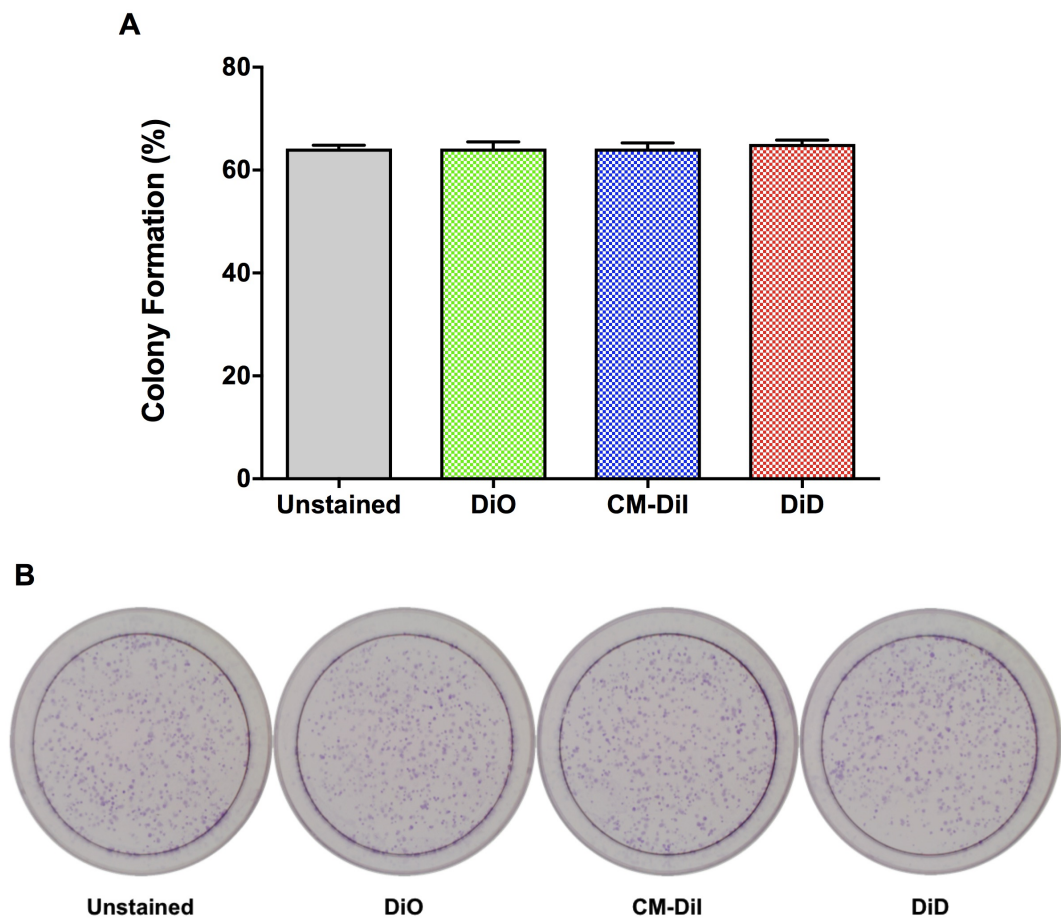
Figure 3.8. Clonogenic Assays for Vybrant® Dye-Stained MDA-MB-231 Cells

A: The number of colonies formed by Vybrant® DiO-, CM-DiI- and DiD-stained MDA-MB-231 cells were compared to data obtained for unstained cells grown under identical conditions using one-way ANOVA followed by Dunnett's Multiple Comparison Test. No statistically significant difference was found between stained and unstained groups. Data are expressed as the mean average ± SEM for n = 3 biologically independent repeat experiments. **B**: Representative images of a crystal violet-stained clonogenic assay plates for unstained and Vybrant® DiO-, CM-DiI- and DiD-stained MDA-MB-231 cells. All images were captured using a 2x stereomicroscopic objective lens.

In order to determine whether Vybrant® dye staining inhibits the intrinsic functional behaviour of cells, such as motility and migratory capability, scratch closure migration assays were undertaken post-staining with Vybrant® dyes. The general scratch closure assay procedure can be found in **Section 2.2.7.** Briefly, samples of 1.0 x 10^6 MDA-MB-231 cells were prepared in serum-free basal culture medium and stained in suspension according to the supplier's instructions (**Section 2.3.1.**). Stained cells were seeded at a density of 7.7 x 10^5 into triplicate wells of 6-well culture plates and placed into incubation for a period of 24 hours to form a confluent monolayer. Cell growth was subsequently arrested by incubation under standard growth conditions for 3 hours in the presence of the potent DNA cross-linking agent Mitomycin C. The Mitomycin C solution was removed before a linear scratch was made in the monolayer using a 200µl pipette tip. Each well was then washed in order to completely remove cell debris. Two reference points were marked at either end of the scratch on the underside of the plate under low-magnification (50X) inverted phase-contrast microscopy using a permanent marker pen. Images were immediately captured at each reference point under inverted phase-contrast microscopy at 100X magnification and further images captured after 24 hours. The area of the scratch within each image field was measured using the open-source image analysis platform ImageJ as described in **Section 2.2.7.** and the percentage closure over the assay time period calculated. The results are depicted in **Figure 3.9.** No significant difference in the migratory capability of cells was found post-staining with Vybrant® DiO, CM-DiI and DiD.
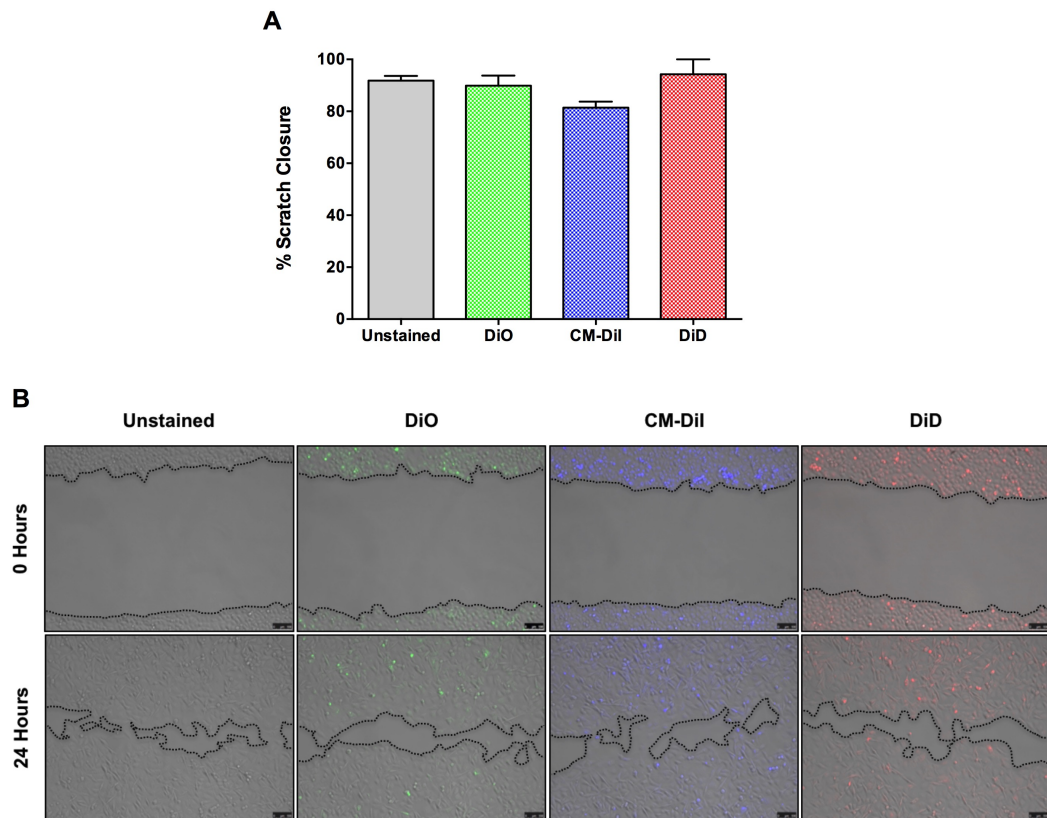
Figure 3.9. Migration Assays for Vybrant® Dye-Stained MDA-MB-231 Cells

A: The migratory capability of Vybrant® DiO-, CM-DiI- and DiD-stained MDA-MB-231 cells assessed by scratch closure assay was compared to data obtained for unstained cells grown under identical conditions using one-way ANOVA followed by Dunnett's Multiple Comparison Test. No statistically significant difference was found between stained and unstained groups. Data are expressed as the mean average ± SEM for n = 3 biologically independent repeat experiments. **B**: Representative examples of images taken during the scratch closure assay of unstained and Vybrant® DiO-, CM-DiI- and DiD-stained MDA-MB-231 cells immediately after the scratch was established and then at a subsequent 24 hour time-point. All images were captured using a 10x objective lens (scale bar = 100μm).

Based on the results of proliferation, colony formation and migration assays it was possible to conclude that any inhibition of the mitochondrial electron transport chain that might have occurred as a result of staining with carbocyanine-derived Vybrant® dyes, as was reported by Anderson and Trgovcich-Zacok (1995), did not result in altered cell culture growth, colony formation or migratory capability. The assessment of cytofluorimetric staining indicated that any of the dyes assayed might be suitable for use in mitotically quiescent cell tracing applications and these data support this conclusion. Vybrant® DiD was chosen over Vybrant® DiO and CM-DiI for routine use in lipophilic dye retention pulse-chase assays. This decision was made based on the fact that initial staining with Vybrant® DiD was more homogenous and considerably brighter than that resulting from the use of DiO and CM-DiI, making Vybrant® DiD better suited to long-term cell tracing.

3.4.3. Identifying Dye-Retaining Sub-Clones in Human Breast Cancer Cell Lines

Cells were initially stained in suspension with Vybrant® DiD according to the supplier's instructions as detailed in **Section 2.3.1.** At the outset of each dye-retention assay, flow cytometric calibration and setting of gates for detection of positively labelled cells was undertaken using an unlabelled sample and a freshly labelled sample of cells. During flow cytometric analyses, single live cell events were determined as described in **Section 2.5.1.** The gates defining event negativity and positivity were set according to the fluorescence profile of an unlabelled sample and a freshly labelled sample of cells, respectively, in the appropriate detector channel (**Figure 3.10.**).
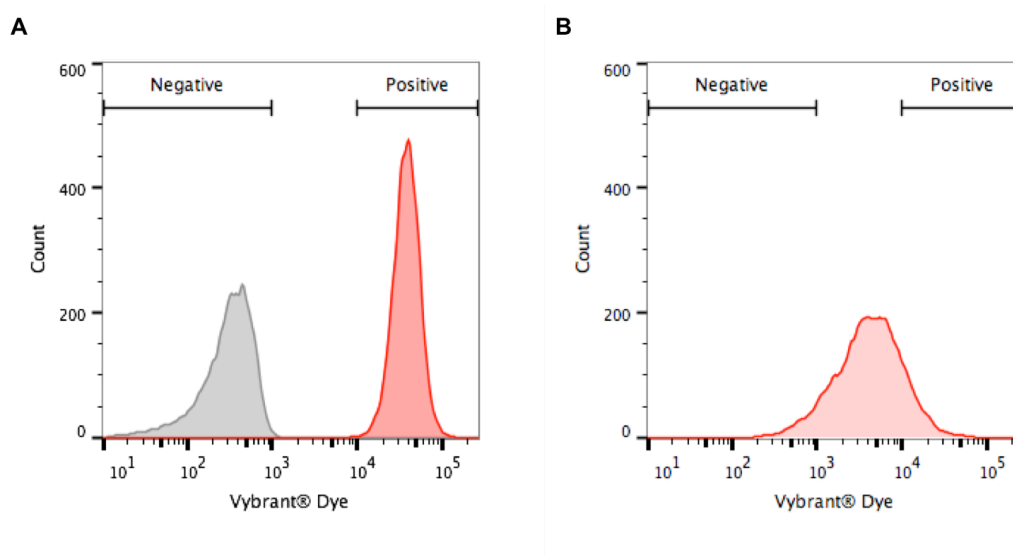
Figure 3.10. Cytofluorimetric Detection of Dye-Retaining Sub-Clones

A: The flow cytometer was initially calibrated for detection of negatively and positively labelled cells using an unlabelled sample (grey) and a freshly labelled sample (red), respectively. **B**: Stained samples of cells were continuously cultured for up to six consecutive passages and the percentage positivity at any given sub-culture interval determined using the initial gate configuration defined for that dye and cell line. Over time, the initial positive fluorescence peak migrated to the left towards, and eventually into, the negative gate as the fluorescence intensity of rapidly dividing cells was lost, leaving only the least mitotically active cells in the positive gate.

Following definition of the flow cytofluorimetric gating strategy, stained cells and unlabelled controls to be grown concomitantly were seeded at the cell line specific optimal density and maintained as described in **Section 2.2.1.1.** At the pre-determined sub-culture interval (**Table 3.1.**), cells were retrieved and counted as detailed previously (**Section 2.2.1.2.** and **Section 2.2.3.**). At each sub-culture, samples of 1.0 x 10^6 cells were prepared for cytofluorimetric analysis by undertaking centrifugation at 150 x *g* for 5 minutes followed by resuspension in serum-free basal medium. Samples were analysed to determine the percentage of positive events present within each sample using the gating tree pre-set at the beginning of the experiment. The percentage positivity of each cell line was monitored in this way for up to six consecutive passages of growth; the results are depicted in **Figure 3.11. - Figure 3.15.** inclusive. Fluorescence photomicroscopy was also undertaken in order to visually demonstrate the changes in Vybrant® DiD staining of cultures over the duration of dye retention assays. Representative images are depicted within the respective figure.

When grown as adherent monolayer cultures, a dye-retaining sub-population was identified within each of the MCF-7, ZR-75-1, MDA-MB-231, MDA-MB-468 and SK-BR-3 cell lines. Initial staining in all cultures resulted in 100% of cells being labelled with Vybrant® DiD. In all cases, a steep decline in the positively labelled population occurred at passage 3 and continued until passage 5, at which the rate of dye loss reduced. Dye-retaining sub-clones comprised < 0.5% of the total cell population at the final passage of dye measurement across all cell lines. In all cases, there was a statistically significant reduction in the median fluorescence intensity (relative brightness) of the Vybrant® DiD-positive population, falling from approximately 260, 000 relative fluorescence units (RFU) at passage 0 to between 20,000 and 10,000 RFU between passages 0 and 6 (P ≤ 0.0001). Whether these dye-retaining cells represent a phenotypically distinct population and whether they possess stem cell-like properties (such as the ability to survive chemotherapy and repopulate the cancer cell population post-cessation of treatment) will be explored in subsequent chapters.

A: 100.00% 99.99% 99.82% 79.17% 17.85% 2.37% 0.23%

Passage 0 Post-Staining · Passage 3 Post-Staining · Passage 6 Post-Staining
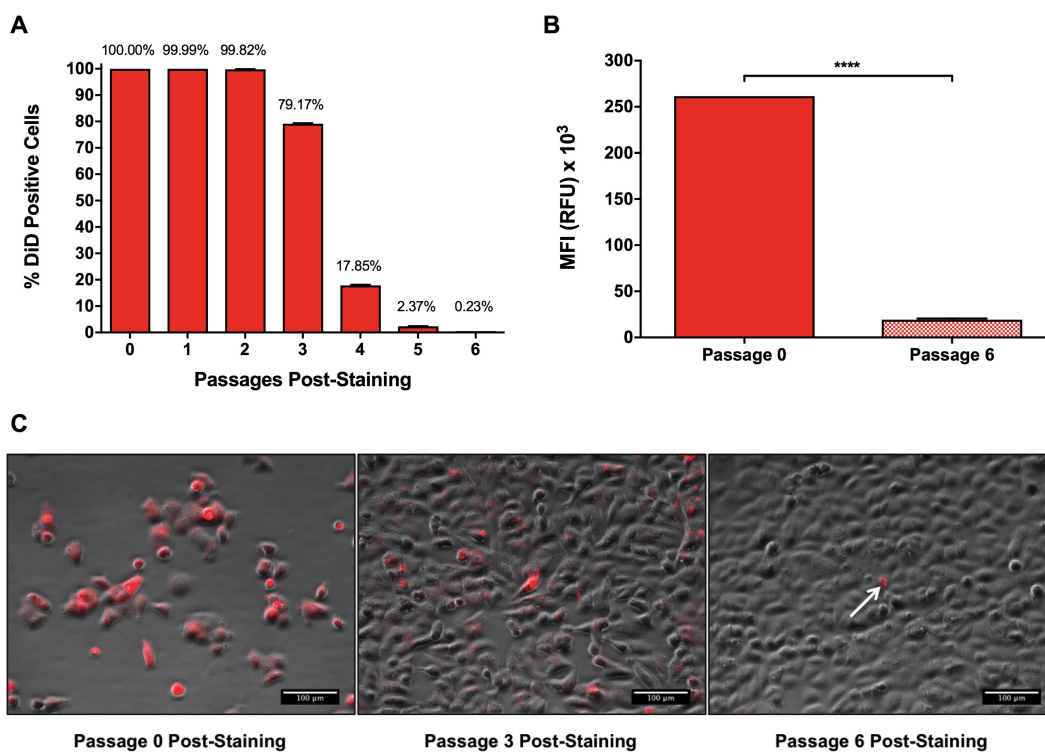
Figure 3.11. Dye-Retaining Cell Frequency in the MCF-7 Cell Line

A: The percentage of Vybrant® DiD-stained MCF-7 cells in adherent monolayer cultures grown under optimal conditions was measured at the time of sub-culture undertaken at 96 hour intervals. Data are expressed as the mean average ± SEM for n = 3 biologically independent repeat experiments; the mean average value is denoted above the respective data bar. **B**: A statistically significant decrease in the relative brightness of dye-retaining cells was revealed when the median fluorescence intensity (MFI) of the gated Vybrant® DiD-positive cell population was compared between samples immediately post-staining and following 6 subsequent passages of culture growth using an unpaired *t*-test (**** = P ≤ 0.0001). Data are expressed as the mean average ± SEM for n = 3 biologically independent repeat experiments. RFU = relative fluorescence units. **C**: Representative images of Vybrant® DiD staining in monolayer MCF-7 cultures at 6 hours (left), passage 3 (centre) and passage 6 (right) post-staining; the white arrow indicates a dye retaining cell evident in the image. All images were captured using a 10x objective lens (scale bar = 100μm).
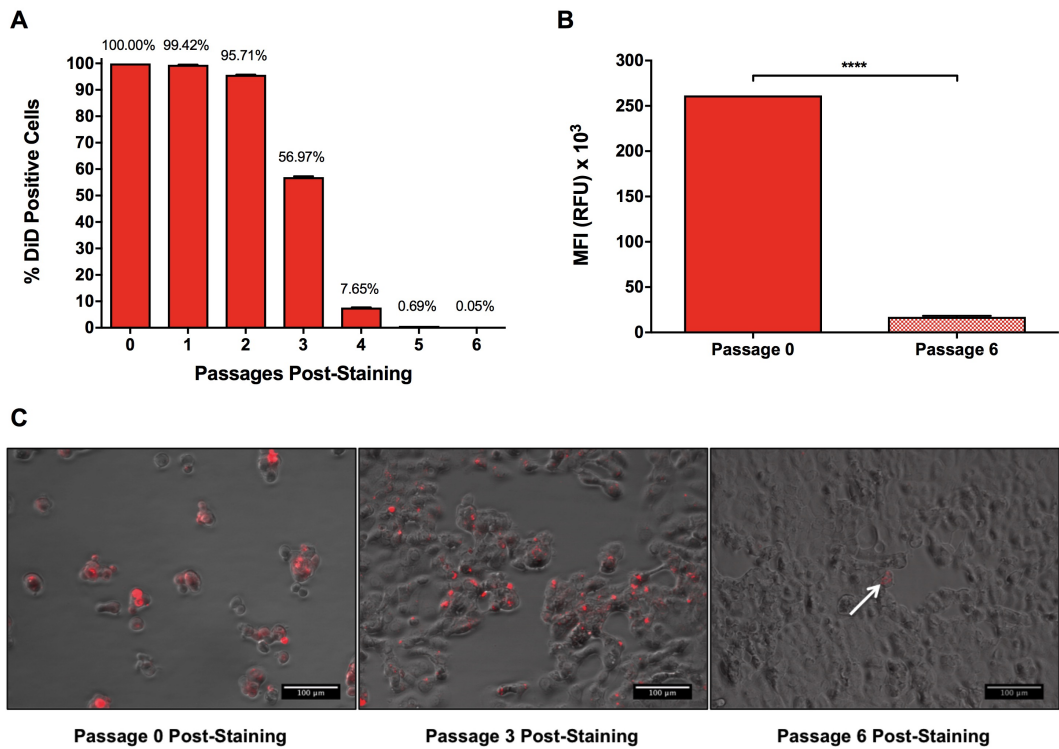
Figure 3.12. Dye-Retaining Cell Frequency in the ZR-75-1 Cell Line

A: The percentage of Vybrant® DiD-stained ZR-75-1 cells in adherent monolayer cultures grown under optimal conditions was measured at the time of sub-culture undertaken at 144 hour intervals. Data are expressed as the mean average ± SEM for n = 3 biologically independent repeat experiments; the mean average value is denoted above the respective data bar. **B**: A statistically significant decrease in the relative brightness of dye-retaining cells was revealed when the median fluorescence intensity (MFI) of the gated Vybrant® DiD-positive cell population was compared between samples immediately post-staining and following 6 subsequent passages of culture growth using an unpaired *t*-test (**** = P ≤ 0.0001). Data are expressed as the mean average ± SEM for n = 3 biologically independent repeat experiments. RFU = relative fluorescence units. **C**: Representative images of Vybrant® DiD staining in monolayer ZR-75-1 cultures at 6 hours (left), passage 3 (centre) and passage 6 (right) post-staining; the white arrow indicates a dye retaining cell evident in the image. All images were captured using a 10x objective lens (scale bar = 100µm).

A: The percentage of Vybrant® DiD-stained MDA-MB-231 cells in adherent monolayer cultures grown under optimal conditions was measured at the time of sub-culture undertaken at 72 hour intervals. Data are expressed as the mean average ± SEM for n = 3 biologically independent repeat experiments; the mean average value is denoted above the respective data bar. **B**: A statistically significant decrease in the relative brightness of dye-retaining cells was revealed when the median fluorescence intensity (MFI) of the gated Vybrant® DiD-positive cell population was compared between samples immediately post-staining and following 6 subsequent passages of culture growth using an unpaired *t*-test (**** = P ≤ 0.0001). Data are expressed as the mean average ± SEM for n = 3 biologically independent repeat experiments. RFU = relative fluorescence units. **C**: Representative images of Vybrant® DiD staining in monolayer MDA-MB-231 cultures at 6 hours (left), passage 3 (centre) passage 6 (right) post-staining; the white arrow indicates a dye retaining cell evident in the image. All images were captured using a 10x objective lens (scale bar = 100µm).
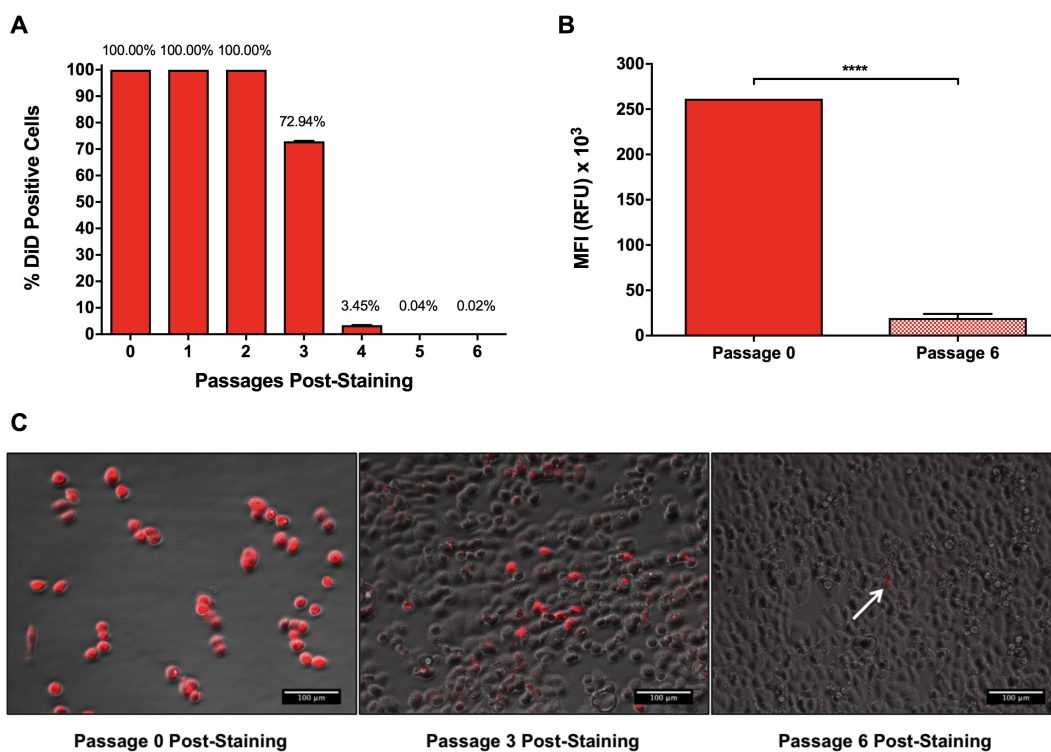
Figure 3.14. Dye-Retaining Cell Frequency in the MDA-MB-468 Cell Line

A: The percentage of Vybrant® DiD-stained MDA-MB-468 cells in adherent monolayer cultures grown under optimal conditions was measured at the time of sub-culture undertaken at 120 hour intervals. Data are expressed as the mean average ± SEM for n = 3 biologically independent repeat experiments; the mean average value is denoted above the respective data bar. **B**: A statistically significant decrease in the relative brightness of dye-retaining cells was revealed when the median fluorescence intensity (MFI) of the gated Vybrant® DiD-positive cell population was compared between samples immediately post-staining and following 6 subsequent passages of culture growth using an unpaired *t*-test (**** = P ≤ 0.0001). Data are expressed as the mean average ± SEM for n = 3 biologically independent repeat experiments. RFU = relative fluorescence units. **C**: Representative images of Vybrant® DiD staining in monolayer MDA-MB-468 cultures at 6 hours (left), passage 3 (centre) and passage 6 (right) post-staining; the white arrow indicates a dye retaining cell evident in the image. All images were captured using a 10x objective lens (scale bar = 100μm).
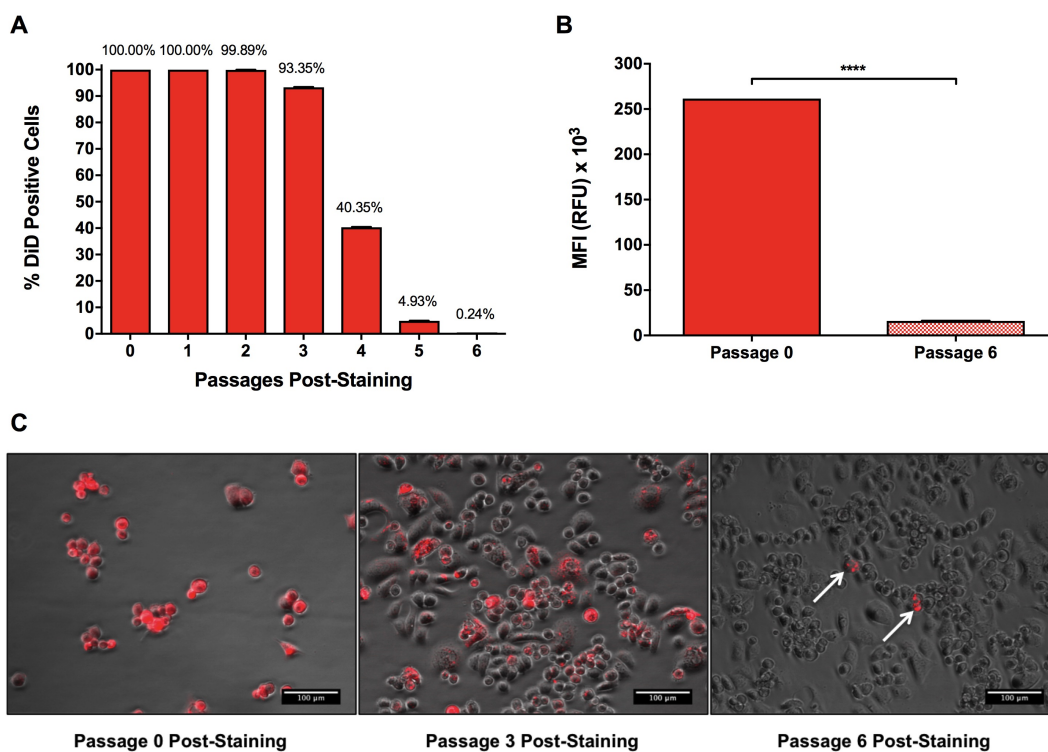
Figure 3.15. Dye-Retaining Cell Frequency in the SK-BR-3 Cell Line

A: The percentage of Vybrant® DiD-stained SK-BR-3 cells in adherent monolayer cultures grown under optimal conditions was measured at the time of sub-culture undertaken at 120 hour intervals. Data are expressed as the mean average ± SEM for n = 3 biologically independent repeat experiments; the mean average value is denoted above the respective data bar. **B**: A statistically significant decrease in the relative brightness of dye-retaining cells was revealed when the median fluorescence intensity (MFI) of the gated Vybrant® DiD-positive cell population was compared between samples immediately post-staining and following 6 subsequent passages of culture growth using an unpaired *t*-test (**** = P ≤ 0.0001). Data are expressed as the mean average ± SEM for n = 3 biologically independent repeat experiments. RFU = relative fluorescence units. **C**: Representative images of Vybrant® DiD staining in monolayer SK-BR-3 cultures at 6 hours (left), passage 3 (centre) and passage 6 (right) post-staining; the white arrows indicate dye retaining cells evident in the image All images were captured using a 10x objective lens (scale bar = 100µm).

3.4.4. Identification of Dye-Retaining Sub-Clones is Not Limited to One Dye Type

In order to demonstrate that the detection of a dye retaining population was not limited to the use of Vybrant® DiD only, lipophilic dye retention assays were repeated in the MDA-MB-231 cell line using Vybrant® CM-DiI. Cells were initially stained in suspension with Vybrant® CM-DiI according to the supplier's instructions as detailed in **Section 2.3.1.** The assay procedure for detection of Vybrant® CM-DiI positive cells was undertaken exactly as described previously for detection of Vybrant® DiD-positive cells (**Section 3.4.3.**). The results, depicted in **Figure 3.16.**, demonstrated that dye-retaining sub-clones were also evident in MDA-MB-231 cells initially labelled with Vybrant® CM-DiI following dye loss from the bulk cell population. At the outset, MDA-MB-231 cultures were 100% positively labelled with Vybrant® CM-DiI. A steep decline in the percentage of positively labelled cells occurred after just one passage of growth and continued up to passage 3, at which point the rate of dye loss reduced considerably. As previously observed using Vybrant® DiD, dye-retaining sub-clones comprised < 0.1% of the total cell population at the final passage of dye measurement, although dye loss from the bulk cell population occurred at an earlier time point using Vybrant® CM-DiI. This was almost certainly due to the lower relative brightness of the initial Vybrant® CM-DiI label and the resultant shorter time period required for sufficient loss of dye to result in migration out of the positive gate. As was previously observed with Vybrant® DiD, the relative intensity of the label in the dye-retaining population was statistically significantly diminished between the first and last passages, falling from approximately 130,000 RFU immediately after initial staining to 13,000 RFU after 4 subsequent passages of culture growth (P ≤ 0.0001).
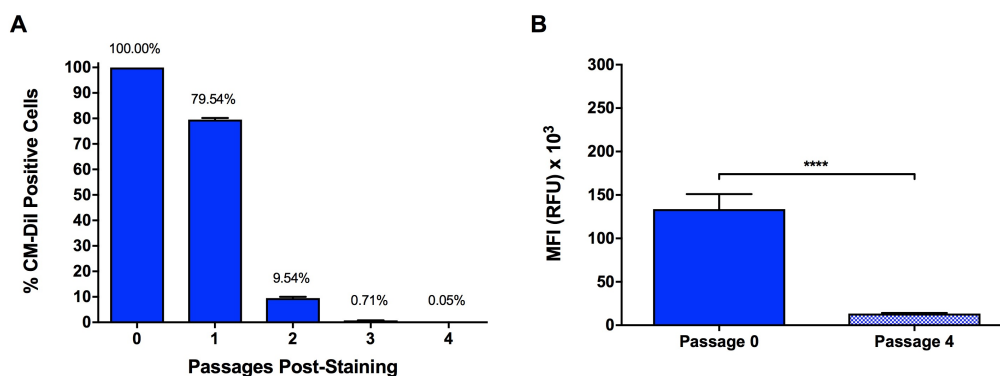
Figure 3.16. Dye-Retention in Vybrant® CM-DiI Stained MDA-MB-231 Cells

A: The percentage of Vybrant® CM-DiI-stained MDA-MB-231 cells in adherent monolayer cultures grown under optimal conditions was measured at the time of sub-culture undertaken at 72 hour intervals. Data are expressed as the mean average ± SEM for n = 3 biologically independent repeat experiments; the mean average value is denoted above the respective data bar. **B**: A statistically significant decrease in the relative brightness of dye-retaining cells was revealed when the median fluorescence intensity (MFI) of the gated Vybrant® CM-DiI-positive cell population was compared between samples immediately post-staining and following 6 subsequent passages of culture growth using an unpaired *t*-test (**** = P ≤ 0.0001). Data are expressed as the mean average ± SEM for n = 3 biologically independent repeat experiments. RFU = relative fluorescence units.

3.4.5. Cell Division is the Primary Determinant of Vybrant® Dye Loss

In order to demonstrate that cell division was the primary determinant of lipophilic fluorescent dye loss, and by extension that dye retention was indicative of mitotic inactivity, samples of MDA-MB-231 cells were pre-treated with the potent DNA cross linking agent Mitomycin C to induce growth arrest prior to staining. Briefly, monolayer cultures were incubated under standard growth conditions for 3 hours in the presence of Mitomycin C freshly prepared in serum-free RPMI-1640 basal medium at a concentration of 10µg/ml before being retrieved as previously described (**Section 2.2.1.2.**). Growth-arrested cells were stained with Vybrant® DiD in suspension according to the supplier instructions, as described in **Section 2.3.1.** Once stained, cells were seeded into 75cm^2 tissue culture flasks at a density of 1.0 x 10^4 cells per cm^2. Equivalent unstained samples were prepared in the same manner and grown concomitantly in order to facilitate flow cytometric analysis at the appropriate time point. Sufficient stained and unstained growth arrested samples were prepared to allow measurement across the entire assay duration of 18 days (equivalent to six passages of culture growth in non-arrested cultures). The percentage of cells retaining the Vybrant® DiD dye was monitored as previously described (**Section 3.4.3.**) at time points equivalent to those used to monitor dye retention in growing cultures.

Mitomycin C-induced growth arrest resulted in the retention of Vybrant® DiD in a high percentage of cells at all time points during the assay period; at passage 6 in non-growth arrested cultures 0.08% of cells retained their Vybrant® DiD label, whereas 99.33% were positively labelled on average in mitomycin C pre-treated cultures at the equivalent time point. The high level of dye retention by growth-arrested cells throughout the assay period is clearly depicted in fluorescence photomicroscopic images of cultures taken at each time point (**Figure 3.17.**).
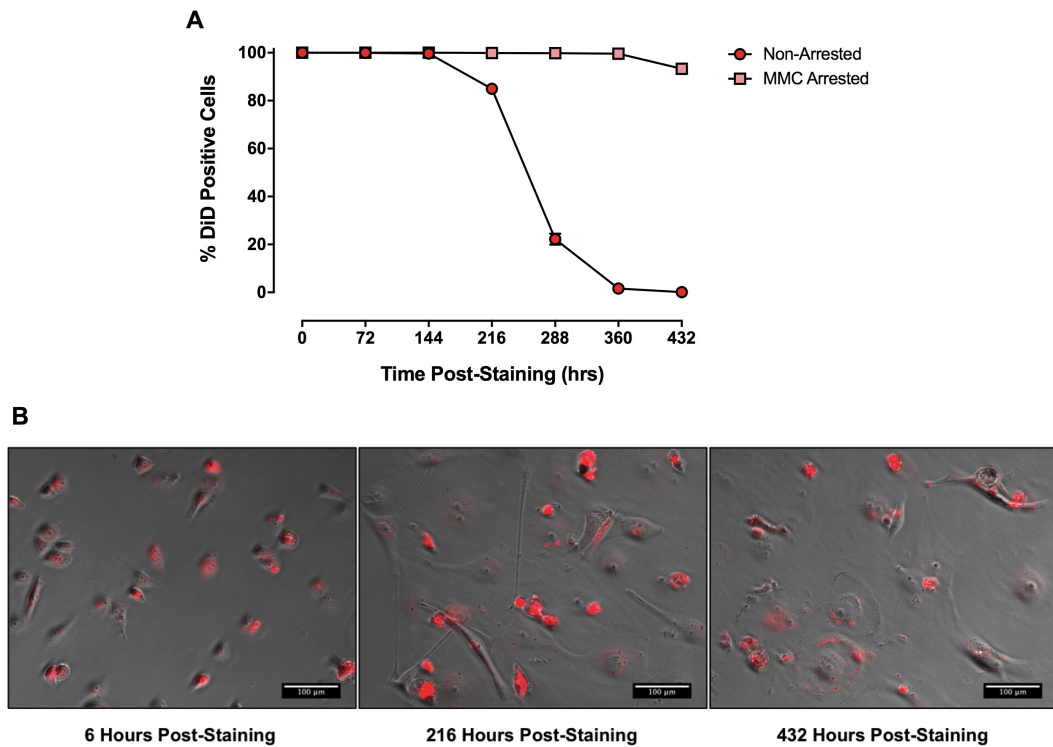
Figure 3.17. Inhibition of Lipophilic Dye Loss Following Growth Arrest

A: The percentage of Vybrant® DiD-stained MDA-MB-231 cells in Mitomycin C (MMC) pre-treated adherent monolayer cultures grown under optimal conditions was measured at 72 hour intervals equivalent to the time of sub-culture in growing cultures. Data are expressed as the mean average ± SEM for n = 3 biologically independent repeat experiments. **B**: Representative images of Vybrant® DiD staining in growth-arrested MDA-MB-231 cultures at 6 hours (left), 216 hours (centre) and 432 hours (right) post-staining. All images were captured using a 10x objective lens (scale bar = 100µm).

3.4.6. Dye-Retaining Cells: Senescent, Absolutely Quiescent or Slowly Cycling?

In order to first determine whether dye-retention represented a senescent state of mitotic inactivity, the activity of senescence-associated β-galactosidase was assayed at pH 6.0 due to the frequent use of this enzyme as a biomarker of cellular senescence. Wild type MDA-MB-231 cells were stained in suspension with Vybrant® DiD according to the manufacturer instructions (**Section 2.3.1.**), seeded at the optimal density of 1.0 x 10^4 cells per cm^2 into 75cm^2 high-quality polystyrene tissue culture flasks and cultured continuously for five passages. Following retrieval of cultures at five passages post-staining, Vybrant® DiD-positive cells were isolated by FACS and were reseeded in triplicate into the wells of 6-well cluster plates. Samples of the BO2 variant MDA-MB-231 cell line engineered to stably express β-galactosidase were prepared concomitantly as a positive control. Cluster plates were placed into incubation overnight to allow cells to adhere to the growth surface. Adherent cells were stained for senescence-associated β-galactosidase activity at pH 6.0 using the β-galactosidase staining kit available from New England Biolabs U.K. Ltd. according to the manufacturer instructions (**Section 2.8.1.**). Stained samples were immediately assessed for positive staining under inverted phase-contrast microscopy and representative images captured. A strong blue coloured staining in the BO2 variant MDA-MB-231 stably expressing β-galactosidase indicated that the assay was working correctly. The complete absence of this staining in isolated Vybrant® DiD-positive cells demonstrated that dye retention in this fraction was not the result of entry into a permanent state of mitotic arrest due to cellular senescence (**Figure 3.18.**).
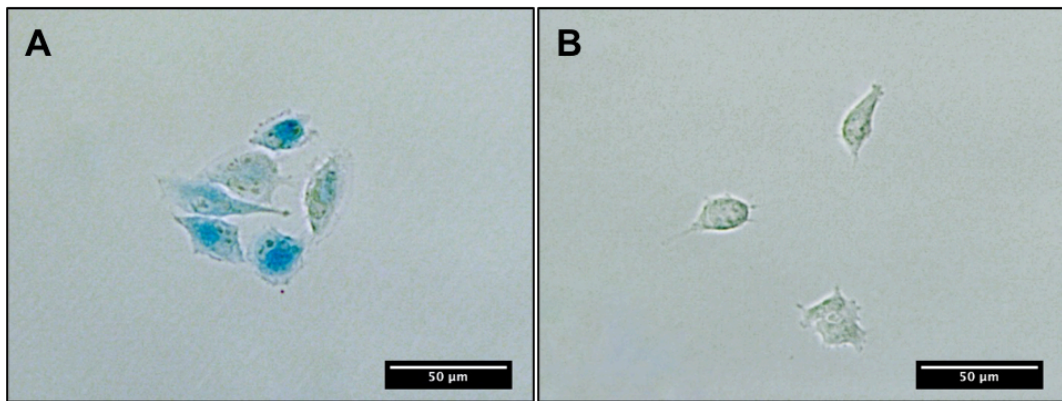
Figure 3.18. β-galactosidase Activity in Vybrant® DiD-Retaining MDA-MB-231 Cells

A: BO2-variant MDA-MB-231 cells stably expressing β-galactosidase used as a positive control for assessment of intracellular β-galactosidase activity at pH 6.0; blue coloured staining is due to 5,5'-dibromo-4,4'-dichloro-indigo resulting from β-galactosidase-catalysed X-gal metabolism. **B**: Isolated Vybrant® DiD-positive MDA-MB-231 cells at 12-hours post-seeding showing negativity for 5,5'-dibromo-4,4'-dichloro-indigo staining indicative of senescence-associated β-galactosidase activity at pH 6.0. All images were captured using a 20x objective lens (scale bar = 50μm).

During lipophilic fluorescent dye pulse-chase assays, a statistically significant reduction in the median fluorescence intensity of the Vybrant® dye-positive population was observed between the first and final passages of culture growth in all cell lines assayed (**Figure 3.11. - Figure 3.16.**). Following the demonstration that dye retaining cells were not senescent, and given that previous experiments demonstrated that a significant reduction in fluorescence intensity of dye staining was indicative of mitotic activity, these results were seen to indicate that dye-retaining cells were in fact a slow-cycling, relatively quiescent population. Indeed, using the median fluorescence intensity of Vybrant® DiD staining to compare the dye-retaining population (MFI = 31744.33 RFU) and the dye-negative population (MFI = 559 RFU) within MDA-MB-231 cultures after five passages post-staining (**Figure 3.19.**), Vybrant® DiD-positive cells were determined to be approximately six cell divisions behind the bulk dye-negative population.
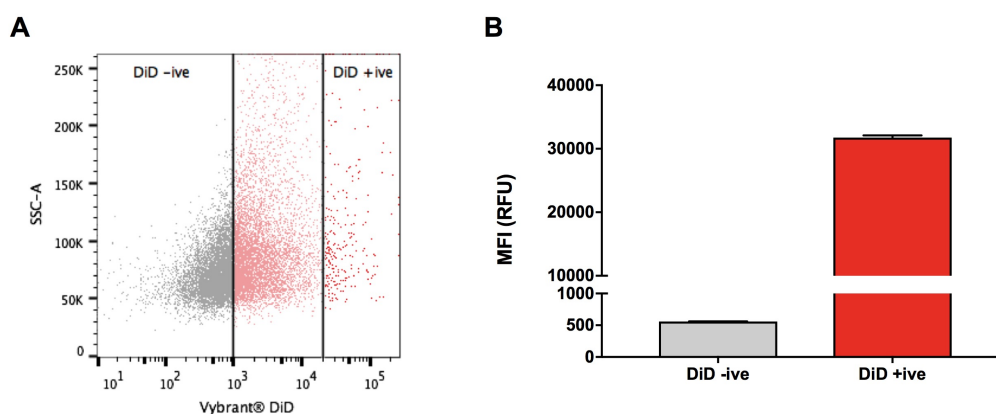
Figure 3.19. Comparison of the MFI of Dye-Retaining and Negative Populations

A: Representative flow cytometric analysis of Vybrant® DiD-stained adherent MDA-MB-231 cultures at five passages post-staining. The gates for detection of the Vybrant® DiD-negative (grey) and most intensely stained Vybrant® DiD-positive (bright red) populations were pre-set at the beginning of the pulse-chase period using unlabelled and freshly labelled samples respectively, allowing the median fluorescence intensity (MFI) of the population defined by each gate to be determined. **B**: The MFI of Vybrant® DiD-negative and Vybrant® DiD-positive populations at five passages post-staining are shown. Data are expressed as the mean average ± SEM for n = 3 biologically independent repeat experiments. RFU = relative fluorescence units.

In order to determine how dye-retaining and non-dye retaining cells differed in their cell cycle status, univariant cytofluorimetric analysis of the cell cycle distribution of Vybrant® DiD-positive and negative MDA-MB-231 cell fractions was undertaken using Hoechst 33342. Briefly, unlabelled and Vybrant® DiD-stained wild-type MDA-MB-231 cells were seeded at the optimal density of 1.0×10^4 cells per cm^2 into $75cm^2$ high-quality polystyrene tissue culture flasks and cultured continuously for five passages. Cultures were retrieved at passage five post-staining and samples of 1.0×10^6 cells prepared in serum-free basal culture medium. Samples were stained with 5μg/ml Hoechst 33342, as described in **Section 2.5.2.2.**, prior to flow cytometric cell cycle profile analysis. During cytofluorimetric analyses, Vybrant® DiD staining status was used to differentiate populations of interest using the gating configuration pre-set using unlabelled samples. Vybrant® DiD-positive and negative populations were then concomitantly analysed for relative Hoechst 33342 content, allowing assessment of the cell cycle profile of each population (**Figure 3.20.**). The outcome of these assays revealed that dye-retaining cells collected in the G_2/M-phase of the cell cycle relative to the dye-negative population (**Figure 3.21.**); approximately 26.73% of Vybrant® DiD-positive cells were found to exist in the G_2/M-phase compared to just 15.40% of Vybrant® DiD-negative cells (P ≤ 0.0001). A corresponding decrease in the G_0/G_1 fraction was observed in the dye-retaining cell population with 49.87% being observed in this phase compared to 63.60% of dye-negative cells on average (P ≤ 0.0001). These observations were seen to indicate that the slow cycling, relatively quiescent nature of the dye-retaining MDA-MB-231 cell fraction was, at least in part, the result of an extended G_2/M-phase transition.
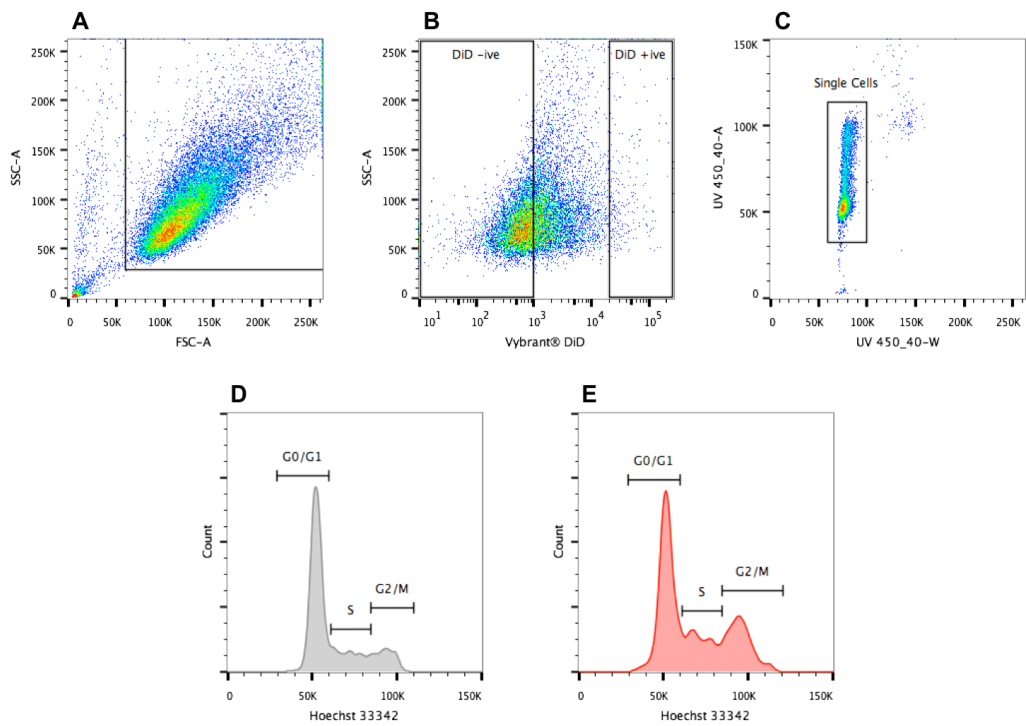
Figure 3.20. Cell Cycle Analysis in Dye-Retaining and Negative Populations

Cellular debris was gated-out of the event population (**A**) and the resultant events divided into Vybrant® DiD-negative and positive populations using gates defined by unlabelled and freshly labelled samples, respectively (**B**). The single cell events within each sub-population were then identified (**C**) before the cell cycle distribution of the Vybrant® DiD-negative (**D**) and Vybrant® DiD-positive (**E**) populations were analysed based on Hoechst 33342 fluorescence which estimates relative DNA content based on stoichiometric binding of the Hoechst dye to cellular DNA.
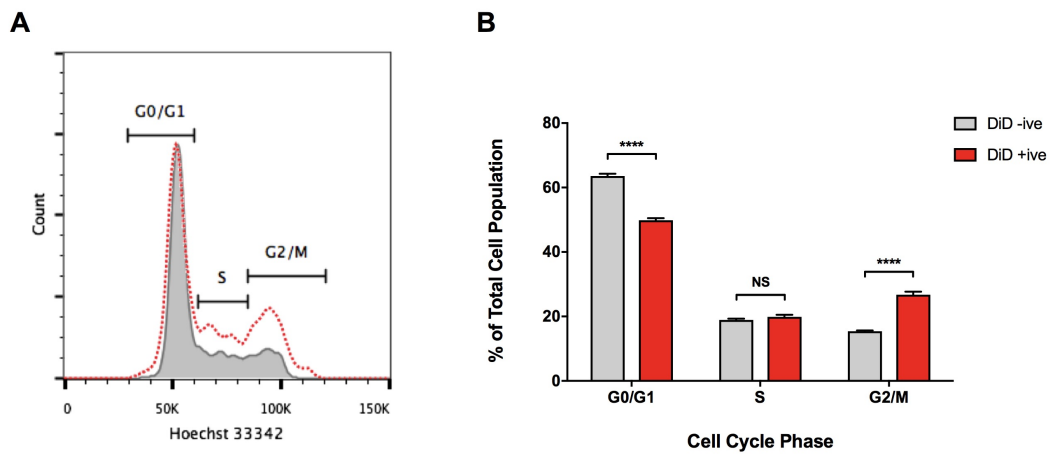
Figure 3.21. Cell Cycle Profiles of Dye-Retaining and Negative Populations

A: The univariant relative cell cycle distribution of Vybrant® DiD-positive (red dotted line) and negative (grey) MDA-MB-231 cells at five passages post-staining are shown. The location of the G_0/G_1-phase (haploid chromosome number), S-phase (intermediate chromosome number) and G_2/M-phase (diploid chromosome number) peaks are illustrated. **B**: The percentage of total cells in each phase of the cell cycle were compared between Vybrant® DiD-positive and negative populations using two-way ANOVA followed by Sidak's Multiple Comparison Test (NS = not statistically significant or $P > 0.05$, **** = $P \leq 0.0001$). Data are expressed as the mean average ± SEM for n = 3 biologically independent repeat experiments.

Univariant cell cycle analyses indicated that Vybrant® DiD-retaining cells were relatively slow cycling due to an extended G_2/M-phase transition. However, it was also possible that the Vybrant® DiD-retaining fraction was made up of both absolutely quiescent (G_0 arrested) and relatively quiescent and slowly cycling cells. In order to establish whether this was the case, immunofluorescent staining for Ki67 was used. The Ki67 protein is a positive marker of active cell proliferation required to maintain individual mitotic chromosomes and is therefore expressed within the nucleus of cells at all active stages of the cell cycle (G_1, S, G_2 and M-phases) but absent during G_0. In order to determine differential expression of Ki67 between Vybrant® DiD-retaining and non-dye-retaining cells, each population was isolated by FACS at passage five post-staining and 2000 cells of each type deposited onto glass microscope slides using a cytocentrifuge as described in **Section 2.3.2.1.** Samples were immunostained for expression of Ki67 using antibodies detailed in **Table 3.2.** according to the protocol for detection of intracellular antigens by indirect immunofluorescence outlined in **Section 2.3.2.2.** The final working protein concentration of antibodies used was determined by preliminary assays carried out in the same manner in which a range of final protein concentrations of primary and secondary antibodies were used; primary antibody concentrations ranged from 0.1µg/ml to 10µg/ml, while secondary antibody concentrations ranged from 2µg/ml to 10µg/ml, as recommended by the supplier. Immunostained samples were imaged under fluorescence microscopy and a series of three non-overlapping fields captured at 100X magnification using the tile scan function of the Leica AF6000LX microscope for manual scoring of marker expression (as described in **Section 2.4.**).

Table 3.2. Antibodies Used in Immunostaining for Ki67 Expression

Target	Host Species	Clonality	Isotype	Conjugate	Final Conc. (µg/ml)	Supplier	Cat. No.
Ki67	Rabbit	Poly	IgG	None	1	Abcam	ab15580
None	Rabbit	Poly	IgG	None	1	Abcam	ab171870
Rabbit IgG H&L	Goat	Poly	IgG	AlexaFluor® 488	4	Abcam	ab150077

An unconjugated anti-Ki67 primary antibody, a matched isotype control antibody and an AlexaFluor® 488-conjugated secondary antibody were sourced from Abcam Plc. (Cambridge, U.K.). The working concentration of the isotype control antibody was matched to the exact working protein concentration of the primary antibody.

Samples that were immunostained for Ki67 expression were imaged under fluorescence microscopy; representative images depicting the staining pattern produced within Vybrant® DiD-positive and DiD-negative samples were initially captured at 200X magnification (**Figure 3.22.**). A series of three non-overlapping fields for each of three technical repeats of both Vybrant® DiD-positive and DiD-negative samples across three biologically independent sample sets were also captured at 100X magnification using the tile scan function of the Leica AF6000LX microscope for manual scoring of Ki67 expression, the results of which are displayed in **Figure 3.22.** The outcome of this scoring for Ki67 expression revealed that approximately 15% more dye-negative cells express Ki67 than in the dye-retaining cell population ($P \leq 0.001$). This result suggests that the overall slow-cycling nature of the dye-retaining MDA-MB-231 cell fraction is the net result of being comprised of a greater number of G_0 arrested cells along with the remaining population having an extended G_2/M-phase transition, as was revealed during cell cycle distribution analyses.
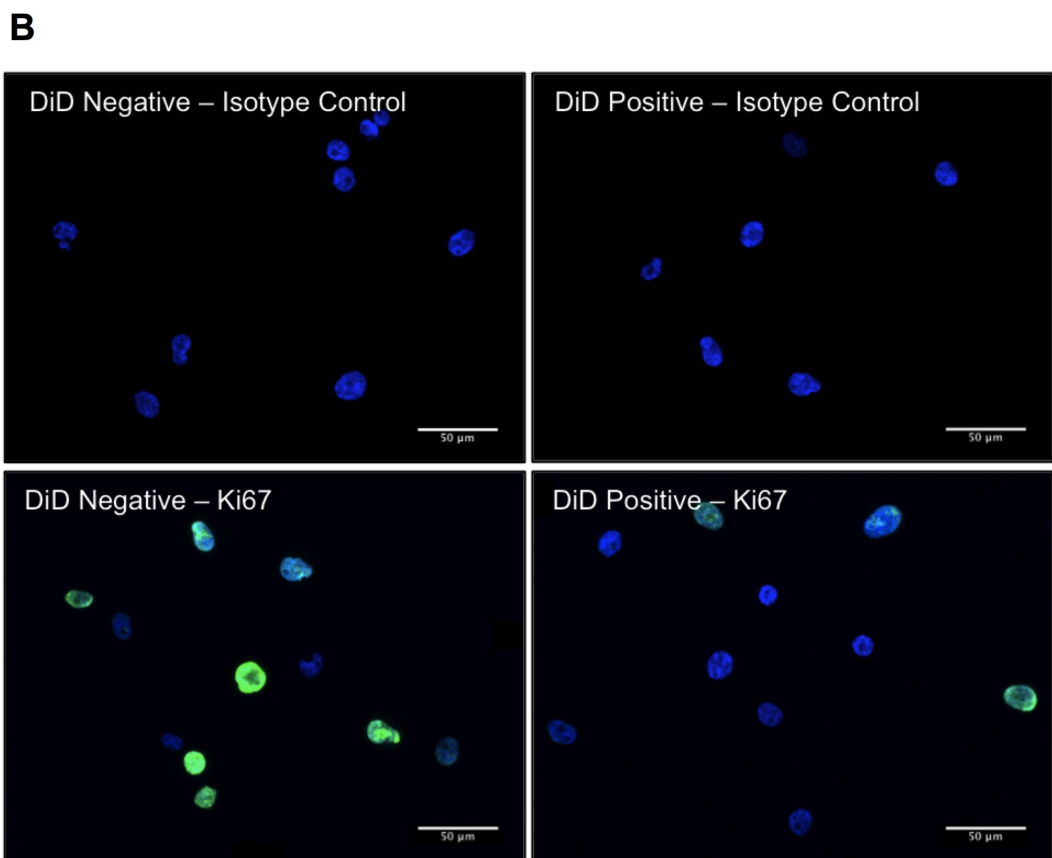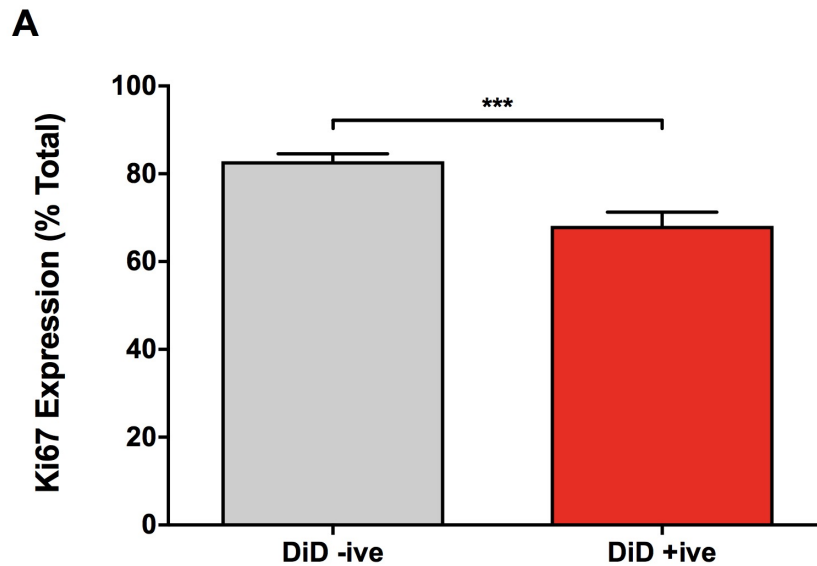
Figure 3.22. Ki67 Expression in Dye-Retaining and Negative Cell Populations

A: The percentage expression of Ki67 in Vybrant® DiD-negative and Vybrant® DiD-positive sub-populations in the MDA-MB-231 cell line at five passages post-staining. Data were compared using a two-tailed unpaired *t*-test (*** = P ≤ 0.001). Data are expressed as the mean average ± SEM for n = 3 biologically independent repeat experiments. **B**: The immunofluorescent staining pattern for Ki67 (green) is shown along with nuclear counterstaining with DAPI (blue). Specificity of staining in each case is indicated by the absence of staining in the matched isotype control sample. All images were captured using a 20x objective lens (scale bar = 50μm).

3.4.7. Suitability of Tumour Spheroid Cultures for Pulse-Chase Analyses

A number of three-dimensional systems for the culture of both primary and immortalised cancer cell lines *in vitro* have been developed. These so-called spheroid cultures aim to recapitulate tumour microenvironmental complexities and better reflect the nutrient, waste metabolite and oxygen tension gradients experienced by cells *in vivo* (Ishiguro *et al.*, 2017). Interestingly, three-dimensional *in vitro* culture systems have been reported to enrich for stem cell traits in some instances (Fillmore and Kuperwasser, 2008; Pece *et al.*, 2010; Raimondi *et al.*, 2016). Given the implicit link between stemness and quiescence, the potential utility of spheroid cultures for the purpose of prospective isolation of mitotically quiescent breast cancer cells by lipophilic dye retention was investigated.

A multitude of techniques have been described for establishing three-dimensional spheroid cultures. These techniques vary in their suitability for generation of tightly formed spheroids and their ability to recapitulate basic characteristics of tumours depending on the cell types used (Friedrich *et al.*, 2007; Lin and Chang, 2008; Friedrich *et al.*, 2009). Notably, it has been reported that the MDA-MB-231 human breast cancer lineage does not readily form uniform and compact spheroid cultures which develop regions of hypoxia and a necrotic core by conventional generation methods such as the hanging drop or agarose-liquid overlay culture (Ivascu and Kubbies, 2006; Moore *et al.*, 2012; Nagelkerke *et al.*, 2013). In order to circumvent this issue, Ivascu and Kubbies (2006) developed a modified version of the non-adherent liquid overlay technique that reliably produced spheroid cultures with the desired characteristics from the MDA-MB-231 cell line. The effectiveness and reproducibility of this approach was later validated by Nagelkerke *et al.* (2013).

Three dimensional spheroid cultures of MDA-MB-231 cells were established using the Ivascu and Kubbies (2006) method (described in detail in **Section 2.2.2.1. - Section 2.2.2.2.**) immediately after staining with Vybrant® DiD. Spheroid samples were collected and digested to form single cell suspensions as described in **Section 2.2.2.3.** at 72-hour intervals, the time-point equivalent to the sub-culture interval in monolayer cultures. At each time point, samples of spheroid-derived single cell suspensions were

analysed cytofluorimetrically and the percentage of Vybrant® DiD-positive events present within each sample was determined using the gating tree pre-set at the beginning of the experiment as previously detailed (**Section 3.4.3.**). Fluorescence photomicroscopy was also undertaken in order to visually demonstrate the changes in Vybrant® DiD staining over the duration of the assay. Assay results and representative images are depicted in **Figures 3.23.**

MDA-MB-231 spheroid cultures were relatively poorly proliferative, resulting in retention of dye by a large proportion of cells at all time points. After 18 days of continuous culture post-staining 68.63% of cells remained positively stained with Vybrant® DiD on average while only 0.08% of cells retained dye at the equivalent time point when grown as an adherent monolayer. Flow cytometric cell cycle profiling using propidium iodide (**Section 2.5.2.1.**) illustrated that when grown as spheroids, the MDA-MB-231 cell cycle profile was significantly skewed towards the G_0/G_1 peak compared to rapidly dividing cells grown as adherent monolayer cultures (**Figure 3.24.**); 74.07% of cells grown as three-dimensional spheroids were found to be in the G_0/G_1 phase compared to 38.83% of cells grown as an adherent monolayer ($P \leq 0.0001$). This G_0/G_1 skewing resulted in a significant reduction in the S-phase population from 35.90% to 14.97% ($P \leq 0.0001$) and in the G_2/M-phase population from 19.37% to 4.57% ($P \leq 0.001$). This loss of proliferative capability and resultant retention of fluorescence by the bulk cell mass indicated that spheroid cultures are not suitable for prospective identification of quiescent cells by pulse-chase analyses in this cell line.

A: The percentage of Vybrant® DiD-stained MDA-MB-231 cells in non-adherent three-dimensional spheroid cultures was measured at 72 hour intervals. Data are expressed as the mean average ± SEM for n = 3 biologically independent repeat experiments; the mean average value is denoted above the respective data bar. **B**: Representative images of Vybrant® DiD staining in three-dimensional MDA-MB-231 cultures at 3 days (left), 9 days (centre) and 18 days (right) post-staining. All images were captured using a 5x objective lens (scale bar = 250µm).

Figure 3.23. Dye-Retaining Cell Frequency in MDA-MB-231 Spheroid Cultures
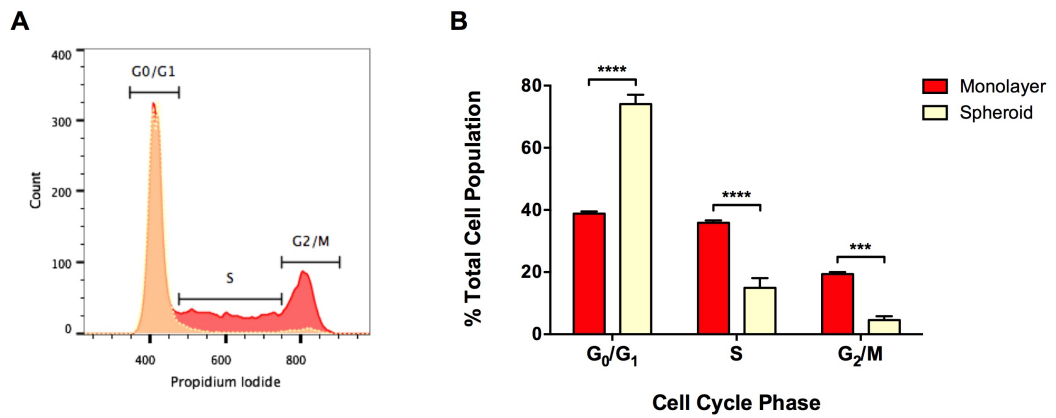
Figure 3.24. Cell Cycle Profiling of Two- and Three-Dimensional Cultures

A: The univariant cell cycle analysis profiles of MDA-MB-231 cells grown as two-dimensional monolayer cultures (red) and three-dimensional spheroid cultures (yellow) are shown. The location of the G_0/G_1-phase (haploid chromosome number), S-phase (intermediate chromosome number) and G_2/M-phase (diploid chromosome number) peaks are illustrated. **B**: The percentage of total cells in each phase of the cell cycle were compared between two-dimensional monolayer and three-dimensional spheroid cultures using two-way ANOVA followed by Sidak's Multiple Comparison Test (*** = $P \leq 0.001$, **** = $P \leq 0.0001$). Data are expressed as the mean average ± SEM for n = 3 biologically independent repeat experiments.

3.5. Discussion

In this chapter, the utility of Vybrant® fluorescent dyes for pulse-chase tracing of cell proliferation in monolayer breast cancer cell cultures has been demonstrated. This technique was shown to have no significant effect on cellular function or culture growth and has proved to be both effective and highly reproducible in facilitating identification of mitotically inactive cells across cell lines of contrasting molecular sub-types. Using a similar method to the one described herein, Moore *et al.* (2012) previously identified a slow-cycling sub-population in the MDA-MB-231 cell line when grown as adherent monolayer cultures. Quiescent cells were isolated in this case based on persistent retention of the fluorescent dye carboxyfluorescein diacetate succinimidyl ester (CFSE) and were found to represent approximately 0.1% of the total cell population. Comparative analysis of fluorescence intensity and cell cycle profiling of dye-retaining and non-dye-retaining populations by Moore *et al.* (2012) indicated that the dye-retaining cells were slowly cycling. The significant decrease in the relative brightness of Vybrant® dye-retaining populations compared to freshly labelled samples observed here suggests some degree of mitotic activity resulting in very gradual loss of the initial dye label. Consequently, it appears that dye-retaining cells are likely to represent a relatively slow cycling sub-population. Moore *et al.* (2012) also attempted to determine whether growing cells as three-dimensional spheroid cultures enriched for cells with the quiescent phenotype, but found that MDA-MB-231 cells formed poorly proliferative spheroids and that this impeded effective application of the lipophilic pulse-chase methodology, as was also demonstrated here.

Although the description of a label-retaining cell sub-set in MDA-MB-231 cells is not entirely novel, prospective functional identification of a mitotically quiescent sub-population has not been reported for MCF-7, ZR-75-1, MDA-MB-468 or SK-BR-3 cell lines. Interestingly, the identification of a discreet population of dye-retaining cells after 5 or 6 passages of continuous culture across multiple cell lines not only indicates the presence of relatively or absolutely mitotically inactive sub-clones in each case, but also suggests that these sub-clones are an intrinsic feature of breast cancer. The considerable degree of continuity between the average quiescent cell population size identified here and that described by Moore *et al.* (2012) might be seen as supporting

this hypothesis. Moreover, the notable comparability between the size of the label-retaining cell population described in these studies and of those described in the closely related works of Wang *et al.* (2015a) and Dembinski and Krauss (2009) in models of prostate and pancreatic cancer, respectively, suggest that a slow cycling or quiescent population is an intrinsic feature of multiple cancer types. Given that cancer stem cells have already been isolated from multiple cancer types and are supposed to exist in a transient state of quiescence like their non-malignant counterparts, the isolation of label-retaining cell sub-sets across multiple cancer types might indicate that quiescent and stem cell populations are non-mutually exclusive. The aforementioned studies by Wang *et al.* (2015a) and Dembinski and Krauss (2009) concurrently indicated that label-retaining quiescent cells do possess stem cell traits and significant metastasis-initiating capacity, despite displaying incomplete overlap with supposed stem cell marker proteins. While Moore *et al.* (2012) were relatively limited in their characterisation of quiescent MDA-MB-231 sub-clones, failing to address both breast cancer stem cell marker expression and many functional parameters, their demonstration of significant therapeutic resistance and tumour re-initiating capability also implies non-mutual exclusivity between quiescent and cancer stem cell populations. As such, redressing a more extensive characterisation of dye-retaining breast cancer cells and their deployment of accepted stem cell traits will form a key focus of work described in subsequent chapters.

While it is entirely feasible that a population of cells that had entered into a state of irreversible cell cycle arrest or senescence would retain a lipophilic fluorescent label post-staining, the dye-retaining cell population identified here was shown to be negative for senescence-associated β-galactosidase activity at pH 6.0. Furthermore, analysis of both cell cycle distribution, changes in average fluorescence of the retained dye label and Ki67 expression collectively indicated that Vybrant® dye retaining cells were primarily actively dividing but slow-cycling relative to the non-label-retaining bulk cell population. Analysis of Ki67 expression also showed that, although the majority of dye-retaining cells existed in a Ki67 positive state and therefore likely to be actively dividing, a significantly lower proportion were Ki67 positive than in the dye-negative fraction. When taken together, these observations indicate that the dye-retaining fraction is comprised of both absolutely quiescent (G_0 arrested and Ki67 negative) and

relatively quiescent but slow cycling (extended G_2/M and Ki67 positive) cells that contribute to an overall lower mitotic activity. This suggests a possible hierarchic organisation within this fraction in which intermittently cycling quiescent cells gives rise to a relatively quiescent transit amplifying population, such has recently been shown to characterise the cellular hierarchy of normal mammary tissue and is an emerging feature of breast cancer (Skibinski and Kuperwasser, 2015). Interestingly, those cells which appear to comprise the most immature sub-set in the breast cancer cellular hierarchy and demonstrate features of the putative metastasis-initiating population (chemoresistance, high metastatic and invasive capability, dormancy competence and stemness) are also characterised by cycling quiescence and a long doubling time (Patel *et al.*, 2012).

3.6.   Conclusions

The Vybrant® dyes DiO, CM-DiI and DiD each stained human breast cancer cell cultures in a homogenous manner. Cell viability, clonogenicity and migratory capability were all unaffected following labelling of cultures with each of these dyes, as were net culture growth characteristics. Vybrant® DiD resulted in the greatest increase in median fluorescence intensity relative to that of unlabelled cultures under cytofluorimetric analysis and was therefore deemed best suited for use in lipophilic dye retention assays. Adherent monolayer cultures were determined to be better suited to use in dye-retention assays than three-dimensional spheroid cultures, owing to the relatively poorly proliferative nature of the latter leading to a high proportion of dye-retaining cells up to 18 days post-staining. Dye retention assays undertaken in monolayer cultures of five distinct human breast cancer cell lines revealed a slow-cycling, relatively quiescent sub-population of cells after five passages of continuous culture. The exact nature of these dye-retaining quiescent cells and the effects that modifying the culture environment have on the dye-retaining quiescent population will be explored in subsequent chapters.

Chapter 4

The Effects of Modulating *In Vitro*

Conditions on the Mitotically Quiescent

Sub-Population in Breast Cancer

4.1. Summary

The contemporary plasticity model of tumoural heterogeneity and emerging experimental evidence both strongly suggest that mitotic quiescence is an inducible phenomenon that is instructed by the tumoural microenvironment, thereby implying that controlled modulation of *in vitro* culture conditions could facilitate the generation of relatively large numbers of quiescent tumour cells for further study. This possibility is a highly desirable prospect as the limiting cost and technical difficulty associated with acquisition of sufficient numbers of quiescent cancer cells from extant *in vivo* model systems has been one of the principal factors impeding progress in understanding the biological processes that underpin tumour cell quiescence. This chapter describes a series of experiments designed to enable a better understanding of how *in vitro* microenvironmental conditions give rise to tumour cells with a mitotically quiescent phenotype.

4.2. Introduction

According to a position paper which was the result of the collaborative efforts of over one hundred internationally recognised specialist breast cancer scientists, clinicians and healthcare professionals, "*understanding the molecular mechanisms of tumour heterogeneity, dormancy, de novo or acquired resistance and how to target key nodes in these dynamic processes*" was one of ten critical research gaps and translational priorities identified for the successful prevention and treatment of breast cancer (Eccles *et al.*, 2013). While there is an obvious requirement for significant advancement in this preeminent area, furthering extant knowledge of these phenomena has been significantly hampered by the difficulty of obtaining sufficient numbers of quiescent cells from the existing *in vivo* model systems used to study breast cancer metastasis.

Previous *in vivo* studies undertaken within the Holen group have demonstrated that a sub-clonal population present in both human breast and prostate tumour cell lines are capable of successful engraftment in the long bones of immunocompromised mice but are able to remain non-proliferative for a protracted period of time (**Figure 4.1.**) (Ottewell *et al.*, 2014a; Ottewell *et al.*, 2014b; Wang *et al.*, 2015b; Wang *et al.*, 2015c). In the preceding chapter, a similar sub-clonal population of cells shown to be either non-dividing or very slowly cycling over an extended time period (up to six passages of culture growth) was identified within multiple human breast cancer cell lines grown *in vitro* using a fluorescent lipophilic dye retention method. Fluorescent dye-retaining human prostate cancer cells that were identified by similar means in the closely related work of Wang *et al.* (2015b) were shown to be significantly more metastatic *in vivo* than the corresponding rapidly dividing population, and had a propensity to colonise the long bones in particular. Taken together, these findings not only suggest that a mitotically quiescent sub-population is a feature of multiple cancer types, but that these slow-cycling cells possess enhanced metastatic potential. Given the discussed limitations of acquiring metastasis-initiating cells from *in vivo* models, the ability to identify, isolate and characterise a relatively large number of inherently quiescent cells from human breast cancer cell lines using the lipophilic dye retention model described previously herein is seemingly a highly attractive prospect that could

potentially enable significant advances in current knowledge of the biological processes underpinning population heterogeneity, the quiescent state and associated enhanced metastatic potential in breast cancer.
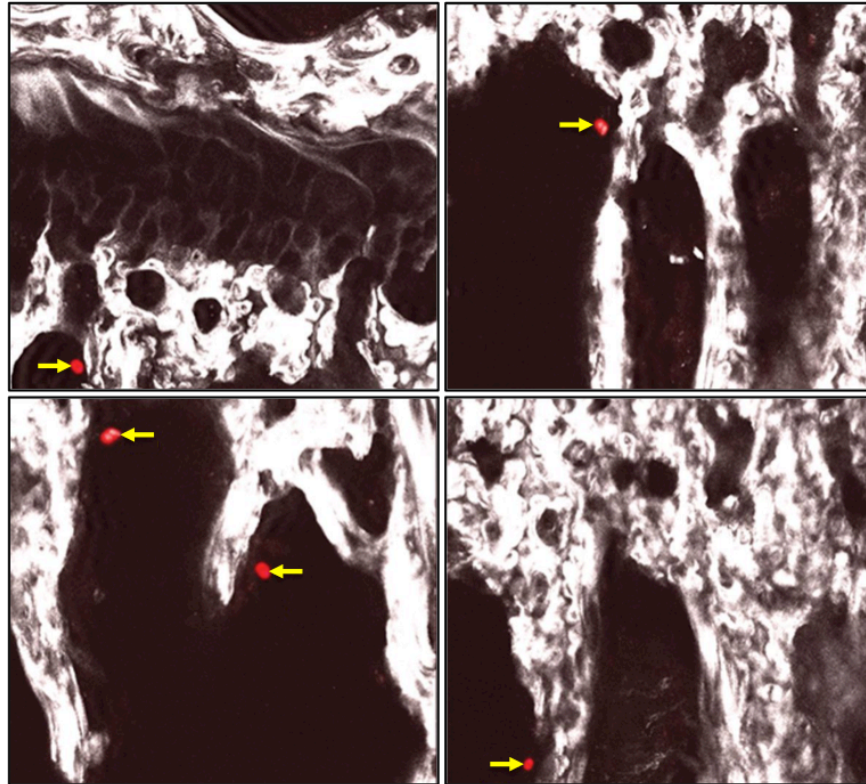
Figure 4.1. Non-Proliferative Tumour Cells in Proximal Trabecular Bone of Mice

Vybrant® DiD-labelled MDA-MB-231 cells (red fluorescent events highlighted by yellow arrows) present in the proximal trabecular region of the tibiae of immunocompromised mice at 35 days post-intravenous injection. These findings demonstrate that tumour cells have successfully homed to bone and engrafted but remain non-proliferative for a protracted period of time. Image modified from Ottewell *et al.* (2014). Zoledronic acid has differential antitumor activity in the pre- and postmenopausal bone microenvironment *in vivo*. Clin Cancer Res, 20, 2922-32 with permission from American Association for Cancer Research.

Given that conditional cellular mitotic quiescence (previously discussed in **Section 1.6.**
- Section 1.7.) is suggested to arise at either pre-metastatic or post-metastatic sites due to a non-growth permissive cellular microenvironment, it is plausible that the quiescent cell population identified within *in vitro* cultures is, at least partially, influenced by microenvironmental stimuli. A greater understanding of how the culture conditions present *in vitro* either give rise to or might be used to enrich the dye-retaining cell population could provide critical insight into the mechanisms governing the existence and survival of cell populations with reduced mitotic activity or enable isolation of greater cell numbers for elucidation of these as yet undefined biological processes. Consequently, the work described within this chapter primarily focuses on the degree to which the intrinsic quiescent cell population size and overt outgrowth of these quiescent sub-clones are influenced by *in vitro* culture conditions. The MDA-MB-231 human breast cancer cell line, the predominant lineage used for *in vivo* modelling of breast cancer bone metastasis, was the principal cell line used in this and subsequent chapters due to the necessity of planned future *in vivo* experiments to determine the intrinsic metastatic potential of dye-retaining and non-dye-retaining populations and to ascertain how findings from the *in vitro* models described herein translate to the *in vivo* setting.

4.3. Aims, Hypothesis and Objectives

The aim of the work described in this chapter was to explore how *in vitro* culture conditions affect the mitotically quiescent breast cancer cell population identified using the fluorescent lipophilic dye retention method and to determine whether this population is an intrinsic feature of breast cancer cell lines or if it emerges under inductive microenvironmental conditions within growing cultures.

The key hypothesis pertaining to the work described in this chapter was that ***the latent mitotically quiescent sub-populations identified within human breast cancer cell lines are not an inherent intrinsic feature but arise due to microenvironmental induction.***

The following objectives were defined in order to test this hypothesis:

1. Determine how monolayer culture conditions affect the size of the slow-cycling cell population (as determined by dye-retention at passage 6 post-staining).

2. Establish whether or not the slow-cycling population is able to re-emerge within cultures of isolated rapidly dividing cells.

3. Determine how culture conditions affect the clonogenicity of the rapidly dividing and slow-cycling cell populations in monolayer colony formation assays.

4. Ascertain whether cells held in a quiescent state by modulating culture conditions can be stimulated to form colonies by re-establishing a standard culture environment.

4.4. Materials and Methods

4.4.1. Assay of the Effect of Confluency at Sub-Culture on Dye-Retention

Wild type MDA-MB-231 and MCF-7 cells were stained in suspension with Vybrant® DiD or Vybrant® CM-DiI according to the manufacturer instructions (**Section 2.3.1.**). Stained cells were seeded at the cell line-specific optimal density (**Table 2.2.**) into 75cm^2 high-quality polystyrene tissue culture flasks along with unlabelled control samples and cultured continuously. The passage-length used for maintaining sub-confluency in growing cultures was 3 days for both MDA-MB-231 and MCF-7 cell lines, while full confluency was reached after 4 days in both cases. Configuration of the flow cytometer was undertaken at the outset of each experiment as described previously (**Section 3.4.3.**). At each sub-culture interval, cells were retrieved and counted before being assessed cytofluorimetrically for percentage dye-positivity. Briefly, samples of 1.0 x 10^6 cells were prepared from each retrieved culture for cytofluorimetric analysis by undertaking centrifugation at 150 x g for 5 minutes followed by resuspension in serum-free basal medium. Prepared cell suspensions were analysed by flow cytometry in order to determine the percentage of Vybrant® dye-positive events present using the gating tree pre-set at the beginning of the experiment. The percentage positivity of each cell line was monitored in this way for up to six consecutive passages of culture growth.

4.4.2. Establishing Dye-Retaining Cell Re-Emergence in Rapidly Dividing Cultures

After a total of five consecutive passages of culture post-staining, Vybrant® DiD-stained MDA-MB-231 cultures were sorted into dye-negative and dye-positive fractions by FACS. The isolated dye-negative fraction was then re-stained according to the manufacturer's instructions (**Section 2.3.1.**) and seeded at the optimal density of 1.0×10^4 cells per cm^2 into 75cm^2 high-quality polystyrene tissue culture flasks, along with unlabelled control samples prepared concomitantly in the same manner. Re-stained cultures were grown for a further six consecutive passages, with dye-retention being monitored at each consecutive sub-culture in the same manner as outlined previously (**Section 3.4.3.**).

4.4.3. Assessing HIF-1α Expression in Dye-Negative and Dye-Retaining Cells

Staining of wild type MDA-MB-231 cells with Vybrant® DiD was undertaken in suspension according to the manufacturer instructions (**Section 2.3.1.**). Stained cells were seeded at the recommended optimal density (**Table 2.2.**) into 75cm^2 high-quality polystyrene tissue culture flasks and cultured continuously for five subsequent passages. Following retrieval of stained cultures at passage five post-staining, Vybrant® DiD-positive and DiD-negative cells were isolated by FACS and 2000 cells of each type deposited onto glass microscope slides using a cytocentrifuge as described in **Section 2.3.2.1.** Samples were immunostained for expression of HIF-1α using antibodies detailed in **Table 4.1.** according to the protocol for detection of intracellular antigens by indirect immunofluorescence outlined in **Section 2.3.2.2.** The final working protein concentration of antibodies used was determined by preliminary assays carried out in the same manner in which a range of final protein concentrations of primary and secondary antibodies were used; primary antibody concentrations ranged from 1μg/ml to 10μg/ml, while secondary antibody concentrations ranged from 1.875μg/ml to 15μg/ml, as recommended by the supplier. Immunostained samples were imaged under fluorescence microscopy and a series of three non-overlapping fields captured at 100X magnification using the tile scan function of the Leica AF6000LX microscope for manual scoring of marker expression (as described in **Section 2.4.**). Representative images of the staining pattern were also captured at 200X magnification.

Table 4.1. Antibodies Used in Immunostaining for HIF-1α Expression

Target	Host Species	Clonality	Isotype	Clone No.	Conjugate	Final Conc. (µg/ml)	Supplier
HIF-1α	Mouse	Mono	IgG2b	H1alpha67	None	5	Abcam
None	Mouse	Mono	IgG2b	7E10G10	None	5	Abcam
Mouse IgG+M	Goat	Poly	IgG	-	AlexaFluor® 488	3.75	Stratech

An unconjugated antibody against HIF-1α and a matched isotype control antibody were sourced from Abcam Plc. (Cambridge, U.K.). An AlexaFluor® 488-conjugated secondary antibody was sourced from Stratech Scientific Ltd. (Newmarket, U.K.). The working concentration of the isotype control antibody was matched to the exact working protein concentration of the primary antibody.

4.4.4. Serum and Glucose Titration Assays

Cells were seeded in triplicate wells of 24-well cluster plates at the optimal density and supplemented with 0.2ml of complete growth medium per cm^2 growth area. Plates were placed into incubation under standard growth conditions for a 12-hour period in order to allow cells to settle and adhere to the plate surface. For glucose titration assays, the medium contained within each well was carefully removed and replaced with an equivalent volume of growth medium containing 10% (v/v) supplemental dialysed FBS and a final concentration of glucose between 0mM and 16.4mM. Glucose concentrations above 11mM were achieved by addition of the required volume of 0.56M D-(+)-glucose solution (Sigma-Aldrich Company Ltd.). For FBS titration assays, the medium contained within each well was carefully removed and replaced with an equal volume of growth medium containing the standard 11mM glucose and a final dialysed FBS concentration between 0% and 15% (v/v). At the end of the logarithmic phase of growth (**Table 3.1.**), all wells were retrieved by trypsinisation as described previously (**Section 2.2.1.2.**) and the viable cell number determined by haemocytometric counting using the trypan blue dye exclusion method (**Section 2.2.3.**).

4.4.5. Monitoring Dye-Retention in Serum- or Glucose-Depleted Cultures

Staining of MDA-MB-231 cells with Vybrant® DiD was undertaken in suspension according to the manufacturer's instructions (**Section 2.3.1.**). A series of 75cm^2 high-quality polystyrene tissue culture flasks were pre-filled with RPMI-1640 basal culture medium containing either 11mM glucose and 10% FBS (control samples), 11mM glucose and the EC$_{50}$ concentration of FBS (4% (v/v)) or the EC$_{50}$ concentration of glucose (2.2mM) and 10% (v/v) FBS. Stained cells and unlabelled samples used for cytofluorimetric configuration were seeded into these flasks at the optimal density of 1.0 x 10^4 cells per cm^2 and cultured continuously for six passages; sub-culture was undertaken at 72-hour intervals. At each sub-culture, cells were retrieved and counted before being assessed cytofluorimetrically for percentage dye-positivity as described previously (**Section 3.4.3.**).

4.4.6. Cell Cycle Profiling Under Varied Culture Conditions Using Propidium Iodide

Wild-type MDA-MB-231 cells were seeded at the optimal density of 1.0 x 10^4 cells per cm^2 into a series of 25cm^2 high-quality polystyrene tissue culture flasks pre-filled with RPMI-1640 culture medium containing either 11mM glucose and 10% FBS (control samples), 11mM glucose and the EC$_{50}$ concentration of FBS (4% (v/v)), or the EC$_{50}$ concentration of glucose (2.2mM) and 10% (v/v) FBS. Cells were placed into incubation for 3 days post-seeding before being retrieved and counted (**Section 2.2.1.2** and **Section 2.2.3.**). Samples of 1.0 x 10^6 cells from each cell suspension were fixed in 70% (v/v) ethanol and incubated with a mixture of 0.002% (w/v) RNase A in 75μM propidium iodide solution prior to cytofluorimetric cell cycle profile analysis, as described previously (**Section 2.5.2.1.**).

4.4.7. Western Blot Analysis of ERR-α Expression in Breast Cancer Cell Lines

Cultures of MCF-7, ZR-75-1, MDA-MB-231, MDA-MB-468 and SK-BR-3 human breast cancer cell lines were grown as detailed in **Section 2.2.1.1.** until approximately 70% confluency was reached. Whole cell lysate were prepared from each cell line and western blot analysis for oestrogen-related receptor-alpha (ERR-α) and the constitutively expressed cytoskeletal protein vinculin (used as a loading control) was carried out according to the methods detailed in **Section 2.7.** The antibodies used are detailed in **Table 4.2.** below. The final working protein concentration of antibodies used was determined by preliminary assays carried out in the same manner in which a range of final protein concentrations of primary antibodies were used; primary antibody concentrations ranged from 1µg/ml to 5µg/ml, while the secondary antibody concentration used was always 0.1µg/ml, as recommended by the supplier.

Table 4.2. Antibodies Used in Western Blot Analysis of ERR-α Expression

Target	Host Species	Clonality	Isotype	Conjugate	Final Conc. (µg/ml)	Supplier	Cat. No.
ERR-α	Rabbit	Poly	IgG	None	2.5	Abcam	ab93173
Vinculin	Rabbit	Poly	IgG	None	1	Abcam	ab73412
Rabbit IgG	Goat	Poly	IgG	Horseradish Peroxidase	2	Agilent	P0448

Unconjugated anti-ERR-α and anti-vinculin primary antibodies were sourced from Abcam Plc. (Cambridge, U.K.), while a horseradish peroxidase-conjugated secondary antibody was sourced from Agilent Technologies LDA U.K. Ltd. (Stockport, U.K.).

4.4.8. Flow Cytometric Analysis of ERR-α Expression in MDA-MB-231 Cells

MDA-MB-231 cells were cultured according to the methods described in **Section 2.2.1.1.** Following harvesting once cultures had reached approximately 70% confluency, samples of 1.0×10^6 cells were prepared and immunostained for ERR-α according to the general protocol for flow cytometric assessment of intracellular markers by indirect immunofluorescence outlined in **Section 2.3.3.3.** using the antibodies detailed in **Table 4.3.** below. The final working protein concentration of antibodies used was determined by preliminary assays carried out in the same manner in which a range of final protein concentrations of primary and secondary antibodies were used; primary antibody concentrations ranged from 10μg/ml to 50μg/ml, while secondary antibody concentrations ranged from 0.5μg/ml to 1μg/ml, as recommended by the supplier.

Table 4.3. Antibodies Used in Flow Cytometric Analysis of ERR-α Expression

Target	Host Species	Clonality	Isotype	Conjugate	Final Conc. (μg/ml)	Supplier	Cat. No.
ERR-α	Rabbit	Poly	IgG	None	10	Abcam	ab93173
None	Rabbit	Poly	IgG	None	10	Abcam	ab171870
Rabbit IgG H&L	Goat	Poly	IgG	AlexaFluor® 488	0.5	Abcam	ab150077

An unconjugated anti-ERR-α primary antibody, a matched isotype control antibody and an AlexaFluor® 488-conjugated secondary antibody were all sourced from Abcam Plc. (Cambridge, U.K.). The working concentration of the isotype control antibody was matched to the exact working protein concentration of the primary antibody.

4.4.9. Preparation of Conditioned Medium

Wild-type MDA-MB-231 cells were seeded into 75cm^2 high-quality polystyrene tissue culture flasks at the optimal density of 1.0 x 10^4 cells per cm^2 and supplemented with 0.2ml of complete culture medium per cm^2 of culture vessel surface area. Conditioned culture medium was removed from growing cultures at the appropriate time interval, which was pre-determined as 96 hours post-seeding for production of glucose-depleted conditioned medium using the MDA-MB-231 cell line (**Section 4.5.7.**). Conditioned medium was immediately centrifuged at 150 x *g* for 5 minutes in order to remove any residual cells contained within the medium. Following centrifugation, the supernatant was decanted and then sterile filtered using a 0.2μm polycarbonate syringe filter. Conditioned medium was kept in a refrigerator maintained at 4°C for short-term storage or at -80°C for long-term storage.

4.4.10. Measurement of Glucose and Lactate in MDA-MB-231 Culture Medium

Wild-type MDA-MB-231 cells were seeded into a series of 25cm^2 high-quality polystyrene tissue culture flasks at the optimal density of 1.0 x 10^4 cells per cm^2. Conditioned medium was collected at 24-hour intervals over a 7-day period and prepared as described above (**Section 4.4.9.**). The concentration of D-glucose and L-lactate present in each solution was determined using the D-glucose or L-lactate assay kit available from Eton Bioscience Inc. as described previously (**Section 2.8.2. - Section 2.8.3.**).

4.4.11. Colony Formation Assays Under Varied Culture Conditions

After a total of five consecutive passages of culture post-staining, Vybrant® DiD-stained MDA-MB-231 cultures were sorted into dye-negative and dye-positive fractions by FACS. Cells from each fraction were seeded at a clonogenic density of 20 cells per cm^2 into triplicate wells of 6-well cluster plates pre-filled with 3ml of culture medium in which either the glucose or serum content had been reduced to the EC$_0$, EC$_{25}$, EC$_{50}$ or EC$_{100}$ concentration (**Table 4.4.**), or which contained 0mM glucose and 22mM lactate (conditioned medium collected from growing MDA-MB-231 cultures at

4-days post-seeding with 10% FBS added). Seeded cluster plates were placed into incubation under standard growth conditions for a period of 6 days. Colony formation assays were subsequently undertaken (as described in **Section 2.2.6.1.**) and the number of colonies formed by Vybrant® DiD-positive and Vybrant® DiD-negative fractions under each set of conditions quantified.

4.4.12. Colony Formation Stimulation Assays

Following five consecutive passages of culture post-staining, Vybrant® DiD-stained MDA-MB-231 cultures were sorted into dye-negative and dye-positive fractions by FACS. Cells from each fraction were seeded at a clonogenic density of 20 cells per cm^2 into triplicate wells of 6-well cluster plates pre-filled with 3ml of culture medium in which either the glucose or serum content had been reduced to either the EC_0 or EC_{25} concentration (**Table 4.4.**), or conditioned medium containing 22mM lactate previously collected from growing MDA-MB-231 cultures at 4-days post-seeding with 10% FBS added. Seeded cluster plates were placed into incubation under standard growth conditions for a period of 6 days. After 6 days of growth post-seeding, colony formation assays were performed on half of each sample set. The culture medium within the wells of the remaining half of each sample set was exchanged for an equal volume of fresh complete culture medium (RPMI-1640 with 11mM glucose + 10% supplemental FBS), effectively replenishing the component from which cells had been deprived. These plates were subsequently replaced in incubation under standard growth conditions for another period of 6 days. Colony formation assays were then undertaken (as described in **Section 2.2.6.1.**) and the number of colonies formed by Vybrant® DiD-positive and Vybrant® DiD-negative fractions under each set of conditions quantified. A summary of the experimental timeline for assays dependent on colony formation stimulation is depicted in **Figure 4.2.**

Stain with Vybrant® DiD
Seed into culture vessels

Retrieve cultures
Isolate DiD- and DiD+ cells by FACS
Seed clonogenic assay plates

Colony formation assay half of each sample set
Change medium (RPMI-1640 + 10% FBS)
remaining half of each sample set

Post-stimulation
colony formation assay

Five Passages of Culture Growth | 6 Days Exposure to Test Conditions | 6 Days
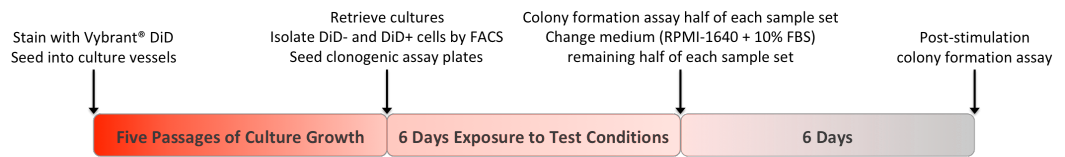
Figure 4.2. Timeline for Colony Formation Stimulation Assays

Vybrant® DiD-stained cells were cultured continuously for five passages prior to being reseeded into 6-well cluster plates and exposed to nutrient deficient medium for six days. Colony formation assays were performed on half of each sample set. The culture medium within the wells of the remaining half of each sample set was exchanged for an equal volume of fresh complete culture medium (RPMI-1640 with 11mM glucose + 10% supplemental FBS), replenishing the component to which cells had been deprived. A further six day incubation period was undertaken prior to determination of the number of colonies formed by Vybrant® DiD-positive and negative cells within each treatment group post-stimulation.

4.4.13. Colony Formation Assays in the Presence of ERR-α Inhibitors

Vybrant® DiD dye-negative and dye-positive MDA-MB-231 populations were isolated by FACS following five consecutive passages of culture post-staining. Each fraction was then seeded at a clonogenic density of 20 cells per cm^2 into triplicate wells of 6-well cluster plates pre-filled with 3ml of pre-conditioned culture medium (22mM lactate with 10% FBS added) that contained either Cpd29 or XCT790 at a final concentration of 10μM. Untreated control samples were composed concomitantly. Seeded cluster plates were placed into incubation under standard growth conditions for a period of 6 days. After 6 days of growth post-seeding, the culture medium in all wells was removed and replaced with an equal volume of complete RPMI-1640 culture medium with 11mM glucose and 10% FBS. Plates were subsequently replaced in incubation under standard growth conditions for another period of 6 days. Colony formation assays were then undertaken as described in **Section 2.2.6.1.** and the number of colonies formed by Vybrant® DiD-positive and Vybrant® DiD-negative fractions under each set of conditions quantified. A summary of the experimental timeline is depicted in **Figure 4.3.**

Figure 4.3. Timeline for Colony Formation Assays Post-ERR-α inhibitor Treatment

Vybrant® DiD-stained cells were cultured continuously for five passages prior to being reseeded into 6-well cluster plates under glucose depleted, lactate rich conditions in the presence of selective ERR-α inhibitors Cpd29 or XCT790 at a final concentration of 10μM for six days. After the initial six-day period, the culture medium within all wells was exchanged for an equal volume of fresh complete culture medium (RPMI-1640 with 11mM glucose + 10% supplemental FBS), effectively removing drug from culture medium, reducing lactate levels and replenishing glucose levels to normal. A further six day incubation period was undertaken prior to determination of the number of colonies formed by Vybrant® DiD-positive and negative cells within each treatment group.

4.4.14. Drug-Resistant Colony Formation Assays in the Presence of ERR-α Inhibitors

Fluorescence activated cell sorting was used to isolate Vybrant® DiD-positive MDA-MB-231 cells at passage five post-staining. Cells were seeded at a clonogenic density of 20 cells per cm^2 into triplicate wells of 6-well cluster plates pre-filled with 3ml of either pre-conditioned culture medium (22mM lactate with 10% FBS added) containing the IC$_{95}$ of doxorubicin (321nM) either alone or in combination with Cpd29 or XCT790 at a final concentration of 10µM. Untreated control samples were composed concomitantly. Seeded cluster plates were placed into incubation under standard growth conditions for a period of 6 days. After 6 days of growth post-seeding, the culture medium in all wells was removed and replaced with an equal volume of complete RPMI-1640 culture medium with 11mM glucose and 10% FBS. Plates were subsequently replaced in incubation under standard growth conditions for another period of 6 days. Colony formation assays were then undertaken as described in **Section 2.2.6.1.** and the number of colonies formed within each treatment group quantified. A summary of the experimental timeline is depicted in **Figure 4.4.**
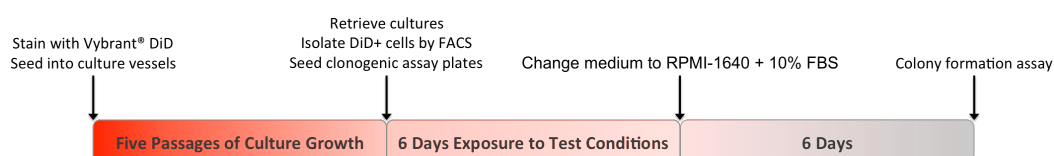
Figure 4.4. Timeline for Drug-Resistant Colony Formation Assays

Vybrant® DiD-retaining cells were isolated at passages five post-staining prior to being reseeded into 6-well cluster plates and exposed to pre-conditioned culture medium (22mM lactate with 10% FBS added) either alone or containing the IC$_{95}$ of doxorubicin (321nM) with or without Cpd29 or XCT790 at a final concentration of 10µM. After six days of exposure to test conditions the culture medium was exchanged for an equal volume of fresh complete culture medium (RPMI-1640 + 10% FBS) and a further six-day incubation period undertaken prior to determination of the number of colonies formed by cells within each treatment group post-stimulation.

4.5. Results

4.5.1. Sub-Culture at Full Confluency Does Not Affect Dye-Retaining Population Size

The established plasticity model of tumoural heterogeneity and emerging experimental evidence both imply that microenvironmental stimuli are able to influence the generation, size and rapid outgrowth of the quiescent or slow-cycling cell population (Rich, 2016; Fluegen *et al.*, 2017). During earlier experiments to determine the existence of a latent slow-cycling or quiescent population within human breast cancer cell lines, growing cultures were maintained at sub-confluent levels and were not allowed to progress further than the logarithmic phase of culture growth. Undertaking sub-culture at the point of complete surface coverage and allowing cultures to progress into the stationary phase of culture growth was therefore used to test the hypothesis that culture overgrowth, and the resultant metabolic stress induced due to loss of metabolic substrates and build-up of metabolic waste products, would increase the size of the latent quiescent population.

In both MDA-MB-231 and MCF-7 cell lines, undertaking sub-culture at full confluency did not result in a significant increase in the overall size of the slow-cycling dye-retaining cell population at the final passage of measurement compared to when cultures were maintained at sub-confluent levels, irrespective of the Vybrant® dye that was used and the resultant duration of the assay (**Figure 4.5.**). Univariant cytofluorimetric analysis of the cell cycle distribution of MDA-MB-231 cells maintained at confluent and sub-confluent levels revealed that cultures maintained at full confluency tended to be distributed more towards the G_0/G_1-phase and were therefore likely slower cycling then cultures maintained at sub-confluent levels (**Figure 4.6.**); an average of $54.73 \pm 1.53\%$ of cells from fully confluent cultures were found to exist in the G_0/G_1-phase compared to just $49.43 \pm 0.55\%$ of cells maintained at sub-confluency ($P \leq 0.01$). Small but statistically insignificant decreases in the S-phase and G_2/M-phase fractions were also measured in cells maintained at confluent levels, corresponding with (and likely cumulatively contributing to) the observed collection of cells in the G_0/G_1-phase. In Vybrant® DiD retention assays, $22.23 \pm 2.34\%$ of MDA-MB-231 cells were dye-positive after four consecutive passages post-staining when sub-

cultured at full confluency, compared to just 14.94 ± 1.47% in cultures maintained at sub-confluent levels, despite passage four being 16 days post-staining in confluent cultures but just 12 days post-staining in sub-confluent cultures. The degree of confluency at the time of sub-culture was therefore deemed to primarily determine the overall cell cycle status of a growing population and thus how rapidly dye was lost from the majority of cells to reveal the latent slow-cycling population. Due to the possibility that relatively subtle metabolic stressors in culture might take a longer period of time to generate slow-cycling populations, or that additional regulatory factors within a growing culture determine the size of a particular cell compartment, these results were not initially deemed to invalidate the presiding hypothesis that the slow-cycling populations in breast cancer cell lines arise due to microenvironmental induction. In order to test this hypothesis more directly, it was subsequently proposed to isolate the rapidly dividing cell fraction and establish whether a latent dye-retaining population was evident following a period of continuous culture. Further experiments to test the effects of more extreme metabolic stress on the size of the slow-cycling population were also planned.
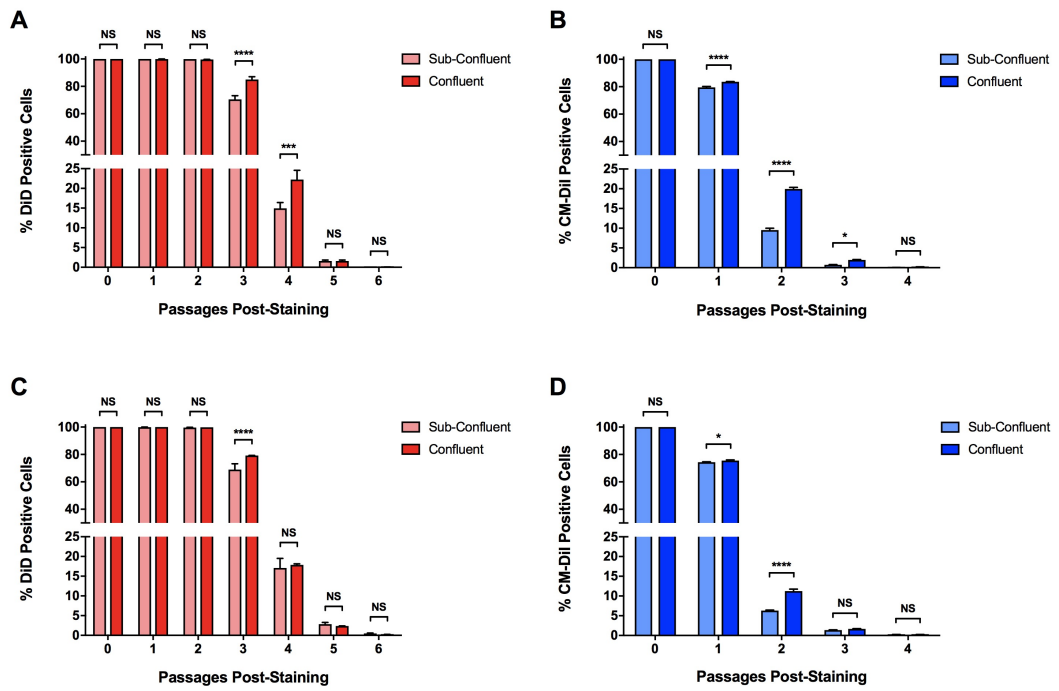
Figure 4.5. Dye Retention in Confluent and Sub-Confluent Cell Cultures

The percentage of Vybrant® DiD-stained or Vybrant® CM-DiI-stained MDA-MB-231 cells (**A** and **B**, respectively) or MCF-7 cells (**C** and **D**, respectively) in adherent monolayer cultures was measured over successive passages at the time of sub-culture, undertaken at either sub-confluency (72 hour intervals) or full confluency (96 hour intervals). The percentage of Vybrant® dye-stained cells was compared between samples over successive time-points using two-way ANOVA followed by Sidak's Multiple Comparison Test (NS = not statistically significant or P > 0.05, * = P ≤ 0.05, *** = P ≤ 0.001, **** = P ≤ 0.0001). Data are expressed as the mean average ± SEM for n = 3 biologically independent repeat experiments.
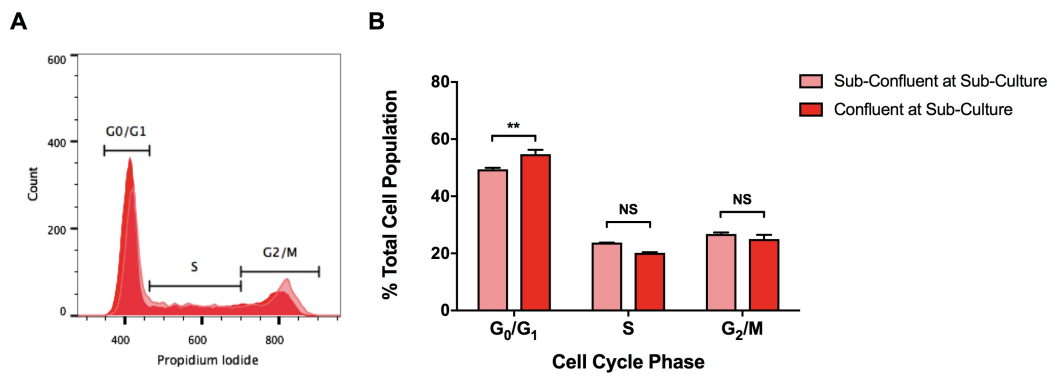
Figure 4.6. Cell Cycle Profile of Confluent and Sub-Confluent Cultures

A: The univariant cell cycle analysis profiles of adherent monolayer cultures of MDA-MB-231 cells grown in complete RPMI-1640 culture medium (10% supplemental FBS) when maintained at sub-confluent or fully confluent levels at the time of sub-culture. The location of the G_0/G_1-phase (haploid chromosome number), S-phase (intermediate chromosome number) and G_2/M-phase (diploid chromosome number) peaks are illustrated. **B**: The percentage of total cells in each phase of the cell cycle was compared between MDA-MB-231 cultures sub-cultured when at sub-confluent or fully confluent levels using two-way ANOVA followed by Sidak's Multiple Comparison Test (NS = not statistically significant or P > 0.05, ** = P ≤ 0.01). Data are expressed as the mean average ± SEM for n = 3 biologically independent repeat experiments.

4.5.2. Dye-Retaining Cells Can Re-Emerge from the Rapidly Dividing Population

In order to test the hypothesis that rapidly-dividing cells within human breast cancer cultures were able to give rise to the latent slow-cycling population previously identified, dye-retention assays were carried out following isolation and re-staining the rapidly-dividing (dye-negative) MDA-MB-231 population (**Section 4.4.2.**). In these re-stained cultures, dye-loss occurred much more rapidly than in the parental control cultures (**Figure 4.7.**); there were 47.77 ± 2.32% (P ≤ 0.0001) and 20.26 ± 2.43% (P ≤ 0.0001) fewer dye-stained cells within re-stained samples at passages three and four post-staining, respectively. In addition, the number of dye-retaining cells present reached < 1% by passage five, one passage of growth earlier than when this occurred in parental control samples. This rapid dye-loss was likely a reflection of the inherently rapidly dividing nature of the isolated dye-negative fraction, allowing effective dilution of the Vybrant® DiD label upon successive divisions to achieve non dye-positive levels over a much shorter timeframe. Interestingly, progressive dye loss ceased at passage five within the re-stained cultures and the number of dye-retaining cells stabilised between passages five and six at approximately 0.04%, a level which was not significantly different from the 0.077 ± 0.015% dye-retaining fraction measured in the parental MDA-MB-231 cultures. The re-emergence of the dye-retaining population within rapidly dividing cultures suggested that factors within the culture microenvironment were indeed responsible for formation of the dye-retaining population. Future experiments aimed to determine which factors could potentially be responsible for this phenomenon.
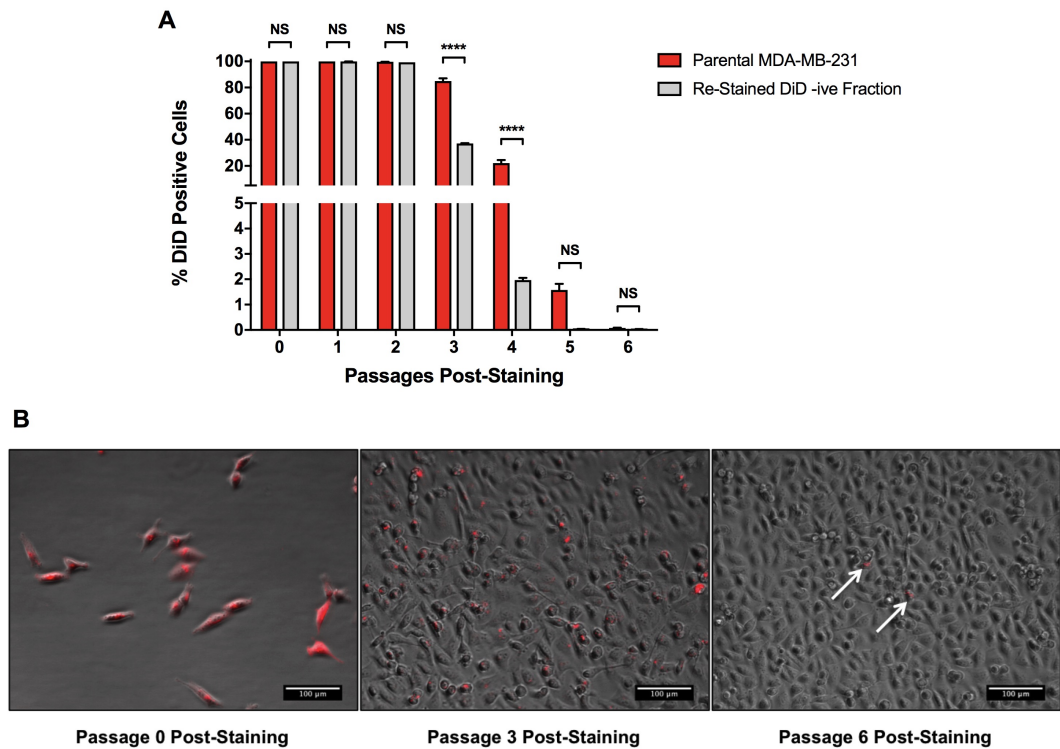
Figure 4.7. Vybrant® DiD Retention in Isolated Dye-Negative Cells after Re-Staining

A: The percentage Vybrant® DiD-stained cells within adherent monolayer cultures of parental MDA-MB-231 cells and re-stained dye-negative cells (previously isolated from parental MDA-MB-231 cultures by FACS at passage 5 post-staining with Vybrant® DiD) was measured over successive passages at the time of sub-culture undertaken at 72 hour intervals. The percentage of Vybrant® DiD-stained cells was compared between samples over successive time-points using two-way ANOVA followed by Sidak's Multiple Comparison Test (NS = not statistically significant or $P > 0.05$, **** = $P \leq 0.0001$). Data are expressed as the mean average ± SEM for n = 3 biologically independent repeat experiments. **B**: Representative images of Vybrant® DiD retention within cultures of re-stained dye-negative MDA-MB-231 cells at 6 hours (left), passage 3 (centre) and passage 6 (right) post-staining; the white arrows indicate dye retaining cells evident in the image. All images were captured using a 10x objective lens (scale bar = 100µm).

4.5.3. Hypoxia as a Potential Mechanism Giving Rise to Slow-Cycling Cells

Based on experimental observations that a dye-retaining population was able to re-emerge within a rapidly dividing culture, it was hypothesised that the localised consumption of oxygen and/or nutrients by rapidly dividing clones in wild-type cultures might lead to induction of a slow-cycling phenotype in neighbouring cells and therefore that dye-retaining cells would express higher levels of markers indicating metabolic stress. In order to test this hypothesis, HIF-1α was selected for assessment due to being regarded as the master transcriptional regulator of cellular response to hypoxic stress, and was assayed in isolated dye-retaining and non-dye-retaining MDA-MB-231 populations (**Section 4.4.3.**). Using the tile scan function of the Leica AF6000LX microscope as described in **Section 2.4.**, nine non-overlapping fields covering the entire immunostained sample were captured at 100X magnification. Representative images of the HIF-1α staining pattern were also captured at 200X magnification (**Figure 4.8.**).

Immunostaining was deemed specific given that the green fluorescent signal used to localise HIF-1α was undetectable in isotype control samples. Upon assessment of the immunostaining produced within both Vybrant® dye-retaining and dye-negative sample sets it became obvious that HIF-1α was ubiquitously expressed irrespective of the initial dye-retention status of the population i.e. 100% of cells expressed HIF-1α. However, it was also clear that Vybrant® DiD-positive cells were considerably brighter across all technical and biological repeat samples, indicating that HIF-1α was present at higher levels in association with reduced mitotic activity. While this is an interesting preliminary finding, it is insufficient to definitively conclude that HIF-1α regulated gene expression governs the quiescent phenotype and as such further experiments will be required to test this hypothesis in a more robust manner.
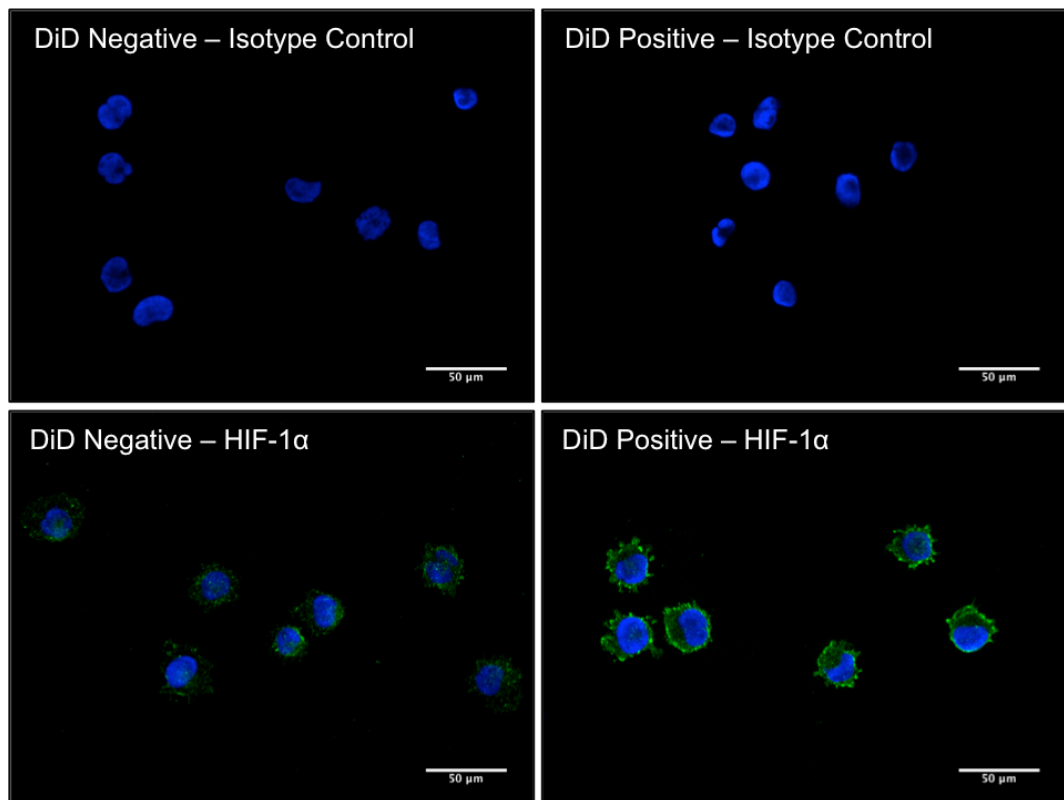
Figure 4.8. Immunofluorescent HIF-1α Staining In Dye-Retaining and Negative Cells

The immunofluorescent staining pattern for HIF-1α (green) is shown along with nuclear counterstaining with DAPI (blue) in Vybrant® DiD-negative and positive MDA-MB-231 cell populations isolated by FACS and deposited onto glass microscope slides by cytocentrifugation. Specificity of staining was indicated by the complete absence of green fluorescence (AlexaFluor®488) used to localise HIF-1α in matched isotype control samples, shown here at the top. All images were captured using a 20x objective lens (scale bar = 50µm).

4.5.4. Defining Sub-Optimal Culture Conditions

In order to begin testing the hypothesis that metabolic stress induced by sub-optimal culture conditions could increase the size of the slow-cycling dye-retaining fraction within growing cultures, it was first necessary to define a series of sub-optimal culture conditions. As the supplementary FBS added to culture medium provides the principal mitogenic stimulus for growing cells and the propagation of cells within culture is primarily reliant on glucose metabolism (be it glycolytic or oxidative), these two factors were deemed to be most suited to modulation for controlled provision of metabolic stress to cells. Titration assays were initially carried out in order to define sub-optimal concentrations of FBS and glucose to which levels could be depleted in subsequent experiments, the results of which are depicted in **Figure 4.9.** and **Figure 4.10.** The final EC_{25} and EC_{50} for FBS and glucose used in all assays was according to the actual dilution used during titration experiments that was closest to the value determined graphically. All of the final serum and glucose concentrations that were defined for use in subsequent assays are summarised in **Table 4.4.** Proliferation assays using the pre-defined EC_{50} of either FBS or glucose were also initially used to determine whether culture growth under adverse conditions was possible, in turn allowing dye-retention assays to be undertaken to determine the effects on the size of the slow-cycling cell population (**Figure 4.9.** and **Figure 4.10.**).

In cultures grown in medium containing only the EC_{50} concentration of FBS, the maximal number of viable cells reached at the end of the log-phase of culture growth was $37.25 \pm 2.39 \times 10^4$ cells; a $6.50 \pm 4.00 \times 10^4$ reduction (~15%) compared to control samples (P ≤ 0.01). In addition, the log-phase population doubling time was determined to be 20.14 hours, 3.32 hours longer than the 16.82 hour log-phase doubling time recorded for control cultures. Similarly, in cultures grown in medium containing the EC_{50} concentration of glucose, the maximal number of viable cells reached was $26.00 \pm 1.47 \times 10^4$ cells, a significant reduction of $10.38 \pm 3.16 \times 10^4$ cells (~30%) when compared to $36.38 \pm 1.69 \times 10^4$ cells in control samples (P ≤ 0.0001), and the log-phase doubling time was extended by 11.95 hours to 28.77 hours. These results indicated that the effective induction of culture stress was successful while still permitting net culture growth.
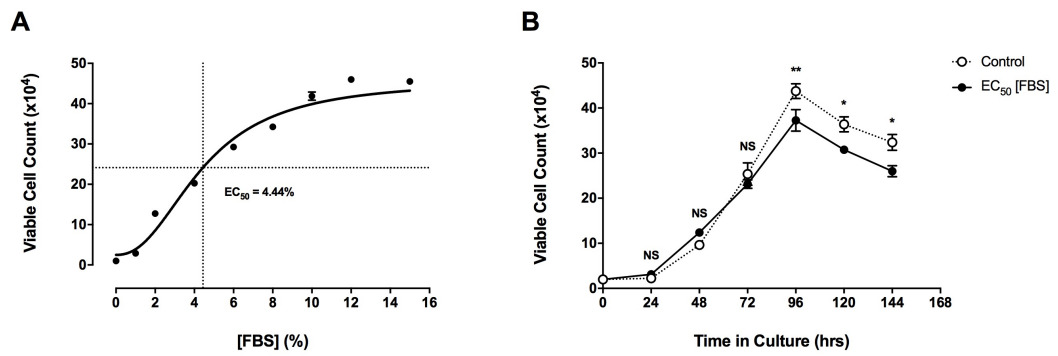
Figure 4.9. MDA-MB-231 Serum Titration and EC$_{50}$ [Serum] Proliferation Assay

A: Dose-response curve for MDA-MB-231 cells grown in RPMI-1640 basal culture medium with varying concentrations of supplemental FBS (0 - 15% (v/v)). **B**: The proliferation curves for MDA-MB-231 cells grown in RPMI-1640 culture medium containing either the EC$_{100}$ (control) or EC$_{50}$ concentration of FBS (10% and 4% (v/v), respectively). The number of viable cells was between treatment groups over successive time-points using two-way ANOVA followed by Sidak's Multiple Comparison Test (NS = not statistically significant or P > 0.05, * = P ≤ 0.05, ** = P ≤ 0.01). Data are expressed as the mean average ± SEM for n = 3 biologically independent repeat experiments.
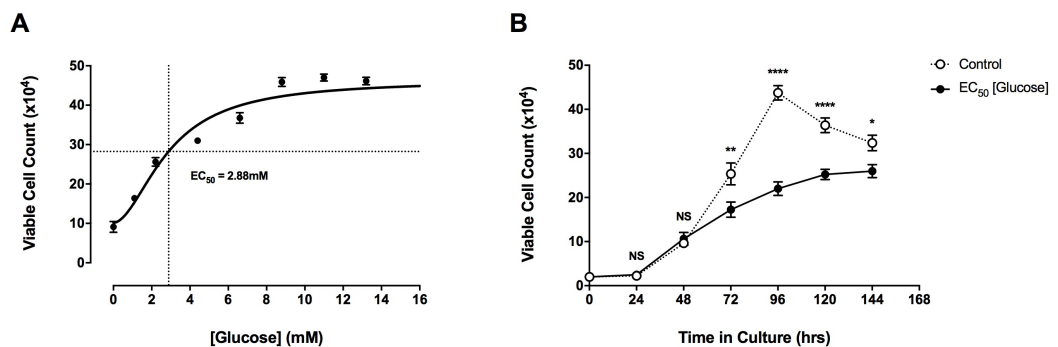
Figure 4.10. MDA-MB-231 Glucose Titration and EC$_{50}$ [Glucose] Proliferation Assay

A: Dose-response curve for MDA-MB-231 cells grown in complete RPMI-1640 culture medium (10% supplemental FBS) and varying concentrations of glucose (0 - 16.5mM). **B**: The proliferation curves for MDA-MB-231 cells grown in complete RPMI-1640 culture medium containing either the EC$_{100}$ (control) or EC$_{50}$ concentration of glucose (11mM and 2.2mM, respectively). The number of viable cells was between treatment groups over successive time-points using two-way ANOVA followed by Sidak's Multiple Comparison Test (NS = not statistically significant or P > 0.05, * = P ≤ 0.05, ** = P ≤ 0.01, **** = P ≤ 0.0001). Data are expressed as the mean average ± SEM for n = 3 biologically independent repeat experiments.

Table 4.4. Composition of Reduced Serum or Glucose Culture Media

Medium Type	Vol. RPMI-1640 11mM D-glucose (% v/v)	Vol. RPMI-1640 0mM D-glucose (% v/v)	Vol. Dialysed FBS (% v/v)
EC_0 Glucose	-	90	10
EC_{25} Glucose	9	81	10
EC_{50} Glucose	18	72	10
EC_{100} Glucose	90	-	10
EC_0 FBS	100	-	-
EC_{25} FBS	98	-	2
EC_{50} FBS	96	-	4
EC_{100} FBS	90	-	10

The EC_0 - EC_{100} concentrations of both FBS and glucose stated were calculated by interpolation from the respective titration curve determined previously for the MDA-MB-231 cell line.

4.5.5. Effects of Modulating Serum and Glucose Concentration on Dye Retention

In order to test the hypothesis that metabolic stress induced by deprivation of mitogenic stimuli (via reduction of the FBS content within culture medium) could induce an increase in the number of latent slow-cycling cells present in a culture, pulse-chase dye-retention assays were undertaken in cultures grown in medium containing serum levels reduced to the pre-determined EC_{50} concentration of 4% (v/v) (**Figure 4.11.**). These experiments were also repeated in parallel using cultures grown in medium containing glucose levels reduced to the pre-determined EC_{50} concentration of 2.2mM in order to test the comparable hypothesis that metabolic stress induced by deprivation of metabolic energy supply (via depletion of the glucose content within culture medium) could induce an increase in the number of latent slow-cycling cells present in a culture (**Figure 4.13.**).

In serum-deprived cultures, there was no significant increase in the overall size of the slow-cycling dye-retaining cell population at the final passage of measurement compared to when cultures were maintained in complete medium containing the EC_{100} concentration of FBS (**Figure 4.11.**). The rate of dye loss from serum-deprived cultures did however appear reduced compared to control cultures, as denoted by the significantly greater dye-retaining cell population over the duration of passages three to five ($P \leq 0.0001$ in all cases), during which dye was lost to residual levels revealing the latent slow-cycling population in control cultures. The reduced proliferative rate of serum-deprived cultures indicated during dye-retention assays was reflected in univariant cytofluorimetric analysis of the cell cycle distribution in serum-deprived cultures, which were skewed more towards the G_0/G_1-phase and therefore most probably slower cycling then control cultures (**Figure 4.12.**). An average of 42.80 ± 0.27% of cells within serum-deprived cultures were found to exist in the G_0/G_1-phase compared to 38.83 ± 0.67% of control cells maintained in culture medium containing 10% (v/v) FBS ($P \leq 0.0001$). A small but statistically significant ($P \leq 0.05$) decrease in the G_2/M-phase fraction was also measured in serum-deprived cultures relative to control samples, while no change in the S-phase fraction was observed.

In contrast, a significant increase in the overall size of the dye-retaining cell population at the final passage of measurement was recorded in glucose-deprived cultures when compared to control cultures maintained in complete medium containing the EC_{100} concentration of glucose (**Figure 4.13.**). However, in accordance with the assays undertaken using reduced serum concentration, glucose-deprived cultures were also significantly slower cycling than control cultures (**Figure 4.14.**). In fact, the re-distribution of the cell population towards the G_0/G_1-phase was considerably more pronounced in glucose-deprived cultures. On average, $49.97 \pm 0.19\%$ of glucose-deprived cells were found to exist in the G_0/G_1-phase compared to $38.83 \pm 0.67\%$ of control cells maintained in culture medium containing 11mM glucose ($P \leq 0.0001$). A $6.47 \pm 1.48\%$ reduction in the S-phase fraction and a 3.50 ± 1.73 reduction in the G_2/M-phase fraction ($P \leq 0.001$ and $P \leq 0.05$, respectively) were also recorded for glucose-deprived cultures relative to control samples. These alterations to the cell cycle distribution were likely the factor underpinning the significantly larger dye-retaining fraction recorded across passages three to five ($P \leq 0.0001$ in all cases).
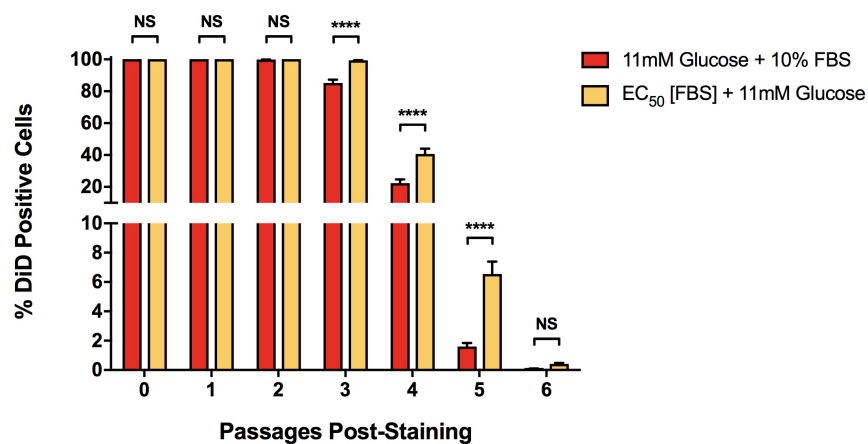
Figure 4.11. Vybrant® Dye Retention in the Presence of EC$_{50}$ [Serum]

The percentage Vybrant® DiD-stained cells within adherent monolayer cultures of MDA-MB-231 cells grown in RPMI-1640 culture medium containing either the EC$_{100}$ or EC$_{50}$ concentration of FBS (10% and 4% (v/v), respectively) was measured over successive passages at the time of sub-culture undertaken at 72 hour intervals. The percentage of Vybrant® DiD-stained cells was compared between samples over successive time-points using two-way ANOVA followed by Sidak's Multiple Comparison Test (NS = not statistically significant or P > 0.05, **** = P ≤ 0.0001). Data are expressed as the mean average ± SEM for n = 3 biologically independent repeat experiments.

Figure 4.12. Cell Cycle Profile of MDA-MB-231 Cells Grown in EC$_{50}$ [Serum]

A: The univariant cell cycle analysis profiles of adherent monolayer cultures of MDA-MB-231 cells grown in RPMI-1640 culture medium containing either the EC$_{100}$ or EC$_{50}$ concentration of FBS (10% and 4% (v/v), respectively) are shown. The location of the G$_0$/G$_1$-phase (haploid chromosome number), S-phase (intermediate chromosome number) and G$_2$/M-phase (diploid chromosome number) peaks are illustrated. **B**: The percentage of total cells in each phase of the cell cycle was compared between MDA-MB-231 cultures grown in RPMI-1640 culture medium containing either the EC$_{100}$ or EC$_{50}$ concentration of FBS using two-way ANOVA followed by Sidak's Multiple Comparison Test (NS = not statistically significant or $P > 0.05$, * = $P \leq 0.05$, **** = $P \leq 0.0001$). Data are expressed as the mean average ± SEM for n = 3 biologically independent repeat experiments.
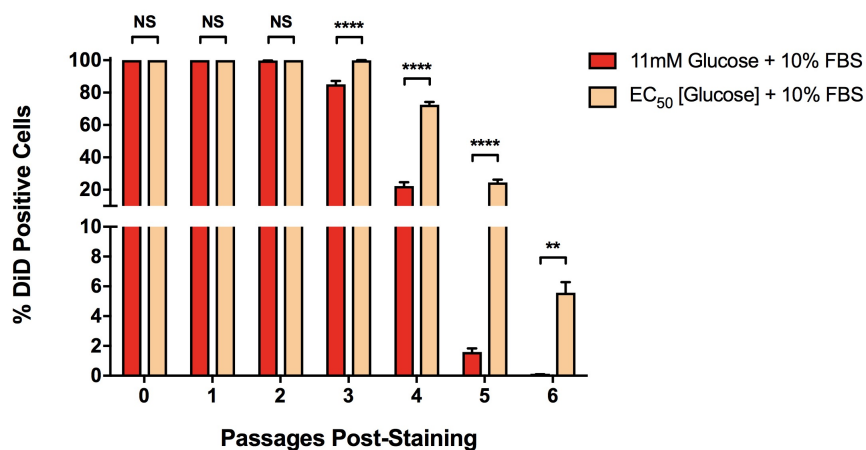
Figure 4.13. Vybrant® Dye Retention in the Presence of EC$_{50}$ [Glucose]

The percentage Vybrant® DiD-stained cells within adherent monolayer cultures of MDA-MB-231 cells grown in complete RPMI-1640 culture medium (10% supplemental FBS) containing either the EC$_{100}$ or EC$_{50}$ concentration of glucose (2.2mM and 11mM, respectively) was measured over successive passages at the time of sub-culture undertaken at 72 hour intervals. The percentage of Vybrant® DiD-stained cells was compared between samples over successive time-points using two-way ANOVA followed by Sidak's Multiple Comparison Test (NS = not statistically significant or P > 0.05, ** = P ≤ 0.01, **** = P ≤ 0.0001). Data are expressed as the mean average ± SEM for n = 3 biologically independent repeat experiments.
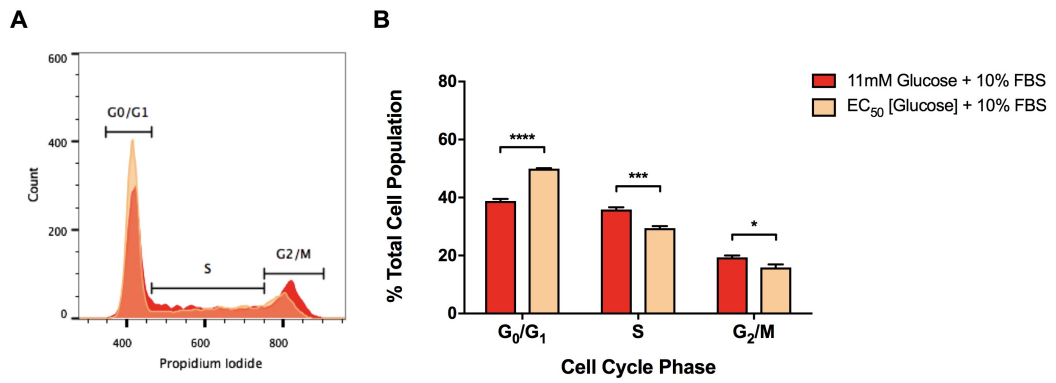
Figure 4.14. Cell Cycle Profile of MDA-MB-231 Cells Grown in EC$_{50}$ [Glucose]

A: The univariant cell cycle analysis profiles of adherent monolayer cultures of MDA-MB-231 cells grown in complete RPMI-1640 culture medium (10% supplemental FBS) containing either the EC$_{100}$ or EC$_{50}$ concentration of glucose (2.2mM and 11mM, respectively) are shown. The location of the G$_0$/G$_1$-phase (haploid chromosome number), S-phase (intermediate chromosome number) and G$_2$/M-phase (diploid chromosome number) peaks are illustrated. **B**: The percentage of total cells in each phase of the cell cycle was compared between MDA-MB-231 cultures grown in RPMI-1640 culture medium containing either the EC$_{100}$ or EC$_{50}$ concentration of glucose using two-way ANOVA followed by Sidak's Multiple Comparison Test (* = P ≤ 0.05, *** = P ≤ 0.001, **** = P ≤ 0.0001). Data are expressed as the mean average ± SEM for n = 3 biologically independent repeat experiments.

4.5.6. Effects of Modulating Serum and Glucose Concentration on Clonogenicity

Based on experimental observations that both rapidly dividing and slow-cycling sub-clones were able to overtly outgrow when isolated from parental cultures, clonogenic assays were used as an alternative means of assessing the effects of *in vitro* conditions on both rapidly- and slowly-dividing sub-populations. Due to the greater requirement for both mitogenic stimuli and metabolic energy supply in rapidly dividing cells, it was hypothesised that slow-cycling cells would have greater survivability following reduction of the supplied concentration of FBS or glucose and therefore would form more colonies than the rapidly dividing fraction following replenishment of the factor to which cells were deprived.

Clonogenic assays undertaken over a six-day period post-isolation of rapidly dividing and dye-retaining MDA-MB-231 fractions by FACS revealed a dose-dependent increase in the number of colonies formed by both dye-negative and dye-positive cells between the EC_0 and EC_{100} concentration of both FBS and glucose (**Figure 4.15.**). Most notably, while there was a trend towards dye-positive cells forming fewer colonies, there was no significant difference between the clonogenicity of dye-negative and dye-positive populations at any of the FBS or glucose concentrations assayed. Across both sets of assays, deprivation of FBS appeared to have a greater impact on clonogenicity; the average number of colonies formed by both dye-negative and dye-positive populations at the EC_0 glucose concentration was approximately 20-25%, while no colonies were detected at the EC_0 FBS concentration, and the average colony count at the EC_{25} was less than 20%.
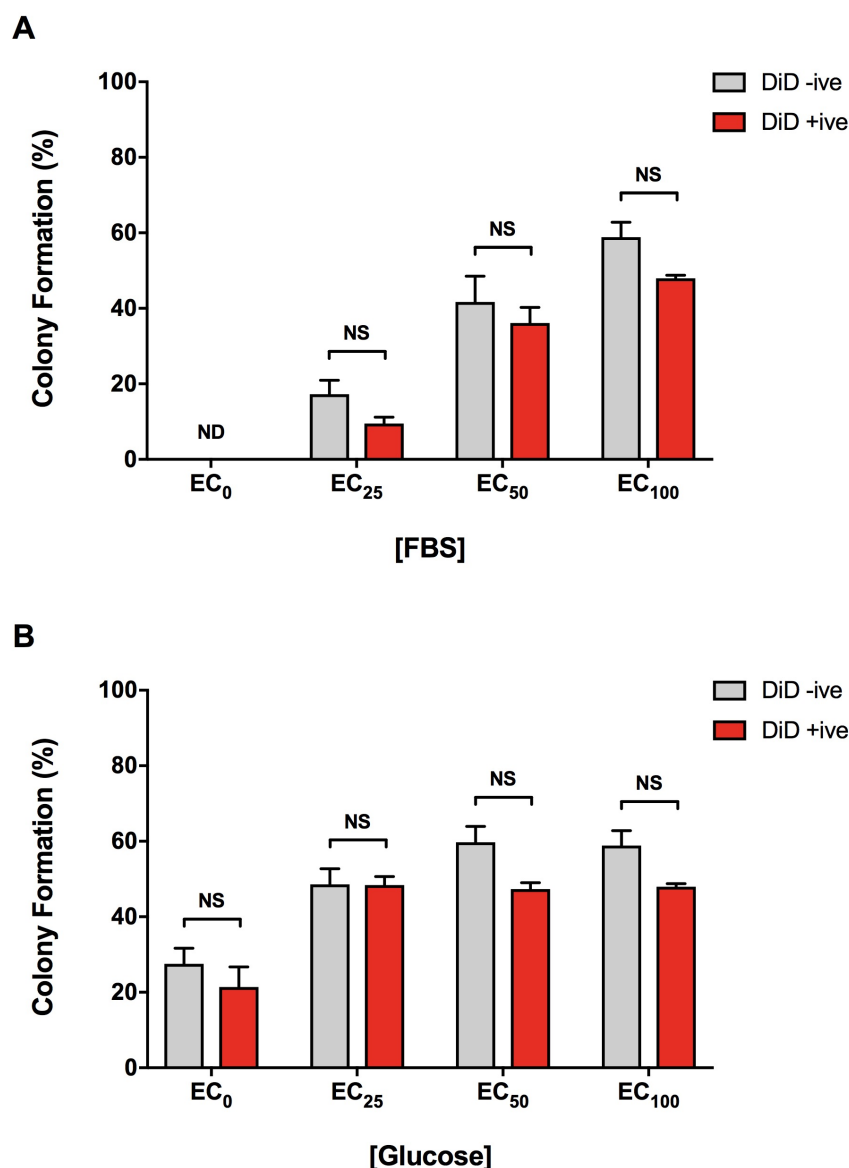
Figure 4.15. Sub-Population Clonogenicity at Varied [Serum] or [Glucose]

A: The percentage colony formation of Vybrant® DiD-negative and Vybrant® DiD-positive MDA-MB-231 cells isolated by FACS at five passages post-staining following a 7 day period of growth in RPMI-1640 basal medium containing either the EC_0, EC_{25}, EC_{50} or EC_{100} concentration of supplemental FBS (0, 2, 4 and 10% (v/v), respectively). ND = not detected. **B**: The percentage colony formation of Vybrant® DiD-negative and Vybrant® DiD-positive MDA-MB-231 cells isolated by FACS at five passages post-staining following a 7 day period of growth in complete RPMI-1640 culture medium (10% supplemental FBS) containing either the EC_0, EC_{25}, EC_{50} or EC_{100} concentration of glucose (0mM, 1.1mM, 2.2mM and 11mM, respectively). The percentage colony formation was compared between the two populations at each FBS or glucose concentration using two-way ANOVA followed by Sidak's Multiple Comparison Test (NS = not statistically significant or $P > 0.05$). Data are expressed as the mean average $\pm$ SEM for n = 3 biologically independent repeat experiments.

In order to determine whether the reduced colony formation at the EC_0 glucose concentration and the EC_0 and EC_{25} FBS concentrations was the result of cell death, permanent senescence or entry into a reversible non-dividing dormant state, clonogenic assays were undertaken in which colony formation was stimulated after the initial six day period of nutrient withdrawal by replacing the component to which cells had been deprived (**Figure 4.16.**). Irrespective of initial dye-retention status, cells seeded into medium completely deficient of FBS (EC_0) did not form any colonies following replenishment of the FBS concentration (data not shown) and no further colonies were formed upon FBS replacement in addition to those initially established in the presence of the EC_{25} concentration of FBS (**Figure 4.16.**). Interestingly, a significant increase in colony formation of approximately 37% ($P \leq 0.01$) was observed following replenishment of glucose in samples initially seeded in medium containing the EC_0 glucose concentration, although there was no significant differential clonogenicity recorded between cells that were initially dye-negative or dye-positive. In fact, in both populations the number of colonies formed following replenishment of glucose following initial deprivation returned to levels that were not significantly different from samples seeded directly into the EC_{100} glucose i.e. a complete rescue of clonogenicity was observed following replenishment of glucose concentration in initially glucose-deprived cultures (**Figure 4.16.**).
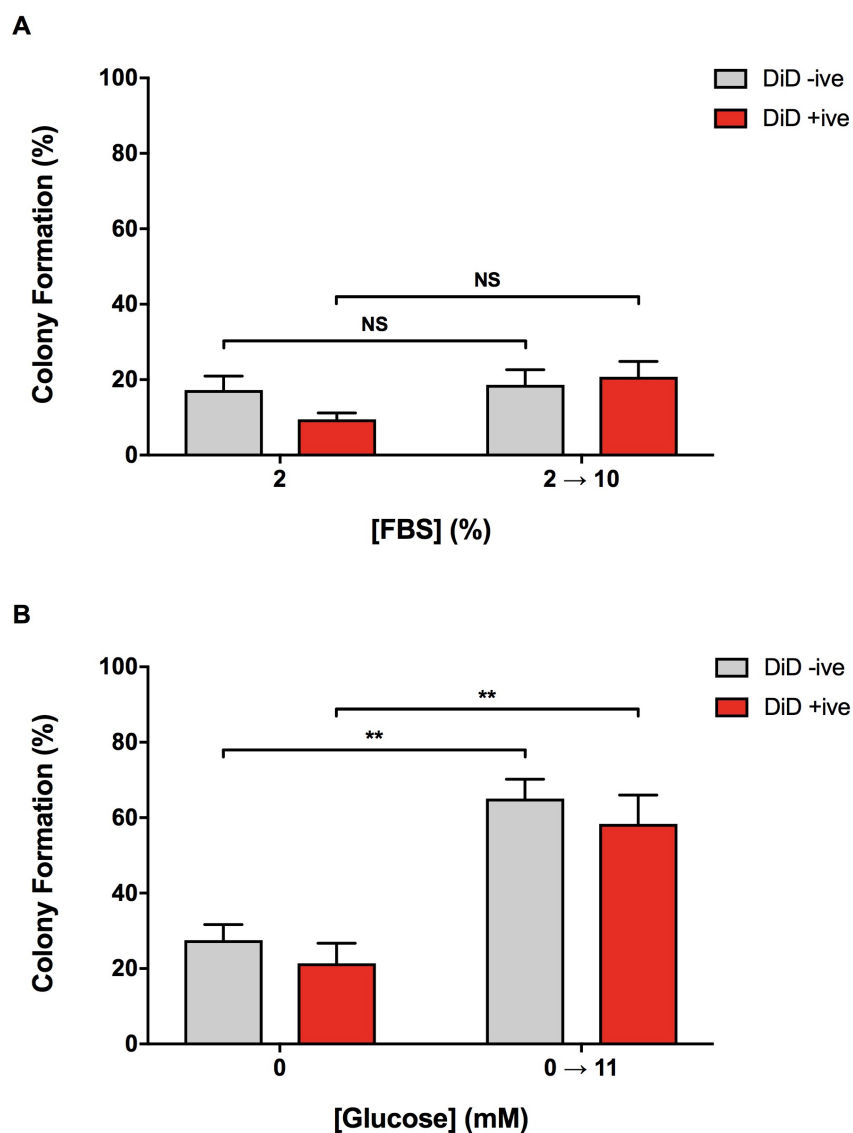
Figure 4.16. Stimulating Clonogenicity Following Serum or Glucose Deprivation

A: The percentage colony formation of Vybrant® DiD-negative and Vybrant® DiD-positive MDA-MB-231 cells isolated by FACS at five passages post-staining following an initial 7 day period of growth in RPMI-1640 basal medium containing 2% supplemental FBS and then a further 7 day period of growth following change to complete RPMI-1640 culture medium containing 10% supplemental FBS. ND = not detected. **B**: The percentage colony formation of Vybrant® DiD-negative and Vybrant® DiD-positive MDA-MB-231 cells isolated by FACS at five passages post-staining following an initial 7 day period of growth in complete RPMI-1640 culture medium (10% supplemental FBS) containing 0mM glucose and then a further 7 day period of growth following change to complete RPMI-1640 culture medium containing 11mM glucose. For each population, the percentage colony formation was compared across each set of growth conditions by two-way ANOVA followed by Sidak's Multiple Comparison Test (NS = not statistically significant or $P > 0.05$, ** = $P \leq 0.01$). Data are expressed as the mean average ± SEM for n = 3 biologically independent repeat experiments.

### 4.5.7. Effects of Lactate on the Clonogenicity of Dye-Retaining and Negative Cells

A recent study by Park *et al.* (2016) demonstrated that some breast cancer cells are capable of metabolic switching to utilise the oxidation of lactate as a primary source of energy, mediated by genes actively regulated by oestrogen-related receptor-alpha (ERR-α), facilitating their survival under conditions of glucose deprivation for extended periods of time. It was therefore hypothesised that slow-cycling cells might be more capable of adapting to utilise lactic acid as a source of metabolic energy, thereby conferring a differential ability to survive under glucose-depleted, high-lactate conditions similar to those which are suggested to occur within the quiescent and/or cancer stem cell niche within primary tumours.

In order to begin testing this hypothesis, the expression of ERR-α by the MDA-MB-231 cell line was determined. Western blot analysis was carried out on whole cell lysates of MDA-MB-231 and four other distinct human breast cancer cell lines as described in **Section 4.4.7.** The results, depicted in **Figure 4.17.**, demonstrate that all breast cancer cell lines tested express ERR-α to greater or lesser extent. Due to the relatively weak expression of ERR-α in the MDA-MB-231 cell line relative to some of the other cell lines tested, the proportion of MDA-MB-231 cells expressing ERR-α was determined by intracellular immunostaining followed by flow cytometric analysis (**Section 4.4.8.**). The fluorescence profile produced during cytofluorimetric analysis demonstrated that all MDA-MB-231 cells express ERR-α (**Figure 4.17.**).
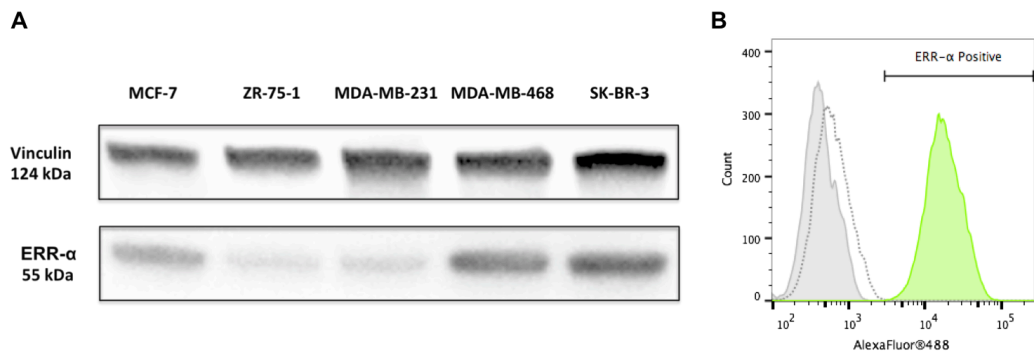
Figure 4.17. ERR-α Expression in Human Breast Cancer Cell Lines

A: Western blot demonstrating the expression of ERR-α in a number of distinct human breast cancer cell lines relative to the constitutively expressed cytoskeletal protein vinculin used as a loading control. **B**: A representative flow cytometric analysis plot depicting the degree of ERR-α positivity within the MDA-MB-231 cell line is shown; an unlabelled control sample profile (grey) and the profile of an isotype control sample (dotted line) are depicted in addition to the positively stained experimental sample (green).

In order to provide glucose-depleted medium in which lactate was the primary metabolic substrate available, the concentration of D-glucose and L-lactate were measured directly in conditioned medium taken from growing MDA-MB-231 cultures (**Section 4.4.10.**). The results depicted in **Figure 4.18.** demonstrate that culture medium removed from growing MDA-MB-231 at 96 hours post-seeding of cells contained 0mM D-glucose and 22mM L-lactate. Consequently, conditioned medium for use in all subsequent assays was prepared at this time point according to the method previously outlined (**Section 4.4.9.**) and 10% supplemental dialysed FBS added immediately prior to use.

No colonies were formed following clonogenic assays undertaken over a six-day period in which rapidly dividing and dye-retaining MDA-MB-231 cells were seeded directly into conditioned medium containing 22mM lactate post-isolation by FACS (data not shown). In order to subsequently determine whether this absence of colony formation under glucose-deprived, lactate-replete conditions was the result of cell death, cells becoming permanently senescent or entering into a reversible non-dividing dormant state, clonogenic assays were undertaken in which colony formation was stimulated after the initial six day period by removing the high-lactate conditioned medium and replacing this with normal complete culture medium containing 11mM glucose and 0mM lactate (**Section 4.4.12.**). Interestingly, the results depicted in **Figure 4.19.** showed a significant increase in colony formation following replenishment of glucose, irrespective of the initial dye-retention status of seeded cells; colony formation was 21.78 ± 5.13% of the total number of cells initially seeded in dye-negative cells while colony formation was measured at 28.17 ± 4.92% in dye-positive cells (P ≤ 0.01 in both cases). The difference in colony formation between the two fractions post-stimulation was not significant.
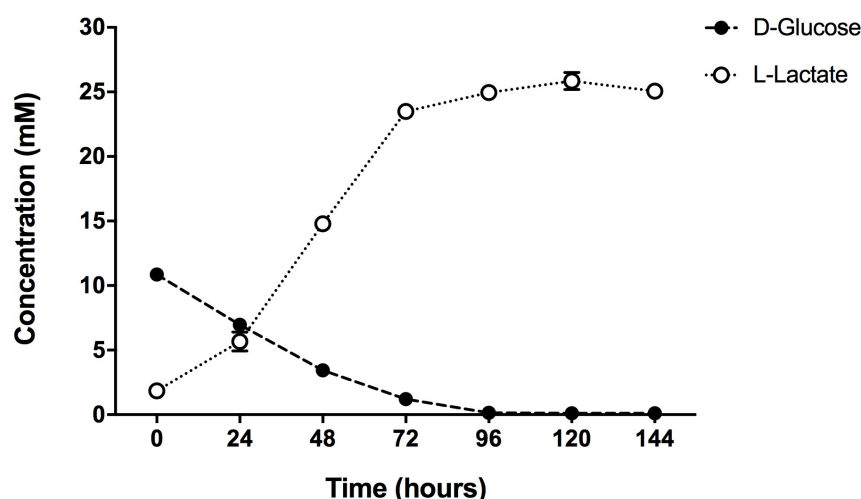
Figure 4.18. [Glucose] and [Lactate] in MDA-MB-231 Cultures Over Time

The concentration of D-glucose and L-lactate in the culture medium (RPMI-1640 + 10% supplemental FBS) of growing MDA-MB-231 cultures over time; the concentration of either compound (Y-axis) is plotted against the duration of culture post-seeding of cells (X-axis). Data are expressed as the mean average ± SEM for n = 3 biologically independent repeat experiments.
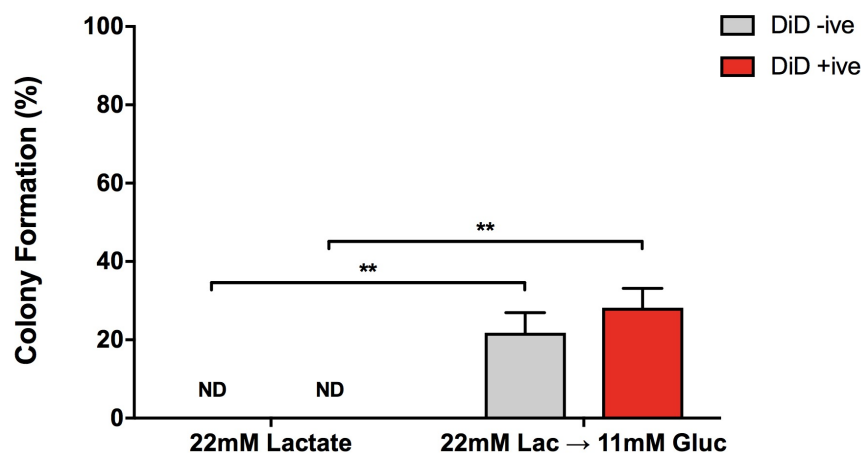
Figure 4.19. Colony Formation in 22mM Lactate and Post-Replacement of Glucose

The percentage colony formation of Vybrant® DiD-negative and Vybrant® DiD-positive MDA-MB-231 cells isolated by FACS at five passages post-staining following an initial 7 day period of growth in complete RPMI-1640 culture medium containing 22mM lactate (0mM glucose) and then a further 7 day period of growth following a change to complete RPMI-1640 culture medium containing 11mM glucose. ND = not detected. For each population, the percentage colony formation was compared across each set of growth conditions by two-way ANOVA followed by Sidak's Multiple Comparison Test (** = P ≤ 0.01). Data are expressed as the mean average ± SEM for n = 3 biologically independent repeat experiments.

4.5.8. Effects of Inhibiting ERR-α on the Survival of Dye-Retaining Cells

A series of experiments described elsewhere in this thesis (**Section 5.5.1.**) demonstrated that the latent slow-cycling population of cells identified by dye-retention methods within human breast cancer cells lines are intrinsically more resistant to anti-neoplastic chemotherapeutics used to treat breast cancer and exclusively contain a sub-clonal population capable of initiating new colonies post-cessation of drug-treatment. It was hypothesised that these drug-resistant sub-clones were also capable of lactate utilisation and survival under glucose-depleted conditions, and that pharmacological inhibition of ERR-α can kill both the cells able to survive when lactate was the primary metabolic substrate and the drug-resistant sub-clonal population.

Two selective ERR-α inhibitors, Cpd29 and XCT790, were kindly provided by Professor Donald P. McDonnell (Duke University, Durham, North Carolina, U.S.A.). In order to first demonstrate that these compounds selectively compromise lactate utilisation but not glucose consumption, adherent MDA-MB-231 cells at 24-hours post-seeding were exposed to either complete culture medium (11mM glucose) or lactate-enriched conditioned medium (22mM lactate) in both the presence and absence of each inhibitor for a period of 72-hours. Inhibitors were used at a final concentration of 10μM according to data previously published for the MDA-MB-231 cell line by the supplier (Park *et al.*, 2016). At each time-interval, the culture medium was harvested from one flask in each treatment group and assayed for either D-glucose or L-lactate content as previously described (**Section 2.8.2. - Section 2.8.3.**). The results clearly demonstrated the selective inhibition of L-lactate consumption by both Cpd29 and XCT790; D-glucose was consumed by MDA-MB-231 cells in untreated and both ERR-α inhibitor-treated cultures while there was a progressive decline in L-lactate levels over the 72 hour assay period in untreated MDA-MB-231 cultures (**Figure 4.20.**). A large statistically significant difference between untreated and inhibitor-treated cultures was measured at each time-point (P ≤ 0.0001 in all cases).
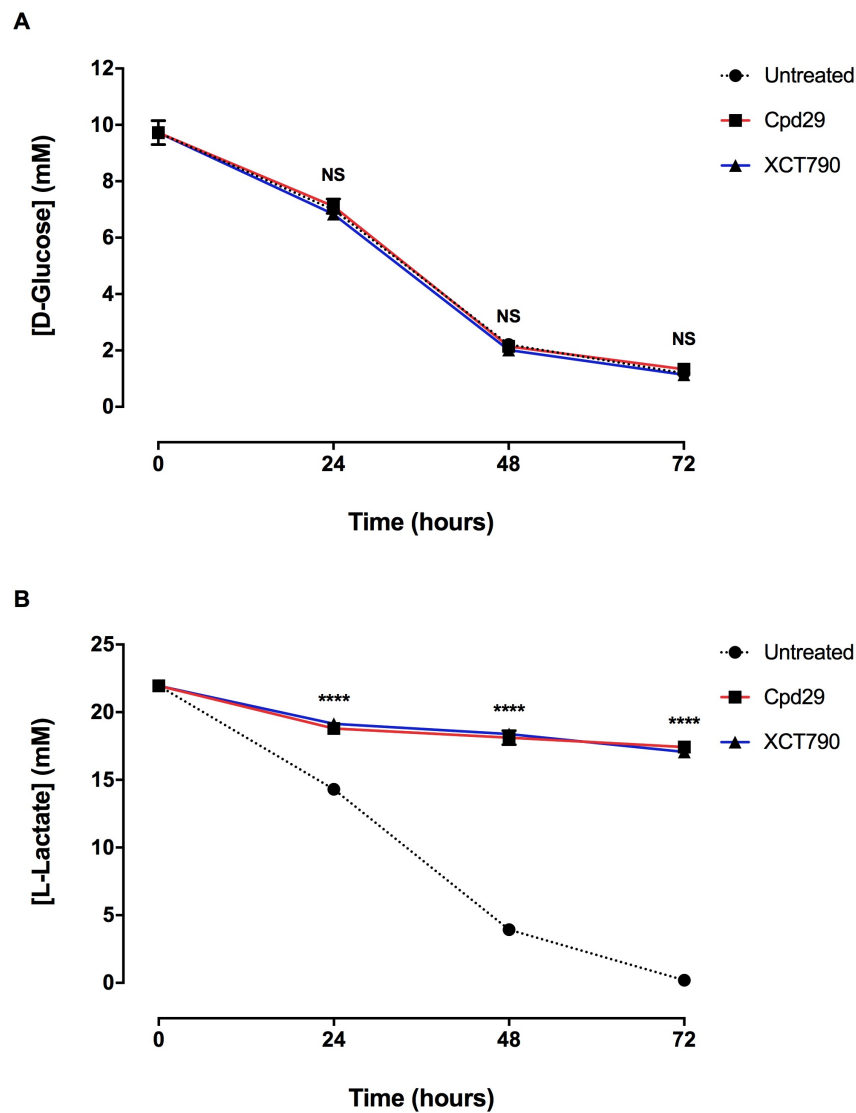
Figure 4.20. Inhibition of ERR-α Prevents Consumption of Lactate But Not Glucose

A: The concentration of D-glucose in the culture medium (RPMI-1640 with 11mM D-glucose and 0mM L-lactate + 10% supplemental FBS) of either untreated, Cpd29-treated (10µM) or XCT790-treated (10µM) MDA-MB-231 cultures over time post-treatment. **B**: The concentration of L-lactate in the culture medium (RPMI-1640 with 0mM D-glucose and 22mM L-lactate + 10% supplemental FBS) of either untreated, Cpd29-treated (10µM) or XCT790-treated (10µM) MDA-MB-231 cultures over time post-treatment. The concentration of either D-glucose or L-lactate was compared between treatment groups at each successive time-points using two-way ANOVA followed by Sidak's Multiple Comparison Test (NS = not statistically significant or $P > 0.05$, **** = $P \leq 0.0001$). Data are expressed as the mean average ± SEM for n = 3 biologically independent repeat experiments.

Colony formation assays were subsequently undertaken to determine whether inhibition of ERR-α under glucose-deficient, lactate-rich conditions would kill both rapidly- and slowly-dividing MDA-MB-231 cell populations (**Figure 4.21.**). These assays were carried out as described in **Section 4.4.13.** Briefly, dye-negative and dye-retaining MDA-MB-231 cells were isolated by FACS at passage five post-staining with Vybrant® DiD, seeded at clonogenic density into 6-well cluster plates pre-filled with either lactate-rich conditioned medium (22mM lactate) only or which contained ERR-α inhibitors Cpd29 or XCT790 (f.c. 10μM). After six days incubation, the medium within all wells was replaced with drug-free complete culture medium (11mM glucose) and a further six days of incubation undertaken prior to carrying out clonogenic assays. The number of colonies formed by untreated Vybrant® DiD-negative and positive cells was comparable to the numbers observed in previous experiments; 29.00 ± 1.26% of Vybrant® DiD-negative cells and 26.33 ± 1.20% of Vybrant® DiD-positive cells seeded formed colonies. No colonies were formed in either of the ERR-α inhibitor-treated groups, irrespective of the intrinsic mitotic capacity of the cells seeded. These results supported the hypothesis that inhibition of ERR-α-regulated lactate metabolism prevents cell survival under nutrient-depleted but lactate-rich conditions.

In order to directly test the hypothesis that inhibition of ERR-α under glucose-depleted but lactate-rich conditions was able to kill the drug-resistant sub-clonal population that is exclusive to the slow-cycling Vybrant® DiD-positive fraction in MDA-MB-231 cultures, clonogenic assays were carried out as described in **Section 4.4.14.** Briefly, Vybrant® DiD-retaining cells were isolated from MDA-MB-231 cultures at passage five post-staining and were subsequently seeded into either lactate-rich conditioned medium (22mM Lactate) only, conditioned medium with the IC_{95} concentration of doxorubicin (321nM), or conditioned medium with 321nM doxorubicin and either Cpd29 or XCT790 (f.c. 10μM). After a six-day initial incubation period, the medium within all samples was changed to complete culture medium only (RPMI-1640 + 10% FBS) and a further six-day period of incubation undertaken prior to carrying out assays of colony formation. The results are depicted in **Figure 4.22.** As would have been expected based on previous results, Vybrant® DiD-positive cells seeded into glucose-depleted medium with 22mM lactate formed 24.33 ± 1.53% colonies on average. Treatment with doxorubicin only under lactate-rich conditions did significantly

decrease the number of colonies formed but a residual population of viable cells was still present leading to $2.33 \pm 1.04\%$ colonies formed post-stimulation by replenishment of glucose. Addition of either inhibitor of ERR-α in combination with doxorubicin under the same conditions completely prevented colony formation, suggesting that blocking metabolic energy supply might be an effective means of eliminating cells inherently resistant to anti-neoplastic drugs.
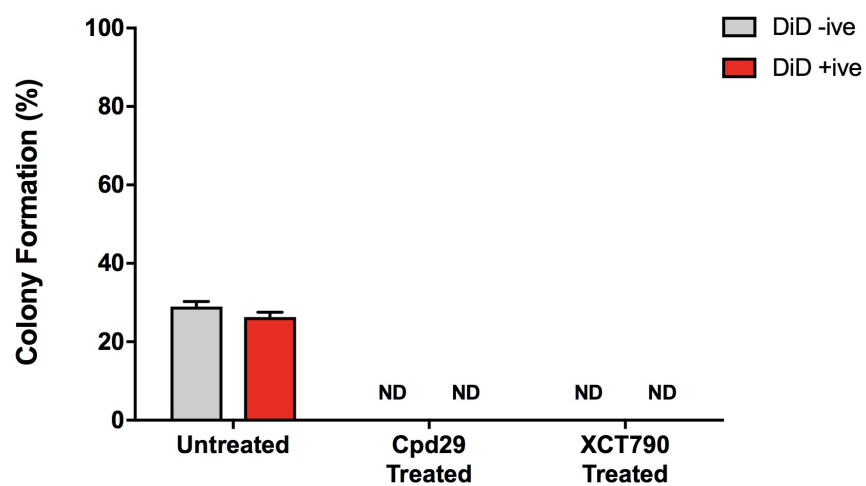
Figure 4.21. Colony Formation Following Inhibition of ERR-α

The percentage colony formation of Vybrant® DiD-negative and Vybrant® DiD-positive MDA-MB-231 cells isolated by FACS at five passages post-staining following an initial 7 day period of growth in complete RPMI-1640 culture medium containing 22mM lactate (0mM glucose), either alone (untreated) or in combination with either Cpd29 (10µM) or XCT790 (10µM), followed by a further 7 day period of growth following a change to complete RPMI-1640 culture medium containing 11mM glucose only. ND = not detected. Data are expressed as the mean average ± SEM for n = 3 biologically independent repeat experiments.
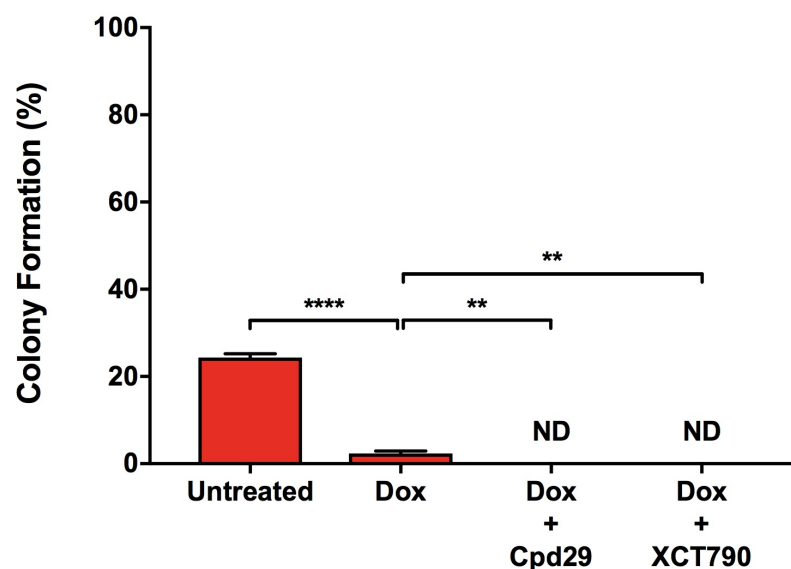
Figure 4.22. Inhibition of ERR-α Can Kill Slow-Cycling Drug-Resistant Sub-Clones

The percentage colony formation of Vybrant® DiD-positive MDA-MB-231 cells isolated by FACS at five passages post-staining following an initial 7 day period of growth in 22mM lactate (0mM glucose), either alone (untreated), in the presence of 321nM doxorubicin only, or 321nM doxorubicin in combination with either Cpd29 (10μM) or XCT790 (10μM), followed by a further 7 day period of growth following a change to drug-free complete RPMI-1640 culture medium. ND = not detected. The number of colonies formed within each treatment group was compared using one-way ANOVA followed by Dunnett's Multiple Comparison Test (** = P ≤ 0.01, **** = P ≤ 0.0001). Data are expressed as the mean average ± SEM for n = 3 biologically independent repeat experiments.

4.6. Discussion

It is well established that tumour cell populations, whether *in vivo* or *in vitro*, are often highly heterogeneous and are comprised of rapidly proliferating, slow-cycling and quiescent cells, cells that have entered into senescence and cells that are undergoing necrotic or apoptotic cell death. Mitotic activity is not the sole functional trait that displays heterogeneity within tumour cell populations; disparities in invasive, migratory and clonogenic behaviour have also been widely reported (Marusyk and Polyak, 2010; Gligorijevic *et al.*, 2014). It is now generally accepted that primary tumoural microenvironments are heterogeneous in composition and that localised adverse microenvironmental conditions can strongly influence cellular phenotype and generate such population diversity (Bragado *et al.*, 2012; Gilkes *et al.*, 2014). Given that similar variance in factors such as oxygenation has also been reported in both three-dimensional and two-dimensional *in vitro* cell cultures (Malda *et al.*, 2007; Demol *et al.*, 2011; Kagawa *et al.*, 2015), it does not seem unreasonable that spatiotemporal fluctuations in the tissue culture microenvironment or indeed controlled modulation of culture conditions might influence the size and behaviour of intrinsic sub-populations, such as those tumour cells that maintain a quiescent phenotype.

The numerous effects of increasing confluency on the biochemical and cell cycle profiles of growing *in vitro* cell cultures are well documented; one of the principal observations being the progressive net redistribution towards the G_0/G_1-phase of the cell cycle as the population density of a culture increases. These changes occur in response to the depletion of nutrients, rapid localised deoxygenation of culture medium, accumulation of waste metabolites and decreased pH, and are reflected in the gross reduction of the overall culture proliferation rate that corresponds with the end of the logarithmic phase of culture growth. A relatively recent study by Matthews *et al.* (2010) highlighted the inherent differences in the biochemical profiles of single prostate cancer cells at varying degrees of culture confluency and cell cycle progression, indicating that individual clones within a culture can vary in their predisposition to the cellular events typically correlated with increased culture

confluency and therefore differ in their susceptibility to potential loss of mitotic activity induced by the adverse conditions arising from culture overgrowth.

Given that the loss of fluorescent dye by progressive dilution during pulse-chase assays is primarily dependent on the rate of culture proliferation, it was not unexpected that extending the sub-culture interval and increasing the degree of culture confluency resulted in a diminished absolute rate of fluorescent dye loss. When the duration of fluorescence pulse-chase assays was expressed as the number of passages post-staining, in order to account for the reduced rate of culture proliferation, the dye-retaining population size was not significantly increased. The relatively modest increase in the magnitude of the G_0/G_1 population measured in confluent cultures suggests that this was perhaps due to the cellular metabolic stress exerted by allowing the culture to reach full confluency being sufficient to limit exponential growth but insufficient to induce reduced mitotic activity in potentially more susceptible sub-clones. Although not undertaken here, it remains possible that a more profound overgrowth of cells would allow generation of further slow-cycling cells; evidence from alternative model systems, such as that described by Pece *et al.* (2010) and Akrap *et al.* (2016), suggest that *de novo* generation of quiescent sub-clones occurs due to microenvironmental conditions that arise within high cell density cultures.

In concurrence with previous studies by Dembinski and Krauss (2009) and Roesch *et al.* (2010), dye-retaining cells were shown to re-emerge within an isolated rapidly dividing cell population, supporting the hypothesis that slow-cycling and quiescent cells can arise within a cell population under microenvironmental instruction. Interestingly, experimental evidence described elsewhere in this thesis (**Section 5.5.7.**) showed that dye-retaining cells could divide asymmetrically to give rise to non-dye retaining cells, thereby recapitulating population mitotic heterogeneity to some degree. A comparable observation by Dembinski and Krauss (2009) led to their proposal of two distinct possibilities; either that a unique latent tumour initiating cell sub-set is enriched within the dye-retaining population but is also present in non-dye-retaining cells and can therefore give rise to each cell type, or that a dynamic relationship between quiescent and tumour initiating cells exists that is context dependent and allows for interconversion between the two states under microenvironmental

regulation. These suggested possibilities now appear somewhat constrained to the classic clonal evolution and cancer stem cell models of tumoural heterogeneity and it could therefore be argued that these two scenarios are more likely to be non-mutually exclusive when conceptualised in the context of the contemporary plasticity model of tumoural heterogeneity. Further work to ascertain the degree of overlap between quiescent and putative tumour initiating phenotypes is described in the following chapter.

During dye-retention assays undertaken following re-staining of isolated dye-negative cells, the rapid decline of dye levels and the subsequent stabilisation of the dye-retaining cell number to one comparable to that observed in wild type cultures suggest that induction of the quiescent phenotype perhaps occurred relatively early following re-establishment of cultures *in vitro*. Given the aforementioned findings of Matthews *et al.* (2010) and that the isolated dye-negative population was inherently rapidly dividing, it appeared entirely plausible that the re-emergence of slow-cycling sub-clones could be due to adverse paracellular conditions generated by aggressively growing sub-clones. Under these hypothetical conditions, a distinct latent sub-population could have been generated from initially more susceptible cells with a size regulated by the number of such niche inductive microenvironments that exist within the culture. This suggestion led to the hypothesis that induction of a HIF-1α-regulated gene expression profile was responsible for initiation of the quiescent phenotype. Indeed, immunostaining of cytocentrifuge preparations showed that in wild type MDA-MB-231 cultures, HIF-1α appeared to be present at a much higher level within the slow-cycling dye-retaining population than in the rapidly dividing dye-negative population. In addition, HIF-1α staining appeared more frequently localised to the nuclei of dye-retaining cells, while in dye-negative cells it appeared to be associated with the cellular periphery. These findings closely mirror those described by Docherty (2014), who indicated that both significantly increased levels of HIF-1α and the propensity for nuclear localisation that was observed in dye-retaining PC-3 human prostate cancer cells was responsible for their mitotically quiescent phenotype. While further work will be required to confirm the findings reported here and to ascertain which HIF-1α-regulated pathways are more active in quiescent cells *in vitro*, it has previously been demonstrated that HIF-1α is able to induce quiescence by enhancing

expression of p21, inhibiting the activity of cyclin-CDK2, -CDK1, and -CDK4/6 complexes and thereby preventing cell cycle progression at G_1- and S-phase (Koshiji *et al.*, 2004). Moreover, a recent report by Fluegen *et al.* (2017) supports that localised hypoxia generates therapy-resistant quiescent cells via induction of a hypoxia-associated transcriptomic signature. Interestingly, this study also reported that hypoxia is not required to maintain this phenotype once induced. The microenvironmental induction of quiescence by hypoxia-regulated mechanisms suggests that other metabolic stressors could also contribute to induction of quiescence. Ascertaining whether nutrient-deprivation-induced gene signatures were associated with the quiescent phenotype fell outside of the achievable scope of this study. However, because isolating sufficient numbers of quiescent cells is one of the primary challenges of studying quiescence, it was deemed a valid line of investigation to establish whether enrichment of this population was possible by modulating the supply of nutrients to *in vitro* cultures.

A number of recent studies have investigated the effects of both partial and severe nutritional deprivation in breast tumour cell lines and have showed that the principal net effect of glucose deprivation is cell cycle redistribution, growth arrest and loss of cell viability (Visagie *et al.*, 2015; Sudhagar *et al.*, 2016; Di Conza *et al.*, 2017). Fewer studies have investigated the effects of serum deprivation, however, there have been reports showing that partial serum deprivation is able to induce pro-survival mechanisms that enabling continued culture growth, but that more prolonged or acute severe serum deprivation induces multiple cell death modalities (Braun *et al.*, 2011; Bartkowiak *et al.*, 2015; Jung *et al.*, 2015). It was therefore not entirely unexpected that a significant reduction in the maximal viable cell number was observed despite continued culture growth upon reduction of the serum or glucose concentration to the respective EC_{50} concentration in growing MDA-MB-231 cultures. In each instance these observations were shown to correspond with a significant G_0/G_1-skewing of the cell cycle distribution, reduced overall rate of culture proliferation and increased retention of fluorescent dye during pulse-chase assays. It appears most likely that the cumulative effects of reduced proliferative activity across several passages of culture growth were primarily responsible for slowing the net rate of dye loss from cultures, and therefore that the measured increase in the number of

dye retaining cells was an in fact the result of this effect and not a true enrichment for the slow-cycling phenotype. These observations did not nullify the hypothesis that nutritional stress could be responsible for induction of quiescence, rather they showed that pulse-chase techniques are not well suited to measuring enrichment of a quiescent population under conditions that result in a lower rate of culture proliferation.

Bartkowiak *et al.* (2015) recently reported that breast cancer sub-clones possessing distinct features of metastasis-initiating cells were able to preferentially survive nutrient deprivation. Given the emerging association of the quiescent phenotype with metastasis-initiating potential, it was hypothesised that the isolated slow-cycling fraction would preferentially survive severe nutrient deprivation and thereby show a differential ability to re-emerge following nutrient replenishment. While the loss of clonogenicity following serum starvation could not be reversed, the reduced colony formation observed under severe glucose deprivation was completely rescued following replenishment of the glucose concentration, in line with the reported findings of Bartkowiak *et al.* (2015) and Visagie *et al.* (2015). Despite this interesting finding, there was no significant difference in the colony forming ability of the dye-negative and dye-positive sub-populations following stimulation by glucose replenishment. When taken together, the results obtained during this series of experiments indicate that severe deprivation of FBS induces cell death and/or irreversible mitotic arrest, while glucose deprivation appears to significantly slow or halt mitotic activity in an entirely reversible manner in large proportion of MDA-MB-231 cells, irrespective of the intrinsic mitotic capacity of the cell population. Whether the localised deprivation of glucose results in cellular stress and the initial induction of mitotic quiescence in pre-disposed sub-clones remains to be elucidated.

One of the historic fundamental questions in primary tumour biology has been how tumor cells modulate their metabolic activity when oxygen tension and glucose levels become limiting in the presence of high exogenous lactate, such as has long been known to occur within the tumoural microenvironment. Amongst a number of less well characterised potential mechanisms, the recently reported metabolic switch from glycolytic metabolism to the ERR-α-regulated oxidative metabolism of lactate has

emerged as one of the principal cellular mechanisms underpinning cancer cell survival under nutrient depleted but lactate rich conditions (Kennedy *et al.*, 2013; Allen *et al.*, 2016; Park *et al.*, 2016). In light of this, it was hypothesised that slow-cycling cells might be more capable of adapting to utilise lactic acid as a source of metabolic energy, thereby conferring a differential ability to survive under glucose-depleted, high-lactate conditions. Interestingly, while no colonies were formed by either rapidly dividing or slow-cycling MDA-MB-231 fractions under nutrient depleted conditions after seven days, replenishment of nutrients and a further seven day culture period resulted in around 25% colony formation in both fractions. While these results did not indicate that inherently slow-cycling cells were more capable of survival under glucose-deficient but lactate-rich conditions, this partial rescue of clonogenicity implies that a considerable proportion of cells within MDA-MB-231 cultures are able to switch to utilisation of oxidative lactate metabolism when deprived of glucose for use as their primary metabolic substrate, while the remainder undergo death or senescence. This observation might in its self have direct implications for the biological processes that underpin formation of the metastasis-initiating population, although this remains to be established. However, the exclusivity of cells able to re-emerge following chemotherapy to the slow-cycling population, as described elsewhere in this thesis (**Section 5.5.1.**), and the demonstration by Park *et al.* (2016) of ERR-α-regulated lactate metabolism to contribute to therapy resistance led to the hypothesis that inhibition of this mechanism might eliminate chemotherapy resistant sub-clones. Indeed, while $2.33 \pm 0.60\%$ of seeded cells formed colonies following treatment with the IC_{95} concentration of doxorubicin for seven days, inhibiting ERR-α using two different pharmacological agents in combination with doxorubicin completely prevented colony formation. While these preliminary results are clearly limited by the inherent simplicity and limitations of the model systems used here, it does provide grounds for future *in vivo* investigations to determine if inhibition of ERR-α can prevent metastatic colonisation of the bone and/or formation of overt metastases by cells that escape initial anti-neoplastic drug treatment.

Throughout the investigations described in this chapter, the primary challenge has been attempting to demonstrate the effects of exogenous conditions on the quiescent cell population while being reliant on dye-retention to identify these slow-cycling cells.

In the case of experiments designed to determine whether it was possible to induce an increase in the quiescent sub-population size by modulating culture conditions, this meant that discerning a true enrichment from the residual effects of reduced culture proliferation was impossible. In experiments in which colony formation was the primary experimental measurement, isolating the quiescent population from parental cultures and thereby stimulating overt outgrowth meant that the quiescent phenotype was inherently lost and therefore some of the results recorded in this way might not reflect the true intrinsic properties of the quiescent population. In light of these limitations, it appears critical that a surrogacy marker profile that accurately identifies quiescent cells will be required. Experiments that attempt to identify differentially expressed markers in the dye-retaining population are described in the next chapter.

4.7. Conclusions

Increasing the degree of culture confluency at successive sub-culture intervals did not result in a significant increase in the overall number of slow cycling, dye-retaining cells, irrespective of the Vybrant® dye or cell line used. While no further increase in the size of the quiescent sub-population was achieved by allowing culture overgrowth, dye-retaining cells were shown to re-emerge within isolated rapidly dividing (non-dye-retaining) cultures, probably due to the influence of microenvironmental conditions and seemingly involving the HIF-1α signalling cascade. When taken together, these results indicate that the quiescent sub-population identified within human breast cancer cell lines initially arise due to microenvironmental induction.

Partial deprivation of either serum or glucose in growing MDA-MB-231 cultures resulted in redistribution of the culture cell cycle profile that led to increased dye-retention during pulse-chase assays but was not seen to represent a true enrichment for quiescent sub-clones. Moderate to severe deprivation of serum or glucose both decreased the monolayer colony formation in both rapidly- and slowly-dividing cell populations but no differential colony forming ability was observed between these populations under any of the conditions tested. While colony formation in both rapidly- and slowly-dividing cell populations was not rescued upon re-establishment of standard culture conditions following serum starvation, the absence of colony formation resulting from severe glucose deprivation was shown to be reversible. The utilisation ERR-α-regulated oxidative lactate metabolism was shown to be one potential mechanism by which cells can survive under glucose deprivation, irrespective of their intrinsic mitotic capacity. Inhibition of ERR-α and blockade of this potentially critical survival mechanism was shown to be effective in preventing colony formation by sub-clones capable of evading anti-neoplastic drug treatment.

Chapter 5

Phenotypic Characterisation of the

Mitotically Quiescent Sub-Population in

Breast Cancer

5.1. Summary

The current literature contains a myriad of evidence for mitotic quiescence being associated with both stemness and inherent resistance to anti-proliferative chemotherapeutic agents. These associations suggest a mechanism of recurrence or relapse that enables mitotically inactive tumour-initiating cell populations to evade the effects of chemotherapeutics and re-emerge following cessation of treatment at either local or post-metastatic sites. The identification of a latent sub-population of cells with reduced mitotic activity within several distinct human breast cancer cell lines (as described in the third chapter of this thesis) was seen to represent a unique opportunity to further characterise a potentially biologically and clinically important cellular sub-set and to elucidate a functionally informed marker signature enabling future isolation of this sub-set from *in vitro* and *in vivo* models, without the requirement for fluorescence dye-dependent lineage tracing. This chapter describes the phenotypic characterisation of mitotically quiescent cells identified within human breast cancer cell lines using a lipophilic dye retention method, with a particular emphasis on cancer stem cell marker expression and chemotherapeutic resistance.

5.2. Introduction

Cancer stem cell (CSC) populations have been shown to contribute to chemoresistance in a number of cancer types. Studies of breast, prostate, ovarian and pancreatic cancers *in vivo* have demonstrated the ability of CSCs to survive concentrations of chemotherapeutic agents in excess of twice that required to elicit cytotoxicity in proliferating cell populations (Naumov *et al.*, 2003; Dembinski and Krauss, 2009; Gao *et al.*, 2010; Liu *et al.*, 2010). In one such study, a significant enrichment of the CSC compartment was observed following culture of patient-derived primary breast tumour cells *in vitro* in the presence of clinically relevant concentrations of cyclophosphamide, 5-fluoruracil and either epirubicin, doxorubicin or methotrexate. Subsequent quantification of the number of CSCs present in paired pre- and post-chemotherapy tumour biopsies indicated an approximate 10-fold increase in CSC frequency in patient samples post-treatment (Yu *et al.*, 2007).

A multitude of drug-resistance mechanisms have been suggested to contribute to the ability of CSCs to resist chemotherapy-induced cell death (**Figure 5.1.**). Enhanced DNA damage repair, up-regulation of xenobiotic pumps such as the multi-drug resistance protein and adenosine 5'-triphosphate-binding cassette transporters, increased enzymatic metabolism by enzymes such as ALDH, expression of anti-apoptotic proteins such as BCL-2 and BCL-XL, and activation of key pro-survival signalling molecules such as NOTCH and nuclear factor-κB (NF-κB) have all been associated with increased survivability of CSCs treated with chemotherapeutic drugs (Eyler and Rich, 2008; Holohan *et al.*, 2013; Cree and Charlton, 2017). At present it remains unclear how the quiescent phenotype contributes to these mechanisms, but it does seem plausible that a reduced proliferative rate would only act to augment their effectiveness. Quiescent cells that resist chemotherapy have been shown to either completely avert drug-induced cell cycle arrest or quickly re-enter the cell cycle once treatment was halted (Fillmore and Kuperwasser, 2008). Whether CSC-associated drug-resistance mechanisms are selectively enriched within quiescent cell populations remains to be elucidated. However, the established ubiquitous association of stemness and quiescence in the normal and neoplastic cellular hierarchies and the observation of a protracted period of dormancy in the natural history of metastatic disease does

suggests that mitotically quiescent and stem-like cell populations in cancer are not mutually exclusive (Moore and Lyle, 2011; Cojoc *et al.*, 2015). The key implication of this suggestion is a potential unified cellular mechanism of tumour initiation, relapse and recurrence in which mitotically inactive CSCs would evade the effects of chemotherapeutics and re-emerge at either primary or secondary sites following cessation of treatment. The series of experiments described within this chapter were aimed at furthering understanding of the degree to which mitotic quiescence, chemotherapeutic resistance and the putative breast cancer stem cell phenotype overlap.
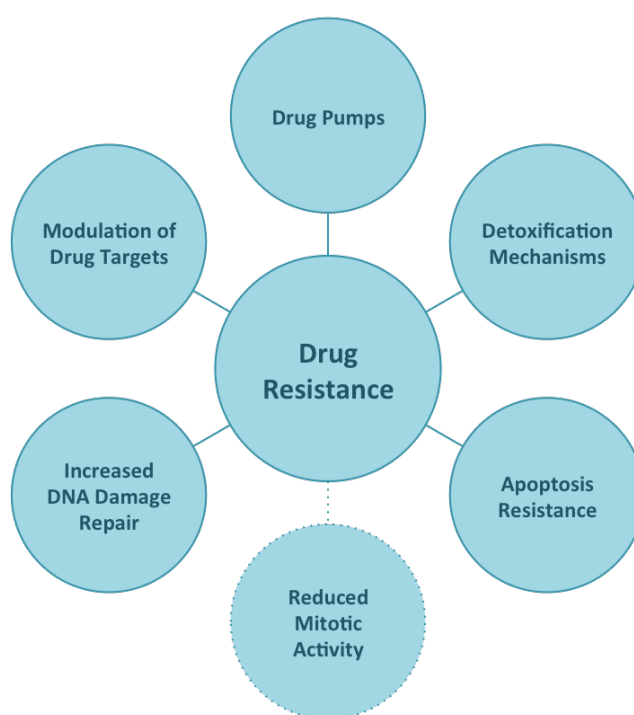
Figure 5.1. Cellular Mechanisms of Drug Resistance in Cancer Stem Cells

The hallmarks of chemotherapeutic resistance in putative cancer stem cell populations; individual cells might modulate or alter expression of drug targets, up-regulate expression of xenobiotic pumps, increase the activity or expression of drug-metabolising enzymes, increase expression of anti-apoptotic proteins or increase DNA damage repair pathways. The direct role of and degree to which these mechanisms are associated with the mitotically quiescent phenotype associated with stem cell populations remains to be elucidated.

5.3. Aims, Hypothesis and Objectives

The aim of the work described in this chapter was to undertake phenotypic and functional characterisation of mitotically quiescent breast cancer cells isolated using the fluorescent lipophilic dye retention method and to determine whether they share characteristics with the purported metastasis-initiating cancer stem cell population in breast cancer.

The key hypothesis pertaining to the work described in this chapter was that ***the latent mitotically quiescent sub-population contained within human breast cancer cell lines shows phenotypic overlap with the putative cancer stem cell population.***

The following objectives were defined in order to test this hypothesis:

1. Determine whether the dye-retaining sub-population was more resistant to the effects of anti-neoplastic drugs than the non-dye-retaining cell population.

2. Establish whether cells within dye-retaining and non-dye-retaining populations that survive anti-neoplastic drug treatment were able to form new clonal populations following cessation of treatment.

3. Ascertain whether the dye-retaining sub-population expressed markers frequently associated with stem cell-like behaviour and compare how the expression of these markers differed with their rapidly proliferating counterparts.

5.4. Materials and Methods

5.4.1. Establishing Dose-Response Curves for Doxorubicin and Paclitaxel

Pegylated liposomal doxorubicin, sourced from the Clinical Research Pharmacy, Weston Park Hospital, Sheffield, U.K., was supplied as an aqueous dispersion in PBS with a concentration of 3.4µM. This solution was sterilised through a 0.2µm filter into a light protected container and stored in a refrigerator maintained at 4°C until required. Immediately prior to use, stock solution was diluted 1:3.4 using complete growth medium as the diluent in order to produce a 1mM working stock. This working stock was then used to carry out a number of 1:10 serial dilutions in complete growth medium to produce a series of working solutions ranging in concentration between 100µM and 1pM.

Paclitaxel (Abcam Plc.) was supplied as 10mg of white crystalline solid. A 10mM stock solution of paclitaxel was prepared by dissolving the total 10mg mass supplied in 1170µl of absolute ethanol. This solution was then stored in a freezer maintained at -20°C until required. Immediately prior use, the stock solution was used to undertake a number of 1:10 serial dilutions in complete growth medium in order to achieve a series of working solutions ranging in concentration between 1µM and 1fM.

The method for seeding of cells and plate configuration for cytotoxicity in 96-well plates is described in detail in **Section 2.6.3.** Working solutions of each drug were added sequentially to adherent MCF-7 or MDA-MB-231 cells that had been seeded into the wells of 96-well cluster plates at the respective optimal density (**Table 2.2.**) 24 hours prior. Cells were incubated in the presence of drug for 72 hours, a period equivalent to the logarithmic phase of culture growth for these cell lines, prior to determination of the viability of cultures at each drug concentration using the MTT assay (**Section 2.6.3.**).

5.4.2. Establishing Sensitivity of Dye-Retaining Cells to Anti-Neoplastic Drugs

Wild type MCF-7 or MDA-MB-231 cells were stained in suspension with Vybrant® DiD according to the manufacturer's instructions (**Section 2.3.1.**) and then seeded at the optimal density (**Table 2.2.**) into 75cm^2 high-quality polystyrene tissue culture flasks. Stained cultures and unstained control samples were cultured for five consecutive passages of growth. Following retrieval of stained cultures at passage five, both stained and unstained cells were reseeded at the optimal density into triplicate wells of 6-well cluster plates pre-filled with 3ml of complete culture medium and were then placed into incubation overnight to allow cell adhesion to the growth surface. Stained cultures and unstained cultures were exposed to chemotherapeutic drugs in complete culture medium for a period of 72 hours (either doxorubicin or paclitaxel at the pre-determined IC$_{95}$ concentration, or a combination of each at the respective IC$_{50}$ concentration). Following 72 hours of incubation in the presence of drugs, the culture medium was removed from all wells and the remaining cells washed twice with PBS. Adherent cells were retrieved by trypsinisation (**Section 2.2.1.2.**) and prepared as suspensions in serum-free basal medium for haemocytometric counting as described previously (**Section 2.2.3.**). Haemocytometric counting was used to determine the number of viable cells present within each well prior to undertaking flow cytometric analysis to determine the percentage of Vybrant® DiD-positive cells. During flow cytometric analyses, unlabelled samples of either untreated, doxorubicin-treated or paclitaxel-treated cells were used to set the gating strategy for the corresponding experimental sample set and propidium iodide (f.c. 7.5µM) was used as a viability dye to ensure only live single cells were analysed for dye-retention. The percentage dye retention and haemocytometric viable cell counts were used to derive the number of viable dye-retaining and dye-negative cells present in untreated and drug treated samples. The relative survivability of Vybrant® DiD-positive and negative fractions was also calculated as a percentage of the untreated control for doxorubicin- and paclitaxel-treated cultures. A summary of the experimental timeline for establishing intrinsic drug resistance in Vybrant® DiD-positive and negative fractions is depicted in **Figure 5.2.**

5.4.3. Determination of the Presence of Drug-Resistant Sub-Clones

Dye-retaining and dye-negative MDA-MB-231 cells that remained viable following 72 hours exposure to the IC_{95} concentration of either doxorubicin or paclitaxel (as described in **Section 5.4.2.**) were isolated by FACS and seeded in triplicate at a clonogenic density of 20 cells per cm^2 into the wells of 6-well cluster plates, each containing a 3ml volume of drug-free complete culture medium. Cluster plates were placed into incubation under standard growth conditions for a period of 6 days. Colony formation assays were subsequently undertaken as described in **Section 2.2.6.1.** and the number of colonies formed by Vybrant® DiD-positive and negative fractions treated with either paclitaxel and doxorubicin quantified. A summary of the experimental timeline for establishing intrinsic drug resistance and determining presence of drug-resistant sub-clones in Vybrant® DiD-positive and negative fractions is depicted in **Figure 5.2.**
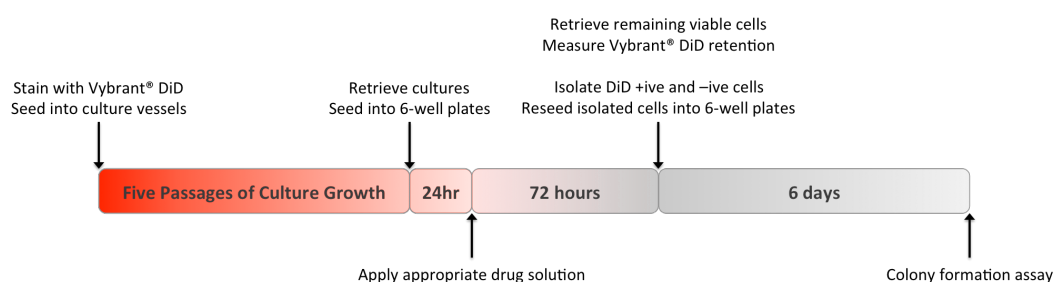
Figure 5.2. Timeline for Investigating Drug-Resistance in Dye-Retaining Cells

Cells stained with Vybrant® DiD were cultured continuously for five passages post-staining before being reseeded into 6-well cluster plates and exposed to the pre-determined IC_{95} concentration of the drug being tested for a 72 hour period. Following drug treatment, viable cells were retrieved and quantified by haemocytometric counting. The percentage Vybrant® DiD positivity of this surviving fraction was determined during the FACS process used to isolate Vybrant® DiD-positive and negative populations. These isolated populations were then re-plated in the absence of drug to allow colony formation. The number of colonies formed by Vybrant® DiD-positive and negative cells that initially survived drug treatment was determined after 6 days of incubation post-cessation of drug exposure.

5.4.4. CD24 and CD44 Expression in Dye-Negative and Dye-Retaining Populations

Staining of wild type MCF-7 or MDA-MB-231 cells with Vybrant® DiD was undertaken in suspension according to the manufacturer's instructions (**Section 2.3.1.**). Stained cells were seeded at the recommended optimal density (**Table 2.2.**) into 75cm^2 high-quality polystyrene tissue culture flasks and cultured continuously for five subsequent passages alongside unlabelled control samples. Following retrieval of cultures at passage five post-staining, samples of 1.0 x 10^6 cells were prepared and immunostained for CD24 and CD44 concomitantly using directly conjugated primary antibodies (**Table 5.1.**) according to the general protocol for detection of cell surface markers by direct immunofluorescence outlined in **Section 2.3.3.1.** The final working protein concentration of antibodies used was pre-determined and validated by the supplier. Stained cultures were analysed cytofluorimetrically for expression of CD24 and CD44 using the gating tree pre-set with an unlabelled control sample while Vybrant® DiD staining status was used to differentiate the two cell populations of interest (**Figure 5.3.**).

Table 5.1. Antibodies Used in CD24 and CD44 Immunostaining

Target	Host Species	Clonality	Isotype	Clone No.	Conjugate	Final Conc. (µg/ml)	Supplier
CD24	Mouse	Mono	IgG1	SN3	Phycoerythrin	6	Abcam
None	Mouse	Mono	IgG1	B11/6	Phycoerythrin	6	Abcam
CD44	Mouse	Mono	IgG2b	G44-26	BV421	10	BD
None	Mouse	Mono	IgG2b	27-35	BV421	10	BD

A phycoerythrin-conjugated anti-CD24 primary antibody and matched isotype control antibody were sourced from Abcam Plc. (Cambridge, U.K.) while a Brilliant Violet 421™-conjugated anti-CD44 primary antibody and matched isotype control antibody were sourced from Beckton, Dickenson and Co. Plc. (Oxford, U.K.). The working concentration of each isotype control antibody was matched to the exact working protein concentration of the primary antibody to which it was paired.
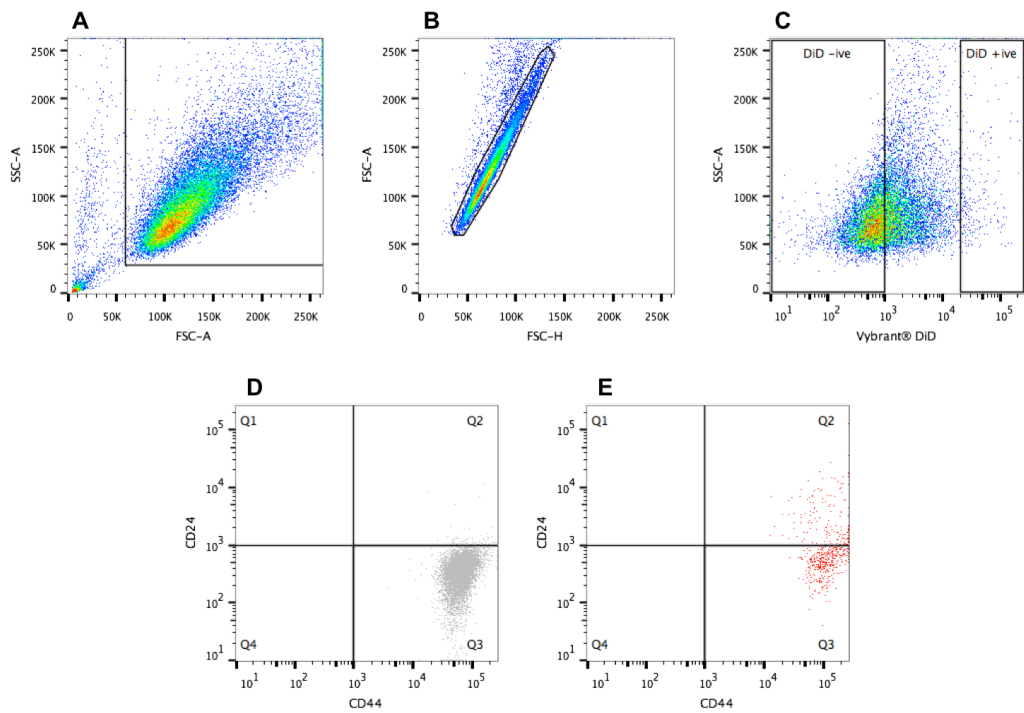
Figure 5.3. CD24 and CD44 Expression by Dye-Retaining and Negative Populations

Cellular debris was gated-out of the event population (**A**), the resultant population divided into single cell and non-single cell events (**B**), and then Vybrant® DiD-negative and positive populations identified using gates predefined by unlabelled and freshly labelled samples, respectively (**C**). Vybrant® DiD-negative (**D**) and Vybrant® DiD-positive (**E**) populations were analysed for expression of CD24 and CD44 concomitantly.

5.4.5. Aldehyde Dehydrogenase Activity of Dye-Negative and Dye-Retaining Cells

Wild type MCF-7 or MDA-MB-231 cells were stained in suspension with Vybrant® DiD according to the manufacturer's instructions (**Section 2.3.1.**) and seeded at the recommended optimal density into 75cm^2 high-quality polystyrene tissue culture flasks (**Table 2.2.**). Stained cells were cultured continuously for five subsequent passages alongside unlabelled control samples. Following retrieval of stained cultures at passage five post-staining, cultures were assayed non-immunologically for ALDH activity using the ALDEFLUOR™ assay, as described in **Section 2.5.3.** During flow cytometric analysis, an unlabelled control sample was used to pre-set the gating strategy for determination of Vybrant® DiD staining status which facilitated differentiation of dye-retaining and dye-negative sub-populations prior to analysis of their respective ALDH positivity. The gate for determination of ALDH positivity, as indicated by fluorescence due to oxidation of BODIPY-aminoacetaldehyde (BAAA), was pre-set using samples pre-treated with the specific ALDH inhibitor diethylaminobenzaldehyde (DEAB). The gating strategy for concomitant cytofluorimetric assessment of the ALDH activity of Vybrant® DiD-retaining and DiD-negative populations is depicted in **Figure 5.4.**
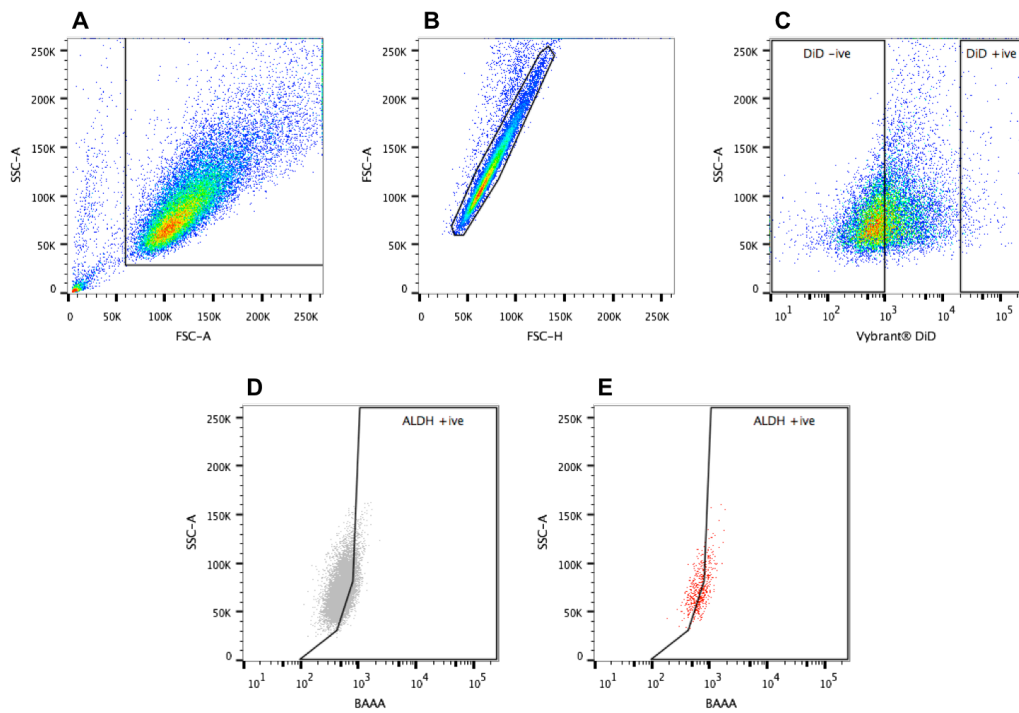
Figure 5.4. ALDH Analysis in Dye-Retaining and Negative Populations

Cellular debris was gated-out of the event population (**A**) and the resultant population divided into single cell and non-single cell events (**B**). The Vybrant® DiD-negative and positive populations within samples were identified using gates predefined by unlabelled and freshly labelled samples, respectively (**C**). A control sample of Vybrant® DiD stained cells treated with the specific aldehyde dehydrogenase (ALDH) inhibitor diethylaminobenzaldehyde (DEAB) was used to set the gating for the detection of oxidised BODIPY-aminoacetaldehyde (BAAA) indicative of cellular ALDH activity in Vybrant® DiD-negative and Vybrant® DiD-positive populations. Experimental samples that were not treated with DEAB were then analysed using the pre-set gating strategy, thereby allowing specific detection of ALDH positive cells in Vybrant® DiD-negative (**D**) and Vybrant® DiD-positive (**E**) populations.

5.4.6. Assessing EMT Marker Expression in Dye-Negative and Dye-Retaining Cells

Staining of wild type MDA-MB-231 cells with Vybrant® DiD was undertaken in suspension according to the manufacturer instructions (**Section 2.3.1.**) before cells were seeded at the recommended optimal density (**Table 2.2.**) into 75cm^2 high-quality polystyrene tissue culture flasks and cultured continuously for five subsequent passages. Following retrieval of stained cultures at passage five post-staining, Vybrant® DiD-positive and DiD-negative cells were isolated by FACS and 2000 cells of each type deposited onto glass microscope slides using a cytocentrifuge as described in **Section 2.3.2.1.** Samples were immunostained for markers of EMT detailed in **Table 5.2.** according to the protocol for detection of intracellular antigens by indirect immunofluorescence outlined in **Section 2.3.2.2.** The final working protein concentration of antibodies used was determined by preliminary assays carried out in the same manner in which a range of final protein concentrations of primary and secondary antibodies were used; primary antibody concentrations ranged from 0.1µg/ml to 20µg/ml, while secondary antibody concentrations ranged from 1.875µg/ml to 15µg/ml, as recommended by the supplier. Immunostained samples were imaged under fluorescence microscopy at 100X magnification and a series of three non-overlapping fields captured using the tile scan function of the Leica AF6000LX microscope for manual scoring of marker expression (**Section 2.4.**). Representative images of the staining pattern in each instance were also captured at 200X magnification.

Table 5.2. Antibodies Used in EMT Marker Immunostaining

Target	Host Species	Clonality	Isotype	Clone No.	Conjugate	Final Conc. (µg/ml)	Supplier
β-Catenin	Mouse	Mono	IgG1	12F7	None	2	Abcam
Vimentin	Mouse	Mono	IgG1	RV202	None	1	Abcam
None	Mouse	Mono	IgG1	15-6E10A7	None	-	Abcam
Mouse IgG+M	Goat	Poly	IgG	-	AlexaFluor® 488	3.75	Stratech

Unconjugated antibodies against β-catenin and vimentin, along a matched isotype control antibody were sourced from Abcam Plc. (Cambridge, U.K.) while an AlexaFluor® 488-conjugated secondary antibody was sourced from Stratech Scientific Ltd. (Newmarket, U.K.). A specific dilution is not stated for the isotype control antibody, as this was dependent on matching the exact working protein concentration of the primary antibody to which it was paired in a particular experiment.

5.4.7. Stem Cell Marker Expression in Dye-Negative and Dye-Retaining Cells

Wild type MDA-MB-231 cells that were stained in suspension with Vybrant® DiD according to the manufacturer instructions (**Section 2.3.1.**) were seeded at the optimal density of 1.0×10^4 cells per cm^2 into $75cm^2$ high-quality polystyrene tissue culture flasks and cultured continuously for five passages post-staining. Following retrieval of stained cultures at passage five post-staining, samples of 1.0×10^6 cells were prepared and subsequently immunostained using a panel of unconjugated primary antibodies for the detection of human embryonic stem cells (hES) and embryocarcinoma stem cells (hEC), depicted in **Table 5.3.** Immunostaining was undertaken according to the general protocol for detection of cell surface markers by indirect immunofluorescence outlined in **Section 2.3.3.2.** The final working protein concentration of all antibodies used was pre-determined and validated by the supplier. Stained cultures were analysed cytofluorimetrically for marker positivity using the gating tree pre-set with an unlabelled control sample while Vybrant® DiD staining status was used to differentiate the two cell populations of interest (**Figure 5.5.**).

Table 5.3. Antibodies Used in Stem Cell Marker Immunostaining

Target	Host Species	Clonality	Isotype	Clone No.	Conjugate	Final Conc. (µg/ml)	Supplier
SSEA-3	Mouse	Mono	IgM	-	None	1	UoS CSCB
SSEA-4	Mouse	Mono	IgG3	-	None	10	UoS CSCB
TRA-1-60S	Mouse	Mono	IgM	-	None	10	UoS CSCB
TRA-1-60R	Mouse	Mono	IgM	-	None	10	UoS CSCB
TRA-1-81	Mouse	Mono	IgM	-	None	10	UoS CSCB
TRA-2-49	Mouse	Mono	IgG1	-	None	10	UoS CSCB
TRA-2-54	Mouse	Mono	IgG1	-	None	10	UoS CSCB
SSEA-1	Mouse	Mono	IgM	-	None	10	UoS CSCB
GD2	Mouse	Mono	IgM	-	None	10	UoS CSCB
GD3	Mouse	Mono	IgM	-	None	10	UoS CSCB
GT3	Mouse	Mono	IgM	-	None	5	UoS CSCB
CD46	Mouse	Mono	IgG1	-	None	10	UoS CSCB
CD56	Mouse	Mono	IgG1	-	None	10	UoS CSCB
CD57	Mouse	Mono	IgM	-	None	10	UoS CSCB
CD271	Mouse	Mono	IgM	-	None	10	UoS CSCB
AA11	Mouse	Mono	IgM	-	None	10	UoS CSCB
AG10	Mouse	Mono	IgM	-	None	10	UoS CSCB
EF12	Mouse	Mono	IgM	-	None	10	UoS CSCB
BE12	Mouse	Mono	IgM	-	None	10	UoS CSCB
BF4	Mouse	Mono	IgM	-	None	10	UoS CSCB
CC9	Mouse	Mono	IgM	-	None	10	UoS CSCB
CH8	Mouse	Mono	IgG1	-	None	10	UoS CSCB
DA9	Mouse	Mono	IgM	-	None	10	UoS CSCB
CD147	Mouse	Mono	IgG1	-	None	2	UoS CSCB
None	Mouse	Mono	IgG1	15-6E10A7	None	-	Abcam
None	Mouse	Mono	IgG3	PPV-07	None	-	Abcam
None	Mouse	Mono	IgM	B11/7	None	-	Abcam
Mouse IgG+M	Goat	Poly	IgG	-	AlexaFluor® 488	15	Stratech

All primary antibodies were raised in-house, pre-validated and supplied by the Centre for Stem Cell Biology, University of Sheffield (Sheffield, U.K.), while isotype control and AlexaFluor® 488-conjugated secondary antibodies were sourced from Abcam Plc. (Cambridge, U.K.) and Stratech Scientific Ltd. (Newmarket, U.K.), respectively. The pan-human antigen CD147 was used as a positive control for immunostaining. Specific dilutions are not stated for isotype control antibodies, as this was dependent on the exact working protein concentration of the primary antibody to which they were matched in any particular experiment.
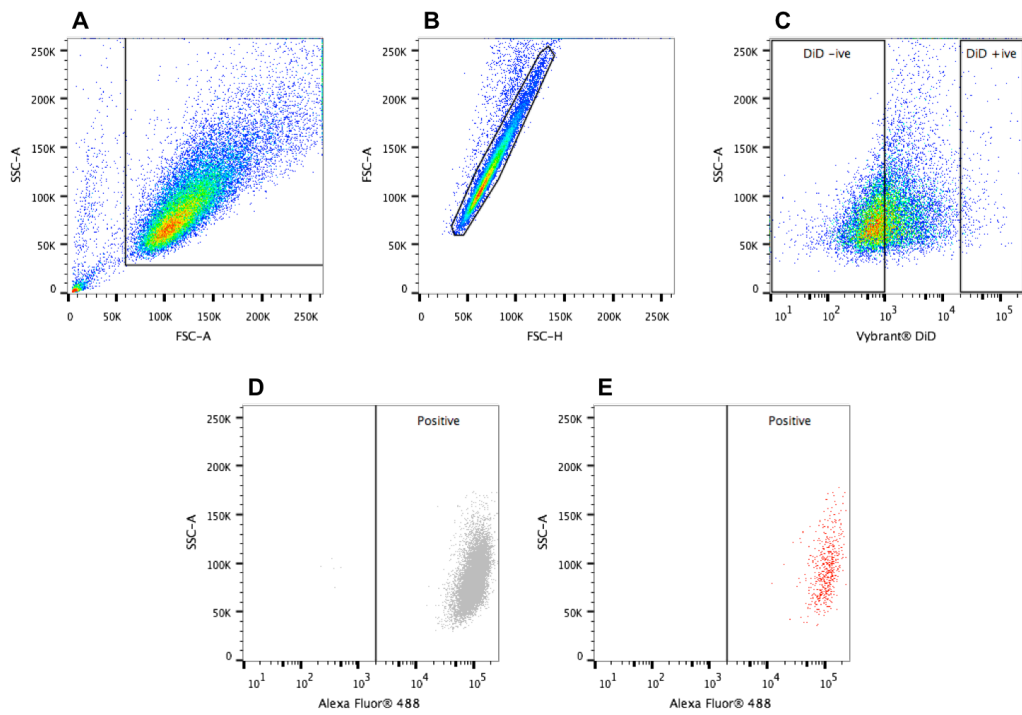
Figure 5.5. Stem Cell Marker Analysis in Dye-Retaining and Negative Populations

Cellular debris was gated-out of the event population (**A**), the resultant population divided into single cell and non-single cell events (**B**), and then Vybrant® DiD-negative and positive populations identified using gates predefined by unlabelled and freshly labelled samples, respectively (**C**). Vybrant® DiD-negative (**D**) and Vybrant® DiD-positive (**E**) populations were then concomitantly analysed for expression of hES or hEC markers according to AlexaFluor® 488 staining status.

5.4.8. Assessment of Mammosphere Formation in Dye-Retaining Cells

After a total of five consecutive passages of culture post-staining with Vybrant® DiD, MDA-MB-231 cultures were sorted into dye-negative and dye-positive populations by FACS and reseeded at a density of 20 cells per cm^2 in a total volume of 3ml complete culture medium into the wells of ultra-low attachment 6-well cluster plates pre-coated with 1.5% (w/v) agarose as described previously (**Section 2.2.6.2.**). Plates were subsequently placed into incubation for a period of 6 days before the mammosphere forming efficiency of the two fractions under routine culture conditions was assessed according to the general protocol described in **Section 2.2.6.2.**

5.4.9. Establishing Mitotic Dynamics of Dye-Retaining Cells

Vybrant® DiD-retaining MDA-MB-231 cells that were isolated by FACS following five consecutive passages of culture growth post-staining were reseeded in triplicate into the wells of 6-well cluster plates pre-filled with 3ml complete culture medium at the clonogenic density of 20 cells per cm^2. Following an initial incubation period of 24 hours to allow cells to adhere to the plate growth surface, single Vybrant® DiD-positive cells were located under inverted phase contrast microscopy using the Leica AF6000LX integrated live cell imaging station and their X and Y coordinates recorded using the "mark and trace" function of the automated microscope stage and proprietary LAS imaging software. At subsequent 24 hour intervals the specimen position was relocated and images recorded.

5.5. Results

5.5.1. Dye-Retaining Cells are Resistant to Anti-Neoplastic Drugs

Conventional chemotherapeutic agents require that cells are actively progressing through the cell cycle in order to elicit their cytotoxic effects (Moore and Lyle, 2011). Mitotically quiescent or slow-cycling cell populations are therefore likely to be less susceptible to such drugs, suggesting an inherent mechanism of recurrence or relapse in which these populations are able to evade the effects of chemotherapeutics and re-emerge at either the primary or secondary sites following cessation of treatment. Vybrant® DiD-stained MCF-7 and MDA-MB-231 cultures were treated with either doxorubicin, paclitaxel or a combination thereof in order to test the hypothesis that the slow-cycling nature of the label-retaining population conferred inherent chemotherapeutic resistance. The IC_{50} and IC_{95} of each drug was first determined using the MTT assay (**Figure 5.6.** and **Figure 5.7.**) before Vybrant® DiD-stained MCF-7 or MDA-MB-231 cultures were treated with drugs for 72 hours (**Section 5.4.2.**). The relative survivability of the dye-negative and dye-retaining fractions was compared when expressed as a percentage of untreated control samples (**Figure 5.8.** and **Figure 5.9.**).
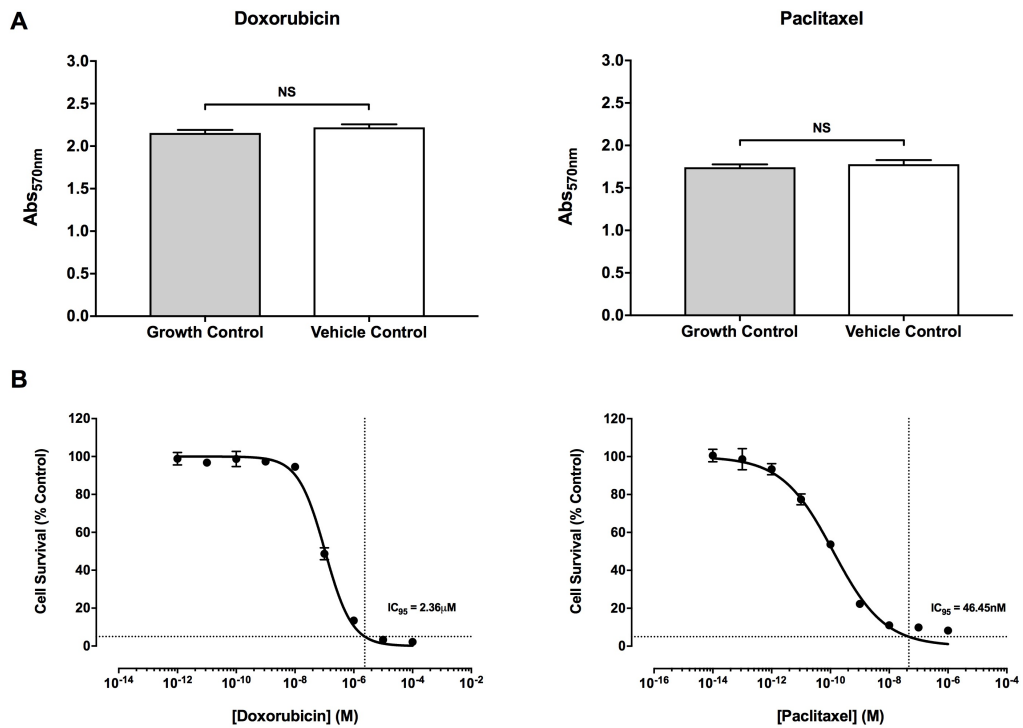
Figure 5.6. MCF-7 Doxorubicin and Paclitaxel Dose-Response Curves

A: Absorbance values measured spectrophotometrically at a wavelength of 570nm (Abs_{570nm}) following MTT assays undertaken on growth control and vehicle control samples included during establishment of the MCF-7 dose-response curves for doxorubicin and paclitaxel. In both cases growth controls were grown in complete culture medium only (RPMI-1640 + 10% (v/v) FBS). Vehicle controls for samples treated with doxorubicin and paclitaxel contained 4.17% (v/v) PBS or 1% (v/v) ethanol respectively in addition to complete culture medium. Data were compared using a two-tailed unpaired *t*-test (NS = not statistically significant or P > 0.05). **B**: MCF-7 dose-response curves established using the MTT assay following a 72-hour period of exposure to either doxorubicin (1pM - 100μM) or paclitaxel (10fM - 1μM). Cell survival at each drug concentration is expressed as a percentage of Abs_{570nm} recorded for samples exposed to the respective vehicle control solution. Data are expressed as the mean average ± SEM for n = 3 biologically independent repeat experiments.
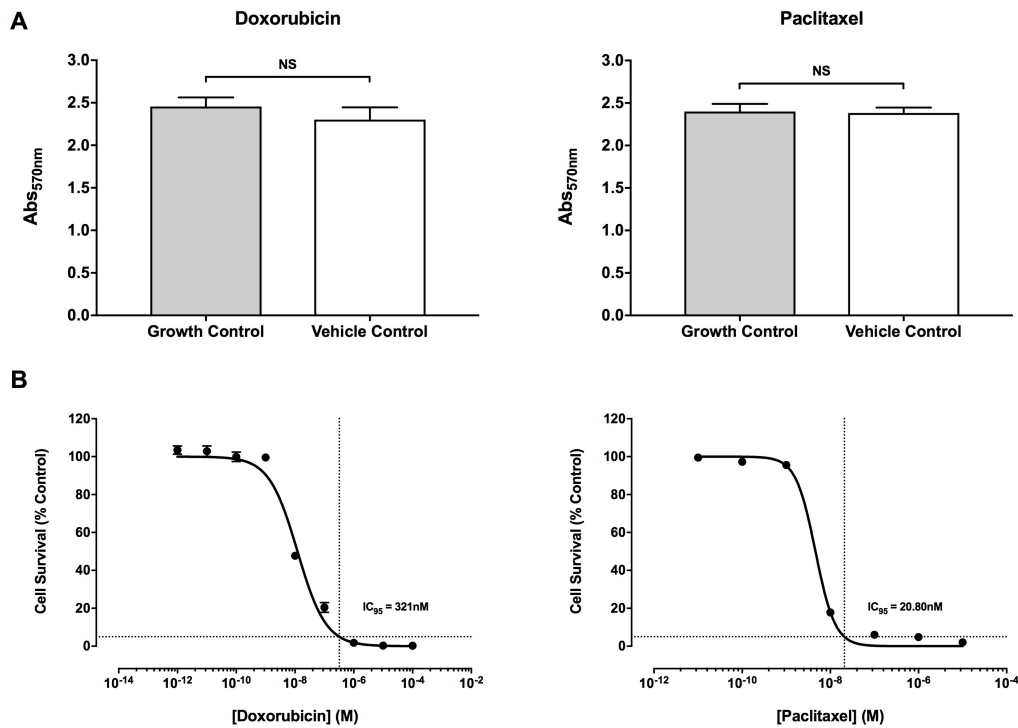
Figure 5.7. MDA-MB-231 Doxorubicin and Paclitaxel Dose-Response Curves

A: Absorbance values measured spectrophotometrically at a wavelength of 570nm (Abs_{570nm}) following MTT assays undertaken on growth control and vehicle control samples included during establishment of the MDA-MB-231 dose-response curves for doxorubicin and paclitaxel. In both cases growth controls were grown in complete culture medium only (RPMI-1640 + 10% (v/v) FBS). Vehicle controls for samples treated with doxorubicin and paclitaxel contained 4.17% (v/v) PBS or 1% (v/v) ethanol respectively in addition to complete culture medium. Data were compared using a two-tailed unpaired *t*-test (NS = not statistically significant or P > 0.05). **B**: MDA-MB-231 dose-response curves established using the MTT assay following a 72-hour period of exposure to either doxorubicin (1pM - 100μM) or paclitaxel (1pM - 1μM). Cell survival at each drug concentration is expressed as a percentage of Abs_{570nm} recorded for samples exposed to the respective vehicle control solution. Data are expressed as the mean average ± SEM for n = 3 biologically independent repeat experiments.

In MCF-7 cultures treated with doxorubicin (IC_{95} = 2.36µM) for 72 hours (**Figure 5.8.**), the Vybrant® DiD-retaining fraction demonstrated significantly increased survival over the non-label-retaining bulk cell population, with 22.68 ± 1.91% of the label retaining population remaining viable following doxorubicin treatment compared with 5.48 ± 0.53% of the bulk cell population ($P ≤ 0.001$). Similarly, when treated with paclitaxel (IC_{95} = 46.45nM) for a 72-hour period, 24.08 ± 1.24% of Vybrant® DiD-retaining MCF-7 cells survived compared with just 6.34 ± 0.58% of the non-labelled bulk population ($P ≤ 0.001$) (**Figure 5.8.**). These findings were reiterated when doxorubicin and paclitaxel were used at lower concentrations in combination (doxorubicin IC_{50} = 0.11µM, paclitaxel IC_{50} = 0.12nM) (**Figure 5.8.**); 93.72 ± 12.84% of Vybrant® DiD-retaining cells survived compared with just 22.60 ± 0.24% of the Vybrant® DiD-negative population ($P ≤ 0.01$).

In MDA-MB-231 cultures treated with doxorubicin (IC_{95} = 321nM) for 72 hours (**Figure 5.9.**), the Vybrant® DiD-retaining MDA-MB-231 fraction demonstrated significantly increased survival over the non-label-retaining bulk cell population, with 40.76 ± 4.60% of the label retaining population remaining viable following doxorubicin treatment compared with 1.63 ± 0.22% of the bulk cell population ($P ≤ 0.0001$). When treated with paclitaxel (IC_{95} = 20.80nM) for a 72-hour period, 102 ± 5.57% of Vybrant® DiD-retaining MDA-MB-231 cells survived compared with just 4.47 ± 0.25% of the non-labelled bulk population ($P ≤ 0.0001$) (**Figure 5.9.**). Similarly, when treated with a combination of doxorubicin and paclitaxel (doxorubicin IC_{50} = 12.14nM, paclitaxel IC_{50} = 4.60nM), 81.43 ± 5.84% of Vybrant® DiD-retaining MDA-MB-231 cells survived compared with 44.41 ± 1.03% of the Vybrant® DiD-negative population ($P ≤ 0.01$) (**Figure 5.9.**). The combined outcome of these assays indicated that the slow-cycling nature of the dye-retaining fraction is associated with an enhanced resistance to the cytotoxic effects of anti-neoplastic chemotherapeutic agents.
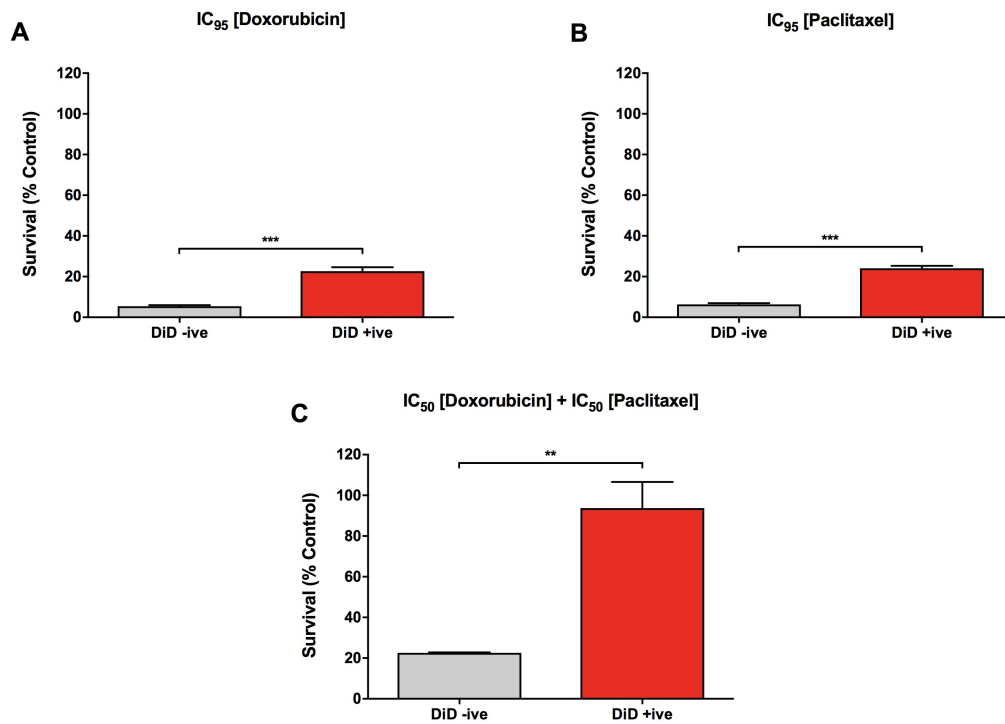
Figure 5.8. Chemoresistance in Dye-Retaining and Negative MCF-7 Cells

The total viable number of Vybrant® DiD-negative and Vybrant® DiD-positive cells present in MCF-7 cultures expressed as a percentage of the corresponding population present in untreated control samples following 72 hours treatment with either the IC_{95} concentration of doxorubicin (**A**), paclitaxel (**B**), or a combination of both at the respective IC_{50} concentration (**C**) at five passages post-staining. Data were compared using one-way ANOVA followed by Dunnett's Multiple Comparison Test (** = $P \leq 0.01$, *** = $P \leq 0.001$). All data are expressed as the mean ± SEM for n = 3 biologically independent repeat experiments.

A IC$_{95}$ [Doxorubicin]

B IC$_{95}$ [Paclitaxel]

C IC$_{50}$ [Doxorubicin] + IC$_{50}$ [Paclitaxel]
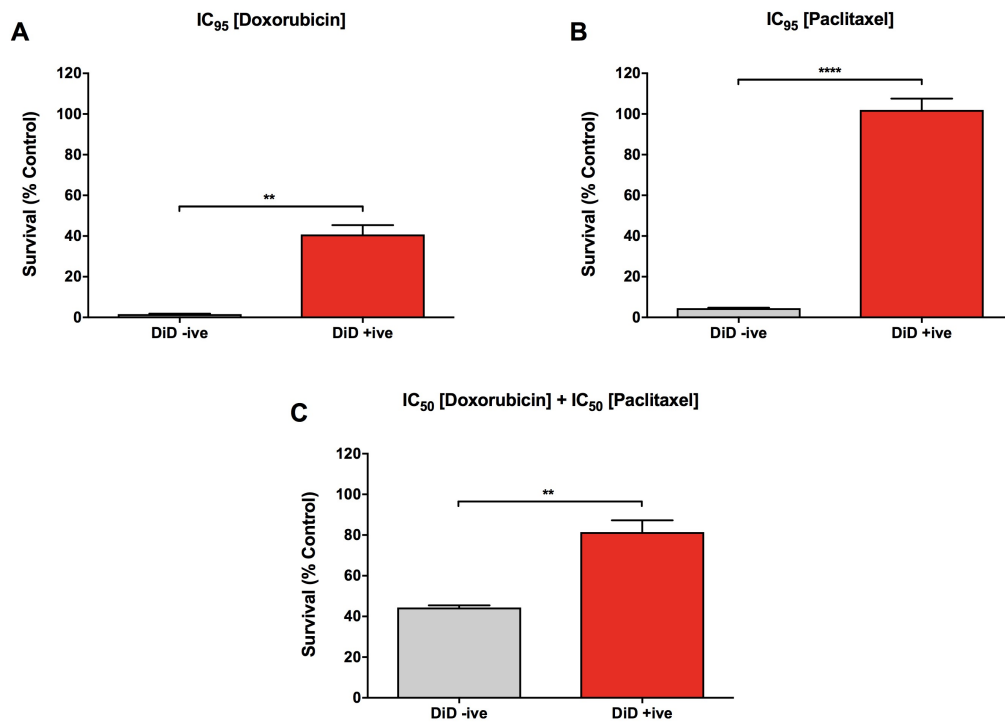
Figure 5.9. Chemoresistance in Dye-Retaining and Negative MDA-MB-231 Cells

The total viable number of Vybrant® DiD-negative and Vybrant® DiD-positive cells present in MDA-MB-231 cultures expressed as a percentage of the corresponding population present in untreated control samples following 72 hours treatment with either the IC$_{95}$ concentration of doxorubicin (**A**), paclitaxel (**B**), or a combination of both at the respective IC$_{50}$ concentration (**C**) at five passages post-staining. Data were compared using one-way ANOVA followed by Dunnett's Multiple Comparison Test (** = P ≤ 0.01, **** = P ≤ 0.0001). All data are expressed as the mean ± SEM for n = 3 biologically independent repeat experiments.

In order to determine whether cells that survived chemotherapeutic drug treatment, such as those depicted in **Figure 5.10.**, were capable of further mitotic activity and subsequent formation of new clonal populations, viable cells from both Vybrant® DiD-negative and Vybrant® DiD-positive fractions were isolated by FACS following 72 hours exposure to the IC_{95} concentration of either doxorubicin or paclitaxel and reseeded at a clonogenic density in drug-free medium (**Section 5.4.3.**). Following six days incubation post-cessation of chemotherapeutic drug exposure, an average of 4.11 ± 0.77 colonies had been formed by Vybrant® DiD-positive cells that initially survived doxorubicin treatment and 4.44 ± 0.56 colonies had been formed by Vybrant® DiD-positive cells that initially survived paclitaxel treatment. In contrast, no detectable colonies were formed by Vybrant® DiD-negative cells that had initially survived treatment with either drug (**Figure 5.11.**) and no undivided single cells were evident in any of the wells when Vybrant® DiD-negative cell assay plates were examined under inverted phase contrast microscopy immediately prior to the colony formation assay. These data demonstrate that cells capable of escaping anti-neoplastic therapy exist within the quiescent fraction. In order to determine whether stem-like cells were equally prevalent within both dye retaining and rapidly dividing cell fractions, or were exclusive to the former population, the expression of widely used breast cancer stem cell markers CD24 and CD44 was next determined.

Untreated	**Doxorubicin-Treated**	**Paclitaxel-Treated**
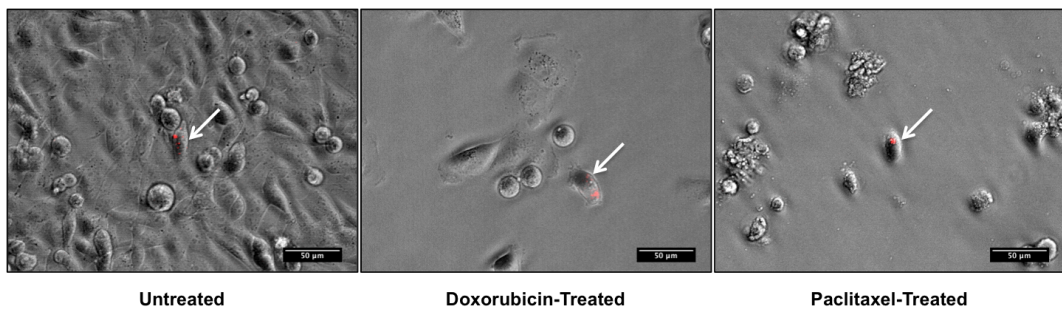
Figure 5.10. Dye-Retaining MDA-MB-231 Cells Surviving Chemotherapy

Representative images of MDA-MB-231 cultures (five passages post-staining with Vybrant® DiD) following 72-hours treatment with the IC_{95} concentration of either doxorubicin (321nM) or paclitaxel (20.80nM). Untreated control cultures are also shown on the left. Dye-retaining cells (red, indicated by white arrows) in drug-treated cultures appear to possess relatively normal morphology despite many surrounding dye-negative cells showing clear evidence of cell death. All images were captured using a 20x objective lens (scale bar = 50µm).
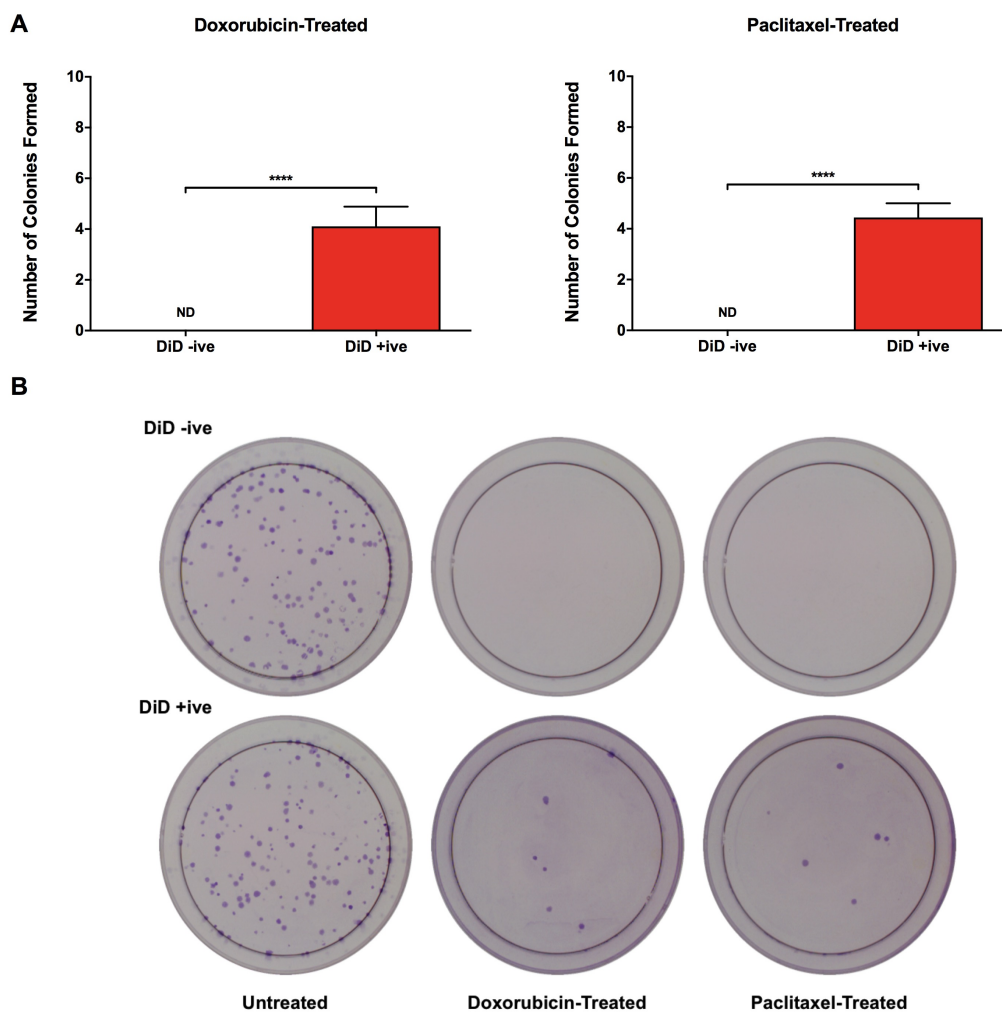
Figure 5.11. Colony Formation by Dye-Retaining Cells Surviving Chemotherapy

A: The number of colonies formed by viable Vybrant® DiD-negative and Vybrant® DiD-positive MDA-MB-231 cells isolated following 72 hours treatment with the IC_{95} concentration of doxorubicin (321nM) or paclitaxel (20.80nM) at five passages post-staining. Data were compared using a two-tailed unpaired *t*-test (**** = P ≤ 0.0001). Data are expressed as the mean average ± SEM for n = 3 biologically independent repeat experiments. **B**: Representative images of a crystal violet-stained clonogenic assay plates for Vybrant® DiD-negative and Vybrant® DiD-positive MDA-MB-231 cells isolated from untreated, paclitaxel- and doxorubicin-treated cultures. All images were captured using a 2x stereomicroscopic objective lens.

5.5.2. CD24 and CD44 Co-Expression is Increased in Dye-Retaining Cells

Since the pioneering study of Al-Hajj *et al.* (2003) the CD44$^+$CD24$^{-/low}$ signature, has been widely used to demark a more tumourigenic putative breast cancer stem cell population. In order to provide an initial indication of the presence and relative distribution of supposed stem-like cells between rapidly dividing and slowly dividing dye-retaining populations, these fractions were distinguished cytofluorimetrically based on Vybrant® DiD staining status following five consecutive passages of culture growth post-staining and then each analysed for CD24 and CD44 expression (**Section 5.4.4.**).

During CD24 and CD44 co-expression analyses it was immediately evident that all MDA-MB-231 cells express CD44 irrespective of their mitotic activity and consequent dye-retention status but that the Vybrant® DiD-negative and Vybrant® DiD-positive populations differed considerably in their relative expression of CD24 (**Figure 5.12.**). A mean average of 0.55 ± 0.01% of Vybrant® DiD-negative cells were CD24$^+$ while 28.99 ± 3.01% of Vybrant® DiD-positive cells were CD24$^+$ (P ≤ 0.0001). Although the overall distribution of the CD24 and CD44 markers was different in the MCF-7 cell line, the same pattern of increased CD24 and CD44 dual positive expression status was observed in the Vybrant® DiD-positive cell population; Vybrant® DiD-negative MCF-7 cells were 52.11 ± 1.39% CD44$^+$CD24$^+$ while the corresponding Vybrant® DiD-positive population was 81.23 ± 0.78% CD44$^+$CD24$^+$ (P ≤ 0.0001).

The observation of significantly increased dual CD24 and CD44 positivity in the Vybrant® DiD-positive fraction of both MDA-MB-231 and MCF-7 cell lines was a somewhat unexpected finding. Relatively recently Liu *et al.* (2014) demonstrated that the CD44$^+$CD24$^{-/low}$ and ALDH$^+$ signatures identify minimally overlapping breast cancer stem cell populations that differ with respect to transcriptomic signatures of EMT. This raised the question as to whether the observed alterations in CD24 and CD44 expression was related to increased relative ALDH activity and altered expression of EMT markers within the Vybrant® DiD-positive population; subsequent experiments were therefore designed in order to address these issues.
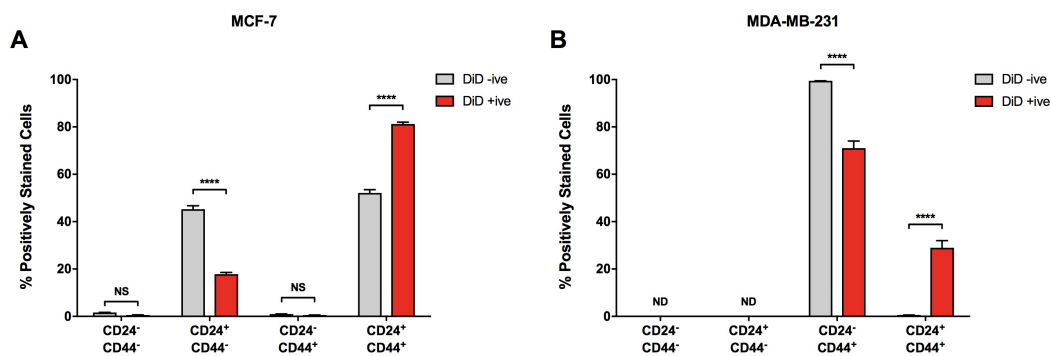
Figure 5.12. CD24 and CD44 Expression in Dye-Retaining and Negative Cells

The percentage co-expression of breast cancer stem cell-associated markers CD24 and CD44 in Vybrant® DiD-negative and Vybrant® DiD-positive sub-populations in the MCF-7 (**A**) and MDA-MB-231 (**B**) cell lines after five consecutive passages post-staining. ND = not detected. Comparison of marker expression between Vybrant® DiD-negative and Vybrant® DiD-positive populations was achieved using two-way ANOVA followed by Sidak's Multiple Comparison Test (NS = not statistically significant or P > 0.05, **** = P ≤ 0.0001). Data are expressed as the mean average ± SEM for n = 3 biologically independent repeat experiments.

5.5.3. Dye Retaining Cells Possess Increased ALDH Activity

Aldehyde dehydrogenase (ALDH) represents a superfamily of $NADP^+$-dependent enzymes responsible for the intracellular oxidation of aldehydes thought to be critical to regulating stem cell differentiation through their role in retinol metabolism (Clark and Palle, 2016). ALDH has been successfully used as a marker for isolation of cells with stem cell properties from multiple cancers and non-malignant tissues. In particular, seminal studies by Ginestier *et al.* (2007) and Charafe-Jauffret *et al.* (2009) demonstrated the utility of ALDH activity for isolation of stem cell-like properties from normal human breast tissue and breast carcinomas. On this basis, the intrinsic ALDH activity of Vybrant® DiD-negative and Vybrant® DiD-positive populations was assessed cytofluorimetrically using the ALDEFLUOR™ assay (**Section 5.4.5.**) in order to better distinguish whether any differential cancer stem cell activity was present within each fraction. A significantly greater number of ALDH-positive cells were detected within the Vybrant® DiD-positive population in both MDA-MB-231 and MCF-7 cell lines compared to the corresponding Vybrant® DiD-negative population (**Figure 5.13.**). In the MDA-MB-231 cell line, an average of 7.68 ± 0.29% of Vybrant® DiD-positive cells were ALDH positive compared to 3.5 ± 0.21% of Vybrant® DiD-negative cells ($P \leq$ 0.001). In the MCF-7 lineage, 8.81 ± 1.27% of Vybrant® DiD-positive cells were ALDH positive compared to 1.24 ± 0.14% positivity in the Vybrant® DiD-negative population ($P \leq$ 0.01). When taken together, CD24 and CD44 expression and ALDH assays suggested that the slowly cycling dye-retaining phenotype is associated with enrichment for $CD44^+CD24^+$ and $ALDH^+$ cells that might represent a distinct relatively quiescent stem cell-like phenotype.
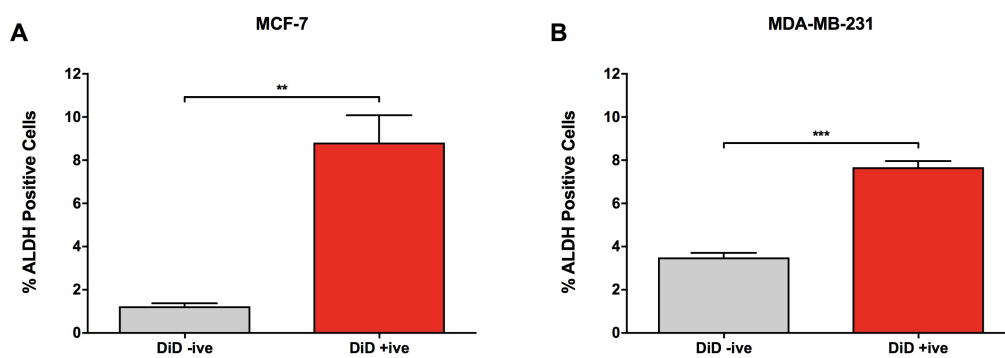
Figure 5.13. ALDH Expression in Dye-Retaining and Negative Cells

The percentage expression of breast cancer stem cell-associated marker enzyme aldehyde dehydrogenase (ALDH) in Vybrant® DiD-negative and Vybrant® DiD-positive sub-populations in the MCF-7 (**A**) and MDA-MB-231 (**B**) cell lines after five consecutive passages post-staining. The relative expression of ALDH by Vybrant® DiD-negative and Vybrant® DiD-positive populations was compared using a two-tailed unpaired *t*-test (** = P ≤ 0.01, *** = P ≤ 0.001). Data are expressed as the mean average ± SEM for n = 3 biologically independent repeat experiments.

5.5.4. EMT Marker Positivity is Unaltered in Dye-Retaining MDA-MB-231 Cells

Given that emerging evidence in breast cancer and other cancer types suggest that stem-like and non-stem-like phenotypes exist along a dynamically transitioning spectrum of states regulated by the EMT programme (Recently reviewed by Fabregat *et al.*, 2016), and that the dye-retaining quiescent phenotype appeared to be associated with CD44$^+$CD24$^+$ and ALDH$^+$ status, it was hypothesised that markers of EMT are differentially regulated between the slow-cycling and rapidly dividing populations. Consequently, the expression of vimentin and β-catenin was assessed by scoring of immunofluorescent staining in cytocentrifuge preparations of the Vybrant® DiD-positive and Vybrant® DiD-negative MDA-MB-231 cell populations following their isolations by FACS (**Section 5.4.6.**). These markers were chosen from those to which antibodies were readily available due to their central roles in the process of EMT and consequent utility as key indicators of cellular EMT-MET status; vimentin is an intermediate filament of mesenchymal origin being correlated with the post-EMT phenotype, while β-catenin is a key downstream effector in the Wnt signalling pathway that plays a key regulatory role in both EMT and stemness (Fabregat *et al.*, 2016). Representative images of staining for each marker in the Vybrant® DiD-positive and Vybrant® DiD-negative MDA-MB-231 cell populations are displayed in **Figure 5.14.** and **Figure 5.15.**

No significant differences in the percentage of cells expressing either vimentin or β-catenin were observed when immunofluorescent staining was quantified in Vybrant® DiD-positive and Vybrant® DiD-negative MDA-MB-231 cell populations; both populations were 100% positive for both markers (data not shown). Interestingly, although scoring was undertaken on the basis of any level of positive staining being considered a positive event, the Vybrant® DiD-positive cell population consistently demonstrated less intense staining than the Vybrant® DiD-negative population for both markers; this was most evident in the case of vimentin which was seemingly distributed slightly differently in the Vybrant® DiD-positive cell population.
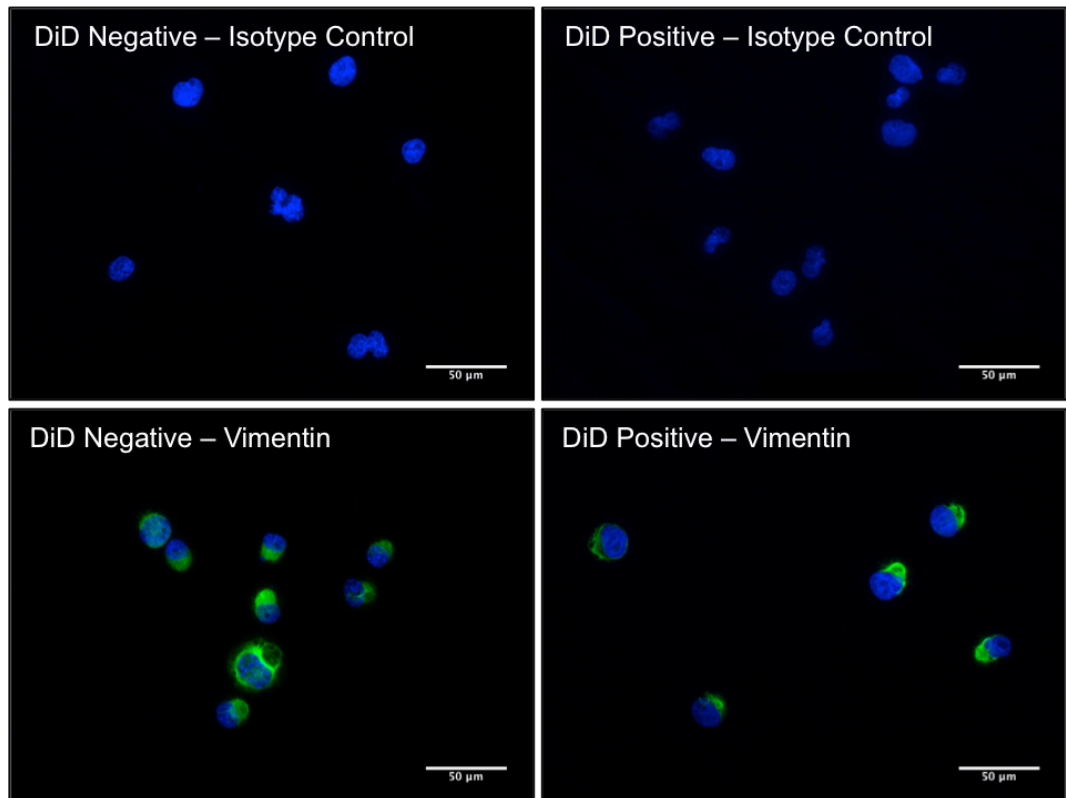
Figure 5.14. Immunofluorescent Staining of EMT Marker Vimentin

The immunofluorescent staining pattern for vimentin (green) is shown along with nuclear counterstaining with DAPI (blue). Specificity of staining in each case is indicated by the absence of staining in the matched isotype control sample. All images were captured using a 20x objective lens (scale bar = 50µm).
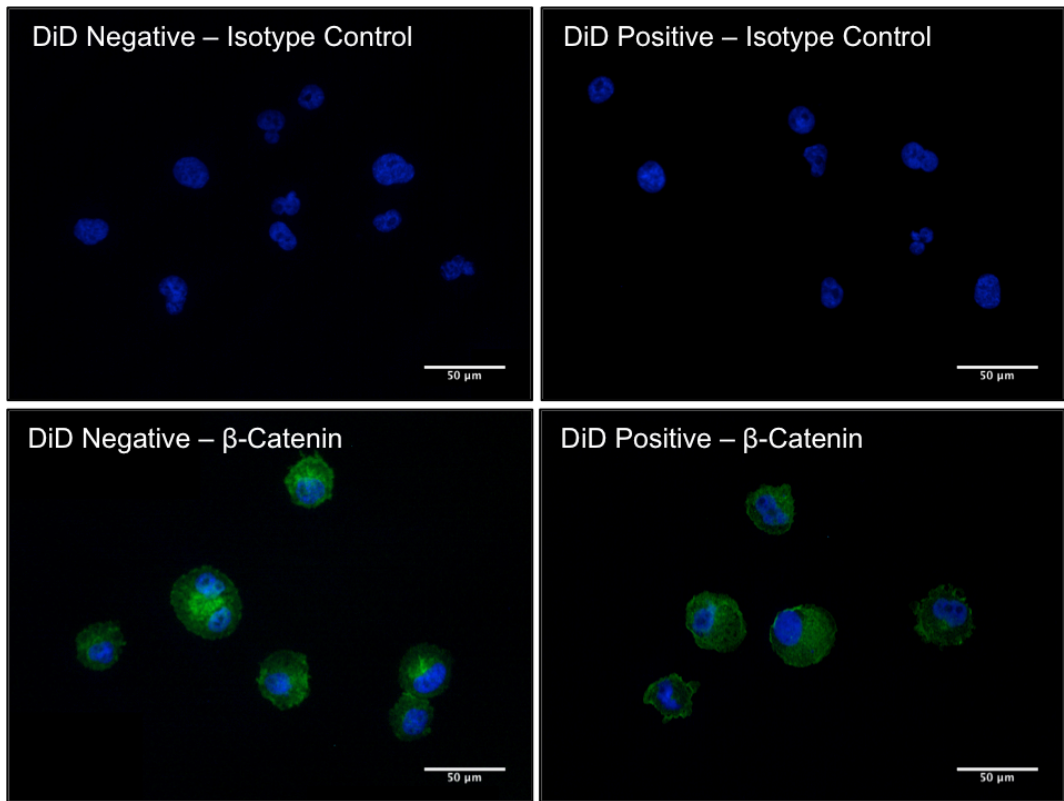
Figure 5.15. Immunofluorescent Staining of EMT Marker β-catenin

The immunofluorescent staining pattern for β-catenin (green) is shown along with nuclear counterstaining with DAPI (blue). Specificity of staining in each case is indicated by the absence of staining in the matched isotype control sample. All images were captured using a 20x objective lens (scale bar = 50μm).

5.5.5. MDA-MB-231 Cells Express Human Embryonal Stem Cell Markers

A number of relatively recent studies have demonstrated that markers expressed by human embryonic stem cells or embryocarcinoma stem cells also demark dedifferentiated and stem-like cell populations in a number of non-germ line cancers, including those of colon, prostate and breast (Battula *et al.*, 2010; Battula *et al.*, 2012; Sivasubramaniyan *et al.*, 2015). In contrast to many of the markers used to identify cell populations associated with enhanced population tumourigenicity following xenotransplantation assays, hES and hEC markers were initially identified in cells of true multipotent nature. Expression of these markers has been associated with enhanced metastatic potential and a worsened prognosis in oropharyngeal, lung, and breast cancer (Gottschling *et al.*, 2013; Hung *et al.*, 2013; Noto *et al.*, 2013).

The antibody panel used by the International Stem Cell Initiative (ISCI) for immunophenotype characterisation of hES and hEC populations was chosen for flow cytometric assays intended to test the hypothesis that slow cycling Vybrant® DiD-retaining cells differentially expresses stem cell markers other than those assayed previously, with the aim of developing a surrogacy marker signature for the slow-cycling phenotype. A second panel of eight fully validated novel antibodies raised to undifferentiated hES and hEC cell lines, originally described by Wright *et al.* (2011), was also used to augment the ability of the ISCI panel to recognise unique sub-states within any extant stem cell compartment within the rapidly- and slowly-dividing MDA-MB-231 cell populations. Immunostaining and cytofluorimetric analyses were carried out according to the methods described previously (**Section 5.4.7.**).

The results, depicted in **Figure 5.16 - Figure 5.18** and summarised in **Table 5.4.**, indicate that the MDA-MB-231 lineage expressed a number of hES and hEC markers but exhibited disparities in expression of five markers that would otherwise demark a true embryonal stem cell population. In terms of differential marker expression, very little difference was detected between rapidly- and slowly-dividing populations. A small but statistically significant reduction in the AG10 marker was observed in the Vybrant® DiD-positive fraction ($P \leq 0.05$) while small, statistically significant increases in expression of BF4 and CC9 antigens ($P \leq 0.01$ and $P \leq 0.05$, respectively) were

detected in the Vybrant® DiD-positive population. The differential expression of these markers between Vybrant® DiD-negative and Vybrant® DiD-positive fractions was deemed to be too small to be of any practical utility; the reduction in AG10 expression was only around 9.5% between Vybrant® DiD-negative and Vybrant® DiD-positive populations, while BF4 and CC9 were increased by 2.77% and 2.02%, respectively, in the Vybrant® DiD-positive sub-population. These findings, while interesting in terms of future study of the MDA-MB-231 cell line and the potential implications of the expression of markers observed here, did not identify a specific marker that could be used in conjunction with CD24 as a surrogate marker profile to denote slow cycling cells.
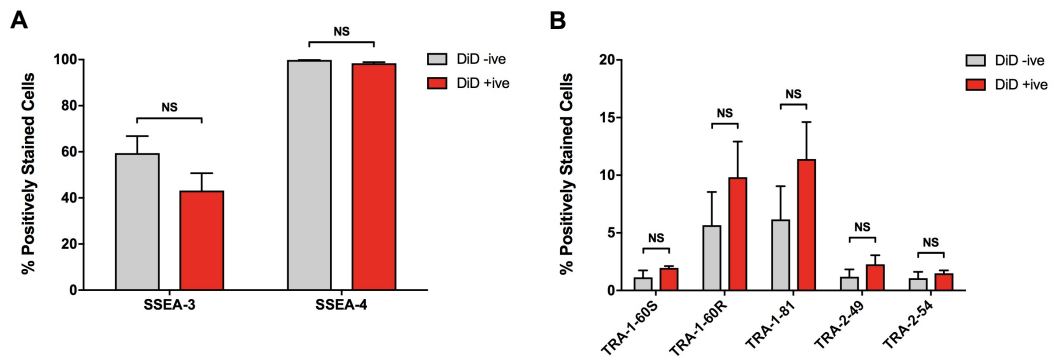
Figure 5.16. Expression of Pre-Differentiation hES and hEC Markers

The percentage expression of pre-differentiation human embryonal and embryocarcinoma stem cell-associated markers in Vybrant® DiD-negative and Vybrant® DiD-positive MDA-MB-231 sub-populations after five consecutive passages post-staining, as determined cytofluorimetrically based on immunofluorescent staining with AlexaFluor®488. **A**: The expression of globoseries glycolipid antigens within Vybrant® DiD-negative and Vybrant® DiD-positive MDA-MB-231 cell fractions is displayed as a percentage of the total cell population with in the respective sub-population. **B**: The expression of high molecular weight keratan sulphate proteoglycan and protein antigens in Vybrant® DiD-negative and Vybrant® DiD-positive MDA-MB-231 cell fractions is displayed as a percentage of the total cell population within the respective sub-population. Data are expressed as the mean average ± SEM for n = 3 biologically independent repeat experiments. Comparison of marker expression between Vybrant® DiD-negative and Vybrant® DiD-positive populations was achieved using two-way ANOVA followed by Sidak's Multiple Comparison Test (NS = not statistically significant or $P > 0.05$).
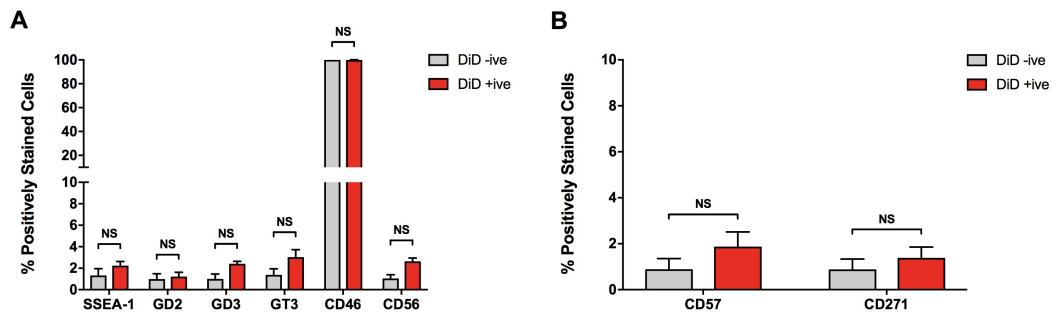
Figure 5.17. Expression of Post-Differentiation hES and hEC Markers

The percentage expression of post-differentiation human embryonal and embryocarcinoma stem cell-associated markers in Vybrant® DiD-negative and Vybrant® DiD-positive MDA-MB-231 sub-populations after five consecutive passages post-staining, as determined cytofluorimetrically based on immunofluorescent staining with AlexaFluor®488. **A**: The expression of miscellaneous antigens commonly expressed by human embryonic stem cells following differentiation within Vybrant® DiD-negative and Vybrant® DiD-positive MDA-MB-231 cell fractions is displayed as a percentage of the total cell population with in the respective sub-population. **B**: The expression of neuronal-, neuroendocrine- and mesenchymal stem cell-associated protein antigens CD57 and CD271 in Vybrant® DiD-negative and Vybrant® DiD-positive MDA-MB-231 cell fractions is displayed as a percentage of the total cell population within the respective sub-population. Data are expressed as the mean average ± SEM for n = 3 biologically independent repeat experiments. Comparison of marker expression between Vybrant® DiD-negative and Vybrant® DiD-positive populations was achieved using two-way ANOVA followed by Sidak's Multiple Comparison Test (NS = not statistically significant or P > 0.05).
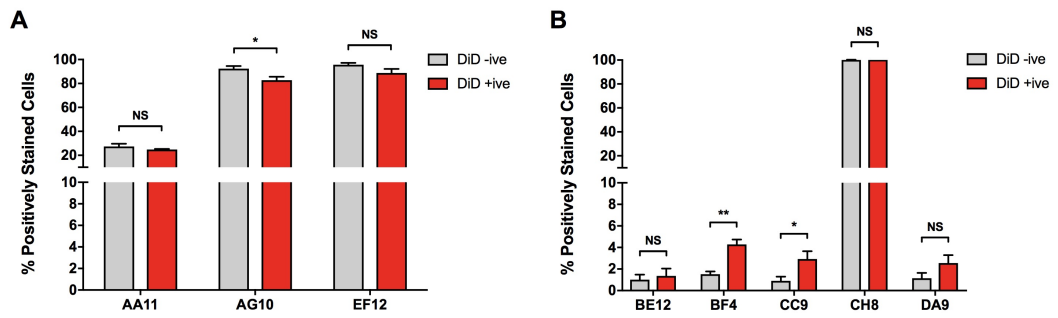
Figure 5.18. Expression of Markers Identified by Novel Anti-Stem Cell Antibodies

The percentage expression of markers identified by novel antibodies raised against human embryonal and embryocarcinoma stem cells (hES) in Vybrant® DiD-negative and Vybrant® DiD-positive MDA-MB-231 sub-populations after five consecutive passages post-staining, as determined cytofluorimetrically based on immunofluorescent staining with AlexaFluor®488. **A**: The expression of glycolipid antigens identified by novel anti-hES antibodies within Vybrant® DiD-negative and Vybrant® DiD-positive MDA-MB-231 cell fractions is displayed as a percentage of the total cell population with in the respective sub-population. **B**: The expression of non-glycolipid antigens identified by novel anti-hES antibodies in Vybrant® DiD-negative and Vybrant® DiD-positive MDA-MB-231 cell fractions is displayed as a percentage of the total cell population within the respective sub-population. Data are expressed as the mean average ± SEM for n = 3 biologically independent repeat experiments. Comparison of marker expression between Vybrant® DiD-negative and Vybrant® DiD-positive populations was achieved using two-way ANOVA followed by Sidak's Multiple Comparison Test (NS = not statistically significant or P > 0.05, * = P ≤ 0.05, ** = P ≤ 0.01).

Table 5.4. Summary of Stem Cell Marker Immunophenotyping

Marker	hES/hEC*	Vybrant® DiD -ive	Vybrant® DiD +ive
SSEA-3	Intermediate	Intermediate	Intermediate
SSEA-4	High	High	High
TRA-1-60S	High	Low	Low
TRA-1-60R	High	Low	Low
TRA-1-81	High	Low	Low
TRA-2-49	Intermediate	Low	Low
TRA-2-54	High	Low	Low
SSEA-1	Low	Low	Low
Ganglioside GD2	Low	Low	Low
Ganglioside GD3	Low	Low	Low
Ganglioside GT 3	Low	Low	Low
CD46	High	High	High
CD56	Low	Low	Low
CD57	Low	Low	Low
CD271	Low	Low	Low

*Immunophenotype of hES and hEC populations taken from Adewumi *et al.* (2007). Expression of a specific marker of 0 - 30% was defined as "low", while an "intermediate" level of expression was defined as being between 30 - 60% and a "high" level of expression being in excess of 60%. Rows shaded in red (TRA-1-60S to TRA-2-54 inclusive) indicate markers at which both Vybrant® DiD-negative and Vybrant® DiD-positive MDA-MB-231 fractions differed from the signature which demarks hES and hEC populations.

5.5.6. Dye-Retaining and Negative Cells Showed Equal Mammosphere Formation

Dontu *et al.* (2003) first reported the ability of putative breast cancer stem cell populations to form tumour-like spheroidal structures, termed mammospheres in the context of breast cancer, under non-adherent conditions. In the years since, the ability of a cancer cell population to self-renew in suspension has frequently been used to assess intrinsic stem cell or progenitor activity *in vitro* (Ponti *et al.*, 2005; Farnie *et al.*, 2007; Fillmore and Kuperwasser, 2008; Grimshaw *et al.*, 2008; Croker *et al.*, 2009). The ability of Vybrant® DiD-negative and Vybrant® DiD-positive MDA-MB-231 populations to form mammospheres was used to determine whether these populations differed in terms of stem cell-like functional capacity. Following their isolation by FACS on day 15 post-staining, the mammosphere forming ability of Vybrant® DiD-negative and Vybrant® DiD-positive MDA-MB-231 fractions was determined according to the methods described in **Section 5.4.8.** Following 168 hours of growth under non-adherent conditions, no statistically significant difference in the mammosphere forming ability of Vybrant® DiD-negative and Vybrant® DiD-positive MDA-MB-231 populations was observed, with Vybrant® DiD-negative cells forming 2.44 ± 0.10% mammospheres on average while Vybrant® DiD-positive cells formed 2.50 ± 0.17% mammospheres on average (**Figure 5.19.**). These results demonstrate that no difference in the intrinsic *in vitro* mammosphere forming potential of the rapidly dividing Vybrant® DiD-negative and relatively quiescent Vybrant® DiD-positive MDA-MB-231 populations exists, reflecting the apparent overall lack of difference in stemness between these two fractions previously identified during marker expression analyses.
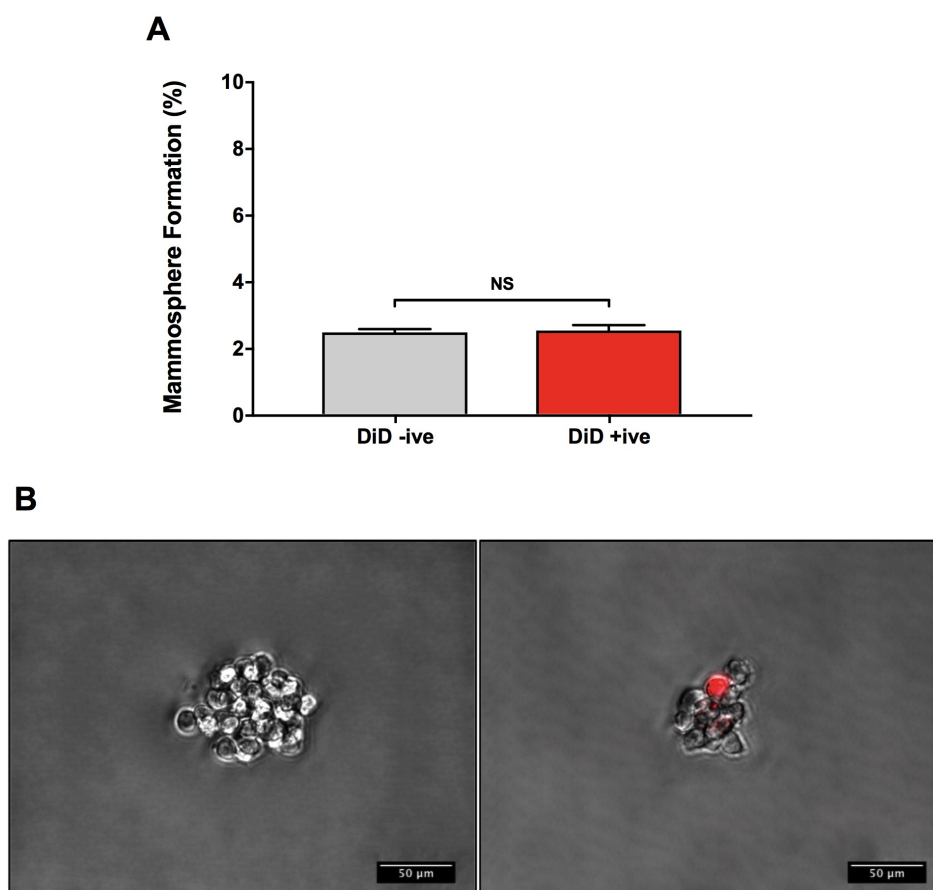
Figure 5.19. Formation of Mammospheres by Dye-Retaining and Negative Cells

A: The number of non-adherent mammospheres formed by Vybrant® DiD-negative and Vybrant® DiD-positive MDA-MB-231 cells isolated at five passages post-staining. Data are expressed as the mean average ± SEM for n = 3 biologically independent repeat experiments and were compared using a two-tailed unpaired *t*-test (NS = not statistically significant or P > 0.05). **B**: Representative images of mammospheres formed by Vybrant® DiD-negative (left) and Vybrant® DiD-positive (right) MDA-MB-231 cells at 168 hours post-isolation; a single intensely fluorescent Vybrant® DiD-positive cell (red) remains evident amongst other less intensely stained and seemingly dye-negative cells having arisen from the same parental cell. All images were captured using a 10x objective lens (scale bar = 50μm).

5.5.7. Dye Retaining Cells Divide Asymmetrically

An interesting observation made during mammosphere formation assays was that mammospheres formed by cells that were initially Vybrant® DiD-positive upon isolation contained single dye-retaining cells but were otherwise dye-negative (**Figure 5.19.**). This observation was seen to indicate that some of the slow-cycling cell population were able to divide asymmetrically, a functional property that is associated with stem cell populations. In order to directly assess whether this was the case, time-course tracking of cell division was undertaken as described in **Section 5.4.9.** In concurrence with the initial observation, some initially dye-retaining cells seeded at clonogenic density were stimulated to divide following isolation from the bulk cell population but did so in an asymmetric manner, with the parental cell that was initially seeded undergoing mitotic division to give rise to a daughter cell which went on to retaining its dye label and another daughter cell which appeared to give rise to non-dye-retaining cells (**Figure 5.20.**).

| 24 Hours Post-FACS | 72 Hours Post-FACS | 120 Hours Post-FACS |
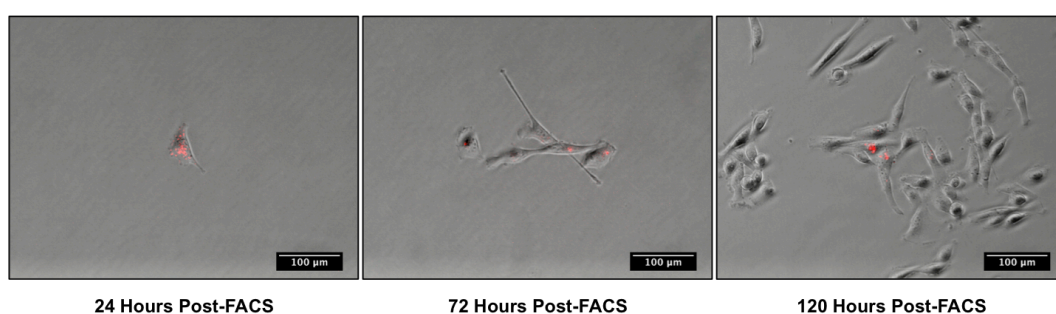
Figure 5.20. Time-Course of Dye-Retaining MDA-MB-231 Cell Division

Representative images depicting the dynamics of Vybrant® DiD-positive MDA-MB-231 cell division for up to 120 hours post-isolation from samples continuously cultured for five consecutive passages post-staining. Distribution of the Vybrant® DiD dye between daughter cells formed appears to be asymmetric upon stimulation of cell division when removed from a mixed population; a single Vybrant® DiD-positive cell gives rise to dye-negative progeny while seemingly retaining the Vybrant® DiD fluorescent label. All images were captured using a 20x objective lens (scale bar = 100µm).

5.6. Discussion

A number of studies have reported a significant expansion of the supposed cancer stem cell compartment following chemotherapy (Naumov *et al.*, 2003; Yu *et al.*, 2007; Dembinski and Krauss, 2009; Gao *et al.*, 2010; Liu *et al.*, 2010). Such enrichment would require either an enormous expansion of the cancer stem cell population or effective reduction of the bulk cell mass. A similar pattern of preferential proliferation or cytotoxicity would also be required to account for the significant increase in the relative proportion of slow-cycling, fluorescent dye-retaining cells surviving following chemotherapy reported here. Calculation of the absolute number of Vybrant® DiD-positive cells present in MDA-MB-231 cultures at the time of seeding and following exposure to a high concentration (IC_{95}) of chemotherapeutic agents demonstrated an increase in the absolute label-retaining cell number from ~1600 to ~2800 across all treatment groups. In the MCF-7 cell line this expansion of the dye-retaining population was from ~1000 cells at the time of seeding to ~3600 cells at the end of the assay period. These increases in dye-retaining cell numbers almost certainly occurred due to mitotic division generating partially labelled daughter cells. However, such expansion alone could not possibly account for the significantly increased relative proportion of label-retaining cells measured within each of the drug-treated cultures compared to untreated cultures. These data not only demonstrate that slow-cycling (label-retaining) cells continued to proliferate when exposed to standard chemotherapeutic agents but that the rapidly dividing (non-label-retaining) population were significantly more susceptible to drug-induced cell death than their slow-cycling counterparts, resulting in a net enrichment for label-retaining cells. These conclusions mirror those drawn from *in vitro* studies reported in the closely-related work of Moore *et al.* (2012), who also demonstrated effective enrichment of a slow-cycling fluorescent label-retaining population *in vivo* using clinically relevant doses of oxaliplatin and fluorouracil to treat tumours derived from the HCT116 human colon cancer cell line.

While the intrinsic ability of cancer cell populations to survive anti-neoplastic chemotherapy is clinically important, cells that are able to initiate tumoural relapse or disease recurrence must also be capable of subsequent proliferation. It was therefore deemed important to establish that the Vybrant® DiD-retaining population were not

avoiding the cytotoxic effects of doxorubicin or paclitaxel by entering a permanently non-dividing state, or that the onset of the cytotoxicity exerted by these drugs was simply delayed due to the slow cycling nature of the label-retaining population. Through measuring incorporation of BrdU into cellular DNA, Moore *et al.* (2012) were able to show that a sub-population of oxaliplatin and fluorouracil-treated label retaining cells could actively proliferate both *in vitro* and *in* vivo shortly after halting treatment. This capability was more directly demonstrated here through the formation of new clonal populations directly from a fraction of cells in the surviving dye-retaining sub-population post-cessation of exposure to chemotherapeutic drugs. When taken together, these results indicate that slow-cycling cells are not only able to survive, but are capable of becoming re-activated after withdrawal of chemotherapy to initiate either local tumoural relapse or formation of a secondary metastatic lesion. However, the data described in this chapter that support this conclusion were solely obtained from *in vitro* models and therefore this hypothesis will require direct testing in the *in vivo* setting in future.

Given the slow-cycling and therapy-resistant nature of the Vybrant® DiD-retaining cell fraction, an associated between slow-cycling cells and the purported cancer stem cell population appears entirely plausible. Indeed, a number of studies across various cancer types have transitively linked quiescence to the cancer stem cell phenotype through retrospective functional validation of putative cancer stem cell populations isolated using cell surface markers (Gao *et al.*, 2010; Roesch *et al.*, 2010). In breast cancer, the seminal study of Al-Hajj *et al.* (2003) identified the CD44^{+}CD24^{-/low} surface marker signature describing the putative CSC population that was associated with enhanced tumourigenic potential following murine xenotransplantation. Fillmore and Kuperwasser (2008) subsequently used this signature to identify stem-like cells in multiple established breast cancer cell lines that were found to be up to 90% label retaining. In contrast, a number of studies in which prospective identification of a quiescent cell population was undertaken through label retention assays demonstrated only partial overlap with cell surface marker signatures associated with the supposed cancer-type-specific stem cell population (Dembinski and Krauss, 2009; Wang *et al.*, 2015a). The findings reported here echo the outcome of these studies; only a modest increase in ALDH activity differentiated the Vybrant® DiD-negative and

Vybrant® DiD-retaining populations, and the latter did not appear to be enriched for the CD44$^+$CD24$^{-/low}$ putative breast CSC marker signature. Interestingly however, the Vybrant® DiD-retaining population in both MCF-7 and MDA-MB-231 cell lines did illustrate a significant enrichment with cells expressing the CD44$^+$CD24$^+$ phenotype (2-fold and 53-fold, respectively). The functional implications of the enrichment for ALDH and CD44$^+$CD24$^+$ cells in the dye-retaining population remain to be established.

As previously discussed, the utility and rigid employment of cell surface marker profiles for definition of cancer stem cell populations through correlative association with tumourigenic potential is not without considerable limitations. Indeed, the concept that exclusive tumour cell sub-sets possess increased nascent capacity for tumour propagation is still evolving. In certain cancer stem cell models, such as those reported in melanoma, the vast majority if not all malignant cells are tumourigenic, while in other cancer types, such as colorectal cancer, purported surface marker signatures have been shown to lack specificity, with marker-positive and negative populations exhibiting tumourigenicity (Ricci-Vitiani *et al.*, 2007; Quintana *et al.*, 2008; Shmelkov *et al.*, 2008). One very notable example of this situation in breast cancer is that of the MDA-MB-231 cell line; in excess of 99% of the total cell population has been reported to express the CD44$^+$CD24$^{-/low}$ marker signature that is supposed to describe breast CSC, yet only a minority fraction of the cell population possesses the ability to initiate population re-growth (Li *et al.*, 2017). The results reported in this chapter reaffirm this lack of specificity; both dye-negative (predominantly CD44$^+$CD24$^{-/low}$) and dye-retaining (predominantly CD44$^+$CD24$^+$) sub-populations of the MDA-MB-231 lineage possessed comparable intrinsic potential to reinitiate tumour growth as estimated by *in vitro* mammosphere forming efficiency assays. Indeed, an often overlooked finding of the landmark study undertaken by Al-Hajj *et al.* (2003) was that CD44$^+$CD24$^+$ breast cancer populations also remained viable and exhibited tumourigenicity in xenotransplantation studies but seemingly possessed reduced proliferative capacity compared to the CD44$^+$CD24$^{-/low}$ cells that were taken to represent the stem-like fraction. Based on these findings it seems plausible that the CD44$^+$CD24$^{-/low}$ signature was implicitly linked to enhanced tumourigenicity simply due to the intrinsic rapid expansion of this population coupled with an insufficient follow up period in mice injected with CD44$^+$CD24$^+$ cells, leading to the conclusion that the former exclusively possessed

tumourigenic potential. In fact, a number of other studies have indicated that stem cell activity in breast cancer is not exclusively limited to the CD44$^+$CD24$^{-/low}$ phenotype but that CD44$^+$CD24$^+$ can be equally tumourigenic in mouse xenograft models, most notably illustrated by Meyer *et al.* (2010) in oestrogen receptor-negative disease. Whether dye-retaining and non-retaining MDA-MB-231 fractions are more dormancy competent but remain tumourigenic *in vivo* remains to be established.

Given the increasing recognition that purported CSC markers are limited in their specificity, an increasing effort has been made to attempt to identify novel marker signatures that more accurately identify tumourigenic, metastasis-initiating or stem-like sub-populations. Amongst these, a number of cell surface antigens that have been used to characterise human embryonic stem cells have been investigated for their expression in various cancer types (Nohara *et al.*, 1998; Sivasubramaniyan *et al.*, 2015). In this chapter, the expression of the standard ISCI panel of human embryonic stem cell markers by the Vybrant® DiD-negative and Vybrant® DiD-retaining populations was investigated. While the rapidly- and slowly-dividing MDA-MB-231 sub-populations did not differentially express any of the standard ISCI markers, the overall pattern of expression in the MDA-MB-231 cell line indicated an overall stem-like phenotype. The ISCI have previously demonstrated that human embryonic stem cells can primarily be defined by their expression of the glycosphingolipid series of cell surface antigens synthesised from the common lactosyl ceramide precursor (Adewumi *et al.*, 2007). Of these markers, the globoseries antigens (SSEA-3 and SSEA-4) are typically found to be highly expressed in human embryonic stem cells pre-differentiation, while the ganglioseries (ganglioside-GD2, -GD3 and -GT3) and lactoseries (SSEA-1) antigens are typically down-regulated (Adewumi *et al.*, 2007; Wright and Andrews, 2009). Hence, the expression pattern of glycosphingolipids and post-differentiation antigens observed in the MDA-MB-231 cell line that is summarised in **Table 5.4.** would typically be considered indicative of the undifferentiated state. This conclusion is further supported by the expression pattern of a number the novel anti-stem cell markers which have been structurally related to certain glycosphingolipid antigens; AA11 appears to be structurally related to SSEA-3 while AG10 and EF12 appear analogous to SSEA-4 and the expression pattern of these antigens observed in the MDA-MB-231 cell line as reported here mirrors that of the globoseries antigens (Wright *et al.*, 2011).

Interestingly, the MDA-MB-231 cell line did differ in their expression of the high molecular weight keratan sulphate antigens (TRA-1-60 isoforms and TRA-1-81) and the two tissue-non-specific alkaline phosphatase antigens (TRA-2-49 and TRA-2-54) that are usually expressed at intermediate to high levels in undifferentiated human embryonic stem cells. The novel anti-stem cell antibody CC9 that has previously been structurally related to TRA-1-60 and TRA-1-81 by Wright *et al.* (2011) was also expressed by MDA-MB-231 cells at minimal levels, somewhat validating these observations. The absence of these antigens might relate to the well-supported hypothesis that cells of the MDA-MB-231 lineage originated in differentiated breast tissue and subsequently underwent spontaneous dedifferentiation, thereby having initially lost the embryonic phenotype during development and only having partially recapitulated this during acquisition of their malignant status. The lack of expression of cell surface alkaline-phosphatase might also relate to their dysregulation and loss during malignancy, as low expression levels have been reported in both human embyrocarcinoma cell lines and cell lines of other cancer types previously (Wright and Andrews, 2009; Wright *et al.*, 2011). The exact basis for the expression pattern of these markers does, however, remain to be established. Indeed, despite a number of studies having investigated the deployment of a number of the human embryonic stem cell markers investigated here in various cancer types, their exact biological function in malignancy and their relationship to stemness in cancer cell sub-populations remains undetermined. Given the overall lack of differential expression of the human embryonic stem cell markers by the Vybrant® DiD-negative and Vybrant® DiD-retaining MDA-MB-231 sub-populations, a different approach such as whole-transcriptomic sequencing or array-based RT-qPCR profiling will be required in future in order to identify a robust quiescence-associated marker signature to act as a surrogate for dye-retention capability.

5.7. Conclusions

The slow-cycling population within both MCF-7 and MDA-MB-231 cell lines identified by long-term fluorescent dye-retention were more resistant to high concentrations of anti-neoplastic drugs routinely used to treat breast cancer in the clinical setting than their rapidly-dividing counterparts. This enhanced drug resistance was associated with up-regulated aldehyde dehydrogenase activity within dye-retaining cells. Whether other established drug-resistance mechanisms are associated with mitotic quiescence remains to be explored. Colonies formed by MDA-MB-231 cells post-cessation of anti-neoplastic drug exposure were exclusively formed by sub-clones within the dye-retaining cell population. The identification of a slow-cycling and inherently therapy resistant cellular sub-set capable of leading to tumour recurrence such as this is both biologically and clinically significant. Breast cancer stem cell markers analysis showed an association of dye-retaining cells within MCF-7 and MDA-MB-231 cell lines with a $CD44^+CD24^+$ phenotype and not the $CD44^+CD24^{-/low}$ profile that has typically been associated with enhanced tumourigenicity in putative breast stem cell populations elsewhere. The functional significance of these findings and whether or not the $CD44^+CD24^+$ signature demarks a transitory epithelial-mesenchymal stem-like state remains to be fully elucidated.

Chapter 6

Discussion, Conclusions and Further Work

6.1. Discussion

Metastatic disease remains the major cause of death in patients diagnosed with advanced breast cancer. Efforts to effectively treat metastasis have been severely hampered by the entry of disseminated tumour cells into a reversible state of mitotic arrest known as dormancy that enables them to evade chemotherapy. Dormant tumour cells often persist within distal tissues for many years or even decades before re-emerging to form lethal overt lesions. Targeting the dormant disseminated tumour cell population, either to maintain dormancy or effect killing, is believed to represent the greatest potential opportunity for therapeutic intervention to improve patient prognosis. However, the development of effective treatments has been severely impeded by a poor understanding of the metastasis-initiating cell population and the biological processes that maintain their dormant phenotype.

An emerging consensus, supported by a growing body of experimental evidence, is that cancer stem cells (CSCs) are the metastasis-initiating population in breast cancer (Luo *et al.*, 2015). However, the predominant means of isolating CSCs using protein marker signatures is increasingly recognised as being unreliable due to cellular plasticity and the poorly defined functional roles of many of these marker proteins. The requirement exists, therefore, for a reliable and functionally informed system enabling the isolation and characterisation of putative metastasis-initiating cancer stem cells. Breast CSCs, like their non-malignant counterparts, are presumed to be mitotically quiescent (Gerdes *et al.*, 2014). Relatively recently, pulse-chase techniques for assessment of stem cells based on their inherent quiescent nature has undergone something of a renaissance due to the advent of lipophilic tracer dyes. The use of fluorescent dyes for monitoring cellular division kinetics offers the distinctive advantage over traditional label-retention methods (e.g. BrdU incorporation) of being able to isolate and further characterise live cell populations (Luo *et al.*, 2015). While a number of studies in other cancer types have demonstrated the prospective identification of CSCs or stem-like populations using this approach, its potential utility in breast cancer has, until now, remained virtually unexplored. The primary aim of this project was to explore the potential utility of lipophilic dye-retention for isolation of

mitotically quiescent breast cancer cells and determine whether these display features of the putative metastasis-initiating cancer stem cell population in breast cancer.

The initial aim of the work presented in **Chapter 3** of this thesis was to determine the suitability of select fluorescent lipophilic tracer dyes for the application of detecting mitotically quiescent breast cancer cells *in vitro*. Fluorescent dyes available for label retention applications may be sub-divided into two predominant groups: cytoplasmic dyes (e.g. Calcein derivatives and CFSE) or membrane-bound dyes (e.g. PKH dye series or Vybrant® dye series). The cytoplasmic dye CFSE is considered a gold standard fluorescent dye for measuring cell proliferation and has been widely used for study of proliferation kinetics and cellular lineage tracing (Parish, 1999; Moore *et al.*, 2012; Hu *et al.*, 2017). However, since their binding to cytoplasmic proteins is able to inhibit the function of cellular enzymes, cytoplasmic dyes can exhibit high levels of cytotoxicity to cells and reduce cellular proliferation and migration (Parish, 1999; Quah *et al.*, 2007; Last'ovicka *et al.*, 2009; Yumoto *et al.*, 2014). In contrast, membrane-bound dyes are generally found to be less toxic (Honig and Hume, 1986; Honig and Hume, 1989). Indeed, the results described in **Chapter 3** and in the closely related works of Yumoto *et al.* (2014), Docherty (2014) and Wang *et al.* (2015b) demonstrate that even relatively high concentrations (2µM - 5µM) of such dyes (e.g. Vybrant® DiD) have no significant effect on cell proliferation, clonogenicity, migration or apoptosis, and hence would be well suited to use in pulse-chase applications for detection of mitotically quiescent breast cancer cells. Although PKH26 has perhaps been the most widely used membrane-bound fluorescent dye for assessment of cell proliferation, it is expensive and relatively complicated to use for labelling, requiring an isosmotic mannitol-based loading medium. By comparison, the equivalent Vybrant® dye, DiD, is inexpensive and can be added directly to culture medium, thereby making handling less technically involved and permitting uniform labelling of cells either in suspension or when growing as adherent monolayers (Honig and Hume, 1986; Honig and Hume, 1989; Yumoto *et al.*, 2014).

Historically, the label-retention technique has been predominantly used in conjunction with other characterisation assays to validate putative stem cell phenotypes (Luo *et al.*, 2015). One of the main criticisms limiting the use of this approach as a primary means of identifying prospective stem cell populations has been that its relative simplicity requires further validation and phenotypic characterisation to be carried out. However, one distinct advantage of this technique is that the progressive dilution or retention of dye is reliant on a functional cellular phenotype and is independent of the expression of protein markers with poorly understood functional roles in mitotic dynamics (Moore *et al.*, 2012; Luo *et al.*, 2015). Indeed, fluorescent label retention has been used to great effect in identifying normal mammary stem cells from patient-derived tissue isolates, identifying stem cell-associated gene signatures that predict clinical outcome in breast cancer and elucidating molecular mechanisms that underpin stem cell function (Pece *et al.*, 2010; Tosoni *et al.*, 2012). The utility of this technique is not limited to application in patient derived tissue. In fact, stem-like label-retaining populations have been identified in multiple established cancer cell lines that were once thought to be largely homogenous and devoid of stem cells (Fillmore and Kuperwasser, 2008; Moore *et al.*, 2012; Akrap *et al.*, 2016). These findings strongly suggest that label retention techniques can be simple yet powerful tools for studying quiescent and stem-like cell populations, even when using commercially available cell lines, as long as the findings are evaluated critically, data interpreted within the context of the experimental parameters, and results confirmed under biologically relevant conditions.

In the early experimental work described in **Chapter 3**, lipophilic dye-retention assays using Vybrant® DiD revealed the presence of a latent label-retaining sub-population within human breast cancer cell lines representing each of the five distinct molecular sub-types originally described by Perou *et al.* (2000) and Sorlie *et al.* (2001). Subsequent cytofluorimetric analysis of the intensity of Vybrant® dye staining in label-retaining cells compared with that of the freshly stained parental culture indicated that some dye loss had occurred during retention assays. Given that dye retention assays undertaken following induction of growth arrest using mitomycin C had previously demonstrated that mitotic activity was the primary determinant of dye loss (**Figure 3.17.**), these findings suggested that label-retaining cells were relatively slowly cycling.

Cell cycle distribution profiling undertaken here confirmed this observation and revealed that label-retaining cells tended to collect in the G_2/M-phase relative to the bulk cell population. Analysis of immunostaining for the proliferation marker Ki67 showed that the label-retaining population was enriched for cells in the G_0-phase of the cell cycle. These results closely mirror those reported elsewhere. Using both *in vitro* and *in vivo* models, Moore *et al.* (2012) showed that chemoresistant, label-retaining MDA-MB-231 human breast cancer cells had a propensity to collect in the G_2/M-phase of the cell cycle. Similarly, the findings reported by Docherty (2014) and Wang *et al.* (2015b) together demonstrated that label-retaining bone-metastatic prostate cancer cells identified within multiple prostate cancer cell lines were also chemoresistant, collected in the G_2/M-phase of the cell cycle and displayed significantly lower Ki67 expression than their non-label-retaining counterparts. When taken together with these reports, the work presented in **Chapter 3** of this thesis suggests that the label-retaining cells identified within human breast cancer cell lines represent a population composed of both absolutely quiescent and infrequently dividing, relatively quiescent cells.

Mitotically quiescent cell sub-populations have been identified in multiple non-malignant human epithelial tissues, including the skin, colon and breast, suggesting that they serve an important functional role in tissue longevity and that their presence in cancer might be a residual characteristic of the tissues of origin (Lyle *et al.*, 1998; Potten *et al.*, 2003; Shackleton *et al.*, 2006). While absolute quiescence or infrequent division are not definitive for adult stem cell populations, published reports do suggest that quiescence plays a critical role in maintenance of stem cell pools by preventing exhaustion of proliferative capacity, inhibiting differentiation, and limiting the accumulation of mutations during frequent rounds of DNA synthesis (Coller *et al.*, 2006; Sang *et al.*, 2008; Viatour *et al.*, 2008). A number of studies in cancer have similarly associated quiescence or a slow cycling nature with preservation of putative cancer stem cell populations through conferring a propensity to resist apoptosis and chemotherapy (Harper *et al.*, 2010; Chikamatsu *et al.*, 2012; Moore *et al.*, 2012). In line with findings reported by Harper *et al.* (2010) and Moore *et al.* (2012), it is plausible that the growth arrest in, or extension of, the G_2/M-phase demonstrated in **Chapter 1** contributed significantly to the enhanced survival and enrichment of label-retaining

cells in cultures treated with anti-neoplastic drugs described in **Chapter 5**. Growth arrest or slowed cell cycle transition would effectively increase the time for drug efflux, drug metabolism or repair of drug-induced cellular stress and thereby enable evasion of pro-apoptotic signals in the relatively quiescent Vybrant® DiD-retaining cell fraction. Indeed, while reduced mitotic activity is likely to contribute to the survival of label-retaining cells in response to chemotherapy, it may not be the sole means by which *de novo* drug resistance occurs and probably works in synergy with other mechanisms to increase their survival. The expression of anti-apoptotic proteins, such as c-FLIP and Bcl-2 family members, are frequently observed in quiescent normal and cancer stem cell populations and have been shown to contribute to enhanced cell survival following chemotherapy (Turton *et al.*, 2001). Enhanced DNA damage repair pathway activation, up-regulation of xenobiotic drug pumps, and increased enzymatic drug metabolism (particularly by ALDH) has also been reported in quiescent stem cell populations (Eyler and Rich, 2008; Cree and Charlton, 2017). Based on these reports, ALDH activity was assayed in quiescent and rapidly-dividing breast cancer cell populations here and was found to be significantly up-regulated within the quiescent, label-retaining fraction of both oestrogen receptor-positive and oestrogen receptor-negative cell lines (**Figure 5.13.**). Although the contribution of quiescence to these established drug-resistance mechanisms remains to be established, it is likely that a reduced proliferative rate only augments their effectiveness. It will be important for future experiments to determine whether other drug-resistance mechanisms are enriched within label-retaining breast cancer cells and whether their inhibition, either alone or in combination, is able to prevent the survival and subsequent outgrowth of drug-resistant sub-clones.

Seminal studies by Ginestier *et al.* (2007) and Charafe-Jauffret *et al.* (2009) have showed that increased ALDH expression demarks stem cells in both normal and malignant breast tissue. High ALDH expression has since been widely employed as a marker for isolation of breast cancer stem cells (Morimoto *et al.*, 2009; Tanei *et al.*, 2009; Park *et al.*, 2010; Charafe-Jauffret *et al.*, 2013). Given that ALDH activity was found to be up-regulated in dye-retaining populations (**Figure 5.13.**), it was hypothesised that other stemness markers might also be differentially expressed by this population. In both the MCF-7 and MDA-MB-231 cell lines, quiescence as denoted by label retention status was associated with a significant enrichment for CD44$^+$CD24$^+$

cells; in the epithelial-like MCF-7 cell line this was associated with a gain in the mesenchymal marker CD44, whereas the mesenchymal-like MDA-MB-231 cell displayed dual positivity due to a gain of the epithelial marker CD24. Although the functional implications of these findings remain to be fully elucidated, dual positivity for these markers (both independent of and in conjunction with ALDH positivity) has recently been associated with stemness, enhanced chemotherapeutic resistance and worsened patient prognosis, particularly in triple-negative breast cancer (Meyer *et al.*, 2010; Qiu *et al.*, 2016; Deng *et al.*, 2017).

A study by Bhat-Nakshatri *et al.* (2010) reported that the generation of either the CD44$^+$CD24$^{-/low}$ or CD44$^+$CD24$^+$ phenotype is dependent on expression of particular EMT-associated gene signatures. Given the apparent re-acquisition of the epithelial marker CD24 in the inherently drug-resistant, dye-retaining cells of the mesenchymal-like MDA-MB-231 lineage, and the emerging association between a transitory epithelial-mesenchymal stem-like phenotype and enhanced chemoresistance (reviewed by Fabregat *et al.*, 2016), it was hypothesised that dye-retention status in MDA-MB-231 cells would be associated with increased epithelial marker expression or, conversely, decreased expression of mesenchymal markers. Although the preliminary assays of EMT marker expression status (**Figure 5.14.** and **Figure 5.15**) did suggest that this might be the case, difficulties in discerning and quantifying the relative degree of marker expression between dye-retaining and non-dye-retaining cells, and the limited number of markers assayed means that a more robust experimental approach across additional cell lines will be required in future to definitively establish how EMT marker expression relates to the quiescent phenotype and how this varies by the molecular sub-type of breast cancer involved. The current working hypothesis regarding the relationship between these characteristics is outlined in **Figure 6.1.**, which highlights how the quiescent breast cancer population identified by label-retention might represent a epithelial-mesenchymal stem cell compartment associated with significant chemoresistance.
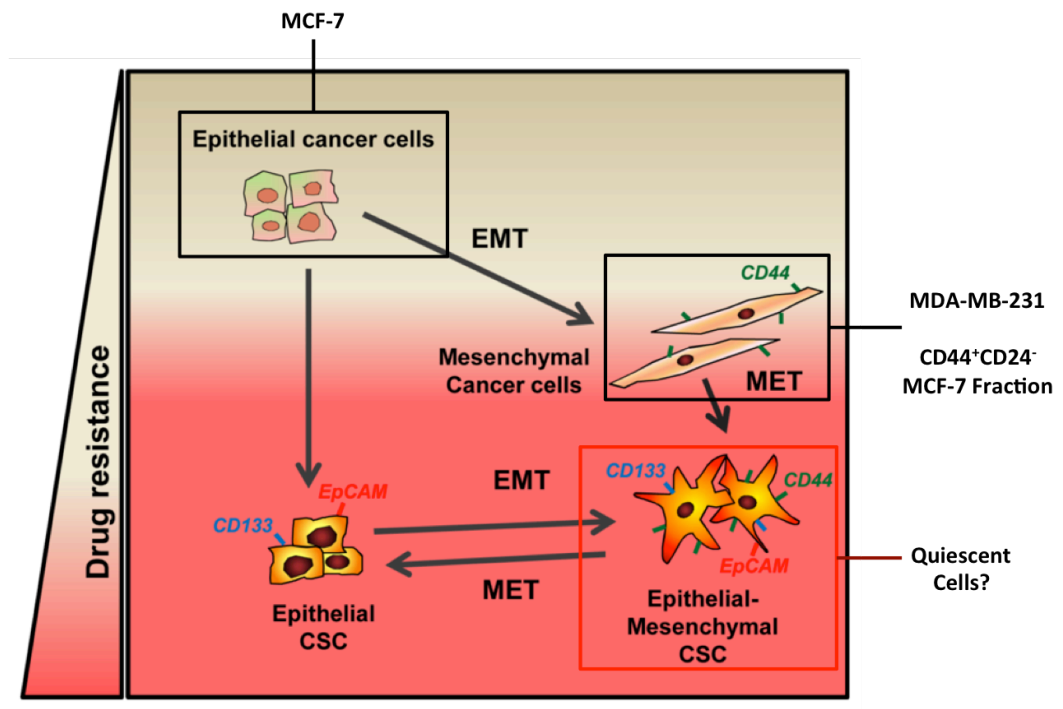
Figure 6.1. Crossroads between EMT, Stemness, Quiescence and Chemoresistance

The combined evidence from published experimental models and data presented herein suggests the conceptual model depicted above, illustrating the interplay between EMT, stemness, chemoresistance and mitotic quiescence. The induction of EMT in epithelial cancer cells, such as the MCF-7 cell line, results in acquisition of a mesenchymal-like phenotype that has been described by the CD44^{+}CD24^{-/low} marker signature. This signature is widely reported to characterise the MDA-MB-231 cell line and the supposed cancer stem cell compartment within MCF-7 cultures. Partial reversion of mesenchymal-like cells to a more epithelial-like phenotype, induced by factors such as hypoxia and TGF-β signalling, results in a transitory epithelial-mesenchymal phenotype associated with enhanced chemotherapeutic resistance. Our current working hypothesis proposes that this state characterises the quiescent, label-retaining cell sub-population identified in breast cancer cell lines. This transitory phenotype, denoted by expression of both epithelial and mesenchymal stemness markers, might give rise to a sub-set of cells that are more epithelial-like and competent to take up long-term residency at post-metastatic sites. Image adapted from Fabregat, I., Malfettone, A. & Soukupova, J. (2016). New Insights into the Crossroads between EMT and Stemness in the Context of Cancer. *J Clin Med*, 5. with permission from Multidisciplinary Digital Publishing Institute (MDPI).

A recent mechanistic study by Deng *et al.* (2017) suggests that the acquisition of CD24 within the label-retaining quiescent MDA-MB-231 sub-population demonstrated in **Chapter 5** could be linked to quiescence-associated signalling programmes described previously. In their study, Deng *et al.* (2017) report that expression of CD24 in triple-negative breast cancer cells is regulated by Bcl-2 and TGF-βRI signalling via ATM-NDRG2 pathways. Interestingly, the TGF-β signalling axis in particular has previously been implicated in acquisition of a chemoresistant, partial epithelial-mesenchymal phenotype and in tumour cell quiescence at both primary and post-metastatic sites. Fernando *et al.* (2015) demonstrated that mesenchymal-like hepatocellular carcinoma cells (HCCs) exhibit autocrine over-activation of the TGF-β pathway and that treating epithelial-like HCCs with exogenous TGF-β resulted in concomitant expression of both epithelial and mesenchymal stem genes and a transitory epithelial-mesenchymal phenotype. Previous studies in head and neck and breast carcinoma by Bragado *et al.* (2013) and Marlow *et al.* (2013), respectively, demonstrated that TGF-β2 signalling via TGF-βRIII and TGF-βRI was able to strongly activate p38 and diminish ERK activation. Altering the p38:ERK signalling ratio in this manner resulted in the induction of p27 and the dormancy-associated transcription factors DEC2 and NR2F1, ultimately leading to entry into a state of mitotic quiescence. Whether these pathways are related to the quiescent phenotype identified by fluorescent dye retention and in the apparent enrichment of CD24 in the quiescent MDA-MB-231 population remains to be elucidated and will be the topic of future studies. However, this hypothesis is supported by the indication that HIF-1α levels were increased within the dye-retaining breast cancer cells depicted in **Figure 4.7.**, comparable findings having previously been reported in dye-retaining prostate cancer cells by Docherty (2014), and a recent study by Fluegen *et al.* (2017) demonstrating that HIF signalling drives the NR2F1^{hi}/DEC2^{hi}/p27^{hi}/TGF-β2^{hi} quiescence-associated gene signature. Further work will first be required to confirm that HIF-1α signalling is differentially activated in association with the quiescent phenotype demarked by fluorescent dye retention, and to determine whether this varies according to the molecular sub-type of breast cancer involved.

While the potential utility of lipophilic dye-retention model in the study of intratumoural mitotic heterogeneity, quiescence and *de novo* drug resistance has been demonstrated in this thesis it is not without limitations. As discussed in **Chapter 4**, the incompatibility of this assay system with experiments designed to identify conditions that generate quiescent sub-clones is a by-product of its reliance on the mitotic activity of the non-quiescent bulk population and the inevitable slowing of culture growth that occurs upon application of metabolic stress. Similarly, the stimulation of overt outgrowth of initially quiescent sub-clones following their replacement into culture post-isolation is not necessarily conducive to determining their differential ability to survive nutritional or cytotoxic stress compared to non-quiescent cells. These limitations could be subverted by employing a surrogate marker profile demarking the quiescent phenotype, thereby removing the reliance of identifying quiescent cells on fluorescent dye-based lineage tracing. The markers currently associated with cellular quiescence, namely the NR2F1^{hi}/DEC2^{hi}/p27^{hi}/TGF-β2^{hi} signature recently described by Linde *et al.* (2016), are intracellular molecules and therefore cannot be used to isolate live cells. While the CD44$^+$CD24$^+$ signature might demark chemoresistant and potentially metastasis-initiating initiating cells in breast cancer, it is enriched within, but not exclusive to, the quiescent breast cancer sub-population. Identifying extracellular markers that more accurately distinguish the quiescent phenotype should therefore be the focus of future work in order to facilitate experimental procedures that require the isolation of live cells for functional studies, both *in vitro* and *in vivo*. In addition, pharmacologically targetable pathways for the removal of quiescent disseminated tumour cells from secondary tissues still remain to be identified. Extending future work beyond identification of a robust surrogate marker profile for quiescence to a more extensive identification of proteins or signalling pathways differentially expressed by quiescent cells might distinguish pharmacologically targetable nodes in the quiescence programme. This broader approach will ultimately result in strategies to eliminate the risk posed by the cells responsible for *de novo* drug resistance and eventual disease relapse and thereby improve the long-term clinical prognosis of patients diagnosed with breast cancer.

6.2. Conclusions

The work presented in this thesis demonstrates that the lipophilic fluorescent dye-retention model system offers the potential to isolate and further characterise live slow-cycling cancer cell populations independent of cell surface protein signatures with ambiguous or poorly understood functional implications for cell dynamics. The slow cycling quiescent cells isolated using this method were shown to exhibit resistance to anti-neoplastic chemotherapeutic agents and appear to exclusively contain a sub-set capable of subsequent outgrowth post-cessation of treatment. Although the exact processes that lead to quiescence and inherent drug-resistance remain to be established, the activity of the drug resistance and stemness marker aldehyde dehydrogenase was significantly up-regulated in the quiescent population of both oestrogen-receptor positive and negative cell lines. Quiescence was also associated with enrichment for the $CD44^+CD24^+$ marker signature that has previously been associated with stemness, enhanced chemotherapeutic resistance and worsened patient prognosis, particularly in triple-negative breast cancer, but did not correlate with enhanced mammosphere formation in the triple-negative MDA-MB-231 cell line. Whether these traits are associated with enhanced metastatic capacity, tumourigenicity or dormancy-competence *in vivo* remains to be established. However, given the potential for a majority of cancer cells or numerous intrinsic sub-populations to display tumourigenicity, the identification of a slow-cycling and inherently therapy resistant cellular sub-set capable of leading to tumor recurrence is both biologically and clinically significant, independent of a cancer stem cell model. Whether this sub-population is capable of establishing colonies within secondary tissues and hence represents the metastasis-initiating population is the subject of on-going studies. Further characterising the cell population identified by quiescence denoted by long-term dye-retention could allow for future live enrichment of quiescent cells and potentially yield novel insight into the cellular biology underpinning tumoural relapse and recurrence leading to the development of new therapeutic approaches to preventing or treating metastatic disease.

6.3. Summary of Future Work

The following list details future work proposed following the work presented in this thesis, some of which will be included in a post-doctoral project awarded by Weston Park Cancer Charity.

1. Undertake whole transcriptomic profiling to characterise the gene expression profile of dye-retaining quiescent cells and compare this to that of the bulk cell population in oestrogen-receptor positive and oestrogen-receptor positive breast cancer cell lines

2. Establish differentially regulated genes and pathways following analysis of transcriptomic profiling data and confirm expression of a select panel of target genes and proteins in order to:

    a. Identify a surrogacy marker signature for the quiescent phenotype

    b. Identify prospective pathways which underpin cellular quiescence and which might represent therapeutic targets for terminal maintenance of dormancy or effective killing of quiescent cells

3. Determine whether drug resistance mechanism other than aldehyde dehydrogenase activity are enriched within dye-retaining quiescent cells across oestrogen-receptor positive and oestrogen receptor negative breast cancer cell lines and whether their inhibition is able to sensitise inherently drug-resistant quiescent cells to the effects of chemotherapeutic agents

4. Establish how the quiescence-associated gene signature identified in (2.) is modulated in quiescent cells that survive chemotherapy

5. Determine whether hypoxia signalling drives the quiescent phenotype in both oestrogen receptor-positive and oestrogen receptor negative cells by:

    a. Establishing whether hypoxia signalling is hyper-activated in quiescent cells

    b. Establishing whether induction of hypoxia in a novel experimental model system developed by our collaborator Dr. Paul Shore (University of Manchester) is able to recapitulate the quiescent phenotype and gene signature identified in (2.)

6. Determine whether dye-retaining quiescent cells are more tumourigenic at primary and metastatic sites or are more prone to long-term dormancy post-metastasis than rapidly dividing cells *in vivo* using limiting dilution xenotransplantation

References

Abraham, B. K., Fritz, P., McClellan, M., Hauptvogel, P., Athelogou, M. & Brauch, H. (2005). Prevalence of CD44+/CD24-/low cells in breast cancer may not be associated with clinical outcome but may favor distant metastasis. *Clin Cancer Res,* **11**, 1154-9.

Adewumi, O., Aflatoonian, B., Ahrlund-Richter, L., Amit, M., Andrews, P. W., Beighton, G., Bello, P. A., Benvenisty, N., Berry, L. S., Bevan, S., Blum, B., Brooking, J., Chen, K. G., Choo, A. B., Churchill, G. A., Corbel, M., Damjanov, I., Draper, J. S., Dvorak, P., Emanuelsson, K., Fleck, R. A., Ford, A., Gertow, K., Gertsenstein, M., Gokhale, P. J., Hamilton, R. S., Hampl, A., Healy, L. E., Hovatta, O., Hyllner, J., Imreh, M. P., Itskovitz-Eldor, J., Jackson, J., Johnson, J. L., Jones, M., Kee, K., King, B. L., Knowles, B. B., Lako, M., Lebrin, F., Mallon, B. S., Manning, D., Mayshar, Y., McKay, R. D., Michalska, A. E., Mikkola, M., Mileikovsky, M., Minger, S. L., Moore, H. D., Mummery, C. L., Nagy, A., Nakatsuji, N., O'Brien, C. M., Oh, S. K., Olsson, C., Otonkoski, T., Park, K. Y., Passier, R., Patel, H., Patel, M., Pedersen, R., Pera, M. F., Piekarczyk, M. S., Pera, R. A., Reubinoff, B. E., Robins, A. J., Rossant, J., Rugg-Gunn, P., Schulz, T. C., Semb, H., Sherrer, E. S., Siemen, H., Stacey, G. N., Stojkovic, M., Suemori, H., Szatkiewicz, J., Turetsky, T., Tuuri, T., van den Brink, S., Vintersten, K., Vuoristo, S., Ward, D., Weaver, T. A., Young, L. A. & Zhang, W. (2007). Characterization of human embryonic stem cell lines by the International Stem Cell Initiative. *Nat Biotechnol,* **25**, 803-16.

Aguirre Ghiso, J. A. (2002). Inhibition of FAK signaling activated by urokinase receptor induces dormancy in human carcinoma cells in vivo. *Oncogene,* **21**, 2513-24.

Aguirre Ghiso, J. A., Kovalski, K. & Ossowski, L. (1999). Tumor dormancy induced by downregulation of urokinase receptor in human carcinoma involves integrin and MAPK signaling. *J Cell Biol,* **147**, 89-104.

Aguirre-Ghiso, J. A. (2007). Models, mechanisms and clinical evidence for cancer dormancy. *Nat Rev Cancer,* **7**, 834-46.

Aguirre-Ghiso, J. A., Liu, D., Mignatti, A., Kovalski, K. & Ossowski, L. (2001). Urokinase receptor and fibronectin regulate the ERK(MAPK) to p38(MAPK) activity ratios that determine carcinoma cell proliferation or dormancy in vivo. *Mol Biol Cell,* **12**, 863-79.

Ahmed, K. M., Zhang, H. & Park, C. C. (2013). NF-kappaB regulates radioresistance mediated by beta1-integrin in three-dimensional culture of breast cancer cells. *Cancer Res,* **73**, 3737-48.

Aigner, K., Dampier, B., Descovich, L., Mikula, M., Sultan, A., Schreiber, M., Mikulits, W., Brabletz, T., Strand, D., Obrist, P., Sommergruber, W., Schweifer, N., Wernitznig, A., Beug, H., Foisner, R. & Eger, A. (2007). The transcription factor ZEB1 (deltaEF1) promotes tumour cell dedifferentiation by repressing master regulators of epithelial polarity. *Oncogene,* **26**, 6979-88.

Akrap, N., Andersson, D., Bom, E., Gregersson, P., Stahlberg, A. & Landberg, G. (2016). Identification of Distinct Breast Cancer Stem Cell Populations Based on Single-Cell Analyses of Functionally Enriched Stem and Progenitor Pools. *Stem Cell Reports,* **6**, 121-36.

Al-Hajj, M., Wicha, M. S., Benito-Hernandez, A., Morrison, S. J. & Clarke, M. F. (2003). Prospective identification of tumorigenic breast cancer cells. *Proc Natl Acad Sci U S A,* **100**, 3983-8.

Allen, E., Mieville, P., Warren, C. M., Saghafinia, S., Li, L., Peng, M. W. & Hanahan, D. (2016). Metabolic Symbiosis Enables Adaptive Resistance to Anti-angiogenic Therapy that Is Dependent on mTOR Signaling. *Cell Rep,* **15**, 1144-60.

Almog, N., Ma, L., Raychowdhury, R., Schwager, C., Erber, R., Short, S., Hlatky, L., Vajkoczy, P., Huber, P. E., Folkman, J. & Abdollahi, A. (2009). Transcriptional switch of dormant tumors to fast-growing angiogenic phenotype. *Cancer Res,* **69**, 836-44.

Anderson, W. M. & Trgovcich-Zacok, D. (1995). Carbocyanine dyes with long alkyl side-chains: broad spectrum inhibitors of mitochondrial electron transport chain activity. *Biochem Pharmacol,* **49**, 1303-11.

Andrade, W., Seabrook, T. J., Johnston, M. G. & Hay, J. B. (1996). The use of the lipophilic fluorochrome CM-DiI for tracking the migration of lymphocytes. *J Immunol Methods,* **194**, 181-9.

Aomatsu, N., Yashiro, M., Kashiwagi, S., Takashima, T., Ishikawa, T., Ohsawa, M., Wakasa, K. & Hirakawa, K. (2012). CD133 is a useful surrogate marker for predicting chemosensitivity to neoadjuvant chemotherapy in breast cancer. *PLoS One,* **7**, e45865.

Baldwin, A. S. (2012). Regulation of cell death and autophagy by IKK and NF-kappaB: critical mechanisms in immune function and cancer. *Immunol Rev,* **246**, 327-45.

Balic, M., Dandachi, N., Lin, H. & Datar, R. H. (2005). Cancer metastasis: advances in the detection and characterization of disseminated tumour cells facilitate clinical translation. *Natl Med J India,* **18**, 250-5.

Balic, M., Lin, H., Young, L., Hawes, D., Giuliano, A., McNamara, G., Datar, R. H. & Cote, R. J. (2006). Most early disseminated cancer cells detected in bone marrow of breast cancer patients have a putative breast cancer stem cell phenotype. *Clin Cancer Res,* **12**, 5615-21.

Bandyopadhyay, S., Pai, S. K., Gross, S. C., Hirota, S., Hosobe, S., Miura, K., Saito, K., Commes, T., Hayashi, S., Watabe, M. & Watabe, K. (2003). The Drg-1 gene suppresses tumor metastasis in prostate cancer. *Cancer Res,* **63**, 1731-6.

Bandyopadhyay, S., Pai, S. K., Hirota, S., Hosobe, S., Takano, Y., Saito, K., Piquemal, D., Commes, T., Watabe, M., Gross, S. C., Wang, Y., Ran, S. & Watabe, K. (2004). Role of the putative tumor metastasis suppressor gene Drg-1 in breast cancer progression. *Oncogene,* **23**, 5675-81.

Bane, A., Viloria-Petit, A., Pinnaduwage, D., Mulligan, A. M., O'Malley, F. P. & Andrulis, I. L. (2013). Clinical-pathologic significance of cancer stem cell marker expression in familial breast cancers. *Breast Cancer Res Treat,* **140**, 195-205.

Barkan, D. & Green, J. E. (2011). An in vitro system to study tumor dormancy and the switch to metastatic growth. *J Vis Exp*.

Barrios, J. & Wieder, R. (2009). Dual FGF-2 and intergrin alpha5beta1 signaling mediate GRAF-induced RhoA inactivation in a model of breast cancer dormancy. *Cancer Microenviron, 2*, 33-47.

Bartkowiak, K., Kwiatkowski, M., Buck, F., Gorges, T. M., Nilse, L., Assmann, V., Andreas, A., Muller, V., Wikman, H., Riethdorf, S., Schluter, H. & Pantel, K. (2015). Disseminated Tumor Cells Persist in the Bone Marrow of Breast Cancer Patients through Sustained Activation of the Unfolded Protein Response. *Cancer Res, 75*, 5367-77.

Battula, V. L., Evans, K. W., Hollier, B. G., Shi, Y., Marini, F. C., Ayyanan, A., Wang, R. Y., Brisken, C., Guerra, R., Andreeff, M. & Mani, S. A. (2010). Epithelial-mesenchymal transition-derived cells exhibit multilineage differentiation potential similar to mesenchymal stem cells. *Stem Cells, 28*, 1435-45.

Battula, V. L., Shi, Y., Evans, K. W., Wang, R. Y., Spaeth, E. L., Jacamo, R. O., Guerra, R., Sahin, A. A., Marini, F. C., Hortobagyi, G., Mani, S. A. & Andreeff, M. (2012). Ganglioside GD2 identifies breast cancer stem cells and promotes tumorigenesis. *J Clin Invest, 122*, 2066-78.

Bernardi, M. A., Logullo, A. F., Pasini, F. S., Nonogaki, S., Blumke, C., Soares, F. A. & Brentani, M. M. (2012). Prognostic significance of CD24 and claudin-7 immunoexpression in ductal invasive breast cancer. *Oncol Rep, 27*, 28-38.

Bhat-Nakshatri, P., Appaiah, H., Ballas, C., Pick-Franke, P., Goulet, R., Jr., Badve, S., Srour, E. F. & Nakshatri, H. (2010). SLUG/SNAI2 and tumor necrosis factor generate breast cells with CD44+/CD24- phenotype. *BMC Cancer, 10*, 411.

Bolos, V., Peinado, H., Perez-Moreno, M. A., Fraga, M. F., Esteller, M. & Cano, A. (2003). The transcription factor Slug represses E-cadherin expression and induces epithelial to mesenchymal transitions: a comparison with Snail and E47 repressors. *J Cell Sci, 116*, 499-511.

Bonnet, D. & Dick, J. E. (1997). Human acute myeloid leukemia is organized as a hierarchy that originates from a primitive hematopoietic cell. *Nat Med, 3*, 730-7.

Bragado, P., Estrada, Y., Parikh, F., Krause, S., Capobianco, C., Farina, H. G., Schewe, D. M. & Aguirre-Ghiso, J. A. (2013). TGF-beta2 dictates disseminated tumour cell fate in target organs through TGF-beta-RIII and p38alpha/beta signalling. *Nat Cell Biol, 15*, 1351-61.

Bragado, P., Sosa, M. S., Keely, P., Condeelis, J. & Aguirre-Ghiso, J. A. (2012). Microenvironments dictating tumor cell dormancy. *Recent Results Cancer Res, 195*, 25-39.

Braun, F., Bertin-Ciftci, J., Gallouet, A. S., Millour, J. & Juin, P. (2011). Serum-nutrient starvation induces cell death mediated by Bax and Puma that is counteracted by p21 and unmasked by Bcl-x(L) inhibition. *PLoS One, 6*, e23577.

Britton, K. M., Eyre, R., Harvey, I. J., Stemke-Hale, K., Browell, D., Lennard, T. W. & Meeson, A. P. (2012). Breast cancer, side population cells and ABCG2 expression. *Cancer Lett,* **323**, 97-105.

Bunting, K. D. (2002). ABC transporters as phenotypic markers and functional regulators of stem cells. *Stem Cells,* **20**, 11-20.

Burrell, R. A., McGranahan, N., Bartek, J. & Swanton, C. (2013). The causes and consequences of genetic heterogeneity in cancer evolution. *Nature,* **501**, 338-45.

Cabrera, M. C., Hollingsworth, R. E. & Hurt, E. M. (2015). Cancer stem cell plasticity and tumor hierarchy. *World J Stem Cells,* **7**, 27-36.

Cailleau, R., Olive, M. & Cruciger, Q. V. (1978). Long-term human breast carcinoma cell lines of metastatic origin: preliminary characterization. *In Vitro,* **14**, 911-5.

Cailleau, R., Young, R., Olive, M. & Reeves, W. J., Jr. (1974). Breast tumor cell lines from pleural effusions. *J Natl Cancer Inst,* **53**, 661-74.

Campbell, P. J., Yachida, S., Mudie, L. J., Stephens, P. J., Pleasance, E. D., Stebbings, L. A., Morsberger, L. A., Latimer, C., McLaren, S., Lin, M. L., McBride, D. J., Varela, I., Nik-Zainal, S. A., Leroy, C., Jia, M., Menzies, A., Butler, A. P., Teague, J. W., Griffin, C. A., Burton, J., Swerdlow, H., Quail, M. A., Stratton, M. R., Iacobuzio-Donahue, C. & Futreal, P. A. (2010). The patterns and dynamics of genomic instability in metastatic pancreatic cancer. *Nature,* **467**, 1109-13.

Chaffer, C. L., Brueckmann, I., Scheel, C., Kaestli, A. J., Wiggins, P. A., Rodrigues, L. O., Brooks, M., Reinhardt, F., Su, Y., Polyak, K., Arendt, L. M., Kuperwasser, C., Bierie, B. & Weinberg, R. A. (2011). Normal and neoplastic nonstem cells can spontaneously convert to a stem-like state. *Proc Natl Acad Sci U S A,* **108**, 7950-5.

Chaffer, C. L. & Weinberg, R. A. (2011). A perspective on cancer cell metastasis. *Science,* **331**, 1559-64.

Charafe-Jauffret, E., Ginestier, C., Bertucci, F., Cabaud, O., Wicinski, J., Finetti, P., Josselin, E., Adelaide, J., Nguyen, T. T., Monville, F., Jacquemier, J., Thomassin-Piana, J., Pinna, G., Jalaguier, A., Lambaudie, E., Houvenaeghel, G., Xerri, L., Harel-Bellan, A., Chaffanet, M., Viens, P. & Birnbaum, D. (2013). ALDH1-positive cancer stem cells predict engraftment of primary breast tumors and are governed by a common stem cell program. *Cancer Res,* **73**, 7290-300.

Charafe-Jauffret, E., Ginestier, C., Iovino, F., Wicinski, J., Cervera, N., Finetti, P., Hur, M. H., Diebel, M. E., Monville, F., Dutcher, J., Brown, M., Viens, P., Xerri, L., Bertucci, F., Stassi, G., Dontu, G., Birnbaum, D. & Wicha, M. S. (2009). Breast cancer cell lines contain functional cancer stem cells with metastatic capacity and a distinct molecular signature. *Cancer Res,* **69**, 1302-13.

Chien, Y., Kim, S., Bumeister, R., Loo, Y. M., Kwon, S. W., Johnson, C. L., Balakireva, M. G., Romeo, Y., Kopelovich, L., Gale, M., Jr., Yeaman, C., Camonis, J. H., Zhao, Y. & White, M. A. (2006). RalB GTPase-mediated activation of the IkappaB family kinase TBK1 couples innate immune signaling to tumor cell survival. *Cell,* **127**, 157-70.

Chikamatsu, K., Ishii, H., Takahashi, G., Okamoto, A., Moriyama, M., Sakakura, K. & Masuyama, K. (2012). Resistance to apoptosis-inducing stimuli in CD44+ head and neck squamous cell carcinoma cells. *Head Neck,* **34**, 336-43.

Chong, M. S., Lim, J., Goh, J., Sia, M. W., Chan, J. K. & Teoh, S. H. (2014). Cocultures of mesenchymal stem cells and endothelial cells as organotypic models of prostate cancer metastasis. *Mol Pharm,* **11**, 2126-33.

Chute, J. P., Muramoto, G. G., Whitesides, J., Colvin, M., Safi, R., Chao, N. J. & McDonnell, D. P. (2006). Inhibition of aldehyde dehydrogenase and retinoid signaling induces the expansion of human hematopoietic stem cells. *Proc Natl Acad Sci U S A,* **103**, 11707-12.

Clark, D. W. & Palle, K. (2016). Aldehyde dehydrogenases in cancer stem cells: potential as therapeutic targets. *Ann Transl Med,* **4**, 518.

Cojoc, M., Mabert, K., Muders, M. H. & Dubrovska, A. (2015). A role for cancer stem cells in therapy resistance: cellular and molecular mechanisms. *Semin Cancer Biol,* **31**, 16-27.

Coleman, R., Body, J. J., Aapro, M., Hadji, P. & Herrstedt, J. (2014a). Bone health in cancer patients: ESMO Clinical Practice Guidelines. *Ann Oncol,* **25 Suppl 3**, iii124-37.

Coleman, R., Cameron, D., Dodwell, D., Bell, R., Wilson, C., Rathbone, E., Keane, M., Gil, M., Burkinshaw, R., Grieve, R., Barrett-Lee, P., Ritchie, D., Liversedge, V., Hinsley, S. & Marshall, H. (2014b). Adjuvant zoledronic acid in patients with early breast cancer: final efficacy analysis of the AZURE (BIG 01/04) randomised open-label phase 3 trial. *Lancet Oncol,* **15**, 997-1006.

Coleman, R. E. (2006). Clinical features of metastatic bone disease and risk of skeletal morbidity. *Clin Cancer Res,* **12**, 6243s-6249s.

Coller, H. A., Sang, L. & Roberts, J. M. (2006). A new description of cellular quiescence. *PLoS Biol,* **4**, e83.

Collins, A. T., Berry, P. A., Hyde, C., Stower, M. J. & Maitland, N. J. (2005). Prospective identification of tumorigenic prostate cancer stem cells. *Cancer Res,* **65**, 10946-51.

Cory, G. (2011). Scratch-wound assay. *Methods Mol Biol,* **769**, 25-30.

Cotsarelis, G., Sun, T. T. & Lavker, R. M. (1990). Label-retaining cells reside in the bulge area of pilosebaceous unit: implications for follicular stem cells, hair cycle, and skin carcinogenesis. *Cell,* **61**, 1329-37.

Cree, I. A. & Charlton, P. (2017). Molecular chess? Hallmarks of anti-cancer drug resistance. *BMC Cancer,* **17**, 10.

Croker, A. K. & Allan, A. L. (2012). Inhibition of aldehyde dehydrogenase (ALDH) activity reduces chemotherapy and radiation resistance of stem-like ALDHhiCD44(+) human breast cancer cells. *Breast Cancer Res Treat,* **133**, 75-87.

Croker, A. K., Goodale, D., Chu, J., Postenka, C., Hedley, B. D., Hess, D. A. & Allan, A. L. (2009). High aldehyde dehydrogenase and expression of cancer stem cell markers selects for breast cancer cells with enhanced malignant and metastatic ability. *J Cell Mol Med,* **13**, 2236-52.

Crosier, P. S., Freeman, S. A., Orlic, D., Bodine, D. M. & Crosier, K. E. (1996). The Dtk receptor tyrosine kinase, which binds protein S, is expressed during hematopoiesis. *Exp Hematol,* **24**, 318-23.

Da Cruz, P. A., Marques, O., Rosa, A. M., M, D. E. F. F., Rema, A. & Lopes, C. (2014). Co-expression of stem cell markers ALDH1 and CD44 in non-malignant and neoplastic lesions of the breast. *Anticancer Res,* **34**, 1427-34.

Da Cruz, P. A., Marques, O., Sampaio, R., Rosa, A., Garcia, J., Rema, A., M, D. E. F. F., Silva, P., Vizcaino, R. & Lopes, C. (2016). Characterization of CD44+ALDH1+Ki-67- Cells in Non-malignant and Neoplastic Lesions of the Breast. *Anticancer Res,* **36**, 4629-38.

Darby, C., Giannola, D. M., Couzens, M. S. & Emerson, S. G. (2000). ETK2 receptor tyrosine kinase promotes survival of factor-dependent FDC-P1 progenitor cells. *Exp Hematol,* **28**, 716-25.

Dembinski, J. L. & Krauss, S. (2009). Characterization and functional analysis of a slow cycling stem cell-like subpopulation in pancreas adenocarcinoma. *Clin Exp Metastasis,* **26**, 611-23.

Demol, J., Lambrechts, D., Geris, L., Schrooten, J. & Van Oosterwyck, H. (2011). Towards a quantitative understanding of oxygen tension and cell density evolution in fibrin hydrogels. *Biomaterials,* **32**, 107-18.

Deng, X., Apple, S., Zhao, H., Song, J., Lee, M., Luo, W., Wu, X., Chung, D., Pietras, R. J. & Chang, H. R. (2017). CD24 Expression and differential resistance to chemotherapy in triple-negative breast cancer. *Oncotarget,* **8**, 38294-38308.

Denizot, F. & Lang, R. (1986). Rapid colorimetric assay for cell growth and survival. Modifications to the tetrazolium dye procedure giving improved sensitivity and reliability. *J Immunol Methods,* **89**, 271-7.

Di Conza, G., Trusso Cafarello, S., Zheng, X., Zhang, Q. & Mazzone, M. (2017). PHD2 Targeting Overcomes Breast Cancer Cell Death upon Glucose Starvation in a PP2A/B55alpha-Mediated Manner. *Cell Rep,* **18**, 2836-2844.

Docherty, F. 2014. *Identifying and Characterising Dormancy in Prostate Cancer Cells.* Ph.D. Thesis, The University of Sheffield.

Dontu, G., Abdallah, W. M., Foley, J. M., Jackson, K. W., Clarke, M. F., Kawamura, M. J. & Wicha, M. S. (2003). In vitro propagation and transcriptional profiling of human mammary stem/progenitor cells. *Genes Dev,* **17**, 1253-70.

Eccles, S. A., Aboagye, E. O., Ali, S., Anderson, A. S., Armes, J., Berditchevski, F., Blaydes, J. P., Brennan, K., Brown, N. J., Bryant, H. E., Bundred, N. J., Burchell, J. M., Campbell, A. M., Carroll, J. S., Clarke, R. B., Coles, C. E., Cook, G. J., Cox, A., Curtin, N. J.,

Dekker, L. V., Silva Idos, S., Duffy, S. W., Easton, D. F., Eccles, D. M., Edwards, D. R., Edwards, J., Evans, D., Fenlon, D. F., Flanagan, J. M., Foster, C., Gallagher, W. M., Garcia-Closas, M., Gee, J. M., Gescher, A. J., Goh, V., Groves, A. M., Harvey, A. J., Harvie, M., Hennessy, B. T., Hiscox, S., Holen, I., Howell, S. J., Howell, A., Hubbard, G., Hulbert-Williams, N., Hunter, M. S., Jasani, B., Jones, L. J., Key, T. J., Kirwan, C. C., Kong, A., Kunkler, I. H., Langdon, S. P., Leach, M. O., Mann, D. J., Marshall, J. F., Martin, L., Martin, S. G., Macdougall, J. E., Miles, D. W., Miller, W. R., Morris, J. R., Moss, S. M., Mullan, P., Natrajan, R., O'Connor, J. P., O'Connor, R., Palmieri, C., Pharoah, P. D., Rakha, E. A., Reed, E., Robinson, S. P., Sahai, E., Saxton, J. M., Schmid, P., Smalley, M. J., Speirs, V., Stein, R., Stingl, J., Streuli, C. H., Tutt, A. N., Velikova, G., Walker, R. A., Watson, C. J., Williams, K. J., Young, L. S. & Thompson, A. M. (2013). Critical research gaps and translational priorities for the successful prevention and treatment of breast cancer. *Breast Cancer Res,* **15**, R92.

Engel, L. W., Young, N. A., Tralka, T. S., Lippman, M. E., O'Brien, S. J. & Joyce, M. J. (1978). Establishment and characterization of three new continuous cell lines derived from human breast carcinomas. *Cancer Res,* **38**, 3352-64.

Eyler, C. E. & Rich, J. N. (2008). Survival of the fittest: cancer stem cells in therapeutic resistance and angiogenesis. *J Clin Oncol,* **26**, 2839-45.

Fabregat, I., Malfettone, A. & Soukupova, J. (2016). New Insights into the Crossroads between EMT and Stemness in the Context of Cancer. *J Clin Med,* **5**.

Farnie, G., Clarke, R. B., Spence, K., Pinnock, N., Brennan, K., Anderson, N. G. & Bundred, N. J. (2007). Novel cell culture technique for primary ductal carcinoma in situ: role of Notch and epidermal growth factor receptor signaling pathways. *J Natl Cancer Inst,* **99**, 616-27.

Fernando, J., Malfettone, A., Cepeda, E. B., Vilarrasa-Blasi, R., Bertran, E., Raimondi, G., Fabra, A., Alvarez-Barrientos, A., Fernandez-Salguero, P., Fernandez-Rodriguez, C. M., Giannelli, G., Sancho, P. & Fabregat, I. (2015). A mesenchymal-like phenotype and expression of CD44 predict lack of apoptotic response to sorafenib in liver tumor cells. *Int J Cancer,* **136**, E161-72.

Fidler, I. J. (1970). Metastasis: guantitative analysis of distribution and fate of tumor embolilabeled with 125 I-5-iodo-2'-deoxyuridine. *J Natl Cancer Inst,* **45**, 773-82.

Fillmore, C. M. & Kuperwasser, C. (2008). Human breast cancer cell lines contain stem-like cells that self-renew, give rise to phenotypically diverse progeny and survive chemotherapy. *Breast Cancer Res,* **10**, R25.

Fluegen, G., Avivar-Valderas, A., Wang, Y., Padgen, M. R., Williams, J. K., Nobre, A. R., Calvo, V., Cheung, J. F., Bravo-Cordero, J. J., Entenberg, D., Castracane, J., Verkhusha, V., Keely, P. J., Condeelis, J. & Aguirre-Ghiso, J. A. (2017). Phenotypic heterogeneity of disseminated tumour cells is preset by primary tumour hypoxic microenvironments. *Nat Cell Biol,* **19**, 120-132.

Friedrich, J., Ebner, R. & Kunz-Schughart, L. A. (2007). Experimental anti-tumor therapy in 3-D: spheroids--old hat or new challenge? *Int J Radiat Biol,* **83**, 849-71.

Friedrich, J., Seidel, C., Ebner, R. & Kunz-Schughart, L. A. (2009). Spheroid-based drug screen: considerations and practical approach. *Nat Protoc,* **4**, 309-24.

Gao, M. Q., Choi, Y. P., Kang, S., Youn, J. H. & Cho, N. H. (2010). CD24+ cells from hierarchically organized ovarian cancer are enriched in cancer stem cells. *Oncogene,* **29**, 2672-80.

Gerdes, M. J., Sood, A., Sevinsky, C., Pris, A. D., Zavodszky, M. I. & Ginty, F. (2014). Emerging understanding of multiscale tumor heterogeneity. *Front Oncol,* **4**, 366.

Gerlinger, M., Rowan, A. J., Horswell, S., Larkin, J., Endesfelder, D., Gronroos, E., Martinez, P., Matthews, N., Stewart, A., Tarpey, P., Varela, I., Phillimore, B., Begum, S., McDonald, N. Q., Butler, A., Jones, D., Raine, K., Latimer, C., Santos, C. R., Nohadani, M., Eklund, A. C., Spencer-Dene, B., Clark, G., Pickering, L., Stamp, G., Gore, M., Szallasi, Z., Downward, J., Futreal, P. A. & Swanton, C. (2012). Intratumor heterogeneity and branched evolution revealed by multiregion sequencing. *N Engl J Med,* **366**, 883-92.

Ghajar, C. M., Peinado, H., Mori, H., Matei, I. R., Evason, K. J., Brazier, H., Almeida, D., Koller, A., Hajjar, K. A., Stainier, D. Y., Chen, E. I., Lyden, D. & Bissell, M. J. (2013). The perivascular niche regulates breast tumour dormancy. *Nat Cell Biol,* **15**, 807-17.

Giancotti, F. G. (2013). Mechanisms governing metastatic dormancy and reactivation. *Cell,* **155**, 750-64.

Gilkes, D. M., Semenza, G. L. & Wirtz, D. (2014). Hypoxia and the extracellular matrix: drivers of tumour metastasis. *Nat Rev Cancer,* **14**, 430-9.

Ginestier, C., Hur, M. H., Charafe-Jauffret, E., Monville, F., Dutcher, J., Brown, M., Jacquemier, J., Viens, P., Kleer, C. G., Liu, S., Schott, A., Hayes, D., Birnbaum, D., Wicha, M. S. & Dontu, G. (2007). ALDH1 is a marker of normal and malignant human mammary stem cells and a predictor of poor clinical outcome. *Cell Stem Cell,* **1**, 555-67.

Giordano, A., Gao, H., Cohen, E. N., Anfossi, S., Khoury, J., Hess, K., Krishnamurthy, S., Tin, S., Cristofanilli, M., Hortobagyi, G. N., Woodward, W. A., Lucci, A. & Reuben, J. M. (2013). Clinical relevance of cancer stem cells in bone marrow of early breast cancer patients. *Ann Oncol,* **24**, 2515-21.

Gligorijevic, B., Bergman, A. & Condeelis, J. (2014). Multiparametric classification links tumor microenvironments with tumor cell phenotype. *PLoS Biol,* **12**, e1001995.

Gomis, R. R. & Gawrzak, S. (2016). Tumor cell dormancy. *Mol Oncol*.

Gottschling, S., Jensen, K., Warth, A., Herth, F. J., Thomas, M., Schnabel, P. A. & Herpel, E. (2013). Stage-specific embryonic antigen-4 is expressed in basaloid lung cancer and associated with poor prognosis. *Eur Respir J,* **41**, 656-63.

Grimshaw, M. J., Cooper, L., Papazisis, K., Coleman, J. A., Bohnenkamp, H. R., Chiapero-Stanke, L., Taylor-Papadimitriou, J. & Burchell, J. M. (2008). Mammosphere culture of metastatic breast cancer cells enriches for tumorigenic breast cancer cells. *Breast Cancer Res,* **10**, R52.

Guan, R. J., Ford, H. L., Fu, Y., Li, Y., Shaw, L. M. & Pardee, A. B. (2000). Drg-1 as a differentiation-related, putative metastatic suppressor gene in human colon cancer. *Cancer Res,* **60**, 749-55.

Guiro, K., Patel, S. A., Greco, S. J., Rameshwar, P. & Arinzeh, T. L. (2015). Investigating breast cancer cell behavior using tissue engineering scaffolds. *PLoS One,* **10**, e0118724.

Gupta, G. P. & Massague, J. (2006). Cancer metastasis: building a framework. *Cell,* **127**, 679-95.

Hadnagy, A., Gaboury, L., Beaulieu, R. & Balicki, D. (2006). SP analysis may be used to identify cancer stem cell populations. *Exp Cell Res,* **312**, 3701-10.

Hafizi, S. & Dahlback, B. (2006). Signalling and functional diversity within the Axl subfamily of receptor tyrosine kinases. *Cytokine Growth Factor Rev,* **17**, 295-304.

Harper, L. J., Costea, D. E., Gammon, L., Fazil, B., Biddle, A. & Mackenzie, I. C. (2010). Normal and malignant epithelial cells with stem-like properties have an extended G2 cell cycle phase that is associated with apoptotic resistance. *BMC Cancer,* **10**, 166.

Harries, M., Taylor, A., Holmberg, L., Agbaje, O., Garmo, H., Kabilan, S. & Purushotham, A. (2014). Incidence of bone metastases and survival after a diagnosis of bone metastases in breast cancer patients. *Cancer Epidemiol,* **38**, 427-34.

Hartkopf, A. D., Taran, F. A., Wallwiener, M., Hahn, M., Becker, S., Solomayer, E. F., Brucker, S. Y., Fehm, T. N. & Wallwiener, D. (2014). Prognostic relevance of disseminated tumour cells from the bone marrow of early stage breast cancer patients - results from a large single-centre analysis. *Eur J Cancer,* **50**, 2550-9.

Hartkopf, A. D., Wallwiener, M., Fehm, T. N., Hahn, M., Walter, C. B., Gruber, I., Brucker, S. Y. & Taran, F. A. (2015). Disseminated tumor cells from the bone marrow of patients with nonmetastatic primary breast cancer are predictive of locoregional relapse. *Ann Oncol,* **26**, 1155-60.

Henckaerts, E., Langer, J. C., Orenstein, J. & Snoeck, H. W. (2004). The positive regulatory effect of TGF-beta2 on primitive murine hemopoietic stem and progenitor cells is dependent on age, genetic background, and serum factors. *J Immunol,* **173**, 2486-93.

Holen, I. (2016). The bone microenvironment - Multiple players involved in cancer progression. *J Bone Oncol,* **5**, 87-89.

Holohan, C., Van Schaeybroeck, S., Longley, D. B. & Johnston, P. G. (2013). Cancer drug resistance: an evolving paradigm. *Nat Rev Cancer,* **13**, 714-26.

Honig, M. G. & Hume, R. I. (1986). Fluorescent carbocyanine dyes allow living neurons of identified origin to be studied in long-term cultures. *J Cell Biol,* **103**, 171-87.

Honig, M. G. & Hume, R. I. (1989). Dil and diO: versatile fluorescent dyes for neuronal labelling and pathway tracing. *Trends Neurosci,* **12**, 333-5, 340-1.

Horan, P. K. & Slezak, S. E. (1989). Stable cell membrane labelling. *Nature,* **340**, 167-8.

Hosseini, H., Obradovic, M. M., Hoffmann, M., Harper, K. L., Sosa, M. S., Werner-Klein, M., Nanduri, L. K., Werno, C., Ehrl, C., Maneck, M., Patwary, N., Haunschild, G., Guzvic, M., Reimelt, C., Grauvogl, M., Eichner, N., Weber, F., Hartkopf, A. D., Taran, F. A., Brucker, S. Y., Fehm, T., Rack, B., Buchholz, S., Spang, R., Meister, G., Aguirre-Ghiso, J. A. & Klein, C. A. (2016). Early dissemination seeds metastasis in breast cancer. *Nature*.

Hu, W. Y., Hu, D. P., Xie, L., Li, Y., Majumdar, S., Nonn, L., Hu, H., Shioda, T. & Prins, G. S. (2017). Isolation and functional interrogation of adult human prostate epithelial stem cells at single cell resolution. *Stem Cell Res,* **23**, 1-12.

Hung, T. C., Lin, C. W., Hsu, T. L., Wu, C. Y. & Wong, C. H. (2013). Investigation of SSEA-4 binding protein in breast cancer cells. *J Am Chem Soc,* **135**, 5934-7.

Husemann, Y., Geigl, J. B., Schubert, F., Musiani, P., Meyer, M., Burghart, E., Forni, G., Eils, R., Fehm, T., Riethmuller, G. & Klein, C. A. (2008). Systemic spread is an early step in breast cancer. *Cancer Cell,* **13**, 58-68.

Ishiguro, T., Ohata, H., Sato, A., Yamawaki, K., Enomoto, T. & Okamoto, K. (2017). Tumor-derived spheroids: Relevance to cancer stem cells and clinical applications. *Cancer Sci*.

Ivascu, A. & Kubbies, M. (2006). Rapid generation of single-tumor spheroids for high-throughput cell function and toxicity analysis. *J Biomol Screen,* **11**, 922-32.

Jaggupilli, A. & Elkord, E. (2012). Significance of CD44 and CD24 as cancer stem cell markers: an enduring ambiguity. *Clin Dev Immunol,* **2012**, 708036.

Joyce, J. A. & Pollard, J. W. (2009). Microenvironmental regulation of metastasis. *Nat Rev Cancer,* **9**, 239-52.

Jung, S., Li, C., Duan, J., Lee, S., Kim, K., Park, Y., Yang, Y., Kim, K. I., Lim, J. S., Cheon, C. I., Kang, Y. S. & Lee, M. S. (2015). TRIP-Br1 oncoprotein inhibits autophagy, apoptosis, and necroptosis under nutrient/serum-deprived condition. *Oncotarget,* **6**, 29060-75.

Kagawa, Y., Matsuura, K., Shimizu, T. & Tsuneda, S. (2015). Direct measurement of local dissolved oxygen concentration spatial profiles in a cell culture environment. *Biotechnol Bioeng,* **112**, 1263-74.

Kennedy, K. M., Scarbrough, P. M., Ribeiro, A., Richardson, R., Yuan, H., Sonveaux, P., Landon, C. D., Chi, J. T., Pizzo, S., Schroeder, T. & Dewhirst, M. W. (2013). Catabolism of exogenous lactate reveals it as a legitimate metabolic substrate in breast cancer. *PLoS One,* **8**, e75154.

Kenny, H. A., Lal-Nag, M., White, E. A., Shen, M., Chiang, C. Y., Mitra, A. K., Zhang, Y., Curtis, M., Schryver, E. M., Bettis, S., Jadhav, A., Boxer, M. B., Li, Z., Ferrer, M. & Lengyel, E. (2015). Quantitative high throughput screening using a primary human three-dimensional organotypic culture predicts in vivo efficacy. *Nat Commun,* **6**, 6220.

Khoury, T., Ademuyiwa, F. O., Chandrasekhar, R., Jabbour, M., Deleo, A., Ferrone, S., Wang, Y. & Wang, X. (2012). Aldehyde dehydrogenase 1A1 expression in breast cancer

is associated with stage, triple negativity, and outcome to neoadjuvant chemotherapy. *Mod Pathol,* **25**, 388-97.

Kim, J. K., Jung, Y., Wang, J., Joseph, J., Mishra, A., Hill, E. E., Krebsbach, P. H., Pienta, K. J., Shiozawa, Y. & Taichman, R. S. (2013). TBK1 regulates prostate cancer dormancy through mTOR inhibition. *Neoplasia,* **15**, 1064-74.

Kinnane, N. (2007). Burden of bone disease. *Eur J Oncol Nurs,* **11 Suppl 2**, S28-31.

Klein, C. A. (2003). The systemic progression of human cancer: a focus on the individual disseminated cancer cell--the unit of selection. *Adv Cancer Res,* **89**, 35-67.

Kobayashi, A., Okuda, H., Xing, F., Pandey, P. R., Watabe, M., Hirota, S., Pai, S. K., Liu, W., Fukuda, K., Chambers, C., Wilber, A. & Watabe, K. (2011). Bone morphogenetic protein 7 in dormancy and metastasis of prostate cancer stem-like cells in bone. *J Exp Med,* **208**, 2641-55.

Korah, R., Boots, M. & Wieder, R. (2004). Integrin alpha5beta1 promotes survival of growth-arrested breast cancer cells: an in vitro paradigm for breast cancer dormancy in bone marrow. *Cancer Res,* **64**, 4514-22.

Korpal, M., Ell, B. J., Buffa, F. M., Ibrahim, T., Blanco, M. A., Celia-Terrassa, T., Mercatali, L., Khan, Z., Goodarzi, H., Hua, Y., Wei, Y., Hu, G., Garcia, B. A., Ragoussis, J., Amadori, D., Harris, A. L. & Kang, Y. (2011). Direct targeting of Sec23a by miR-200s influences cancer cell secretome and promotes metastatic colonization. *Nat Med,* **17**, 1101-8.

Koshiji, M., Kageyama, Y., Pete, E. A., Horikawa, I., Barrett, J. C. & Huang, L. E. (2004). HIF-1alpha induces cell cycle arrest by functionally counteracting Myc. *Embo j,* **23**, 1949-56.

Kreso, A. & Dick, J. E. (2014). Evolution of the cancer stem cell model. *Cell Stem Cell,* **14**, 275-91.

Kreso, A., O'Brien, C. A., van Galen, P., Gan, O. I., Notta, F., Brown, A. M., Ng, K., Ma, J., Wienholds, E., Dunant, C., Pollett, A., Gallinger, S., McPherson, J., Mullighan, C. G., Shibata, D. & Dick, J. E. (2013). Variable clonal repopulation dynamics influence chemotherapy response in colorectal cancer. *Science,* **339**, 543-8.

Lagadec, C., Vlashi, E., Della Donna, L., Meng, Y., Dekmezian, C., Kim, K. & Pajonk, F. (2010). Survival and self-renewing capacity of breast cancer initiating cells during fractionated radiation treatment. *Breast Cancer Res,* **12**, R13.

Langley, R. R. & Fidler, I. J. (2011). The seed and soil hypothesis revisited--the role of tumor-stroma interactions in metastasis to different organs. *Int J Cancer,* **128**, 2527-35.

Last'ovicka, J., Budinsky, V., Spisek, R. & Bartunkova, J. (2009). Assessment of lymphocyte proliferation: CFSE kills dividing cells and modulates expression of activation markers. *Cell Immunol,* **256**, 79-85.

Lawler, P. R. & Lawler, J. (2012). Molecular basis for the regulation of angiogenesis by thrombospondin-1 and -2. *Cold Spring Harb Perspect Med,* **2**, a006627.

Lawson, D. A., Bhakta, N. R., Kessenbrock, K., Prummel, K. D., Yu, Y., Takai, K., Zhou, A., Eyob, H., Balakrishnan, S., Wang, C. Y., Yaswen, P., Goga, A. & Werb, Z. (2015). Single-cell analysis reveals a stem-cell program in human metastatic breast cancer cells. *Nature,* **526**, 131-5.

Li, C., Heidt, D. G., Dalerba, P., Burant, C. F., Zhang, L., Adsay, V., Wicha, M., Clarke, M. F. & Simeone, D. M. (2007). Identification of pancreatic cancer stem cells. *Cancer Res,* **67**, 1030-7.

Li, P., Zhang, R., Sun, H., Chen, L., Liu, F., Yao, C., Du, M. & Jiang, X. (2013). PKH26 can transfer to host cells in vitro and vivo. *Stem Cells Dev,* **22**, 340-4.

Li, W., Ma, H., Zhang, J., Zhu, L., Wang, C. & Yang, Y. (2017). Unraveling the roles of CD44/CD24 and ALDH1 as cancer stem cell markers in tumorigenesis and metastasis. *Sci Rep,* **7**, 13856.

Li, X., Lewis, M. T., Huang, J., Gutierrez, C., Osborne, C. K., Wu, M. F., Hilsenbeck, S. G., Pavlick, A., Zhang, X., Chamness, G. C., Wong, H., Rosen, J. & Chang, J. C. (2008). Intrinsic resistance of tumorigenic breast cancer cells to chemotherapy. *J Natl Cancer Inst,* **100**, 672-9.

Lim, E., Vaillant, F., Wu, D., Forrest, N. C., Pal, B., Hart, A. H., Asselin-Labat, M. L., Gyorki, D. E., Ward, T., Partanen, A., Feleppa, F., Huschtscha, L. I., Thorne, H. J., Fox, S. B., Yan, M., French, J. D., Brown, M. A., Smyth, G. K., Visvader, J. E. & Lindeman, G. J. (2009). Aberrant luminal progenitors as the candidate target population for basal tumor development in BRCA1 mutation carriers. *Nat Med,* **15**, 907-13.

Lim, P. K., Bliss, S. A., Patel, S. A., Taborga, M., Dave, M. A., Gregory, L. A., Greco, S. J., Bryan, M., Patel, P. S. & Rameshwar, P. (2011). Gap junction-mediated import of microRNA from bone marrow stromal cells can elicit cell cycle quiescence in breast cancer cells. *Cancer Res,* **71**, 1550-60.

Lin, R. Z. & Chang, H. Y. (2008). Recent advances in three-dimensional multicellular spheroid culture for biomedical research. *Biotechnol J,* **3**, 1172-84.

Linde, N., Fluegen, G. & Aguirre-Ghiso, J. A. (2016). The Relationship Between Dormant Cancer Cells and Their Microenvironment. *Adv Cancer Res,* **132**, 45-71.

Liu, D., Aguirre Ghiso, J., Estrada, Y. & Ossowski, L. (2002). EGFR is a transducer of the urokinase receptor initiated signal that is required for in vivo growth of a human carcinoma. *Cancer Cell,* **1**, 445-57.

Liu, S., Cong, Y., Wang, D., Sun, Y., Deng, L., Liu, Y., Martin-Trevino, R., Shang, L., McDermott, S. P., Landis, M. D., Hong, S., Adams, A., D'Angelo, R., Ginestier, C., Charafe-Jauffret, E., Clouthier, S. G., Birnbaum, D., Wong, S. T., Zhan, M., Chang, J. C. & Wicha, M. S. (2014). Breast cancer stem cells transition between epithelial and mesenchymal states reflective of their normal counterparts. *Stem Cell Reports,* **2**, 78-91.

Liu, T., Xu, F., Du, X., Lai, D., Liu, T., Zhao, Y., Huang, Q., Jiang, L., Huang, W., Cheng, W. & Liu, Z. (2010). Establishment and characterization of multi-drug resistant, prostate

carcinoma-initiating stem-like cells from human prostate cancer cell lines 22RV1. *Mol Cell Biochem,* **340**, 265-73.

Liu, T. J., Sun, B. C., Zhao, X. L., Zhao, X. M., Sun, T., Gu, Q., Yao, Z., Dong, X. Y., Zhao, N. & Liu, N. (2013). CD133+ cells with cancer stem cell characteristics associates with vasculogenic mimicry in triple-negative breast cancer. *Oncogene,* **32**, 544-53.

Liu, W., Xing, F., Iiizumi-Gairani, M., Okuda, H., Watabe, M., Pai, S. K., Pandey, P. R., Hirota, S., Kobayashi, A., Mo, Y. Y., Fukuda, K., Li, Y. & Watabe, K. (2012). N-myc downstream regulated gene 1 modulates Wnt-beta-catenin signalling and pleiotropically suppresses metastasis. *EMBO Mol Med,* **4**, 93-108.

Lu, X., Mu, E., Wei, Y., Riethdorf, S., Yang, Q., Yuan, M., Yan, J., Hua, Y., Tiede, B. J., Lu, X., Haffty, B. G., Pantel, K., Massague, J. & Kang, Y. (2011). VCAM-1 promotes osteolytic expansion of indolent bone micrometastasis of breast cancer by engaging alpha4beta1-positive osteoclast progenitors. *Cancer Cell,* **20**, 701-14.

Lu, Z., Luo, R. Z., Lu, Y., Zhang, X., Yu, Q., Khare, S., Kondo, S., Kondo, Y., Yu, Y., Mills, G. B., Liao, W. S. & Bast, R. C., Jr. (2008). The tumor suppressor gene ARHI regulates autophagy and tumor dormancy in human ovarian cancer cells. *J Clin Invest,* **118**, 3917-29.

Luo, M., Clouthier, S. G., Deol, Y., Liu, S., Nagrath, S., Azizi, E. & Wicha, M. S. (2015). Breast cancer stem cells: current advances and clinical implications. *Methods Mol Biol,* **1293**, 1-49.

Lyle, S., Christofidou-Solomidou, M., Liu, Y., Elder, D. E., Albelda, S. & Cotsarelis, G. (1998). The C8/144B monoclonal antibody recognizes cytokeratin 15 and defines the location of human hair follicle stem cells. *J Cell Sci,* **111 (Pt 21)**, 3179-88.

Ma, S., Chan, K. W., Hu, L., Lee, T. K., Wo, J. Y., Ng, I. O., Zheng, B. J. & Guan, X. Y. (2007). Identification and characterization of tumorigenic liver cancer stem/progenitor cells. *Gastroenterology,* **132**, 2542-56.

Malda, J., Klein, T. J. & Upton, Z. (2007). The roles of hypoxia in the in vitro engineering of tissues. *Tissue Eng,* **13**, 2153-62.

Marlow, R., Honeth, G., Lombardi, S., Cariati, M., Hessey, S., Pipili, A., Mariotti, V., Buchupalli, B., Foster, K., Bonnet, D., Grigoriadis, A., Rameshwar, P., Purushotham, A., Tutt, A. & Dontu, G. (2013). A novel model of dormancy for bone metastatic breast cancer cells. *Cancer Res,* **73**, 6886-99.

Marsden, C. G., Wright, M. J., Carrier, L., Moroz, K., Pochampally, R. & Rowan, B. G. (2012). "A novel in vivo model for the study of human breast cancer metastasis using primary breast tumor-initiating cells from patient biopsies". *BMC Cancer,* **12**, 10.

Marusyk, A. & Polyak, K. (2010). Tumor heterogeneity: causes and consequences. *Biochim Biophys Acta,* **1805**, 105-17.

Matthews, Q., Jirasek, A., Lum, J., Duan, X. & Brolo, A. G. (2010). Variability in Raman spectra of single human tumor cells cultured in vitro: correlation with cell cycle and culture confluency. *Appl Spectrosc,* **64**, 871-87.

McGranahan, N. & Swanton, C. (2017). Clonal Heterogeneity and Tumor Evolution: Past, Present, and the Future. *Cell,* **168**, 613-628.

Mendoza, A., Hong, S. H., Osborne, T., Khan, M. A., Campbell, K., Briggs, J., Eleswarapu, A., Buquo, L., Ren, L., Hewitt, S. M., Dakir el, H., Garfield, S., Walker, R., Merlino, G., Green, J. E., Hunter, K. W., Wakefield, L. M. & Khanna, C. (2010). Modeling metastasis biology and therapy in real time in the mouse lung. *J Clin Invest,* **120**, 2979-88.

Meyer, M. J., Fleming, J. M., Lin, A. F., Hussnain, S. A., Ginsburg, E. & Vonderhaar, B. K. (2010). CD44posCD49fhiCD133/2hi defines xenograft-initiating cells in estrogen receptor-negative breast cancer. *Cancer Res,* **70**, 4624-33.

Michor, F., Iwasa, Y. & Nowak, M. A. (2004). Dynamics of cancer progression. *Nat Rev Cancer,* **4**, 197-205.

Michor, F. & Polyak, K. (2010). The origins and implications of intratumor heterogeneity. *Cancer Prev Res (Phila),* **3**, 1361-4.

Mishra, A., Wang, J., Shiozawa, Y., McGee, S., Kim, J., Jung, Y., Joseph, J., Berry, J. E., Havens, A., Pienta, K. J. & Taichman, R. S. (2012). Hypoxia stabilizes GAS6/Axl signaling in metastatic prostate cancer. *Mol Cancer Res,* **10**, 703-12.

Moody, S. E., Perez, D., Pan, T. C., Sarkisian, C. J., Portocarrero, C. P., Sterner, C. J., Notorfrancesco, K. L., Cardiff, R. D. & Chodosh, L. A. (2005). The transcriptional repressor Snail promotes mammary tumor recurrence. *Cancer Cell,* **8**, 197-209.

Moore, N., Houghton, J. & Lyle, S. (2012). Slow-cycling therapy-resistant cancer cells. *Stem Cells Dev,* **21**, 1822-30.

Moore, N. & Lyle, S. (2011). Quiescent, slow-cycling stem cell populations in cancer: a review of the evidence and discussion of significance. *J Oncol,* **2011**.

Morimoto, K., Kim, S. J., Tanei, T., Shimazu, K., Tanji, Y., Taguchi, T., Tamaki, Y., Terada, N. & Noguchi, S. (2009). Stem cell marker aldehyde dehydrogenase 1-positive breast cancers are characterized by negative estrogen receptor, positive human epidermal growth factor receptor type 2, and high Ki67 expression. *Cancer Sci,* **100**, 1062-8.

Mosmann, T. (1983). Rapid colorimetric assay for cellular growth and survival: application to proliferation and cytotoxicity assays. *J Immunol Methods,* **65**, 55-63.

Mundy, G. R. (1997). Mechanisms of bone metastasis. *Cancer,* **80**, 1546-56.

Nagelkerke, A., Bussink, J., Sweep, F. C. & Span, P. N. (2013). Generation of multicellular tumor spheroids of breast cancer cells: how to go three-dimensional. *Anal Biochem,* **437**, 17-9.

Nakanishi, T., Chumsri, S., Khakpour, N., Brodie, A. H., Leyland-Jones, B., Hamburger, A. W., Ross, D. D. & Burger, A. M. (2010). Side-population cells in luminal-type breast

cancer have tumour-initiating cell properties, and are regulated by HER2 expression and signalling. *Br J Cancer,* **102**, 815-26.

Narita, T., Kimura, N., Sato, M., Matsuura, N. & Kannagi, R. (1998). Altered expression of integrins in adriamycin-resistant human breast cancer cells. *Anticancer Res,* **18**, 257-62.

Naumov, G. N., Townson, J. L., MacDonald, I. C., Wilson, S. M., Bramwell, V. H., Groom, A. C. & Chambers, A. F. (2003). Ineffectiveness of doxorubicin treatment on solitary dormant mammary carcinoma cells or late-developing metastases. *Breast Cancer Res Treat,* **82**, 199-206.

Nguyen, D. X., Bos, P. D. & Massague, J. (2009). Metastasis: from dissemination to organ-specific colonization. *Nat Rev Cancer,* **9**, 274-84.

Nguyen, L. V., Vanner, R., Dirks, P. & Eaves, C. J. (2012). Cancer stem cells: an evolving concept. *Nat Rev Cancer,* **12**, 133-43.

Nogami, T., Shien, T., Tanaka, T., Nishiyama, K., Mizoo, T., Iwamto, T., Ikeda, H., Taira, N., Doihara, H. & Miyoshi, S. (2014). Expression of ALDH1 in axillary lymph node metastases is a prognostic factor of poor clinical outcome in breast cancer patients with 1-3 lymph node metastases. *Breast Cancer,* **21**, 58-65.

Nohara, K., Wang, F. & Spiegel, S. (1998). Glycosphingolipid composition of MDA-MB-231 and MCF-7 human breast cancer cell lines. *Breast Cancer Res Treat,* **48**, 149-57.

Noto, Z., Yoshida, T., Okabe, M., Koike, C., Fathy, M., Tsuno, H., Tomihara, K., Arai, N., Noguchi, M. & Nikaido, T. (2013). CD44 and SSEA-4 positive cells in an oral cancer cell line HSC-4 possess cancer stem-like cell characteristics. *Oral Oncol,* **49**, 787-95.

O'Brien, C. A., Pollett, A., Gallinger, S. & Dick, J. E. (2007). A human colon cancer cell capable of initiating tumour growth in immunodeficient mice. *Nature,* **445**, 106-10.

Oakes, S. R., Gallego-Ortega, D. & Ormandy, C. J. (2014). The mammary cellular hierarchy and breast cancer. *Cell Mol Life Sci,* **71**, 4301-24.

Ombrato, L. & Malanchi, I. (2014). The EMT universe: space between cancer cell dissemination and metastasis initiation. *Crit Rev Oncog,* **19**, 349-61.

Ono, M., Kosaka, N., Tominaga, N., Yoshioka, Y., Takeshita, F., Takahashi, R. U., Yoshida, M., Tsuda, H., Tamura, K. & Ochiya, T. (2014). Exosomes from bone marrow mesenchymal stem cells contain a microRNA that promotes dormancy in metastatic breast cancer cells. *Sci Signal,* **7**, ra63.

Orian-Rousseau, V. (2015). CD44 Acts as a Signaling Platform Controlling Tumor Progression and Metastasis. *Front Immunol,* **6**, 154.

Ottewell, P. D., Wang, N., Brown, H. K., Reeves, K. J., Fowles, C. A., Croucher, P. I., Eaton, C. L. & Holen, I. (2014a). Zoledronic acid has differential antitumor activity in the pre- and postmenopausal bone microenvironment in vivo. *Clin Cancer Res,* **20**, 2922-32.

Ottewell, P. D., Wang, N., Meek, J., Fowles, C. A., Croucher, P. I., Eaton, C. L. & Holen, I. (2014b). Castration-induced bone loss triggers growth of disseminated prostate cancer cells in bone. *Endocr Relat Cancer,* **21**, 769-81.

Pantel, K., Brakenhoff, R. H. & Brandt, B. (2008). Detection, clinical relevance and specific biological properties of disseminating tumour cells. *Nat Rev Cancer,* **8**, 329-40.

Papadaki, M. A., Kallergi, G., Zafeiriou, Z., Manouras, L., Theodoropoulos, P. A., Mavroudis, D., Georgoulias, V. & Agelaki, S. (2014). Co-expression of putative stemness and epithelial-to-mesenchymal transition markers on single circulating tumour cells from patients with early and metastatic breast cancer. *BMC Cancer,* **14**, 651.

Parish, C. R. (1999). Fluorescent dyes for lymphocyte migration and proliferation studies. *Immunol Cell Biol,* **77**, 499-508.

Park, J. M., Munoz, J. L., Won, B. W., Bliss, S. A., Greco, S. J., Patel, S. A., Kandouz, M. & Rameshwar, P. (2013). Exogenous CXCL12 activates protein kinase C to phosphorylate connexin 43 for gap junctional intercellular communication among confluent breast cancer cells. *Cancer Lett,* **331**, 84-91.

Park, S., Chang, C. Y., Safi, R., Liu, X., Baldi, R., Jasper, J. S., Anderson, G. R., Liu, T., Rathmell, J. C., Dewhirst, M. W., Wood, K. C., Locasale, J. W. & McDonnell, D. P. (2016). ERRalpha-Regulated Lactate Metabolism Contributes to Resistance to Targeted Therapies in Breast Cancer. *Cell Rep,* **15**, 323-35.

Park, S. Y., Lee, H. E., Li, H., Shipitsin, M., Gelman, R. & Polyak, K. (2010). Heterogeneity for stem cell-related markers according to tumor subtype and histologic stage in breast cancer. *Clin Cancer Res,* **16**, 876-87.

Patel, S. A., Ramkissoon, S. H., Bryan, M., Pliner, L. F., Dontu, G., Patel, P. S., Amiri, S., Pine, S. R. & Rameshwar, P. (2012). Delineation of breast cancer cell hierarchy identifies the subset responsible for dormancy. *Sci Rep,* **2**, 906.

Patrawala, L., Calhoun, T., Schneider-Broussard, R., Zhou, J., Claypool, K. & Tang, D. G. (2005). Side population is enriched in tumorigenic, stem-like cancer cells, whereas ABCG2+ and ABCG2- cancer cells are similarly tumorigenic. *Cancer Res,* **65**, 6207-19.

Pece, S., Tosoni, D., Confalonieri, S., Mazzarol, G., Vecchi, M., Ronzoni, S., Bernard, L., Viale, G., Pelicci, P. G. & Di Fiore, P. P. (2010). Biological and molecular heterogeneity of breast cancers correlates with their cancer stem cell content. *Cell,* **140**, 62-73.

Perou, C. M., Sorlie, T., Eisen, M. B., van de Rijn, M., Jeffrey, S. S., Rees, C. A., Pollack, J. R., Ross, D. T., Johnsen, H., Akslen, L. A., Fluge, O., Pergamenschikov, A., Williams, C., Zhu, S. X., Lonning, P. E., Borresen-Dale, A. L., Brown, P. O. & Botstein, D. (2000). Molecular portraits of human breast tumours. *Nature,* **406**, 747-52.

Plaks, V., Kong, N. & Werb, Z. (2015). The cancer stem cell niche: how essential is the niche in regulating stemness of tumor cells? *Cell Stem Cell,* **16**, 225-38.

Ponti, D., Costa, A., Zaffaroni, N., Pratesi, G., Petrangolini, G., Coradini, D., Pilotti, S., Pierotti, M. A. & Daidone, M. G. (2005). Isolation and in vitro propagation of

tumorigenic breast cancer cells with stem/progenitor cell properties. *Cancer Res,* **65**, 5506-11.

Potten, C. S., Booth, C., Tudor, G. L., Booth, D., Brady, G., Hurley, P., Ashton, G., Clarke, R., Sakakibara, S. & Okano, H. (2003). Identification of a putative intestinal stem cell and early lineage marker; musashi-1. *Differentiation,* **71**, 28-41.

Potten, C. S., Kellett, M., Roberts, S. A., Rew, D. A. & Wilson, G. D. (1992). Measurement of in vivo proliferation in human colorectal mucosa using bromodeoxyuridine. *Gut,* **33**, 71-8.

Prince, M. E., Sivanandan, R., Kaczorowski, A., Wolf, G. T., Kaplan, M. J., Dalerba, P., Weissman, I. L., Clarke, M. F. & Ailles, L. E. (2007). Identification of a subpopulation of cells with cancer stem cell properties in head and neck squamous cell carcinoma. *Proc Natl Acad Sci U S A,* **104**, 973-8.

Progatzky, F., Dallman, M. J. & Lo Celso, C. (2013). From seeing to believing: labelling strategies for in vivo cell-tracking experiments. *Interface Focus,* **3**, 20130001.

Qiu, Y., Pu, T., Guo, P., Wei, B., Zhang, Z., Zhang, H., Zhong, X., Zheng, H., Chen, L., Bu, H. & Ye, F. (2016). ALDH(+)/CD44(+) cells in breast cancer are associated with worse prognosis and poor clinical outcome. *Exp Mol Pathol,* **100**, 145-50.

Quah, B. J., Warren, H. S. & Parish, C. R. (2007). Monitoring lymphocyte proliferation in vitro and in vivo with the intracellular fluorescent dye carboxyfluorescein diacetate succinimidyl ester. *Nat Protoc,* **2**, 2049-56.

Quintana, E., Shackleton, M., Sabel, M. S., Fullen, D. R., Johnson, T. M. & Morrison, S. J. (2008). Efficient tumour formation by single human melanoma cells. *Nature,* **456**, 593-8.

Raimondi, M., Marcassa, E., Cataldo, F., Arnandis, T., Mendoza-Maldonado, R., Bestagno, M., Schneider, C. & Demarchi, F. (2016). Calpain restrains the stem cells compartment in breast cancer. *Cell Cycle,* **15**, 106-16.

Rameshwar, P., Poddar, A. & Gascon, P. (1997). Hematopoietic regulation mediated by interactions among the neurokinins and cytokines. *Leuk Lymphoma,* **28**, 1-10.

Ren, G., Esposito, M. & Kang, Y. (2015). Bone metastasis and the metastatic niche. *J Mol Med (Berl),* **93**, 1203-12.

Ricardo, S., Vieira, A. F., Gerhard, R., Leitao, D., Pinto, R., Cameselle-Teijeiro, J. F., Milanezi, F., Schmitt, F. & Paredes, J. (2011). Breast cancer stem cell markers CD44, CD24 and ALDH1: expression distribution within intrinsic molecular subtype. *J Clin Pathol,* **64**, 937-46.

Ricci-Vitiani, L., Lombardi, D. G., Pilozzi, E., Biffoni, M., Todaro, M., Peschle, C. & De Maria, R. (2007). Identification and expansion of human colon-cancer-initiating cells. *Nature,* **445**, 111-5.

Rich, J. N. (2016). Cancer stem cells: understanding tumor hierarchy and heterogeneity. *Medicine (Baltimore),* **95**, S2-7.

Rodriguez, L. G., Wu, X. & Guan, J. L. (2005). Wound-healing assay. *Methods Mol Biol,* **294**, 23-9.

Roesch, A., Fukunaga-Kalabis, M., Schmidt, E. C., Zabierowski, S. E., Brafford, P. A., Vultur, A., Basu, D., Gimotty, P., Vogt, T. & Herlyn, M. (2010). A temporarily distinct subpopulation of slow-cycling melanoma cells is required for continuous tumor growth. *Cell,* **141**, 583-94.

Sakamoto, S., Inoue, H., Ohba, S., Kohda, Y., Usami, I., Masuda, T., Kawada, M. & Nomoto, A. (2015). New metastatic model of human small-cell lung cancer by orthotopic transplantation in mice. *Cancer Sci,* **106**, 367-74.

Samlowski, W. E., Robertson, B. A., Draper, B. K., Prystas, E. & McGregor, J. R. (1991). Effects of supravital fluorochromes used to analyze the in vivo homing of murine lymphocytes on cellular function. *J Immunol Methods,* **144**, 101-15.

Sang, L., Coller, H. A. & Roberts, J. M. (2008). Control of the reversibility of cellular quiescence by the transcriptional repressor HES1. *Science,* **321**, 1095-100.

Scheel, C., Eaton, E. N., Li, S. H., Chaffer, C. L., Reinhardt, F., Kah, K. J., Bell, G., Guo, W., Rubin, J., Richardson, A. L. & Weinberg, R. A. (2011). Paracrine and autocrine signals induce and maintain mesenchymal and stem cell states in the breast. *Cell,* **145**, 926-40.

Schewe, D. M. & Aguirre-Ghiso, J. A. (2008). ATF6alpha-Rheb-mTOR signaling promotes survival of dormant tumor cells in vivo. *Proc Natl Acad Sci U S A,* **105**, 10519-24.

Shackleton, M., Vaillant, F., Simpson, K. J., Stingl, J., Smyth, G. K., Asselin-Labat, M. L., Wu, L., Lindeman, G. J. & Visvader, J. E. (2006). Generation of a functional mammary gland from a single stem cell. *Nature,* **439**, 84-8.

Shen, R. R. & Hahn, W. C. (2011). Emerging roles for the non-canonical IKKs in cancer. *Oncogene,* **30**, 631-41.

Sheridan, C., Kishimoto, H., Fuchs, R. K., Mehrotra, S., Bhat-Nakshatri, P., Turner, C. H., Goulet, R., Jr., Badve, S. & Nakshatri, H. (2006). CD44+/CD24- breast cancer cells exhibit enhanced invasive properties: an early step necessary for metastasis. *Breast Cancer Res,* **8**, R59.

Shimono, Y., Zabala, M., Cho, R. W., Lobo, N., Dalerba, P., Qian, D., Diehn, M., Liu, H., Panula, S. P., Chiao, E., Dirbas, F. M., Somlo, G., Pera, R. A., Lao, K. & Clarke, M. F. (2009). Downregulation of miRNA-200c links breast cancer stem cells with normal stem cells. *Cell,* **138**, 592-603.

Shiozawa, Y., Eber, M. R., Berry, J. E. & Taichman, R. S. (2015). Bone marrow as a metastatic niche for disseminated tumor cells from solid tumors. *Bonekey Rep,* **4**, 689.

Shiozawa, Y., Havens, A. M., Jung, Y., Ziegler, A. M., Pedersen, E. A., Wang, J., Wang, J., Lu, G., Roodman, G. D., Loberg, R. D., Pienta, K. J. & Taichman, R. S. (2008). Annexin II/annexin II receptor axis regulates adhesion, migration, homing, and growth of prostate cancer. *J Cell Biochem,* **105**, 370-80.

Shiozawa, Y., Pedersen, E. A., Havens, A. M., Jung, Y., Mishra, A., Joseph, J., Kim, J. K., Patel, L. R., Ying, C., Ziegler, A. M., Pienta, M. J., Song, J., Wang, J., Loberg, R. D., Krebsbach, P. H., Pienta, K. J. & Taichman, R. S. (2011). Human prostate cancer metastases target the hematopoietic stem cell niche to establish footholds in mouse bone marrow. *J Clin Invest,* **121**, 1298-312.

Shiozawa, Y., Pedersen, E. A., Patel, L. R., Ziegler, A. M., Havens, A. M., Jung, Y., Wang, J., Zalucha, S., Loberg, R. D., Pienta, K. J. & Taichman, R. S. (2010). GAS6/AXL axis regulates prostate cancer invasion, proliferation, and survival in the bone marrow niche. *Neoplasia,* **12**, 116-27.

Shmelkov, S. V., Butler, J. M., Hooper, A. T., Hormigo, A., Kushner, J., Milde, T., St Clair, R., Baljevic, M., White, I., Jin, D. K., Chadburn, A., Murphy, A. J., Valenzuela, D. M., Gale, N. W., Thurston, G., Yancopoulos, G. D., D'Angelica, M., Kemeny, N., Lyden, D. & Rafii, S. (2008). CD133 expression is not restricted to stem cells, and both CD133+ and CD133- metastatic colon cancer cells initiate tumors. *J Clin Invest,* **118**, 2111-20.

Singh, A. & Settleman, J. (2010). EMT, cancer stem cells and drug resistance: an emerging axis of evil in the war on cancer. *Oncogene,* **29**, 4741-51.

Singh, D., Joshi, D. D., Hameed, M., Qian, J., Gascon, P., Maloof, P. B., Mosenthal, A. & Rameshwar, P. (2000). Increased expression of preprotachykinin-I and neurokinin receptors in human breast cancer cells: implications for bone marrow metastasis. *Proc Natl Acad Sci U S A,* **97**, 388-93.

Singh, S. K., Hawkins, C., Clarke, I. D., Squire, J. A., Bayani, J., Hide, T., Henkelman, R. M., Cusimano, M. D. & Dirks, P. B. (2004). Identification of human brain tumour initiating cells. *Nature,* **432**, 396-401.

Sivasubramaniyan, K., Harichandan, A., Schilbach, K., Mack, A. F., Bedke, J., Stenzl, A., Kanz, L., Niederfellner, G. & Buhring, H. J. (2015). Expression of stage-specific embryonic antigen-4 (SSEA-4) defines spontaneous loss of epithelial phenotype in human solid tumor cells. *Glycobiology,* **25**, 902-17.

Skibinski, A. & Kuperwasser, C. (2015). The origin of breast tumor heterogeneity. *Oncogene,* **34**, 5309-16.

Smith, M. R., Saad, F., Coleman, R., Shore, N., Fizazi, K., Tombal, B., Miller, K., Sieber, P., Karsh, L., Damiao, R., Tammela, T. L., Egerdie, B., Van Poppel, H., Chin, J., Morote, J., Gomez-Veiga, F., Borkowski, T., Ye, Z., Kupic, A., Dansey, R. & Goessl, C. (2012). Denosumab and bone-metastasis-free survival in men with castration-resistant prostate cancer: results of a phase 3, randomised, placebo-controlled trial. *Lancet,* **379**, 39-46.

Sorlie, T., Perou, C. M., Tibshirani, R., Aas, T., Geisler, S., Johnsen, H., Hastie, T., Eisen, M. B., van de Rijn, M., Jeffrey, S. S., Thorsen, T., Quist, H., Matese, J. C., Brown, P. O., Botstein, D., Lonning, P. E. & Borresen-Dale, A. L. (2001). Gene expression patterns of breast carcinomas distinguish tumor subclasses with clinical implications. *Proc Natl Acad Sci U S A,* **98**, 10869-74.

Sosa, M. S., Bragado, P. & Aguirre-Ghiso, J. A. (2014). Mechanisms of disseminated cancer cell dormancy: an awakening field. *Nat Rev Cancer,* **14**, 611-22.

Sosa, M. S., Bragado, P., Debnath, J. & Aguirre-Ghiso, J. A. (2013). Regulation of tumor cell dormancy by tissue microenvironments and autophagy. *Adv Exp Med Biol,* **734**, 73-89.

Sosa, M. S., Parikh, F., Maia, A. G., Estrada, Y., Bosch, A., Bragado, P., Ekpin, E., George, A., Zheng, Y., Lam, H. M., Morrissey, C., Chung, C. Y., Farias, E. F., Bernstein, E. & Aguirre-Ghiso, J. A. (2015). NR2F1 controls tumour cell dormancy via SOX9- and RARbeta-driven quiescence programmes. *Nat Commun,* **6**, 6170.

Soule, H. D., Vazguez, J., Long, A., Albert, S. & Brennan, M. (1973). A human cell line from a pleural effusion derived from a breast carcinoma. *J Natl Cancer Inst,* **51**, 1409-16.

Sudhagar, S., Sathya, S., Gokulapriya, G. & Lakshmi, B. S. (2016). AKT-p53 axis protect cancer cells from autophagic cell death during nutrition deprivation. *Biochem Biophys Res Commun,* **471**, 396-401.

Taichman, R. S., Patel, L. R., Bedenis, R., Wang, J., Weidner, S., Schumann, T., Yumoto, K., Berry, J. E., Shiozawa, Y. & Pienta, K. J. (2013). GAS6 receptor status is associated with dormancy and bone metastatic tumor formation. *PLoS One,* **8**, e61873.

Tanei, T., Morimoto, K., Shimazu, K., Kim, S. J., Tanji, Y., Taguchi, T., Tamaki, Y. & Noguchi, S. (2009). Association of breast cancer stem cells identified by aldehyde dehydrogenase 1 expression with resistance to sequential Paclitaxel and epirubicin-based chemotherapy for breast cancers. *Clin Cancer Res,* **15**, 4234-41.

Theodoropoulos, P. A., Polioudaki, H., Agelaki, S., Kallergi, G., Saridaki, Z., Mavroudis, D. & Georgoulias, V. (2010). Circulating tumor cells with a putative stem cell phenotype in peripheral blood of patients with breast cancer. *Cancer Lett,* **288**, 99-106.

Thiery, J. P., Acloque, H., Huang, R. Y. & Nieto, M. A. (2009). Epithelial-mesenchymal transitions in development and disease. *Cell,* **139**, 871-90.

Tivari, S., Korah, R., Lindy, M. & Wieder, R. (2015). An In Vitro Dormancy Model of Estrogen-sensitive Breast Cancer in the Bone Marrow: A Tool for Molecular Mechanism Studies and Hypothesis Generation. *J Vis Exp,* e52672.

Tosoni, D., Di Fiore, P. P. & Pece, S. (2012). Functional purification of human and mouse mammary stem cells. *Methods Mol Biol,* **916**, 59-79.

Trempe, G. L. (1976). Human breast cancer in culture. *Recent Results Cancer Res,* 33-41.

Turton, N. J., Judah, D. J., Riley, J., Davies, R., Lipson, D., Styles, J. A., Smith, A. G. & Gant, T. W. (2001). Gene expression and amplification in breast carcinoma cells with intrinsic and acquired doxorubicin resistance. *Oncogene,* **20**, 1300-6.

Valastyan, S. & Weinberg, R. A. (2011). Tumor metastasis: molecular insights and evolving paradigms. *Cell,* **147**, 275-92.

Viatour, P., Somervaille, T. C., Venkatasubrahmanyam, S., Kogan, S., McLaughlin, M. E., Weissman, I. L., Butte, A. J., Passegue, E. & Sage, J. (2008). Hematopoietic stem cell quiescence is maintained by compound contributions of the retinoblastoma gene family. *Cell Stem Cell,* **3**, 416-28.

Visagie, M. H., Mqoco, T. V., Liebenberg, L., Mathews, E. H., Mathews, G. E. & Joubert, A. M. (2015). Influence of partial and complete glutamine-and glucose deprivation of breast-and cervical tumorigenic cell lines. *Cell Biosci,* **5**, 37.

Wang, N., Docherty, F., Brown, H. K., Reeves, K., Fowles, A., Lawson, M., Ottewell, P. D., Holen, I., Croucher, P. I. & Eaton, C. L. (2015a). Mitotic quiescence, but not unique "stemness," marks the phenotype of bone metastasis-initiating cells in prostate cancer. *FASEB J.*

Wang, N., Docherty, F., Brown, H. K., Reeves, K., Fowles, A., Lawson, M., Ottewell, P. D., Holen, I., Croucher, P. I. & Eaton, C. L. (2015b). Mitotic quiescence, but not unique "stemness," marks the phenotype of bone metastasis-initiating cells in prostate cancer. *Faseb j,* **29**, 3141-50.

Wang, N., Docherty, F. E., Brown, H. K., Reeves, K. J., Fowles, A. C., Ottewell, P. D., Dear, T. N., Holen, I., Croucher, P. I. & Eaton, C. L. (2014). Prostate cancer cells preferentially home to osteoblast-rich areas in the early stages of bone metastasis - evidence from in vivo models. *J Bone Miner Res.*

Wang, N., Reeves, K. J., Brown, H. K., Fowles, A. C., Docherty, F. E., Ottewell, P. D., Croucher, P. I., Holen, I. & Eaton, C. L. (2015c). The frequency of osteolytic bone metastasis is determined by conditions of the soil, not the number of seeds; evidence from in vivo models of breast and prostate cancer. *J Exp Clin Cancer Res,* **34**, 124.

Weber, G. F. (2013). Why does cancer therapy lack effective anti-metastasis drugs? *Cancer Lett,* **328**, 207-11.

Wei, W., Hu, H., Tan, H., Chow, L. W., Yip, A. Y. & Loo, W. T. (2012). Relationship of CD44+CD24-/low breast cancer stem cells and axillary lymph node metastasis. *J Transl Med,* **10 Suppl 1**, S6.

Weilbaecher, K. N., Guise, T. A. & McCauley, L. K. (2011). Cancer to bone: a fatal attraction. *Nat Rev Cancer,* **11**, 411-25.

Weinstat-Saslow, D. L., Zabrenetzky, V. S., VanHoutte, K., Frazier, W. A., Roberts, D. D. & Steeg, P. S. (1994). Transfection of thrombospondin 1 complementary DNA into a human breast carcinoma cell line reduces primary tumor growth, metastatic potential, and angiogenesis. *Cancer Res,* **54**, 6504-11.

Weiswald, L. B., Bellet, D. & Dangles-Marie, V. (2015). Spherical cancer models in tumor biology. *Neoplasia,* **17**, 1-15.

Wellner, U., Schubert, J., Burk, U. C., Schmalhofer, O., Zhu, F., Sonntag, A., Waldvogel, B., Vannier, C., Darling, D., zur Hausen, A., Brunton, V. G., Morton, J., Sansom, O., Schuler, J., Stemmler, M. P., Herzberger, C., Hopt, U., Keck, T., Brabletz, S. & Brabletz,

T. (2009). The EMT-activator ZEB1 promotes tumorigenicity by repressing stemness-inhibiting microRNAs. *Nat Cell Biol,* **11**, 1487-95.

Wheeler, S. E., Clark, A. M., Taylor, D. P., Young, C. L., Pillai, V. C., Stolz, D. B., Venkataramanan, R., Lauffenburger, D., Griffith, L. & Wells, A. (2014). Spontaneous dormancy of metastatic breast cancer cells in an all human liver microphysiologic system. *Br J Cancer,* **111**, 2342-50.

White, D. E., Kurpios, N. A., Zuo, D., Hassell, J. A., Blaess, S., Mueller, U. & Muller, W. J. (2004). Targeted disruption of beta1-integrin in a transgenic mouse model of human breast cancer reveals an essential role in mammary tumor induction. *Cancer Cell,* **6**, 159-70.

Wright, A., Andrews, N., Bardsley, K., Nielsen, J. E., Avery, K., Pewsey, E., Jones, M., Harley, D., Nielsen, A. R., Moore, H., Gokhale, P., Rajpert-De Meyts, E., Andrews, P. W., Walsh, J. & Harrison, N. J. (2011). Mapping the stem cell state: eight novel human embryonic stem and embryonal carcinoma cell antibodies. *Int J Androl,* **34**, e175-87; discussion e187-8.

Wright, A. J. & Andrews, P. W. (2009). Surface marker antigens in the characterization of human embryonic stem cells. *Stem Cell Res,* **3**, 3-11.

Yang, F., Cao, L., Sun, Z., Jin, J., Fang, H., Zhang, W. & Guan, X. (2016). Evaluation of Breast Cancer Stem Cells and Intratumor Stemness Heterogeneity in Triple-negative Breast Cancer as Prognostic Factors. *Int J Biol Sci,* **12**, 1568-1577.

Yang, J., Mani, S. A., Donaher, J. L., Ramaswamy, S., Itzykson, R. A., Come, C., Savagner, P., Gitelman, I., Richardson, A. & Weinberg, R. A. (2004). Twist, a master regulator of morphogenesis, plays an essential role in tumor metastasis. *Cell,* **117**, 927-39.

Ye, F., Qiu, Y., Li, L., Yang, L., Cheng, F., Zhang, H., Wei, B., Zhang, Z., Sun, L. & Bu, H. (2015). The Presence of EpCAM(-)/CD49f(+) Cells in Breast Cancer Is Associated with a Poor Clinical Outcome. *J Breast Cancer,* **18**, 242-8.

Yu, F., Yao, H., Zhu, P., Zhang, X., Pan, Q., Gong, C., Huang, Y., Hu, X., Su, F., Lieberman, J. & Song, E. (2007). let-7 regulates self renewal and tumorigenicity of breast cancer cells. *Cell,* **131**, 1109-23.

Yumoto, K., Berry, J. E., Taichman, R. S. & Shiozawa, Y. (2014). A novel method for monitoring tumor proliferation in vivo using fluorescent dye DiD. *Cytometry A,* **85**, 548-55.

Zhou, Y., Zhao, L., Xiong, T., Chen, X., Zhang, Y., Yu, M., Yang, J. & Yao, Z. (2013). Roles of full-length and truncated neurokinin-1 receptors on tumor progression and distant metastasis in human breast cancer. *Breast Cancer Res Treat,* **140**, 49-61.

Zhou, Y., Zuo, D., Wang, M., Zhang, Y., Yu, M., Yang, J. & Yao, Z. (2014). Effect of truncated neurokinin-1 receptor expression changes on the interaction between human breast cancer and bone marrow-derived mesenchymal stem cells. *Genes Cells,* **19**, 676-91.